INNOVATION IN GLAUCOMA

EDITED BY: Michele Lanza, Dariusz Dobrowolski and Soosan Jacob
PUBLISHED IN: Frontiers in Medicine

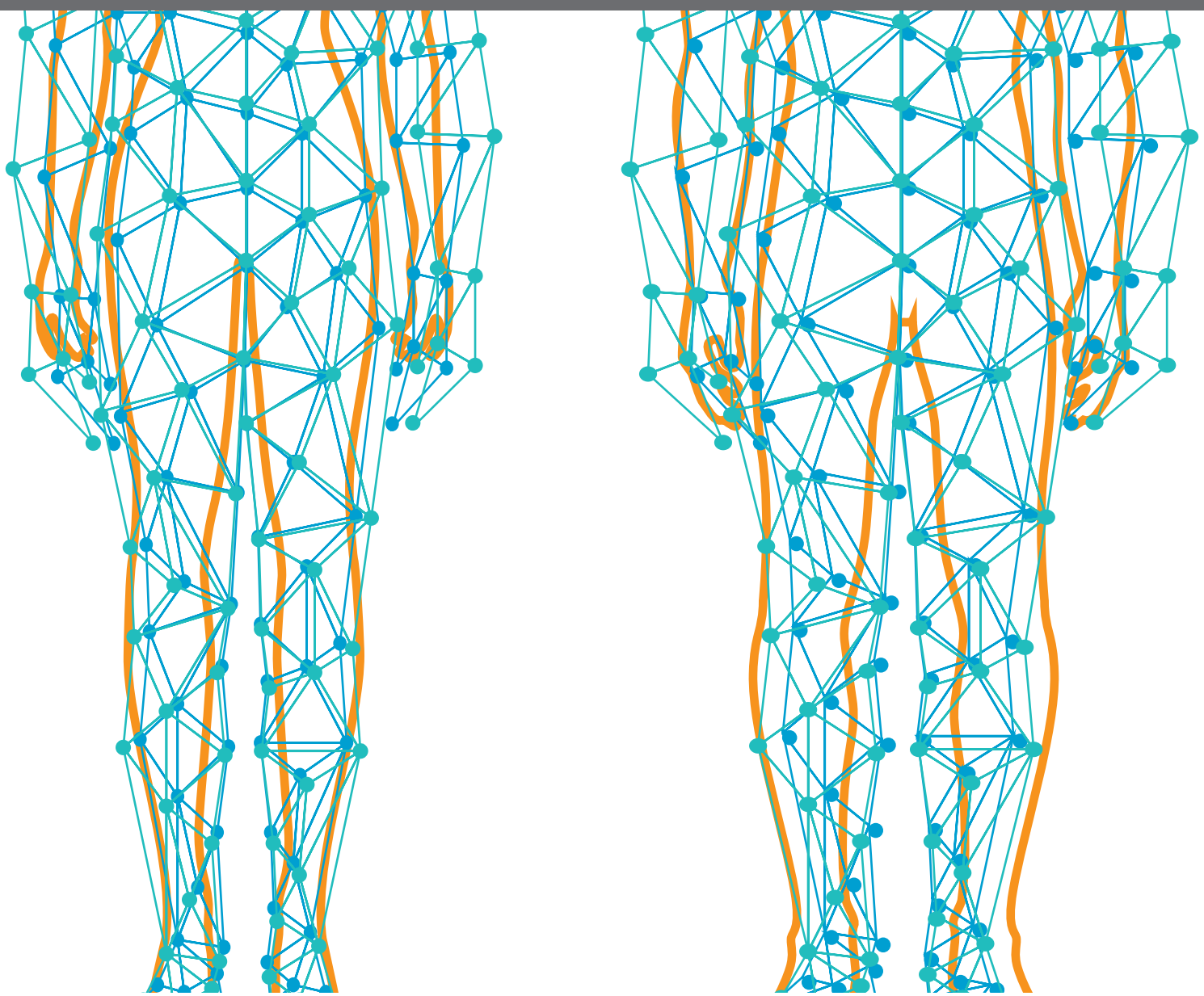

frontiers Research Topics

frontiers

ISSN 1664-8714
ISBN 978-2-88974-756-6
DOI 10.3389/978-2-88974-756-6

About Frontiers

Frontiers is more than just an open-access publisher of scholarly articles: it is a pioneering approach to the world of academia, radically improving the way scholarly research is managed. The grand vision of Frontiers is a world where all people have an equal opportunity to seek, share and generate knowledge. Frontiers provides immediate and permanent online open access to all its publications, but this alone is not enough to realize our grand goals.

Frontiers Journal Series

The Frontiers Journal Series is a multi-tier and interdisciplinary set of open-access, online journals, promising a paradigm shift from the current review, selection and dissemination processes in academic publishing. All Frontiers journals are driven by researchers for researchers; therefore, they constitute a service to the scholarly community. At the same time, the Frontiers Journal Series operates on a revolutionary invention, the tiered publishing system, initially addressing specific communities of scholars, and gradually climbing up to broader public understanding, thus serving the interests of the lay society, too.

Dedication to Quality

Each Frontiers article is a landmark of the highest quality, thanks to genuinely collaborative interactions between authors and review editors, who include some of the world's best academicians. Research must be certified by peers before entering a stream of knowledge that may eventually reach the public - and shape society; therefore, Frontiers only applies the most rigorous and unbiased reviews.
Frontiers revolutionizes research publishing by freely delivering the most outstanding research, evaluated with no bias from both the academic and social point of view. By applying the most advanced information technologies, Frontiers is catapulting scholarly publishing into a new generation.

What are Frontiers Research Topics?

Frontiers Research Topics are very popular trademarks of the Frontiers Journals Series: they are collections of at least ten articles, all centered on a particular subject. With their unique mix of varied contributions from Original Research to Review Articles, Frontiers Research Topics unify the most influential researchers, the latest key findings and historical advances in a hot research area! Find out more on how to host your own Frontiers Research Topic or contribute to one as an author by contacting the Frontiers Editorial Office: frontiersin.org/about/contact

INNOVATION IN GLAUCOMA

Topic Editors:
Michele Lanza, University of Campania Luigi Vanvitelli, Italy
Dariusz Dobrowolski, Medical University of Silesia in Katowice, Poland
Soosan Jacob, Dr. Agarwal's Eye Hospital, India

Citation: Lanza, M., Dobrowolski, D., Jacob, S., eds. (2022). Innovation in Glaucoma. Lausanne: Frontiers Media SA. doi: 10.3389/978-2-88974-756-6

Table of Contents

05 ***Editorial: Innovation in Glaucoma***
Michele Lanza, Dariusz Dobrowolski and Soosan Jacob

07 ***Prevalence of Primary Angle Closure Glaucoma in the Last 20 Years: A Meta-Analysis and Systematic Review***
Nan Zhang, Jiaxing Wang, Biyue Chen, Ying Li and Bing Jiang

17 ***Comparison of the Humphrey Field Analyzer and Photopic Negative Response of Focal Macular Electroretinograms in the Evaluation of the Relationship Between Macula Structure and Function***
Kazuyuki Hirooka, Kenji Yokoyama, Kana Tokumo and Yoshiaki Kiuchi

24 ***Evaluation of the Effectiveness of a Chronic Ocular Hypertension Mouse Model Induced by Intracameral Injection of Cross-Linking Hydrogel***
Junjue Chen, Jun Sun, Huan Yu, Ping Huang and Yisheng Zhong

40 ***Corrigendum: Evaluation of the Effectiveness of a Chronic Ocular Hypertension Mouse Model Induced by Intracameral Injection of Cross-Linking Hydrogel***
Junjue Chen, Jun Sun, Huan Yu, Ping Huang and Yisheng Zhong

41 ***Development and Validation of Automated Visual Field Report Extraction Platform Using Computer Vision Tools***
Murtaza Saifee, Jian Wu, Yingna Liu, Ping Ma, Jutima Patlidanon, Yinxi Yu, Gui-Shuang Ying and Ying Han

54 ***Low-Contrast High-Pass Visual Acuity Might Help to Detect Glaucoma Damage: A Structure-Function Analysis***
Yun Wen, Zidong Chen, Chengguo Zuo, Yangfan Yang, Jiangang Xu, Yang Kong, Hui Cheng and Minbin Yu

65 ***Extended Ganglion Cell Layer Thickness Deviation Maps With OCT in Glaucoma Diagnosis***
Paul Lehmann, Bettina Hohberger, Robert Lämmer and Christian Mardin

76 ***Optical Coherence Tomography Evaluation of Peripapillary and Macular Structure Changes in Pre-perimetric Glaucoma, Early Perimetric Glaucoma, and Ocular Hypertension: A Systematic Review and Meta-Analysis***
Yuxin Tong, Tiantian Wang, Xinyu Zhang, Yi He and Bing Jiang

94 ***Non-invasive Clinical Measurement of Ocular Rigidity and Comparison to Biomechanical and Morphological Parameters in Glaucomatous and Healthy Subjects***
Yanhui Ma, Sayoko E. Moroi and Cynthia J. Roberts

103 ***Oral Scutellarin Treatment Ameliorates Retinal Thinning and Visual Deficits in Experimental Glaucoma***
Jingyuan Zhu, Anoop Sainulabdeen, Krystal Akers, Vishnu Adi, Jeffrey R. Sims, Eva Yarsky, Yi Yan, Yu Yu, Hiroshi Ishikawa, Christopher K. Leung, Gadi Wollstein, Joel S. Schuman, Wenbin Wei and Kevin C. Chan

114 ***Microcatheter-Assisted Trabeculotomy Combined With Deep Sclerectomy and Trabeculectomy in Young to Middle-Aged Adults With Advanced Primary Open-Angle Glaucoma: 1-Year Result***
Hengli Zhang, Xiaowei Yan, Fan Li, Lihua Ma, Yulei Geng, Kexin Jiao and Guangxian Tang

124 ***Glaucoma Clinical Research: Trends in Treatment Strategies and Drug Development***
Line Storgaard, Thuy Linh Tran, Josefine Clement Freiberg, Alexander S. Hauser and Miriam Kolko

138 ***Change of Retinal Vessel Density After Lowering Intraocular Pressure in Ocular Hypertension***
Xuhao Chen, Ying Hong, Haohao Di, Qianru Wu, Di Zhang and Chun Zhang

147 ***The Relationship Between Plasma Tetrahydrocannabinol Levels and Intraocular Pressure in Healthy Adult Subjects***
Sameh Mosaed, Andrew K. Smith, John H. K. Liu, Donald S. Minckler, Robert L. Fitzgerald, David Grelotti, Emily Sones, Robert N. Weinreb and Thomas D. Marcotte

frontiers in Medicine

EDITORIAL
published: 03 March 2022
doi: 10.3389/fmed.2022.863131

Editorial: Innovation in Glaucoma

Michele Lanza[1,2]*, *Dariusz Dobrowolski*[3] *and Soosan Jacob*[4]

[1] University of Campania Luigi Vanvitelli, Caserta, Italy, [2] Dipartimento di Specialità Mediche, Chirurgiche ed Odontoiatriche, Università della Campania Luigi Vanvitelli, Naples, Italy, [3] Medical University of Silesia, Katowice, Poland, [4] Dr. Agarwal's Eye Hospital, Chennai, India

Keywords: glaucoma, glaucoma surgery, glaucoma diagnosis, glaucoma treatment, intraocular pressure (IOP), standardized automated perimetry, OCT

Editorial on the Research Topic

Innovation in Glaucoma

Glaucoma is one of the main causes of blindness worldwide, among the various forms existing of this disease, the most diffuse is primary open-angle glaucoma but many other types of glaucoma are known. Nowadays, this disease is defined as a multifactorial optic neuropathy characterized by a progressive optic nerve damage causing loss of retinal ganglion cells and their axons, developing specific visual field abnormalities, affecting eyes with open anterior chamber angles.

The goal of its treatment is to conserve the quality of life and the visual function of patients by lowering the intraocular pressure (IOP). Among the possible therapeutic options, physicians can choose a medical therapy with topical glaucoma drugs, laser, or surgical therapy.

Last years have witnessed many innovations both in glaucoma diagnostics and in treatments.

Early diagnosis is always considered a key factor in the successful management of every disease and more, the chronic and subtle ones such as glaucoma. OCT is considered an extremely important device also in glaucoma management. Lehmann et al. suggest considering retinal ganglion cell layer thickness as a very useful tool in highlighting the first alterations in eyes difficult to classify. Tong et al. provided an interesting review showing the relevance of OCT evaluations, both peripapillary and both in macular area to be very helpful in distinguish pre-perimetric glaucoma, early perimetric glaucoma and ocular hypertension.

Another interesting contribution about OCT and Glaucoma came from Chen X. et al. that detected a significant correlation between vessel density measured by OCT angiography and changes in IOP.

Hirooka et al. conducted a very interesting study evaluating morpho-functional changes in glaucoma eyes comparing results obtained with standardized automated perimetry (SAP), electroretinograms (ERG) and OCT showing data that could be very useful both in better understand this disease.

Others helps in improving the timing and the sensitivity of glaucoma diagnosis came from Wen et al., purposing a low contrast visual acuity test to check visual acuity in glaucoma patients, and from Saifee et al., purposing a new software to extract data from SAP report imagines.

Two very interesting reviews, one showing the prevalence of primary angle closure glaucoma by Zhang N. et al., and the other one investigating the trends in treatment approaches by Storgaard et al. have been included in this Research Topic.

The more experimental studies purposed in this section are one related to the correlation between the plasma level of Δ9-tetrahydrocannabinol and the IOP fluctuations by Chen J. et al. and the other one providing a new model of chronic ocular hypertension obtainable in laboratory by Mosaed et al..

Ma et al. suggested an innovative model of measuring ocular biomechanical properties.

About innovation in treatments, Zhu et al., purposed a brief report detailing the results of using

OPEN ACCESS

Edited and reviewed by:
Jodhbir Mehta,
Singapore National Eye Center, Singapore

***Correspondence:**
Michele Lanza
mic.lanza@gmail.com

Specialty section:
This article was submitted to Ophthalmology, a section of the journal Frontiers in Medicine

Received: *26 January 2022*
Accepted: *09 February 2022*
Published: *03 March 2022*

Citation:
Lanza M, Dobrowolski D and Jacob S (2022) Editorial: Innovation in Glaucoma. Front. Med. 9:863131. doi: 10.3389/fmed.2022.863131

a drug supposed to be a neuro-enhancer in glaucoma patients: Scutellarin, whereas Zhang H. et al. provided a study showing their experience in combining Microcatheter-Assisted Trabeculotomy and Deep Sclerectomy and Trabeculectomy in young glaucoma patients.

This sections provided very interesting and useful information to better manage the glaucoma patients.

Altogether this collection of articles emphasizes the importance of measuring the CSF to assess visual function in both basic research and clinical settings. It presents some methods to perform and improve those measures, and considers their interpretation and implications.

AUTHOR CONTRIBUTIONS

All authors contributed to manuscript revision, read, and approved the submitted version.

Conflict of Interest: The authors declare that the research was conducted in the absence of any commercial or financial relationships that could be construed as a potential conflict of interest.

frontiers in Medicine

SYSTEMATIC REVIEW
published: 18 January 2021
doi: 10.3389/fmed.2020.624179

Prevalence of Primary Angle Closure Glaucoma in the Last 20 Years: A Meta-Analysis and Systematic Review

Nan Zhang[1,2†], *Jiaxing Wang*[2†], *Biyue Chen*[1], *Ying Li*[2] *and Bing Jiang*[1,3*]

[1] Department of Ophthalmology of Second Xiangya Hospital, Central South University, Changsha, China, [2] Department of Ophthalmology, School of Medicine, Emory University, Atlanta, GA, United States, [3] Hunan Clinical Research Center of Ophthalmic Disease, Changsha, China

OPEN ACCESS

Edited by:
Michele Lanza,
University of Campania Luigi Vanvitelli, Italy

Reviewed by:
Shengjie Li,
Fudan University, China
Daniela Montorio,
University of Naples Federico II, Italy
Ahmed Mousa,
King Saud University, Saudi Arabia
Eray Atalay,
Eskişehir Osmangazi University, Turkey

***Correspondence:**
Bing Jiang
drjiangb@csu.edu.cn

[†] These authors have contributed equally to this work

Specialty section:
This article was submitted to Ophthalmology, a section of the journal Frontiers in Medicine

Received: 30 October 2020
Accepted: 30 November 2020
Published: 18 January 2021

Citation:
Zhang N, Wang J, Chen B, Li Y and Jiang B (2021) Prevalence of Primary Angle Closure Glaucoma in the Last 20 Years: A Meta-Analysis and Systematic Review. Front. Med. 7:624179. doi: 10.3389/fmed.2020.624179

Purpose: This meta-analysis aims to investigate the worldwide prevalence of primary angle-closure glaucoma (PACG) and its risk factors in the last 20 years.

Methods: We conducted a systematic review and meta-analysis of 37 population-based studies and 144,354 subjects. PubMed, Embase, and Web of Science databases were searched for cross-sectional or cohort studies published in the last 20 years (2000–2020) that reported the prevalence of PACG. The prevalence of PACG was analyzed according to various risk factors. A random-effects model was used for the meta-analysis.

Results: The global pooled prevalence of PACG was 0.6% [95% confidence interval (CI) = 0.5–0.8%] for the last 20 years. The prevalence of PACG increases with age. Men are found less likely to have PACG than women (risk ratio = 0.71, 95% CI = 0.53–0.93, $p < 0.01$). Asia is found to have the highest prevalence of PACG (0.7%, 95% CI = 0.6–1.0%). The current estimated population with PACG is 17.14 million (95% CI = 14.28–22.85) for people older than 40 years old worldwide, with 12.30 million (95% CI = 10.54–17.57) in Asia. It is estimated that by 2050, the global population with PACG will be 26.26 million, with 18.47 million in Asia.

Conclusion: PACG affects more than 17 million people worldwide, especially leading a huge burden to Asia. The prevalence of PACG varies widely across different ages, sex, and population geographic variation. Asian, female sex, and age are risk factors of PACG.

Keywords: glaucoma, prevalence, PACG, risk factor, age, gender, Asia

INTRODUCTION

Glaucoma is one of the leading causes of irreversible blindness worldwide (1). It is defined as a group of optic neuropathies associated with characteristic structural changes at the optic nerve head that cause the death of retinal ganglion cells and their axons, leading to visual field loss and blindness (2, 3). In contrast to primary open-angle glaucoma, the most common type of glaucoma, primary angle-closure glaucoma (PACG), is associated with the closure of the anterior chamber angle of the eye and is known to have a greater propensity of bilateral blindness, which lead to a huge burden to families and the society (4, 5).

In 2013, the worldwide prevalence of PACG was reported to be 0.5% [95% confidence interval (CI) = 0.11–1.36%] (6). It was also estimated that the global population with PACG would be 23.36 million in 2020 and 32.04 million in 2040, in which Asia accounts for more than three-quarters of PACG population (6). PACG has been associated with many risk factors, including ethnicity, age, and sex (6–8), and they all contribute to the prevalence. Updates in study designs and diagnostic methods of PACG alter the estimations of prevalence and population, whereas the International Society for Geographical and Epidemiological Ophthalmology (ISGEO) provides a standard PACG definition for survey (9). Prevalence of PACG varies across different ethnicities and geographical regions (10). With the rapid increase in global population and aging trends, it is critical to pool PACG prevalence and estimate up-to-date and accurate PACG prevalence, providing evidence for a future health-care plan. Besides, there have been increasing surveys of PACG with a large number of participants in recent years across the world, especially in Asia and Africa. In this study, we aimed to estimate the detailed prevalence of PACG globally in a risk factor-specific manner for the last two decades.

METHODS

The study was conducted following the Preferred Reporting Items for guidelines of Systemic Reviews and Meta-Analysis guidelines (11, 12).

Eligibility Criteria

Studies published between January 2000 to September 2020 were included in this meta-analysis when they met the following inclusion criteria: (1) Population-based cross-sectional or cohort studies in which the prevalence of PACG from a defined geographic region was provided; (2) Studies with a clear definition of random or clustered sampling procedure; (3) PACG defined by using ISGEO (9) criteria or similar to ISGEO that based on structure and/or functional evidence of glaucomatous optic neuropathy with occludable anterior chamber angle; (4) Studies that prevalence data for PACG can be extracted or calculated. Exclusion criteria included: (1) Self-reported diagnosis of glaucoma included; (2) Non-English articles; (3) Articles using repeated data from the author's previous publications.

Search Strategy

We conducted a systematic and comprehensive search in three electronic databases (PubMed, Embase, and Web of Science) from August to September 2020. A combination of keywords related to PACG (glaucoma, PACG, and primary angle-closure glaucoma) and epidemiology (prevalence, population, and survey) was used to identify all published papers, abstracts, and letters between January 2000 and September 2020. Besides, a hand search was used to identify target articles from the other reference list. The detailed search strategy of different databases was provided in **Supplementary Table 1**.

Data Extraction

Two reviewers (NZ and BC) conducted data extraction independently based on inclusion and exclusion criteria; disagreements received final consensus after several full discussions between reviewers. Full data extraction in the data extraction sheet was completed after reviewers independently identified cases from every targeted article and reached final agreement. The following data were extracted and reported for each study: first author, year of publication, sex, age, continent, country, habitation area (urban or rural), numbers of cases, sample size, prevalence with 95% CI, and response rate (**Supplementary Table 2**).

Statistical Analysis

Data are presented as prevalence (95%CIs). Forest plots were performed using the software R version 3.6.3 (R Foundation for Statistical Computing, Vienna, Austria) and the R package "meta" 13. We selected the prevalence of PACG as the main outcome. The relative risk ratios and 95% CIs of the results were compared. Heterogeneity between studies was assessed using the I^2 statistic (13–16). Due to the high likelihood of heterogeneity among the selected studies, we used a random-effects model to evaluate pooled effects. Publication bias was calculated using the Funnel plots (17, 18), P-curve analysis (19), and Egger test (17) ($p < 0.05$ was considered as significant publication bias). Detailed bias for each study was described in **Supplementary Tables 3, 4**.

The p-value for prevalence difference among groups for age, sex, continent, habitation area, and decades was calculated using "metaprop" from R package "meta," random-effects model. The p-value for prevalence difference among groups for sex was calculated using "metabin" from R package "meta," random-effects model. A meta-regression test was performed for subgroup analysis, with the first category of each subgroup used as intercept. The statistical output includes a test of whether the intercept differs significantly from zero and whether other groups differ from the intercept. A value of $p < 0.05$ was considered statistically significant.

The number of people older than 40 years old with PACG was estimated by different continents. The population projection data were from the latest data of the World Population Prospects of the United Nations (20), which consisted of the latest results of national population consensus and demographic surveys from countries worldwide and also consider mortality rate and fertility rate in its projection of world population number. The estimated numbers of PACG population were calculated by multiplying the age- and region-specific prevalence from our random-effects model and the corresponding population number. Age- and region-specific prevalence were assumed to be consistent in the next 30 years' projection, as no significant difference has been found between the prevalence of last two decades by the random-effects model ($Q = 0.22$, df $= 1$, $p = 0.64$).

Risk of Bias Assessment

Articles included in the study were assessed for risk of bias using two domains of the Quality in Prognosis Studies tool (21) that are relevant to observational studies (study participation and outcome measurement) (22). Appraisal of each

domain provides a subjective assessment of the risk of bias (ranked as low, moderate, or high). A summary of the areas considered in the assessment of each domain is included in **Supplementary Tables 3, 4**.

RESULTS

Search Results

In this study, we reviewed the full text of 68 studies about PACG prevalence published in the last 20 years, and 31 were excluded based on inclusion and exclusion criteria. The screening process is detailed in **Figure 1**. A total of 37 publications (23–59) that include 144,354 subjects were recruited. The sample size of the study ranged from 790 (Bourne, 2003, Thailand) (27) to 15,122 (Chassis, 2018, Israel) (56). Detailed information is provided in forest plots given different risk factors and summarized in **Supplementary Table 2**, including author, year of publication, country, continent, age range, detailed number of cases and sample size, and response rate.

Risk of Bias

A summary of the risk of bias of the included articles is provided in **Supplementary Figures 1, 2**; a justification of each rating is provided in **Supplementary Tables 3, 4**.

Egger test result revealed a significant publication bias ($p < 0.01$) in this meta-analysis. Funnel plots and P-curve analysis results are shown in **Supplementary Figures 3, 4**.

Meta-Analysis

The prevalence of PACG is provided in **Table 1**. The overall PACG pooled prevalence worldwide is 0.6% (95% CI = 0.5–0.8%) for the last 20 years (**Figure 2**).

Twenty-six articles presented prevalence data by sex. Prevalence was higher for women in 69.2% of the studies (18 of 26). The male-to-female portions were ranged from 0.50 (Rotchford, 2003, South Africa) (28) to 1.09 (Paul, 2015, India) (55). Sex-specific prevalence of PACG is provided in **Table 1**; **Supplementary Figure 5**. This meta-analysis showed men are less likely to suffer from PACG than women with a relative risk of 0.71 (95% CI = 0.53–0.93, $p < 0.01$) in **Figure 3**. As summarized in **Figure 4**, the prevalence of PACG in the female sex is higher than the male sex in every age group. Subgroup differences test by random-effects model resulted in a significant difference between the prevalence of male and female groups ($Q = 70.59$, $df = 25$, $p < 0.001$).

Twenty-one studies reported age-specific prevalence of PACG; the detailed prevalence for each age group is listed in **Table 1**. Prevalence of PACG increased with aging steadily (**Figure 4**; **Supplementary Figure 6**). People older than 80 years old have highest prevalence (2.8%, 95% CI = 1.7–4.7%, $p < 0.01$). People aged 40–49 years have the lowest prevalence compared with other age groups (0.1%, 95% CI = 0.1–0.3%, $p < 0.01$). Subgroup differences tested using the random-effects model revealed a statistically significant difference among different age groups ($Q = 64.71$, $df = 6$, $p < 0.001$).

Most of the surveys we included in this study were conducted in Asia (28 of 37). A survey from Oceania and North America was lacking. Among all continents, Asia is found to have the highest prevalence of PACG (0.7%, 95% CI = 0.6–1.0%). South America has the same prevalence as Asia (0.7%, 95% CI = 0.4–1.3%). Europe has the lowest PACG prevalence compared with others (0.2%, 95% CI = 0.1–0.6%). Detailed prevalence of each continent is provided in **Table 1**; **Supplementary Figure 7**. Subgroup differences tested using the random-effects model revealed a statistically significant difference among different continents ($Q = 12.84$, $df = 3$, $p = 0.005$).

In this meta-analysis, 9 studies were conducted in urban, 15 in rural, and 17 were unknown or mixed. The prevalence of urban or rural population is listed in **Table 1**; **Supplementary Figure 8**. No statistical difference has been found between rural and urban populations using the random-effects model ($p = 0.2387$, $Q = 2.87$, $df = 2$).

Risk Factors of Primary Angle-Closure Glaucoma

In this meta-analysis, we analyzed the prevalence of PACG according to various risk factors. Female sex ($Q = 70.59$, $p < 0.001$), Asian ($Q = 12.84$, $p = 0.005$), and aging ($Q = 64.71$, $p < 0.001$) are main risk factors of PACG.

Number of People With Primary Angle-Closure Glaucoma Worldwide in 2020

The estimated number of aged populations (older than 40 years old) with PACG worldwide in 2020 and the next few decades are provided in **Table 2**. The populations with PACG are estimated based on our results and estimated world population number from the United Nations (20). The global population of PACG is 17.14 million (95% CI = 14.28–22.85) for population older than 40 years old in 2020, 20.73 million (95% CI = 17.27–27.63) in 2030, 23.73 million (95% CI = 19.78–31.64) in 2040, and 26.26 million (95% CI = 21.88–35.01) in 2050. Asia has the highest population of PACG among all continents in 2020 (12.30 million, 95% CI = 10.54–17.57) and also in the next few decades, accounts for more than 70% of the PACG population worldwide.

DISCUSSION

This study provided the most updated worldwide prevalence of PACG for the last 20 years. Based on our results, the overall pooled PACG prevalence worldwide is 0.6% (95% CI = 0.5–0.8%). Asia has the highest PACG prevalence among all continents (0.7%, 95% CI = 0.6–1.0%). We estimated that the population of PACG is 17.14 million (95% CI = 14.28–22.85) for people older than 40 years old in 2020 globally, of which Asia accounts for over 70%. Our estimated PACG prevalence is similar to Tham et al.'s study, which reported the pooled PACG prevalence is 0.50% (95% CI = 0.11–1.36%) (6). PACG is still a worldwide public health burden that requires improvement in diagnostic and therapeutic approaches, particularly in Asia. The risk factors for PACG, including age, sex, and ethnicity, were discussed in detail as follows.

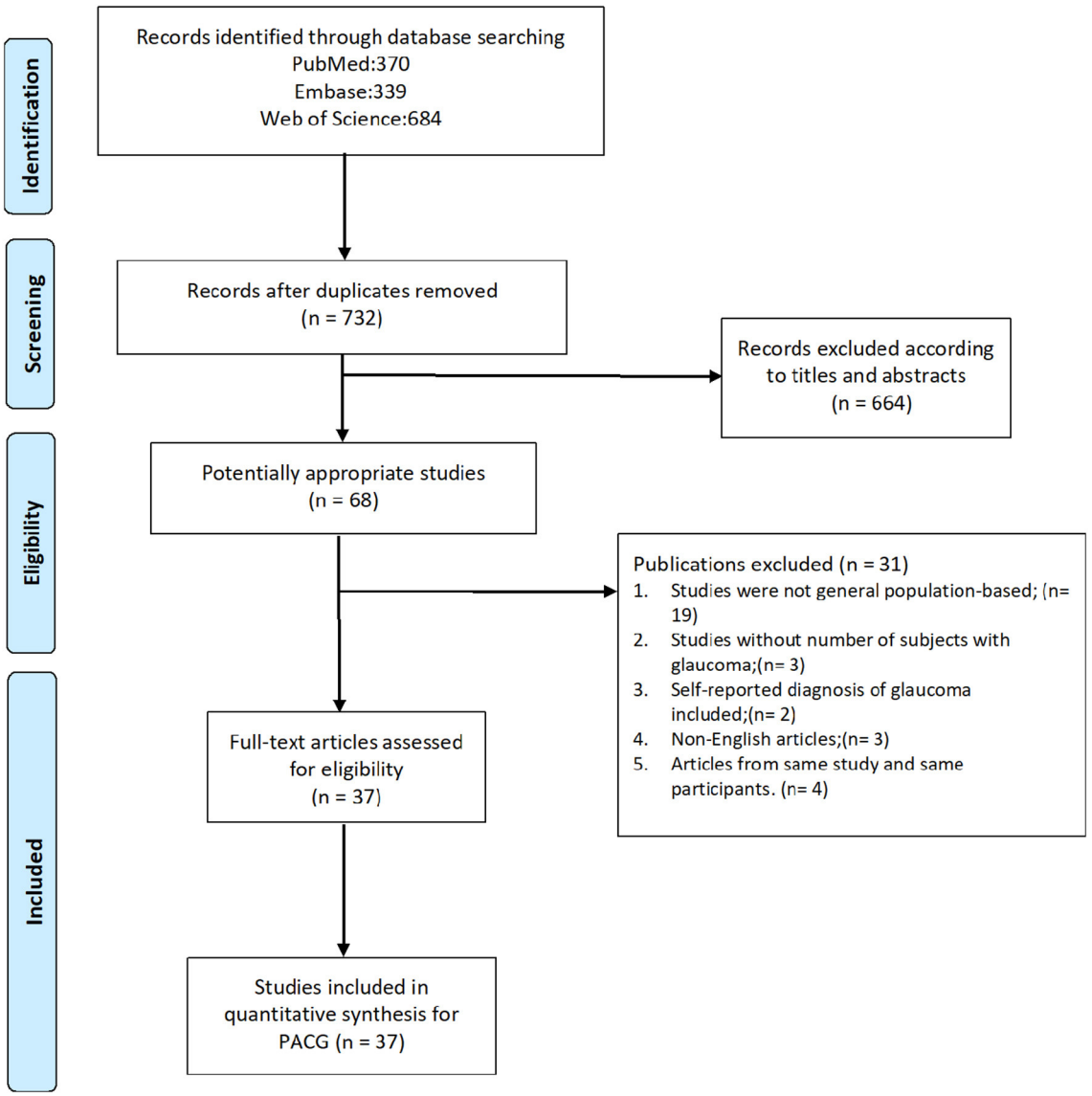

FIGURE 1 | Flow charts of search process. PACG, primary angle-closure glaucoma.

Age

Age is known to be the major risk factor for all types of glaucoma, as the prevalence increase with age (7, 60, 61). This is confirmed in this meta-analysis. Aging per decade is consistently associated with higher intraocular pressure, thinner central corneal thickness, and higher mean ocular perfusion pressure (62). For PACG pathogenesis, multiple mechanisms contributed to angle closure, including pupillary block and plateau iris, resulting in increased intraocular pressure and neurodegeneration (63). Anatomical changes could explain the increase of morbidity, and narrow anterior chamber depth (ACD) increases the risk of PACG. ACD and anterior chamber area both significantly decreased with age (−0.0119 mm/year, −0.0845 mm^2/year, $p < 0.0001$), which was caused by increment of iris cross-sectional area, iris curvature, and lens vault (64). Besides the lens becomes more compact and thicker with increasing age, proportionately large lens contributed to pupillary block and angle-crowding (65). Moreover, morphological studies have indicated that the outflow ability decreased with age and resulted in increased intraocular pressure, which was caused by the accumulation of extracellular materials in trabecular meshwork (66).

Sex

In this study, sex is found to be a significant risk factor for PACG; females are more likely to have PACG than males at all age groups (**Figures 3**, **4**). Various studies had associated shallow anterior chamber and narrow chamber angle with female sex

TABLE 1 | Results of subgroup analyses and meta-regression analyses based on age, sex, geographical location, habitation area, decades, and risk of bias.

	Subgroup analysis			Meta-regression	
	Number of estimates	Pooled estimate (95% CIs)	I^2, %	Mean difference (95% CIs)	*P*-value
All estimates	37	0.6 (0.5–0.8)	94.4		
Age range, years				Intercept = "<40"	
<40	1	0.2 (0–0.6)	-	−6.56 (−8.63 to −4.49)	<0.01
40–49	18	0.1 (0–0.3)	88.6	0.18 (−1.95 to 2.31)	0.87
50–59	21	0.5 (0.3–0.8)	85.8	1.26 (−0.85 to 3.37)	0.24
60–69	21	1.0 (0.7–1.5)	81.4	1.97 (−0.14 to 4.07)	0.07
70–79	11	1.4 (0.9–2.3)	73.2	2.25 (0.11 to 4.39)	0.04
70+	9	2.1 (1.2–3.3)	88.0	2.65 (0.50 to 4.79)	0.02
80+	10	2.8 (1.7–4.7)	25.3	2.79 (0.61 to 4.96)	0.01
Sex				Intercept = Male	
Male	26	0.8 (0.6–1.1)	90.5	−5.24 (−5.60 to −4.89)	<0.01
Female	26	0.5 (0.3–0.8)	90.8	−0.41 (−0.07 to 0.90)	0.09
Geographical location				Intercept = Africa	
Africa	5	0.4 (0.2–0.5)	46.3	−5.69 (−6.39 to −4.99)	<0.01
Asia	28	0.7 (0.6–1.0)	94.3	0.78 (0.04 to 1.53)	0.04
Europe	3	0.2 (0.1–0.6)	85.4	−0.42 (−1.53 to 0.68)	0.45
S. America	1	0.7 (0.4–1.3)	-	0.75 (−0.85 to 2.34)	0.36
Habitation area				Intercept = Urban	
Urban	9	0.7 (0.5–1.2)	90.6	−4.90 (−5.39 to −4.40)	<0.01
Rural	15	0.8 (0.5–1.2)	94.4	0.06 (−0.56 to 0.69)	0.84
Mixed or unknown	17	0.5 (0.3–0.7)	93.6	−0.39 (−1.01 to 0.22)	0.21
Decades				Intercept = 2000–2009	
2000–2009	17	0.6 (0.4–0.8)	89.5	−5.18 (−5.57 to −4.78)	<0.01
2010–2019	20	0.6 (0.4–0.9)	95.9	0.13 (−0.40 to 0.66)	0.63
Risk of bias				Intercept = Low	
Low	21	0.7 (0.5–1.0)	95.4	−4.97 (−5.31 to −4.63)	<0.01
Moderate	15	0.5 (0.3–0.7)	90.0	−0.36 (−0.88 to 0.17)	0.18
High	1	0.1 (0.7–1.3)	–	0.35 (−1.16 to 1.87)	0.65

S. America, South America.

(67–69). Moreover, females were shown to have greater ACD shallowing with aging than males (70). The mean ACD values were significantly different from men [2.59 mm (2.56; 2.62)] to women [2.42 mm (2.39; 2.44)] in elderly Chinese (older than 50 years old) (71). Such anatomical differences could contribute to the sex difference in PACG. Other factors such as endocrinologic difference and menopausal status might also be involved in sex differences for the prevalence of PACG (72).

Ethnicity and Continent

In this meta-analysis, most of the included studies (28 of 37) were conducted in Asian countries. Although the majority of the ethnicity from Asian countries are from Asia, people from other countries such as the Europeans were of mixed ethnicity. Because most of the studies lack detailed prevalence data for each ethnicity, it is not possible to perform a meta-analysis for ethnicity based on such limited information. Hence, continent differences were analyzed instead.

As we mentioned earlier, the majority of the population from Asian countries are Asians. The results from the continent of Asia may represent the prevalence of PACG for Asians (0.7%, 95% CI = 0.6–1.0%, $p < 0.01$). It is previously reported that Asians have a higher prevalence of PACG (73, 74), consistent with findings from this meta-analysis (**Table 1**; **Supplementary Figure 7**). Chan et al. reported that the PACG prevalence in Asia was 0.73% (95% CI = 0.18–1.96%) in 2013, which is similar to our results (75). They also estimated that the population with PACG would be 13.43 million (95% CI = 4.01–31.79) in 2020 and 17.51 million (95% CI = 5.21–41.37) in 2040. Our estimated PACG prevalence of Asia is slightly lower than Tham et al. (1.09%, 95% CI = 0.43–2.32%) (6), which might be due to the newly included seven studies (51–53, 55–58) conducted after the year 2012, which accounted for more than half of the Asian participants (64,380 of 110,833) in this meta-analysis. Our study provides a more up-to-date PACG prevalence. Anatomical differences might be contributed to the high prevalence of PACG in Asians. A prospective study from the United States found that

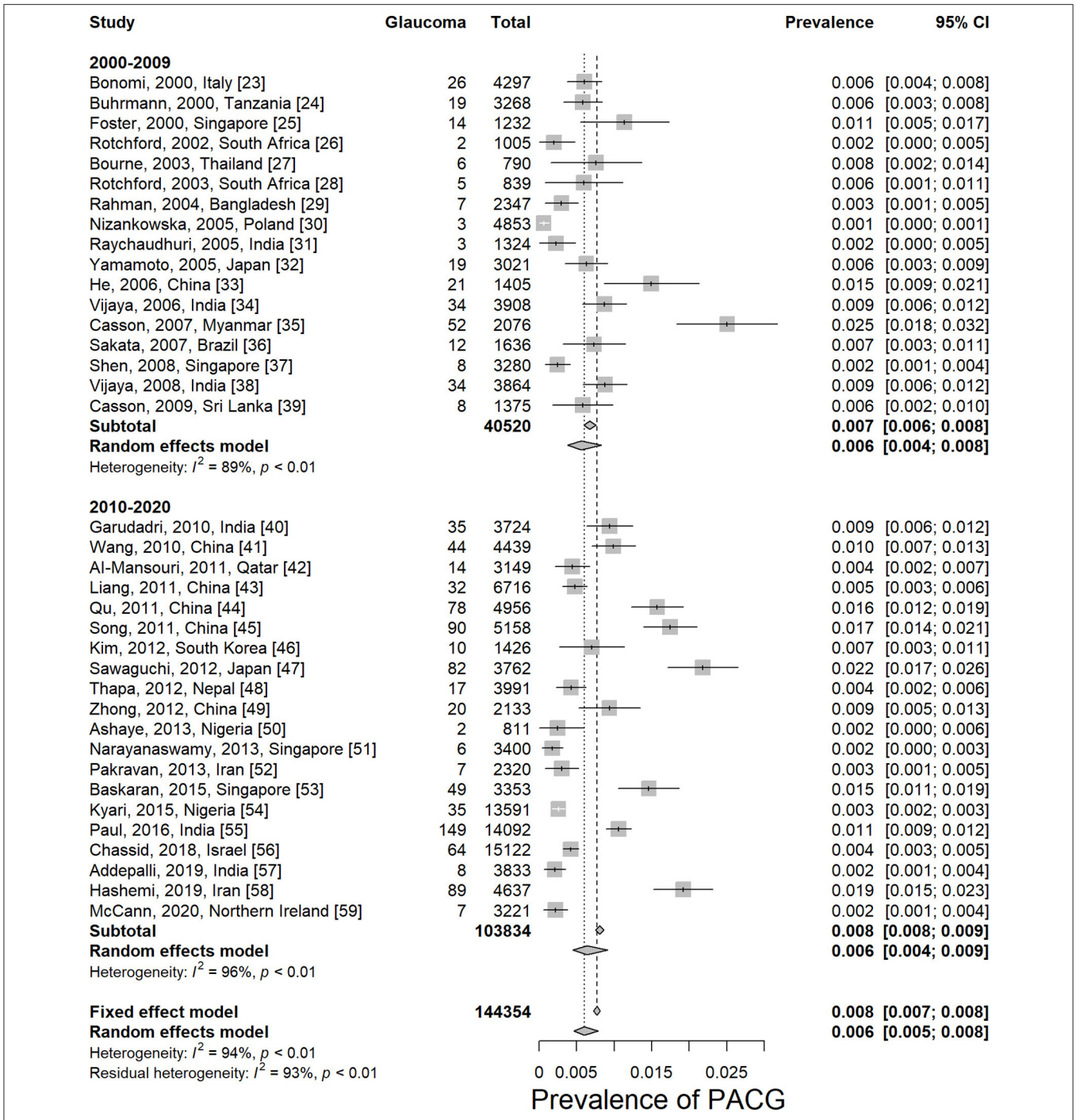

FIGURE 2 | Prevalence of primary angle-closure glaucoma worldwide by decades. PACG, primary angle-closure glaucoma.

Chinese–American people had a significantly thick iris at 750 and 2,000 μm from the scleral spurs (76). Another reported that Chinese and Hispanic subjects had the highest mean value of iris thickness at 750 μm from the scleral spurs, lowest anterior chamber area, anterior chamber volume, and anterior chamber width compared with Whites and Africans (77). The prevalence of PACG also varies in different Asian regions. South-central Asia was considered to have the highest overall glaucoma and primary open-angle glaucoma burden than other regions, whereas East Asia has a higher PACG prevalence (75).

Habitation Area

Besides sex, age, and continents, habitation area (urban or rural) was also analyzed in this study (**Supplementary Figure 8**). No statistical difference was found in the prevalence of PACG between rural and urban populations. However, this part of the

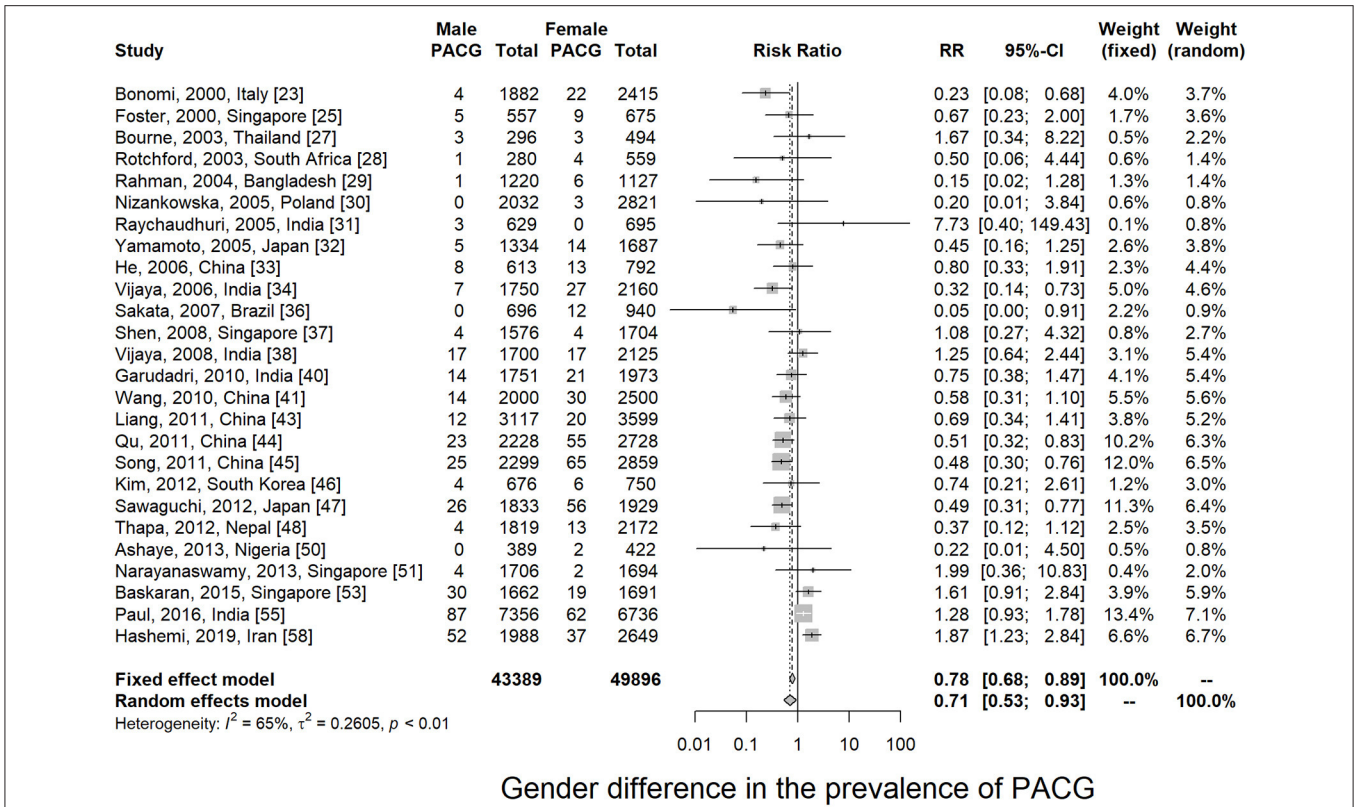

FIGURE 3 | Sex comparison of primary angle-closure glaucoma. PACG, primary angle-closure glaucoma.

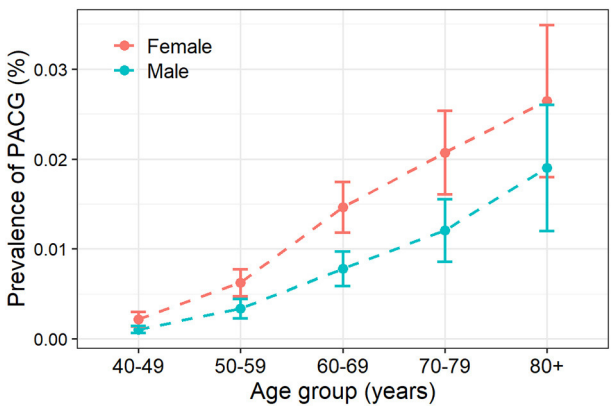

FIGURE 4 | Prevalence of primary angle-closure glaucoma increased with aging. PACG, primary angle-closure glaucoma.

TABLE 2 | Estimated global population of PACG.

Continent	Estimated PACG cases (million, 95% CI)			
	2020	2030	2040	2050
Africa	1.07 (0.53; 1.33)	1.49 (0.74; 1.86)	2.02 (1.01; 2.52)	2.71 (1.36; 3.39)
Asia	14.05 (10.54; 17.57)	15.02 (12.87; 21.45)	17.07 (14.63; 24.38)	18.47 (15.83; 26.39)
Europe	0.80 (0.40; 2.40)	0.85 (0.42; 2.54)	0.85 (0.42; 2.54)	0.83 (0.41; 2.48)
S. America	1.14 (0.65; 2.12)	2.06 (1.18; 3.84)	2.44 (1.40; 4.54)	2.73 (1.56; 5.06)
World	17.14 (14.28; 22.85)	20.73 (17.27; 27.63)	23.73 (19.78; 31.64)	26.26 (21.88; 35.01)

PACG, primary angle-closure glaucoma; S. America, South America.

analysis represents substantial bias for the following reasons: (1) The information habitation area is usually vaguely described in the majority of the studies; (2) There are only a few studies that have included both urban and rural populations in the study, and therefore, the comparison between urban and rural across studies represent ethnicity and country bias. The only study that has reported the prevalence of PACG for both habitation areas is Paul et al.'s study of the Indian population in 2016 (55). They showed that the prevalence of PACG is slightly higher in the rural (1.15%) than urban area (0.97%). However, because our meta-analysis represents bias for the reasons mentioned earlier, more evidence is needed to reveal the role of the habitation area in the risk of PACG in future studies.

Bias and Heterogeneity

The risk of bias in this meta-analysis was from the following three major aspects: the selection of participants, response

rate, and diagnostic criteria for the outcome measurement (**Supplementary Table 3**). The overall risk of bias for this study is low because low-quality studies were excluded, as mentioned in the method. In this meta-analysis, the overall heterogeneity is high ($I^2 = 94.4\%$). Commonly, a meta-analysis for prevalence studies yields very high heterogeneities, usually more than 90% of the I^2 value (22, 78–81). The impact of study quality on pooled prevalence was assessed by excluding low-quality studies and by conducting a meta-regression, comparing studies at low risk of bias with those at moderate-to-high risk. Meta-regression demonstrated little evidence of risk of bias, giving a consistent level of prevalence. It is noted that in this meta-analysis, the heterogeneity dropped dramatically in people with the age of 80+ years ($I^2 = 25.3\%$) and among studies from Africa ($I^2 = 46.3\%$, **Table 1**), indicating that the risk factors of age and geographical location are possibly the main sources of the heterogeneity.

LIMITATIONS

The major limitation of this study is that the number of studies conducted in the last 20 years varies a lot across continents, and therefore, the overall prevalence for some continents represents selection bias. There is only one study for South America (36) and three studies for Europe (23, 30, 59). The data from North America and Oceania lack in this meta-analysis.

CONCLUSION

In this meta-analysis, we reviewed 37 studies of 144,354 subjects for the prevalence of PACG in the last 20 years. Up to date, PACG is still a worldwide vision-threatening disease with high prevalence (0.6%, 95% CI = 0.5–0.8%), which is affecting about 17.14 million aged people in the world, especially in Asia (12.30 million). Asian, female sex, and aging are considered to be risk factors of PACG. Early screening in people with high risks is needed in early intervention of PACG, particularly in Asian countries.

DATA AVAILABILITY STATEMENT

The original contributions presented in the study are included in the article/**Supplementary Material**, further inquiries can be directed to the corresponding author/s.

AUTHOR CONTRIBUTIONS

NZ, JW, and BJ: research design. NZ, JW, and BC: data acquisition, research execution, and data analysis. NZ, JW, BC, YL, and BJ: manuscript preparation. All authors: contributed to the article and approved the submitted version.

FUNDING

Supported by grants from the National Science Foundation of China (82070967 and 81770930 to BJ), Natural Science Foundation of Hunan Province Grant (2020jj4788 to BJ). The sponsor or funding organization had no role in the design or conduct of this research.

SUPPLEMENTARY MATERIAL

The Supplementary Material for this article can be found online at: https://www.frontiersin.org/articles/10.3389/fmed.2020.624179/full#supplementary-material

REFERENCES

1. Jonas JB, Aung T, Bourne RR, Bron AM, Ritch R, Panda-Jonas S. Glaucoma. *Lancet.* (2017) 390:2183–93. doi: 10.1016/S0140-6736(17)31469-1
2. Gupta D, Chen PP. Glaucoma. *Am Fam Physician.* (2016) 93:668–74.
3. Almasieh M, Levin LA. Neuroprotection in glaucoma: animal models and clinical trials. *Annu Rev Vis Sci.* (2017) 3:91–120. doi: 10.1146/annurev-vision-102016-061422
4. Foster PJ. The epidemiology of primary angle closure and associated glaucomatous optic neuropathy. *Semin Ophthalmol.* (2002) 17:50–8. doi: 10.1076/soph.17.2.50.14718
5. Ang LP, Ang LP. Current understanding of the treatment and outcome of acute primary angle-closure glaucoma: an Asian perspective. *Ann Acad Med Singap.* (2008) 37:210–5.
6. Tham YC, Li X, Wong TY, Quigley HA, Aung T, Cheng CY. Global prevalence of glaucoma and projections of glaucoma burden through 2040: a systematic review and meta-analysis. *Ophthalmology.* (2014) 121:2081–90. doi: 10.1016/j.ophtha.2014.05.013
7. Unterlauft JD, Bohm MRR. Role of the aging visual system in glaucoma. *Ophthalmologe.* (2017) 114:108–13. doi: 10.1007/s00347-016-0430-6
8. Zetterberg M. Age-related eye disease and gender. *Maturitas.* (2016) 83:19–26. doi: 10.1016/j.maturitas.2015.10.005
9. Foster PJ, Buhrmann R, Quigley HA, Johnson GJ. The definition and classification of glaucoma in prevalence surveys. *Br J Ophthalmol.* (2002) 86:238–42. doi: 10.1136/bjo.86.2.238
10. Cedrone C, Mancino R, Cerulli A, Cesareo M, Nucci C. Epidemiology of primary glaucoma: prevalence, incidence, and blinding effects. *Prog Brain Res.* (2008) 173:3–14. doi: 10.1016/S0079-6123(08)01101-1
11. Moher D, Shamseer L, Clarke M, Ghersi D, Liberati A, Petticrew M, et al. Preferred reporting items for systematic review and meta-analysis protocols (PRISMA-P) 2015 statement. *Syst Rev.* (2015) 4:1. doi: 10.1186/2046-4053-4-1
12. Shamseer L, Moher D, Clarke M, Ghersi D, Liberati A, Petticrew M, et al. Preferred reporting items for systematic review and meta-analysis protocols (PRISMA-P) 2015: elaboration and explanation. *BMJ.* (2015) 350:g7647. doi: 10.1136/bmj.g7647
13. Ma Q, Su J, Li Y, Wang J, Long W, Luo M, et al. The chance of permanent cure for micro- and macroprolactinomas, medication or surgery? A systematic review and meta-analysis. *Front Endocrinol.* (2018) 9:636. doi: 10.3389/fendo.2018.00636
14. Zhang S, Wang J, Li Y, Liu Y, He L, Xia X. The role of primary intraocular lens implantation in the risk of secondary glaucoma following congenital cataract surgery: a systematic review and meta-analysis. *PLoS ONE.* (2019) 14:e0214684. doi: 10.1371/journal.pone.0214684
15. Zhang X, Wang J, Li Y, Jiang B. Diagnostic test accuracy of spot and plusoptix photoscreeners in detecting amblyogenic risk factors in children: a systemic review and meta-analysis. *Ophthalmic Physiol Opt.* (2019) 39:260–71. doi: 10.1111/opo.12628
16. Li Y, Wang J, Chen Z, Tang X. Effect of hydrophobic acrylic versus hydrophilic acrylic intraocular lens on posterior capsule opacification: meta-analysis. *PLoS ONE.* (2013) 8:e77864. doi: 10.1371/journal.pone.0077864

17. Egger M, Davey Smith G, Schneider M, Minder C. Bias in meta-analysis detected by a simple, graphical test. *BMJ.* (1997) 315:629–34. doi: 10.1136/bmj.315.7109.629
18. Sterne JA, Sutton AJ, Ioannidis JP, Terrin N, Jones DR, Lau J, et al. Recommendations for examining and interpreting funnel plot asymmetry in meta-analyses of randomised controlled trials. *BMJ.* (2011) 343:d4002. doi: 10.1136/bmj.d4002
19. Head ML, Holman L, Lanfear R, Kahn AT, Jennions MD. The extent and consequences of p-hacking in science. *PLoS Biol.* (2015) 13:e1002106. doi: 10.1371/journal.pbio.1002106
20. United Nations Population Division, Population Estimates and Projections Section *World Population Prospects: The 2019 Revision [database online]*. (2019) Available online at: http://esaunorg/wpp/
21. Hayden JA, van der Windt DA, Cartwright JL, Cote P, Bombardier C. Assessing bias in studies of prognostic factors. *Ann Intern Med.* (2013) 158:280–6. doi: 10.7326/0003-4819-158-4-201302190-00009
22. Mansfield KE, Sim J, Jordan JL, Jordan KP. A systematic review and meta-analysis of the prevalence of chronic widespread pain in the general population. *Pain.* (2016) 157:55–64. doi: 10.1097/j.pain.0000000000000314
23. Bonomi L, Marchini G, Marraffa M, Bernardi P, De Franco I, Perfetti S, et al. Epidemiology of angle-closure glaucoma: prevalence, clinical types, and association with peripheral anterior chamber depth in the Egna-Neumarket Glaucoma Study. *Ophthalmology.* (2000) 107:998–1003. doi: 10.1016/S0161-6420(00)00022-1
24. Buhrmann RR, Quigley HA, Barron Y, West SK, Oliva MS, Mmbaga BB. Prevalence of glaucoma in a rural East African population. *Invest Ophthalmol Vis Sci.* (2000) 41:40–8.
25. Foster PJ, Oen FT, Machin D, Ng TP, Devereux JG, Johnson GJ, et al. The prevalence of glaucoma in Chinese residents of Singapore: a cross-sectional population survey of the Tanjong Pagar district. *Arch Ophthalmol.* (2000) 118:1105–11. doi: 10.1001/archopht.118.8.1105
26. Rotchford AP, Johnson GJ. Glaucoma in Zulus: a population-based cross-sectional survey in a rural district in South Africa. *Arch Ophthalmol.* (2002) 120:471–8. doi: 10.1001/archopht.120.4.471
27. Bourne RR, Sukudom P, Foster PJ, Tantisevi V, Jitapunkul S, Lee PS, et al. Prevalence of glaucoma in Thailand: a population based survey in Rom Klao District, Bangkok. *Br J Ophthalmol.* (2003) 87:1069–74. doi: 10.1136/bjo.87.9.1069
28. Rotchford AP, Kirwan JF, Muller MA, Johnson GJ, Roux P. Temba glaucoma study: a population-based cross-sectional survey in urban South Africa. *Ophthalmology.* (2003) 110:376–82. doi: 10.1016/S0161-6420(02)01568-3
29. Rahman MM, Rahman N, Foster PJ, Haque Z, Zaman AU, Dineen B, et al. The prevalence of glaucoma in Bangladesh: a population based survey in Dhaka division. *Br J Ophthalmol.* (2004) 88:1493–7. doi: 10.1136/bjo.2004.043612
30. Nizankowska MH, Kaczmarek R. Prevalence of glaucoma in the wroclaw population. The wroclaw epidemiological study. *Ophthalmic Epidemiol.* (2005) 12:363–71. doi: 10.1080/09286580500212904
31. Raychaudhuri A, Lahiri SK, Bandyopadhyay M, Foster PJ, Reeves BC, Johnson GJ. A population based survey of the prevalence and types of glaucoma in rural West Bengal: the West Bengal Glaucoma Study. *Br J Ophthalmol.* (2005) 89:1559–64. doi: 10.1136/bjo.2005.074948
32. Yamamoto T, Iwase A, Araie M, Suzuki Y, Abe H, Shirato S, et al. The Tajimi Study report 2: prevalence of primary angle closure and secondary glaucoma in a Japanese population. *Ophthalmology.* (2005) 112:1661–9. doi: 10.1016/j.ophtha.2005.05.012
33. He M, Foster PJ, Ge J, Huang W, Zheng Y, Friedman DS, et al. Prevalence and clinical characteristics of glaucoma in adult Chinese: a population-based study in Liwan District, Guangzhou. *Invest Ophthalmol Vis Sci.* (2006) 47:2782–8. doi: 10.1167/iovs.06-0051
34. Vijaya L, George R, Arvind H, Baskaran M, Paul PG, Ramesh SV, et al. Prevalence of angle-closure disease in a rural southern Indian population. *Arch Ophthalmol.* (2006) 124:403–9. doi: 10.1001/archopht.124.3.403
35. Casson RJ, Newland HS, Muecke J, McGovern S, Abraham L, Shein WK, et al. Prevalence of glaucoma in rural Myanmar: the Meiktila Eye Study. *Br J Ophthalmol.* (2007) 91:710–4. doi: 10.1136/bjo.2006.107573
36. Sakata K, Sakata LM, Sakata VM, Santini C, Hopker LM, Bernardes R, et al. Prevalence of glaucoma in a South brazilian population: projeto glaucoma. *Invest Ophthalmol Vis Sci.* (2007) 48:4974–9. doi: 10.1167/iovs.07-0342
37. Shen SY, Wong TY, Foster PJ, Loo JL, Rosman M, Loon SC, et al. The prevalence and types of glaucoma in malay people: the Singapore Malay eye study. *Invest Ophthalmol Vis Sci.* (2008) 49:3846–51. doi: 10.1167/iovs.08-1759
38. Vijaya L, George R, Arvind H, Baskaran M, Ve Ramesh S, Raju P, et al. Prevalence of primary angle-closure disease in an urban south Indian population and comparison with a rural population. The Chennai Glaucoma Study. *Ophthalmology.* (2008) 115:655–60 e651. doi: 10.1016/j.ophtha.2007.05.034
39. Casson RJ, Baker M, Edussuriya K, Senaratne T, Selva D, Sennanayake S. Prevalence and determinants of angle closure in central Sri Lanka: the Kandy eye study. *Ophthalmology.* (2009) 116:1444–9. doi: 10.1016/j.ophtha.2009.03.005
40. Garudadri C, Senthil S, Khanna RC, Sannapaneni K, Rao HB. Prevalence and risk factors for primary glaucomas in adult urban and rural populations in the Andhra Pradesh eye disease study. *Ophthalmology.* (2010) 117:1352–9. doi: 10.1016/j.ophtha.2009.11.006
41. Wang YX, Xu L, Yang H, Jonas JB. Prevalence of glaucoma in North China: the Beijing Eye Study. *Am J Ophthalmol.* (2010) 150:917–24. doi: 10.1016/j.ajo.2010.06.037
42. Al-Mansouri FA, Kanaan A, Gamra H, Khandekar R, Hashim SP, Al Qahtani O, et al. Prevalence and determinants of glaucoma in citizens of qatar aged 40 years or older: a community-based survey. *Middle East Afr J Ophthalmol.* (2011) 18:141–9. doi: 10.4103/0974-9233.80703
43. Liang Y, Friedman DS, Zhou Q, Yang XH, Sun LP, Guo L, et al. Prevalence and characteristics of primary angle-closure diseases in a rural adult Chinese population: the Handan Eye Study. *Invest Ophthalmol Vis Sci.* (2011) 52:8672–9. doi: 10.1167/iovs.11-7480
44. Qu W, Li Y, Song W, Zhou X, Kang Y, Yan L, et al. Prevalence and risk factors for angle-closure disease in a rural Northeast China population: a population-based survey in Bin County, Harbin. *Acta Ophthalmol.* (2011) 89:e515–20. doi: 10.1111/j.1755-3768.2011.02146.x
45. Song W, Shan L, Cheng F, Fan P, Zhang L, Qu W, et al. Prevalence of glaucoma in a rural northern china adult population: a population-based survey in kailu county, inner mongolia. *Ophthalmology.* (2011) 118:1982–8. doi: 10.1016/j.ophtha.2011.02.050
46. Kim YY, Lee JH, Ahn MD, Kim CY, Namil Study Group KGS. Angle closure in the Namil study in central South Korea. *Arch Ophthalmol.* (2012) 130:1177–83. doi: 10.1001/archophthalmol.2012.1470
47. Sawaguchi S, Sakai H, Iwase A, Yamamoto T, Abe H, Tomita G, et al. Prevalence of primary angle closure and primary angle-closure glaucoma in a southwestern rural population of Japan: the Kumejima Study. *Ophthalmology.* (2012) 119:1134–42. doi: 10.1016/j.ophtha.2011.12.038
48. Thapa SS, Paudyal I, Khanal S, Twyana SN, Paudyal G, Gurung R, et al. A population-based survey of the prevalence and types of glaucoma in Nepal: the Bhaktapur glaucoma study. *Ophthalmology.* (2012) 119:759–64. doi: 10.1016/j.ophtha.2011.10.021
49. Zhong H, Li J, Li C, Wei T, Cha X, Cai N, et al. The prevalence of glaucoma in adult rural Chinese populations of the Bai nationality in Dali: the Yunnan minority eye study. *Invest Ophthalmol Vis Sci.* (2012) 53:3221–5. doi: 10.1167/iovs.11-9306
50. Ashaye A, Ashaolu O, Komolafe O, Ajayi BG, Olawoye O, Olusanya B, et al. Prevalence and types of glaucoma among an indigenous African population in southwestern Nigeria. *Invest Ophthalmol Vis Sci.* (2013) 54:7410–6. doi: 10.1167/iovs.13-12698
51. Narayanaswamy A, Baskaran M, Zheng Y, Lavanya R, Wu R, Wong WL, et al. The prevalence and types of glaucoma in an urban Indian population: the Singapore Indian eye study. *Invest Ophthalmol Vis Sci.* (2013) 54:4621–7. doi: 10.1167/iovs.13-11950
52. Pakravan M, Yazdani S, Javadi MA, Amini H, Behroozi Z, Ziaei H, et al. A population-based survey of the prevalence and types of glaucoma in central Iran: the Yazd eye study. *Ophthalmology.* (2013) 120:1977–84. doi: 10.1016/j.ophtha.2013.02.029
53. Baskaran M, Foo RC, Cheng CY, Narayanaswamy AK, Zheng YF, Wu R, et al. The prevalence and types of glaucoma in an Urban Chinese population: the Singapore Chinese eye study. *JAMA Ophthalmol.* (2015) 133:874–80. doi: 10.1001/jamaophthalmol.2015.1110
54. Kyari F, Entekume G, Rabiu M, Spry P, Wormald R, Nolan W, et al. A population-based survey of the prevalence and types of glaucoma in Nigeria:

results from the Nigeria National Blindness and Visual Impairment Survey. *BMC Ophthalmol.* (2015) 15:176. doi: 10.1186/s12886-015-0160-6
55. Paul C, Sengupta S, Choudhury S, Banerjee S, Sleath BL. Prevalence of glaucoma in Eastern India: the Hooghly River Glaucoma Study. *Indian J Ophthalmol.* (2016) 64:578–83. doi: 10.4103/0301-4738.191497
56. Chassid O, Epstein I, Sharabi-Nov A, Pikkel J. Prevalence of glaucoma in the Israeli Arab population. *Int J Ophthalmol.* (2018) 11:163–5. doi: 10.18240/ijo.2018.01.25
57. Addepalli UK, Jonnadula GB, Garudadri CS, Khanna RC, Papas EB. Prevalence of primary glaucoma as diagnosed by study optometrists of l. v. prasad eye institute - glaucoma epidemiology and molecular genetics study. *Ophthalmic Epidemiol.* (2019) 26:150–4. doi: 10.1080/09286586.2018.1551961
58. Hashemi H, Mohammadi M, Zandvakil N, Khabazkhoob M, Emamian MH, Shariati M, et al. Prevalence and risk factors of glaucoma in an adult population from Shahroud, Iran. *J Curr Ophthalmol.* (2019) 31:366–72. doi: 10.1016/j.joco.2018.05.003
59. McCann P, Hogg R, Wright DM, Pose-Bazarra S, Chakravarthy U, Peto T, et al. Glaucoma in the Northern Ireland Cohort for the Longitudinal Study of Ageing (NICOLA): cohort profile, prevalence, awareness and associations. *Br J Ophthalmol.* (2020) 104:1492–9. doi: 10.1136/bjophthalmol-2019-315330
60. Casson RJ, Marshall D, Newland HS, McGovern S, Muecke J, Tan EW, et al. Risk factors for early angle-closure disease in a Burmese population: the Meiktila Eye Study. *Eye.* (2009) 23:933–9. doi: 10.1038/eye.2008.102
61. Leske MC, Wu SY, Hennis A, Honkanen R, Nemesure B, Group BES. Risk factors for incident open-angle glaucoma: the Barbados Eye Studies. *Ophthalmology.* (2008) 115:85–93. doi: 10.1016/j.ophtha.2007.03.017
62. Coleman AL, Miglior S. Risk factors for glaucoma onset and progression. *Surv Ophthalmol.* (2008) 53(Suppl. 1):S3–10. doi: 10.1016/j.survophthal.2008.08.006
63. Sun X, Dai Y, Chen Y, Yu DY, Cringle SJ, Chen J, et al. Primary angle closure glaucoma: what we know and what we don't know. *Prog Retin Eye Res.* (2017) 57:26–45. doi: 10.1016/j.preteyeres.2016.12.003
64. Sun JH, Sung KR, Yun SC, Cheon MH, Tchah HW, Kim MJ, et al. Factors associated with anterior chamber narrowing with age: an optical coherence tomography study. *Invest Ophthalmol Vis Sci.* (2012) 53:2607–10. doi: 10.1167/iovs.11-9359
65. Tarongoy P, Ho CL, Walton DS. Angle-closure glaucoma: the role of the lens in the pathogenesis, prevention, and treatment. *Surv Ophthalmol.* (2009) 54:211–25. doi: 10.1016/j.survophthal.2008.12.002
66. Gabelt BT, Kaufman PL. Changes in aqueous humor dynamics with age and glaucoma. *Prog Retin Eye Res.* (2005) 24:612–37. doi: 10.1016/j.preteyeres.2004.10.003
67. Xu L, Cao WF, Wang YX, Chen CX, Jonas JB. Anterior chamber depth and chamber angle and their associations with ocular and general parameters: the Beijing Eye Study. *Am J Ophthalmol.* (2008) 145:929–36. doi: 10.1016/j.ajo.2008.01.004
68. Nongpiur ME, Sakata LM, Friedman DS, He M, Chan YH, Lavanya R, et al. Novel association of smaller anterior chamber width with angle closure in Singaporeans. *Ophthalmology.* (2010) 117:1967–73. doi: 10.1016/j.ophtha.2010.02.007
69. Congdon NG, Foster PJ, Wamsley S, Gutmark J, Nolan W, Seah SK, et al. Biometric gonioscopy and the effects of age, race, and sex on the anterior chamber angle. *Br J Ophthalmol.* (2002) 86:18–22. doi: 10.1136/bjo.86.1.18
70. Phu J, Tong J, Zangerl B, Le JL, Kalloniatis M. Cluster analysis reveals patterns of age-related change in anterior chamber depth for gender and ethnicity: clinical implications. *Ophthalmic Physiol Opt.* (2020) 40:632–49. doi: 10.1111/opo.12714
71. He M, Huang W, Zheng Y, Alsbirk PH, Foster PJ. Anterior chamber depth in elderly Chinese: the Liwan eye study. *Ophthalmology.* (2008) 115:1286–90:1290 e1281–1282. doi: 10.1016/j.ophtha.2007.12.003
72. Vajaranant TS, Grossardt BR, Maki PM, Pasquale LR, Sit AJ, Shuster LT, et al. Risk of glaucoma after early bilateral oophorectomy. *Menopause.* (2014) 21:391–8. doi: 10.1097/GME.0b013e31829fd081
73. Wright C, Tawfik MA, Waisbourd M, Katz LJ. Primary angle-closure glaucoma: an update. *Acta Ophthalmol.* (2016) 94:217–25. doi: 10.1111/aos.12784
74. Cheng JW, Zong Y, Zeng YY, Wei RL. The prevalence of primary angle closure glaucoma in adult Asians: a systematic review and meta-analysis. *PLoS ONE.* (2014) 9:e103222. doi: 10.1371/journal.pone.0103222
75. Chan EW, Li X, Tham YC, Liao J, Wong TY, Aung T, et al. Glaucoma in Asia: regional prevalence variations and future projections. *Br J Ophthalmol.* (2016) 100:78–85. doi: 10.1136/bjophthalmol-2014-306102
76. Lee RY, Huang G, Porco TC, Chen YC, He M, Lin SC. Differences in iris thickness among African Americans, Caucasian Americans, Hispanic Americans, Chinese Americans, and Filipino-Americans. *J Glaucoma.* (2013) 22:673–8. doi: 10.1097/IJG.0b013e318264ba68
77. Lee RY, Chon BH, Lin SC, He M, Lin SC. Association of ocular conditions with narrow angles in different ethnicities. *Am J Ophthalmol.* (2015) 160:506–15 e501. doi: 10.1016/j.ajo.2015.06.002
78. Assefa A, Bihon A. A systematic review and meta-analysis of prevalence of Escherichia coli in foods of animal origin in Ethiopia. *Heliyon.* (2018) 4:e00716. doi: 10.1016/j.heliyon.2018.e00716
79. Li R, Li W, Lun Z, Zhang H, Sun Z, Kanu JS, et al. Prevalence of metabolic syndrome in Mainland China: a meta-analysis of published studies. *BMC Public Health.* (2016) 16:296. doi: 10.1186/s12889-016-2870-y
80. Bacigalupo I, Mayer F, Lacorte E, Di Pucchio A, Marzolini F, Canevelli M, et al. A systematic review and meta-analysis on the prevalence of dementia in Europe: estimates from the highest-quality studies adopting the DSM IV Diagnostic Criteria. *J Alzheimers Dis.* (2018) 66:1471–81. doi: 10.3233/JAD-180416
81. Navarro P, Arias A, Arias-Gonzalez L, Laserna-Mendieta EJ, Ruiz-Ponce M, Lucendo AJ. Systematic review with meta-analysis: the growing incidence and prevalence of eosinophilic oesophagitis in children and adults in population-based studies. *Aliment Pharmacol Ther.* (2019) 49:1116–25. doi: 10.1111/apt.15231

Conflict of Interest: The authors declare that the research was conducted in the absence of any commercial or financial relationships that could be construed as a potential conflict of interest.

frontiers in Medicine

ORIGINAL RESEARCH
published: 26 February 2021
doi: 10.3389/fmed.2021.649971

Comparison of the Humphrey Field Analyzer and Photopic Negative Response of Focal Macular Electroretinograms in the Evaluation of the Relationship Between Macula Structure and Function

Kazuyuki Hirooka, Kenji Yokoyama, Kana Tokumo and Yoshiaki Kiuchi*

Department of Ophthalmology and Visual Science, Graduate School of Biomedical Sciences, Hiroshima University, Hiroshima, Japan

OPEN ACCESS

Edited by:
Michele Lanza, University of Campania Luigi Vanvitelli, Italy

Reviewed by:
Teresa Rolle, Università di Torino, Italy
Luigi Di Perna, University of Campania Luigi Vanvitelli, Italy

***Correspondence:**
Kazuyuki Hirooka
khirooka9@gmail.com

Specialty section:
This article was submitted to Ophthalmology, a section of the journal Frontiers in Medicine

Received: *06 January 2021*
Accepted: *08 February 2021*
Published: *26 February 2021*

Citation:
Hirooka K, Yokoyama K, Tokumo K and Kiuchi Y (2021) Comparison of the Humphrey Field Analyzer and Photopic Negative Response of Focal Macular Electroretinograms in the Evaluation of the Relationship Between Macula Structure and Function. Front. Med. 8:649971. doi: 10.3389/fmed.2021.649971

Purpose: To investigate the association between macular inner retinal layer thickness and macula visual field (VF) mean deviation as measured by the Humphrey Field Analyzer (HFA) or macular function as measured by focal macular electroretinograms (ERGs) in patients with glaucoma.

Methods: The participants in this cross-sectional study were 71 patients with glaucoma and 10 healthy controls. Macular inner retinal layer thickness and function were measured in all participants using optical coherence tomography (OCT) and HFA or focal macular ERGs, respectively. Macular OCT images were segmented into the macular retinal nerve fiber layer (mRNFL), macular ganglion cell layer/inner plexiform layer (GCL/IPL), and ganglion cell complex (GCC). Spearman correlation analysis was used to assess the relationship between macular inner retinal layer thickness and function.

Results: Focal macular ERGs were composed of a negative wave (N1), a positive wave (P1), and a slow negative wave (N2). The N2 response density was significantly reduced in eyes with glaucoma, and was significantly associated with the thickness of the mRNFL ($R = 0.317$), GCL/IPL ($R = 0.372$), or GCC ($R = 0.367$). The observed structure–function relationship was also significantly correlated with the HFA VF mean deviation for each thickness [mRNFL ($R = 0.728$), GCL/IPL ($R = 0.603$), or GCC ($R = 0.754$)].

Conclusions: Although a significant correlation was found between the N2 response density and the thickness of the macular inner layer, the observed structure–function relationship with the mean deviation of the HFA VF was higher than that of the N2 response density.

Keywords: visual field, optical coherance tomography, electroretinogram (ERG), glaucoma, structure-function

INTRODUCTION

Glaucoma is a group of ocular diseases known to be characterized by retinal ganglion cell (RGC) soma and axon loss (1, 2). As about 50% of the RGCs are within 4.5 mm of the foveal center (3), measuring macular RGC function could be useful for diagnosing glaucoma or predicting disease progression. Some studies investigated the relationship between local sensitivity loss on 10-2 visual field (VF) loss and macular ganglion cell/inner plexiform layer (GCL/IPL) thickness (4–7). Clarifying the relationship between macular GCL/IPL thickness and central visual function could help clinicians gain a better understanding of how to detect glaucomatous damage at the early stage and disease progression. The Humphrey Field Analyzer (HFA; Carl Zeiss Meditec, Dublin, CA) has been confirmed to have high test–retest variability, with fixation errors being one of the major factors (8).

The photopic negative response (PhNR), which originates from the activity of RGCs and their axons (9), is a negative wave that follows the photopic b-wave. Increasing evidence has shown that the PhNR can be useful in evaluating the functional condition of neurons in patients with glaucoma (10, 11). The amplitude of the focal PhNR has been shown to be significantly correlated with a reduction in both visual sensitivity as determined by standard automated perimetry (SAP) (11) and retinal nerve fiber layer (RNFL) thickness (10) in patients with glaucoma. The PhNR recorded from the macular area can be used to assess the function of associated RGCs (12). The PhNR recorded using multifocal electroretinograms (mfERGs) with pseudorandom sequence stimulation has been found to be reduced in patients with glaucoma compared with controls, and this reduction in multifocal PhNR (mfPhNR) amplitude was correlated with disease severity (13). Due to recent improvements in the mfERG technique, the pupil does not need to be dilated before recording the mfPhNR.

To improve the ability to detect the presence and progression of glaucomatous damage, numerous studies have applied spectral-domain optical coherence tomography (OCT) to examine the association between structural and functional damage. Given this background, the present study aimed to compare macular function measurements made by the HFA and focal macular PhNR, and to assess whether any potential relationships exist between these measurements and the thickness of the macular inner retinal layer.

MATERIALS AND METHODS

Patients

This cross-sectional study was carried out at Hiroshima University Hospital. The participants were all patients examined between November 2019 and August 2020. Before the study began, in accordance with the principles outlined in the Declaration of Helsinki, all participants were given a detailed explanation of the study purpose and methods and then asked to provide written informed consent. This study was approved by the Institutional Review Board of the Hiroshima University Faculty of Medicine.

First, all participants underwent a complete ophthalmic examination, which included visual acuity testing with refraction, intraocular pressure, gonioscopy, and a dilated fundus examination with stereoscopic biomicroscopy of the optic nerve head using indirect ophthalmoscopy and a slit lamp. Participants with a best-corrected visual acuity of $\geq$20/25, a spherical error within a range of +4.0 and −6.0 diopters, a cylinder within ± 2.0 diopters, an axial length <26 mm, and open angles (grades 3 and 4 according to the Shaffer grading

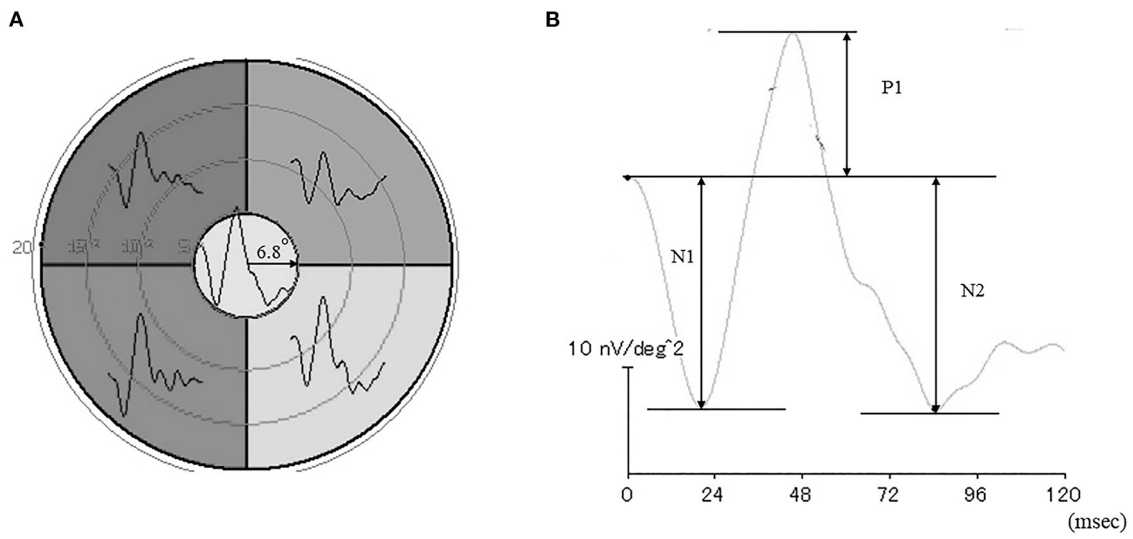

FIGURE 1 | Stimulus patterns used to elicit the multifocal electroretinograms (mfERGs) **(A)**. Representative waveforms of the mfERGs recorded from five retinal loci. **(B)** Focal electroretinogram.

system) were included in the analysis. An optical biometer (IOLMaster, Carl Zeiss Meditec) was used to acquire axial length. Participants with a history of retinal pathology or neurologic disease or who had undergone a retinal laser procedure or either retinal or intraocular surgery were excluded. If both eyes met the inclusion criteria, the right eye was assessed. Control subjects were required to have an intraocular pressure $\leq$21 mmHg and a normal VF. All included eyes had to show the following structural glaucomatous changes to meet the definition of glaucoma: a vertical cup-disc asymmetry of $\geq$0.2 between the eyes, a cup-to-disc ratio of $\geq$0.6, neuroretinal rim narrowing, notches, localized pallor, or RNFL defects with glaucomatous VF loss in the corresponding hemifield. To meet the definition of glaucomatous VF, the participant had to have undergone a glaucoma hemifield test outside of the normal limits in a minimum of two consecutive baseline tests, with at least three contiguous test points within the same hemifield on a pattern deviation plot at $P < 1\%$ and at least one contiguous test point at $P < 0.5\%$, after excluding test points that were on the edge of the field or directly above and below the blind spot.

Measurement of Macular Inner Retinal Layer Thickness

Raster scanning [scan density of 512 (vertical) × 128 (horizontal) scans] of a 7 mm^2 area centered on the fovea was performed using a high-resolution fundus camera (Topcon 3D OCT-2000; Topcon, Inc., Tokyo, Japan). The built-in protocol measured a 6 × 6-mm area centered on the fovea using embedded software. The data were divided into 10 × 10 grids and exported by the Topcon software. Then, the mean thickness of the macular retinal nerve fiber layer (mRNFL), GCL/IPL, and ganglion cell complex (GCC), which consists of the mRNFL and GCL/IPL, were calculated. Images with a quality factor < 30 were excluded from the analysis.

Visual Sensitivity of the 10-2 HFA

Visual sensitivity was examined using static automated white-on-white threshold perimetry (HFA; 10-2 Swedish Interactive Threshold Algorithm Standard test). The VF results were considered reliable when the fixation losses and false-positive/false-negative rates were <20%. The subsequent analyses use only reliable test data.

mfERG Recordings

As described in a previous study on mfERG recordings (13) and shown in **Figure 1A**, stimuli consisting of five stimulus elements were generated on a cathode-ray tube monitor (VERIS? 7, Electro-Diagnostic Imaging, San Mateo, CA). mfERGs were elicited by a circular stimulus with a 6.8° radius centered on the fovea and a quarter of an annulus placed around the macula, with the radius of the outer border of the annulus set to 20°. White (200 cd/mm^2) or black (4 cd/mm^2) elements were presented in a pseudorandom binary m-sequence at a frequency of 6.25 Hz, with a steady background of 100 cd/m^2 surrounding the stimulus field.

A Burian-Allen bipolar contact lens electrode (Hansen Ophthalmic Laboratories, Coralville, IA) was placed on the cornea following corneal anesthesia. A chloride silver electrode as the ground electrode was placed on the left ear lobe. All responses were digitally band-pass filtered between 3 and 30 Hz. VERIS software (VERIS Science 4.1.1; Maya, Nagoya, Japan) was used to analyzed the mfERGs. The local retinal responses from the five different retinal loci were averaged to obtain the all-trace waveforms of the first-order kernels (**Figure 1A**) The response density of focal ERGs in the center area were evaluated as a macular function.

The N1 and P1 amplitudes were measured from the baseline to the trough of the first negative response and the peak of the following positive wave, respectively, and the N2 amplitude was measured from the baseline to the following trough (**Figure 1B**). The focal ERG amplitudes were expressed as response density (nV/deg^2), which represents the amplitude as a function of the stimulus area.

Statistical Analysis

For continuous variables, variance equality was assessed using Levene's test. Based on the results obtained, a Student's *t*-test or Welch's test was used to assess differences between the control and glaucoma groups. The chi-square test for categorical parameters was used to assess differences between the control and glaucoma groups. Spearman rank order correlations were used to examine the correlation between mRNFL, GCL/IPL, and GCC thickness and VF mean deviation or N2 response density, and tests of equality of dependent correlation coefficients were used to evaluate comparisons of the strength of the structure–function association. All statistical values are presented as means

TABLE 1 | Clinical characteristics of the study population.

	Glaucoma ($n = 71$)	Normal ($n = 10$)	*P*-value
Age (y)	71.0 ± 1.5	68.2 ± 3.9	0.50
Gender (M/F)	39/32	6/4	0.76
Diagnosis			
POAG	46		
NTG	8		
EG	17		
Refraction (D)	−1.3 ± 0.2	−0.3 ± 0.6	0.13
Axial length (mm)	24.0 ± 0.1	23.5 ± 0.3	0.046

M, male; F, female; POAG, primary open-angle glaucoma; NTG, normal-tension glaucoma; EG, exfoliation glaucoma; D, diopter.

TABLE 2 | Macular inner retinal layer thickness and function.

	Glaucoma	Normal	*P*-value
GCC thickness (μm)	71.7 ± 1.2	101.0 ± 3.2	<0.001[a]
GCL/IPL thickness (μm)	51.6 ± 0.6	63.4 ± 1.5	<0.001[a]
mRNFL thickness (μm)	20.2 ± 0.9	37.8 ± 2.3	<0.001[b]
MD of 10-2 (dB)	14.01 ± 0.87	1.06 ± 2.31	<0.001[b]
N2 response density (nV/deg^2)	7.52 ± 0.76	14.14 ± 2.04	0.003[a]

GCC, ganglion cell complex; GCL, ganglion cell layer; IPL, inner plexiforma layer; mRNFL, macular retinal nerve fiber layer; MD, mean deviation.
[a] *Student's t-test.*
[b] *Welch test.*

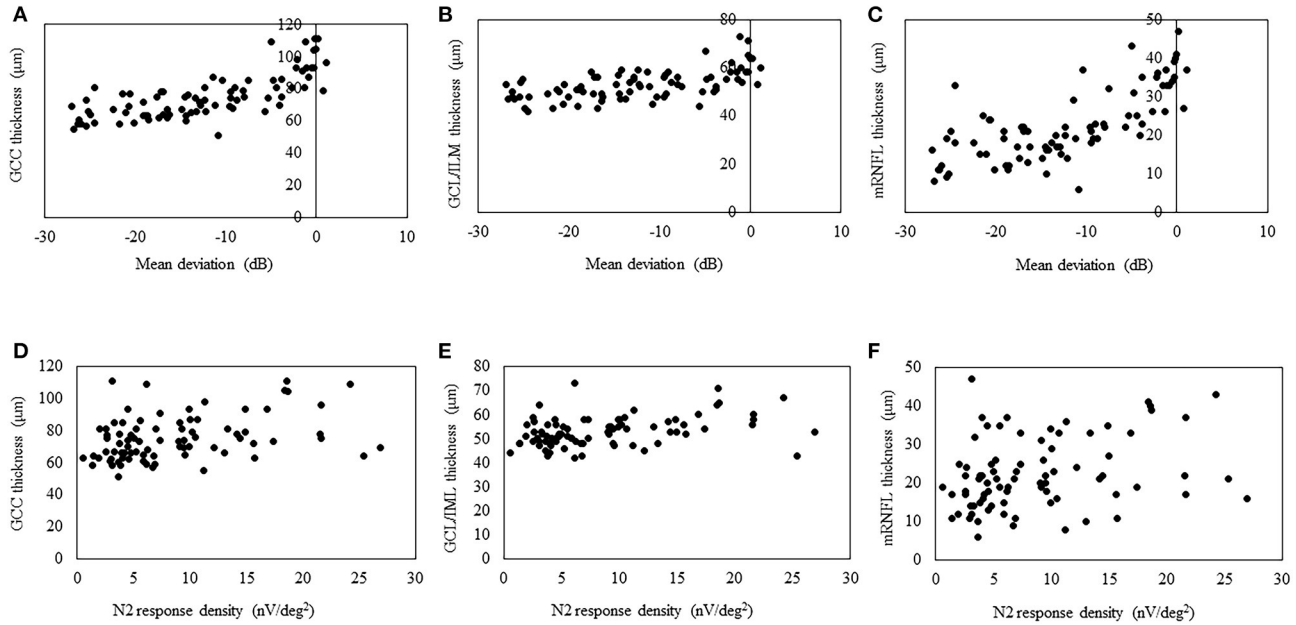

FIGURE 2 | Scatterplots showing the association between the 3D OCT-2000 thickness parameters and the corresponding retinal sensitivity (decibels) measured by the Humphrey Field Analyzer or center N2 response density. Association between the average thickness of the ganglion cell complex (GCC) **(A)**, macular ganglion cell layer/inner plexiform layer (GCL/IPL) **(B)**, or macular retinal nerve fiber layer (mRNFL) **(C)** and macular mean deviation. Association between the average thickness of the GCC **(D)**, GCL/IPL **(E)**, or mRNFL **(F)** and the center N2 response.

± standard deviations (SDs), with $P < 0.05$ considered to be statistically significant. JMP software (version 15; SAS Inc., Cary, NC) was used for all statistical analyses.

RESULTS

Demographic Characteristics

The demographic characteristics of the 71 patients with glaucoma and 10 healthy controls who participated in the study are shown in **Table 1**. Disease grade in the glaucomatous eyes of the 71 patients, which was based on the standard VF severity grading scale (14), ranged from early to moderate, with 13 (18.3%), 17 (23.9%), and 41 (57.7%) eyes classified as early, moderate, and severe, respectively.

Comparison of the Normal and Glaucoma Groups

A significant difference in mRNFL, GCL/IPL, or GCC thickness was observed between the glaucoma and healthy control groups, as shown in **Table 2**. The mean deviation was significantly lower in the glaucomatous than in the healthy eyes, and the N2 response density was significantly reduced in the glaucomatous eyes, as shown in **Table 2**.

Correlation Between Macular Inner Layer Thickness and Mean Sensitivity and N2 Response Density

The structure–function relationship was evaluated based on the mRNFL, GCL/IPL, or GCC thickness and VF mean deviation or N2 response density (**Figure 2** and **Table 3**). In each mRNFL, GCL/IPL, or GCC thickness, the structure–function relationship observed HFA VF mean deviation was higher than those of N2 response density. The Spearman correlation coefficient was the highest (0.754) for the GCC thickness-HFA VF mean sensitivity measurements. **Table 4** shows the structure–function relationship in each glaucoma type.

TABLE 3 | Comparison of the strength of the structure-function relationship between the Humphrey Field Analyzer and focal electroretinograms.

	Statistic	HFA	Focal ERG	*P*-value
GCC	Correlation coefficient	0.754	0.367	<0.001
	95% bootstrapped CI	0.625–0.826	0.172–0.550	
GCL/IPL	Correlation coefficient	0.603	0.372	0.06
	95% bootstrapped CI	0.444–0.727	0.155–0.537	
mRNFL	Correlation coefficient	0.728	0.317	<0.001
	95% bootstrapped CI	0.599–0.813	0.089–0.488	

HFA, humphrey field analyzer; ERG, electroretinogram; CI, confidence interval; GCC, ganglion cell complex; GCL, ganglion cell layer; IPL, inner plexiform layer; mRNFL, macular retinal nerve fiber layer.

DISCUSSION

The retina contains about 1.07 million RGCs on average, approximately half of which are located within 4.5 mm of the foveal center (3, 15). During the early stages of glaucoma, RGC

TABLE 4 | Comparison of the strength of structure-function relationship between Humphrey Field Analyzer and multifocal electroretinogram in each glaucoma type.

		POAG ($n = 46$)		NTG ($n = 8$)		EG ($n = 17$)	
	Statistic	**HFA**	**Focal ERG**	**HFA**	**Focal ERG**	**HFA**	**Focal ERG**
GCC	Correlation coefficient	0.783	0.367	0.715	0.336	0.676	0.486
	95% bootstrapped CI	0.661–0.864	0.087–0.538	0.270–0.908	0.263–0.749	0.405–0.838	0.138–0.727
GCL/IPL	Correlation coefficient	0.614	0.313	0.514	0.319	0.615	0.491
	95% bootstrapped CI	0.429–0.750	0.067–0.524	0.051–0.830	0.281–0.740	0.314–0.803	0.144–0.703
mRNFL	Correlation coefficient	0.782	0.299	0.799	0.347	0.659	0.457
	95% bootstrapped CI	0.661–0.864	0.052–0.513	0.444–0.938	0.252–0.754	0.380–0.829	0.102–0.709

POAG, primary open-angle glaucoma; NTG, normal-tension glaucoma; EG, exfoliation glaucoma; HFA, humphrey field analyzer; ERG, electroretinogram; CI, confidence interval; GCC, ganglion cell complex; GCL, ganglion cell layer; IPL, inner plexiform layer; mRNFL, macular retinal nerve fiber layer.

loss is evident around the fovea (16), which highlights the importance of assessing the central macular structure–function relationship. The N2 component of mfERGs recorded from the central area represents the RGC activity in the corresponding macular area (13).

Structure–Function Relationship of Glaucomatous Damage

Some researchers have recently reported on the diagnostic performance of mfERG in glaucoma patients (17, 18) or an animal model of glaucoma (19). The combination of mfERG and OCT improved diagnostic performance and monitoring of disease progression (17). By analyzing the mfPhNR/b-wave ratio, Al-Nosairy et al. (18) achieved the best performance for discriminating between controls and glaucoma suspects. The diagnostic performance and structure–function relationship were strongest for mfERG when compared with full-field flash ERG PhNR or pattern-reversal ERG in an experimental animal model of glaucoma (19). A combined approach using structural and functional assessment of glaucomatous retinal damage offers great promise for uncovering the interrelationship between the different components of ocular damage in glaucoma.

Correlation Between Macular Inner Layer Thickness and N2 Response Density

The high test–retest variability of SAP is often explained by poor patient vigilance and inattention in subjective examinations. By contrast, measurements of mfPhNR amplitude tend to show better test–retest reliability because of this is an objective test (20). Therefore, we hypothesized that the structure–function relationship for the observed N2 response would be higher than that for the HFA VA mean deviation. Although a significant correlation was found between N2 response density and macular inner layer thickness in this study, the structure–function relationship for the observed HFA VF mean deviation was higher than that for the N2 response density. Macular focal ERGs were elicited by a circular stimulus with a 6.8° radius centered on the fovea. The built-in protocol measured a 6 × 6-mm area centered on the fovea corresponding to a 20° square of the retina in the macular area. The 3D-OCT used in this study and the 10-2 HFA measure similar macular areas (the 10-2 HFA analyzes 68 data points located within a central arc of 10°). Therefore, we assume that the results may be affected by the measurement area of each instrument. Moreover, the N2 may not represent the neural activity of RGCs only. In rodents, the PhNR has been shown to be affected by the neural activity of amacrine cells (21, 22).

In the present study, although a significant correlation was observed between the N2 response density and GCC thickness, the correlation coefficient was lower than that in a previous study ($R = 0.363$ vs. 0.575, respectively) (13), in which SD-OCT (RS-3000 Advance; Nidek Co., Ltd.) was used to obtain the GCC thickness. It is therefore difficult to compare the strength of the structure–function relationship in this study with that in their study because it can be affected by sample size, disease severity, and OCT instruments.

Limitations

This study did have some limitations. First, the present study did not include any patients with preperimetric glaucoma; such patients should be examined and compared with regard to the structure–function relationship in a future study. Second, although we observed no obvious differences in the structure–function relationship among patients with primary open-angle, normal tension, or exfoliation glaucoma, the sample size was small. Therefore, a large number of subjects will need to be closely examined for each glaucoma type in a future study.

CONCLUSIONS

The results of this study revealed that the N2 response density was affected by glaucoma in the central macular area. In addition, a significant correlation was found between the N2 amplitude and macular inner layer thickness; however, this correlation was weaker than that between the macular inner layer thickness and HFA VF mean deviation.

DATA AVAILABILITY STATEMENT

The datasets presented in this study can be found in online repositories. The names of the repository/repositories and accession number(s) can be found in the article/supplementary material.

ETHICS STATEMENT

The studies involving human participants were reviewed and approved by Institutional Review Board of the Hiroshima University Faculty of Medicine. The patients/participants provided their written informed consent to participate in this study.

AUTHOR CONTRIBUTIONS

KH: conception of design of the work acquisition, analysis, and interpretation of the data final approval of the version to be published and agreement to be accountable for all aspects of the work in ensuring that questions related to the accuracy and integrity of any part of the work are appropriately investigated and resolved. KY: acquisition of the data final approval of the version to be published and agreement to be accountable for all aspects of the work in ensuring that questions related to the accuracy and integrity of any part of the work are appropriately investigated and resolved. KT: acquisition of the data final approval of the version to be published and agreement to be accountable for all aspects of the work in ensuring that questions related to the accuracy and integrity of any part of the work are appropriately investigated and resolved. YK: final approval of the version to be published and agreement to be accountable for all aspects of the work in ensuring that questions related to the accuracy and integrity of any part of the work are appropriately investigated and resolved. All authors contributed to the article and approved the submitted version.

FUNDING

This work was supported by a Grant-in-Aid for Scientific Research from the Ministry of Education, Culture, Sports, Science, and Technology of Japan (20K09827).

ACKNOWLEDGMENTS

We thank Forte Science Communications, Inc., for editing the draft of this manuscript.

REFERENCES

1. Danias J, Shen F, Kavalarakis M, Chen B, Goldblum D, Lee K, et al. Characterization of retinal damage in the episcleral vein cauterization rat glaucoma model. *Exp Eye Res.* (2006) 82:219–28. doi: 10.1016/j.exer.2005.06.013
2. Soto I, Pease ME, Son JL, Shi X, Quigley HA, Marsh-Armstrong N. Retinal ganglion cell loss in a rat ocular hypertension model is sectional and involves early optic nerve axon loss. *Invest Ophthalmol Vis Sci.* (2011) 52:434–41. doi: 10.1167/iovs.10-5856
3. Curcio CA, Allen KA. Topography of ganglion cells in human retina. *J Comp Neurol.* (1990) 300:5–25. doi: 10.1002/cne.903000103
4. Raza AS, Cho J, de Moraes CG, Wang M, Zhang X, Kardon RH, et al. Retinal ganglion cell layer thickness and local visual field sensitivity in glaucoma. *Arch Ophthalmol.* (2011) 129:1529–36. doi: 10.1001/archophthalmol.2011.352
5. Ohkubo S, Higashide T, Udagawa S, Sugiyama K, Hangai M, Yoshimura N, et al. Focal relationship between structure and function within the central 10 degrees in glaucoma. *Invest Ophthalmol Vis Sci.* (2014) 55:5269–77. doi: 10.1167/iovs.14-14153
6. Hirooka K, Misaki K, Nitta E, Ukegawa K, Sato S, Tsujikawa A. Comparison of macular integrity assessment (MAIA^{TM}), MP-3, and the humphrey field analyzer in the evaluation of the relationship between the structure and function of the macula. *PLoS ONE.* (2016) 11:e0151000. doi: 10.1371/journal.pone.0151000
7. Lee JW, Morales E, Sharifipour F, Amini N, Yu F, Afifi AA, et al. The relationship between central visual field sensitivity and macular ganglion cell/inner plexiform layer thickness in glaucoma. *Br J Ophthalmol.* (2017) 101:1052–8. doi: 10.1136/bjophthalmol-2016-309208
8. Maddess T. Modeling the relative influence of fixation and sampling errors on retest variability in perimetry. *Graefes Arch Clin Exp Ophthalmol.* (2014) 252:1611–9. doi: 10.1007/s00417-014-2751
9. Viswanathan S, Frishman LJ, Robson JG, Harwerth RS, Smith EL III. The photopic negative response of the macaque electroretinogram: reduction by experimental glaucoma. *Invest Ophthalmol Vis Sci.* (1999) 40:1124–36.
10. Machida S, Toba Y, Ohtaki A, Gotoh Y, Kaneko M, Kurosaka D. Photopic negative response of focal electroretinograms in glaucomatous eyes. *Invest Ophthalmol Vis Sci.* (2008) 49:5636–44. doi: 10.1167/iovs.08-1946
11. Tamada K, Machida S, Oikawa T, Yokoyama D, Kaneko M, Kurosaka D. Correlation between photopic negative response of focal electroretinograms and local loss of retinal neurons in glaucoma. *Curr Eye Res.* (2010) 35:155–64. doi: 10.3109/02713680903447926
12. Machida S, Tamada K, Oikawa T, Yokoyama D, Kaneko M, Kurosaka D. Sensitivity and specificity of photopic negative response of focal electroretinogram to detect glaucomatous eyes. *Br J Ophthalmol.* (2010) 94:202–8. doi: 10.1136/bjo.2009.161166
13. Kaneko M, Machida S, Hoshi Y, Kurosaka D. Alterations of photopic negative response of multifocal electroretinogram in patients with glaucoma. *Curr Eye Res.* (2015) 40:77–86. doi: 10.3109/02713683.2014.915575
14. Hodapp E, Parrish RK II, Anderson DR. *Clinical Detection in Glaucoma*. St. Louise, MO: Mosby (1993).
15. Wässle H, Grünert U, Röhrenbeck J, Boycott BB. Retinal ganglion cell density and cortical magnification factor in the primate. *Vision Res.* (1990) 30:1897–911. doi: 10.1016/0042-6989(90)90166-i
16. Quigley HA, Dunkelberger GR, Green WR. Retinal ganglion cell atrophy correlated with automated perimetry in human eyes with glaucoma. *Am J Ophthalmol.* (1989) 107:453–64. doi: 10.1016/0002-9394(89)90488-1
17. Al-Nosairy KO, Prabhakaran GT, Pappelis K, Thieme H, Hoffmann MB. Damage with electroretinography and optical coherence tomography/angiogeaphy. *Trans Vis Sci Tech.* (2020) 9:7. doi: 10.1167//tvst.9.12.7
18. Al-Nosairy KO, Thieme H, Hoffmann MB. Diagnostic performance of multifocal photopic negative responses, pattern electroretinogram and optical coherence tomography in glaucoma. *Exp Eye Res.* (2020) 200:108242. doi: 10.1016/j.exer.2020.108242
19. Wilsey L, Gowrisankaran S, Cull G, Hardin C, Burgoyne CF, Fortune B. Comparing three different modes of electroretinography in experimental glaucoma: diagnostic performance and correlation to structure. *Doc Ophthalmol.* (2017) 134:111–28. doi: 10.1007//s10633-017-9578-x
20. Van Alstine AW, Viswanathan S. Test-retest reliability of the multifocal photopic negative response. *Doc Ophthalmol.* (2017) 134:25–36. doi: 10.1007/s10633-016-9569-3
21. Bui BV, Fortune B. Ganglion cell contributions to the rat full-field electroretinogram. *J Physiol.* (2004) 555:153–73. doi: 10.1113/jphysiol.2003.052738
22. Machida S, Raz-Prag D, Fariss RN, Sieving PA, Bush RA. Photopic ERG negative response from amacrine

cell signaling in RCS rat retinal degeneration. *Invest Ophthalmol Vis Sci.* (2008) 49:442–52. doi: 10.1167/iovs.07-0291

Conflict of Interest: The authors declare that the research was conducted in the absence of any commercial or financial relationships that could be construed as a potential conflict of interest.

frontiers in Medicine

ORIGINAL RESEARCH
published: 22 March 2021
doi: 10.3389/fmed.2021.643402

Evaluation of the Effectiveness of a Chronic Ocular Hypertension Mouse Model Induced by Intracameral Injection of Cross-Linking Hydrogel

Junjue Chen[1†], *Jun Sun*[1†], *Huan Yu*[1], *Ping Huang*[2*] *and Yisheng Zhong*[1*]

[1] *Department of Ophthalmology, Rujin Hospital, Shanghai Jiao Tong University School of Medicine, Shanghai, China,*
[2] *Shanghai Key Laboratory for Bone and Joint Diseases, Shanghai Institute of Traumatology and Orthopedics, Rujin Hospital Affiliated Medical School, Shanghai Jiaotong University, Shanghai, China*

OPEN ACCESS

Edited by:
Michele Lanza, University of Campania Luigi Vanvitelli, Italy

Reviewed by:
Sabrina Reinehr, Ruhr-University Bochum, Germany
Kin-Sang CHO, Schepens Eye Research Institute, United States
Ana I. Ramírez, Complutense University of Madrid, Spain

***Correspondence:**
Yisheng Zhong
yszhong68@126.com
Ping Huang
pinghpingh@126.com

[†]*These authors have contributed equally to this work and share first authorship*

Specialty section:
This article was submitted to Ophthalmology, a section of the journal Frontiers in Medicine

Received: *18 December 2020*
Accepted: *10 February 2021*
Published: *22 March 2021*

Citation:
Chen J, Sun J, Yu H, Huang P and Zhong Y (2021) Evaluation of the Effectiveness of a Chronic Ocular Hypertension Mouse Model Induced by Intracameral Injection of Cross-Linking Hydrogel. Front. Med. 8:643402. doi: 10.3389/fmed.2021.643402

Background: Glaucoma is an irreversible and blinding neurodegenerative disease that is characterized by progressive loss of retinal ganglion cells. The current animal models of glaucoma fail to provide a chronic elevated intraocular pressure and cannot maintain the optical media clarity for a long time, which brings some difficulties to the study of glaucoma. Here, we developed a new chronic ocular hypertension model of mice induced by cross-linking hydrogel intracameral injection.

Methods: C57BL/6J mice aged 6–8 weeks were randomly divided into the control group and the operation group. The mice of the operation group were injected with cross-linking hydrogel to induce ocular hypertension. Intraocular pressure was measured preoperatively, 3 days after surgery, and weekly until the end of the study. Flash visual evoked potential (F-VEP) was used to observe optic nerve function at different times (preoperatively and 2, 4, and 6 weeks) after chronic ocular hypertension (COH). Retinal TNF-α, IL-1β, and IL-17A protein expression were measured by western blotting in the control group and in mice at 2, 4, and 6 weeks after COH. Microglial cell activation was evaluated by immunofluorescence staining and western blotting. Apoptosis and loss of retinal ganglion cells after 2, 4, and 6 weeks of intracameral injection of cross-linking hydrogel were observed by the TUNEL assay and Brn3a protein labeling. The loss of optic nerve axons in COH mice was evaluated by neurofilament heavy polypeptide protein labeling.

Results: Intracameral injection of the cross-linking hydrogel induces increased intraocular pressure (IOP) to a mean value of 19.3 ± 4.1 mmHg, which was sustained for at least 8 weeks. A significant difference in IOP was noted between COH mice and sham-operation mice ($p < 0.0001$). The success rate was 75%. The average amplitude of F-VEP in mice with COH was reduced ($p = 0.0149$, 0.0012, and 0.0009 at 2, 4, and 6 weeks after COH vs. the control group, respectively), and the average latent period in mice with COH was longer ($p = 0.0290$, <0.0001, and <0.0001 at 2, 4, and 6 weeks after COH vs. the control group, respectively) compared with that in the control group. TNF-α, IL-1β, IL-17A, Iba-1, and CD68 protein expression increased in COH mice. During the processing of COH, the number of microglial cells increased along

with cellular morphological changes of rounder bodies and thicker processes compared with the control group. Apoptosis of retinal ganglion cells (RGCs) was clearly observed in mice at 2, 4, and 6 weeks after COH ($p = 0.0061$, 0.0012, <0.0001, and 0.0371 at 2, 4, and 6 weeks after COH vs. the control group, respectively). The RGC density decreased significantly in the COH mice compared with the control group ($p = 0.0042$, 0.0036, and <0.0001 at 2, 4, and 6 weeks after COH vs. the control group, respectively). There was a significant loss of optic nerve axons in mice after intracameral injection of cross-linking hydrogel ($p = 0.0095$, 0.0002, and <0.0001 at 2, 4, and 6 weeks after COH vs. the control group, respectively).

Conclusions: A single intracameral injection of cross-linking hydrogel can effectively induce chronic ocular hypertension in mice, which causes progressive loss of retinal ganglion cells, increased expression levels of inflammatory cytokines and microglial cell activation, and deterioration of optic nerve function.

Keywords: glaucoma, animal model, mice, cross-linking hydrogel, intracameral injection

INTRODUCTION

Glaucoma, a leading cause of irreversible blindness, is characterized by retinal ganglion cell (RGC) death and axonal damage of the optic nerve (1). Glaucoma affects an estimated 64.3 million people between the ages of 40 and 80 worldwide and is expected to reach 111.8 million by 2040 (2). The pathogenesis of glaucoma has not been elucidated, and the elevated intraocular pressure (IOP) is thought to be a major risk factor (3). However, progressive RGC loss, optic axon injury, and visual field defects are still present in glaucoma patients with normal IOP. This finding suggests that mechanisms other than stress-mediated neurodegenerative injury exist (4). A growing body of literature, particularly from a variety of animal models, suggests that neuroinflammation (often considered to be an immune response associated with the central nervous system) is a key process in glaucoma (5). Retinal microglial cells are one of the main cells involved in immune inflammation in the retina and optic nerve. Microglial cells in the optic nerve head are activated in the early stages of glaucoma. In the case of retinal and optic nerve injury, microglial cells can be rapidly activated to play a beneficial neuroprotective role, but overactivation of microglial cells can lead to damage of the nerve tissue by releasing a series of toxic substances. Simultaneously, activated microglia can deliver antigens to activated T cells in the retina and optic nerve and participate in T-cell-mediated neuroprotective immunity and immunopathological damage (6, 7). However, the specific roles of neuroinflammation and microglia in the development of glaucoma have not been completely elucidated.

Therefore, effective animal models are needed for further study of glaucoma. To date, there are some established animal models of glaucoma, including spontaneous ocular hypertension animal models and induced ocular hypertension animal models. Among the animal models of hereditary glaucoma, the DBA/2J mouse is a commonly used animal model for glaucoma research. However, this model of persistent injury develops slowly, and severe injuries are typically observed at 9 months of age (8). The animal models of induced ocular hypertension include the microbead occlusion glaucoma model, the laser-induced glaucoma model, the optic nerve axotomy model, and the scleral cauterization glaucoma model (9–11). An ideal model of experimental glaucoma should be able to preserve optical media clarity and exhibit chronic, progressive loss of RGCs (12). In addition, the operation is simple, and the cost is reasonable. However, many of the existing models of experimental glaucoma fall short of demonstrating these attributes.

In this study, we used a new method to establish a model of experimental glaucoma—a single cross-linked hydrogel intracameral injection—to induce elevated IOP in mice. The increase in IOP in this model was stable and sustained for at least 8 weeks, leading to the loss of RGCs, increased expression levels of inflammatory cytokines and microglial cell activation, and deterioration of optic nerve function in mice. Our model has the characteristics of strong operability.

MATERIALS AND METHODS

Animals

Six- to 8-week-old male C57BL/6J mice (Charles River Laboratories, Shanghai, China) were used in this study. All animal experimental protocols were approved by Ruijin Hospital, Shanghai Jiao Tong University School of Medicine Animal Care and Use Committee. All animal procedures in this study adhered to the National Institutes of Health (NIH) guidelines for the Care and Use of Laboratory Animals and the Association for Research in Vision and Ophthalmology (ARVO) statement for the Use of Animals in Ophthalmic and Vision Research. All mice were fed *ad libitum*, and the environment was maintained at approximately 21°C with a 12-h light and 12-h dark cycle. The number of animals used in the experimental procedures is listed in **Table 1**.

Surgical Induction of the Glaucoma Model

Chronic ocular hypertension (COH) was induced in the right eyes of mice. To avoid potential inflammatory reactions caused by contralateral COH eyes, the left eye was not considered the control eye (13). Mice were anesthetized by intraperitoneal administration of 80 mg/kg ketamine hydrochloride (Sigma-Aldrich, St. Louis, MO, USA) and 16 mg/kg xylazine (Sigma-Aldrich, St. Louis, MO, USA). Topical anesthesia was delivered to the ocular surface by a drop of 0.5% proparacaine hydrochloride (Bausch & Lomb, Tampa, FL, USA). Before injection, an *in situ* cross-linking hydrogel (Sigma-Aldrich, St. Louis, MO, USA) was mixed. The cross-linking hydrogel consisted of a thiol-modified carboxymethyl hyaluronic acid (HyStem) and a thiol-reactive polyethylene glycol diacrylate (Extralink). Both substances were dissolved in degassed water according to the manufacturer's instructions and shaken in a 37°C thermostat water bath for 2 h before mixing. Anterior chamber puncture is performed from the peripheral area of the cornea to the center with a 31-gauge needle to form a sufficiently long tunnel incision. Then, the premixed hydrogel was immediately injected into the anterior chamber through the incision with a Hamilton syringe (Hamilton Bonaduz AG, Switzerland). The cross-linking hydrogel was mixed at a ratio of 4:1 immediately before the injection and occurred *in situ* for approximately 5 min in the anterior chamber. A total of 3 μl of the mixture including 2.4 μl HyStem and 0.6 μl Extralink was aspirated by a pulled glass micropipette needle and injected into the anterior chamber targeted at the anterior chamber angle (**Figure 1**). Sham operations were performed on the right eyes of other mice to be used as the control group. Briefly, an equivalent volume of phosphate buffered saline (PBS) was injected into the anterior chamber, and other procedures were the same as described for COH induction.

IOP measurements were performed as previously described (14). Briefly, IOP was measured using a rebound tonometer (TonoLab, Vantaa, Finland) under brief systemic anesthesia by isoflurane inhalation (2–4%) immediately preoperation and 3 days postoperation and weekly until the end point of the experimental period. All IOP measurements were obtained between 10 a.m. and 2 p.m., and the average of six readings was calculated for each IOP measurement.

TABLE 1 | Number of mice used in separate procedures.

Procedure	*N* (Mice)
Intracameral injections for model building and IOP profile	90
Immunofluorescence staining	54
VEP test	24
Western blot	20

Quantification of RGCs and Microglial Cells in Retinal Whole Mounts

Mice were anesthetized and perfused in sequence with saline and 4% paraformaldehyde (PFA) transcardially. The right eyes were enucleated and further fixed in 4% PFA for 1 h at 4°C. Whole retinas were isolated and placed in cold 0.3% Triton X-100 for 30 min and blocked in 10% donkey serum (Jackson ImmunoResearch Laboratories, West Grove, PA, USA) containing 1% bovine serum albumin and 0.05% Tween-20 (Sigma-Aldrich, St. Louis, MO, USA) at room temperature for 1 h. The whole retinas were incubated with rabbit polyclonal anti-Brn3a (1:100 dilution, ab53025; Abcam, Cambridge, UK) primary antibodies for RGCs and rabbit monoclonal anti-Iba-1 (1:500 dilution, ab178846; Abcam, Cambridge, UK) primary antibodies for microglial cells at 4°C overnight. Visualization of immunoreactive proteins was enabled by incubation with goat anti-rabbit secondary antibody (1:1,000 dilution; Thermo Fisher Scientific, Waltham, MA, USA). Immunofluorescence images were scanned and captured with a confocal laser-scanning microscope (LSM 510 META; Zeiss, Jena, Germany). The number of RGCs and microglial cells was measured in areas of approximately the same distances of 1/6, 3/6, and 5/6 retinal radius from the optic disc in each quadrant (each piece of the retina was calculated four times at each distance, the magnification was ×200). A digital image analysis system is used for automatic analysis and counting (Image-Pro Plus Version 6.0, Media Cybernetics, Silver Spring, MD, USA). The average RGC

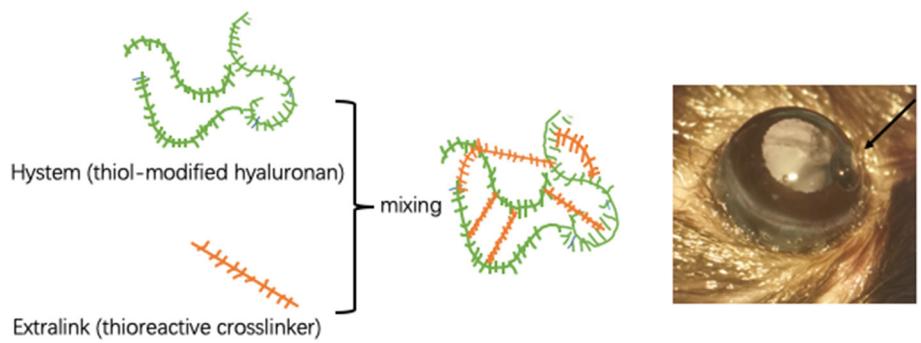

FIGURE 1 | Intracameral injection of cross-linking hydrogel. Schematic diagram of cross-linking hydrogels. The proportion of HyStem and Extralink is 4:1. The hydrogel is injected into the anterior chamber to form solidified gel droplets at the anterior chamber angle.

and microglial cell densities were considered the mean density of RGCs and microglial cells for a certain position in each retina.

Immunofluorescence Staining

Mice were anesthetized and transcardially perfused with saline and 4% PFA. The right eyes and optic nerves were dissected and further fixed in 4% PFA at 4°C overnight, and then cryoprotection was achieved with gradient concentrations of sucrose solutions (the concentration gradients of sucrose solution were 20, 30, and 40%). The eyecups and optic nerves were embedded in optimum cutting temperature compound (Sakura Finetek, Torrance, CA, USA) and frozen. The retinas were nasotemporally sectioned around the optic disc into slices 12 μm thick using a Leica microtome (CM1950, Wetzlar, Germany) and mounted on gelatin-coated slides. The optic nerve cross-sections (12-μm) were cut with a cryostat (CM1950, Leica, Wetzlar, Germany) and mounted on gelatin-coated slides. Slices were permeated with cold 0.3% Triton X-100 for 30 min and blocked in 10% donkey serum (Jackson ImmunoResearch Laboratories, West Grove, PA, USA) containing 1% bovine serum albumin and 0.05% Tween-20 (Sigma-Aldrich, St. Louis, MO, USA) at room temperature for 1 h. The retinal slices were incubated with rabbit polyclonal anti-Brn3a (1:100 dilution, ab53025; Abcam, Cambridge, UK) primary antibodies, and the optic nerves slices were incubated with rabbit monoclonal anti-neurofilament heavy polypeptide (1:100 dilution, ab207176; Abcam, Cambridge, UK) primary antibodies at 4°C overnight. Visualization of immunoreactive proteins was enabled by incubation with goat anti-rabbit secondary antibody (1:1,000 dilution; Thermo Scientific, Waltham, MA, USA). For RGCs, nuclear DNA fragmentation of apoptotic cells was evaluated using the terminal deoxynucleotidyl transferase-mediated deoxyuridine triphosphate nick end labeling (TUNEL) method, employing an *in situ* Cell Death Detection Kit (Roche Diagnostics Corporation, Indianapolis, IN, USA). The procedures followed the manufacturer's instructions. Briefly, after incubation with goat anti-rabbit secondary antibody, the slices were incubated with 50 μl of TUNEL reaction agent, containing 5 μl of enzyme solution and 45 μl of label solution, in a humidified incubator for 1 h at 37°C. Finally, the nuclear was mounted with a ProLong Antifade medium combined with 4′,6-diamidino-2-phenylindole (DAPI; Life Technologies, Waltham, MA, USA). The fluorescence images were scanned and captured with a confocal laser-scanning microscope (LSM 510 META; Zeiss, Jena, Germany). Quantitative analysis of fluorescence density was performed according to a previous study (14, 15). Briefly, for retinal slices, three randomly selected nonoverlapping subranges of 300 μm within a 1-mm distance from the optic disc margin of each unilateral side were outlined for a total of six subranges for each slice. Then, the mean optical density of immunoreactive fluorescence staining was measured within distinct areas. The numbers of Brn3a-positive cells and double-staining-positive cells within the ganglion cell layer (GCL) were counted; thus, the proportion of TUNEL-positive neurons in the GCL was obtained. Finally, for each staining target, 18 values obtained from one eye were expressed as an average for individual mice. For optic nerves, five sections per slide and three images per optic nerve were captured. Images were converted into gray scales and the background was subtracted. Then, the lower and upper threshold values were determined for each image. Finally, a digital image analysis system was used to calculate the average fluorescence intensity of the selected area. All the image analysis work was performed with the help of a digital image analysis system (Image-Pro Plus Version 6.0, Media Cybernetics, Silver Spring, MD, USA).

Flash Visual Evoked Potential

The flash visual evoked potential (F-VEP) test (UTAS-E3000LKC, Multi-focal Visual Diagnostic Test System, IKC Technologies, Gaithersburg, MD, USA) was performed in mice preoperatively and 2, 4, and 6 weeks postoperatively. The method was performed according to the standards of the International Clinical Electrophysiology of Vision (16). The silver needle electrode was used with an impedance of 2k. Using a full-field Ganzfeld flash stimulator, the stimulated light intensity was 3.12 cd s^{-1} m^{-2}. The magnification was 20,000 times. The low frequency was 0.1 Hz and the high frequency was 300 Hz. The single stimulus mode was adopted, and the stimulus frequency was 1.0 Hz. The analysis time was 250 ms, and the waveform was superposed 100 times. The mice were anesthetized and dilated with tropicamide. The mice were placed on a homemade mouse fixation device. The recording electrode was placed under the occipital tuberosity scalp. The reference electrode was placed under the nose, and the ground electrode was placed under the mastoid process. After the electrodes were placed, the mice underwent dark adaptation for 15 min. When one eye was examined, the opaque black blindfold completely covered the opposite eye. F-VEP inspection was performed using the two-channel recording method and measured at least thrice consecutively.

Western Blotting Analysis

The COH mice were sacrificed by cervical dislocation, and the retinas were collected immediately and homogenized. Total protein content was extracted from the homogenate using radioimmunoprecipitation assay buffer (RIPA; Sigma-Aldrich, St. Louis, MO, USA) with a protease inhibitor cocktail (Sigma-Aldrich, St. Louis, MO, USA). Retinal tissue ($n = 2$/group) was homogenized in 100 μl RIPA containing a protease inhibitor cocktail on ice for 1 h. Subsequently, all samples were centrifuged at 15,000×g at 4°C for 15 min, and the supernatant was applied to determine the protein concentration. The protein concentrations were measured using the Bicinchoninic Acid Kit (Beyotime, Shanghai, China) (the protein concentration was 3 μg/μl). Briefly, 5× SDS buffer was added to each protein sample (4:1) and denaturized at 100°C for 10 min. Equal amounts of protein samples were separated by electrophoresis in a Mini-Protean three electrophoresis system (Bio-Rad, Hercules, CA, USA) with sodium dodecyl sulfate polyacrylamide gel. Then, proteins were electroblotted to polyvinylidene fluoride membranes in a Mini Trans-Blot electrophoretic transfer system (Bio-Rad, Hercules, CA, USA). The membranes were blocked with 5% skimmed milk at room temperature for 2 h and subsequently incubated with rabbit polyclonal anti-actin (1:5,000

dilution; ab179467; Abcam, Cambridge, UK), mouse monoclonal anti-TNF-α (1:1,000 dilution; ab1793; Abcam, Cambridge, UK), rabbit polyclonal anti-IL-1β (1:1,000; ab9722; Abcam, Cambridge, UK), rabbit monoclonal anti-Iba-1 (1:1,000 dilution; ab178846; Abcam, Cambridge, UK), rabbit monoclonal anti-IL-17A (1:1,000 dilution; ab79056; Abcam, Cambridge, UK), and mouse monoclonal anti-CD68 (1:200 dilution; ab201340; Abcam, Cambridge, UK) primary antibodies at 4°C overnight. The membranes were then washed sufficiently with Tris-buffered saline with Tween and incubated with horseradish peroxidase-conjugated goat anti-rabbit (1:1,000 dilution; Abcam, Cambridge, UK) and goat anti-mouse (1:1,000 dilution; Abcam, Cambridge, UK) secondary antibodies at room temperature for 1 h according to the sources of primary antibodies. The protein bands on the membranes were visualized with a chemofluorescence reagent (Beyotime, Shanghai, China) under an ImageQuant LAS 4000 mini system (GE Healthcare Bio-Sciences, Piscataway, NJ, USA). Gray values of the images were analyzed semiquantitatively with Image-Pro Plus Version 6.0 software (Media Cybernetics, Silver Spring, MD, USA).

Statistical Methods

Statistical analyses were performed using SPSS software (19.0 IBM Corporation, Armonk, NY, USA). First, the normal distribution of the data was tested. Then the data were analyzed using two-tailed independent-samples *t* test and one-way ANOVA followed by Tukey's *post hoc* test. These tests were used to evaluate statistical significance. $p < 0.05$ indicated that the difference was statistically significant.

RESULTS

Longitudinal Profile of IOP Elevation

Mice were randomly assigned for anterior chamber injection. Fifty-four eyes exhibited elevated IOP after intracameral injection of cross-linking hydrogel and the success rate was 68% (54/80). A total of 80 mice were injected with cross-linking hydrogel. However, eight of them showed postoperative opacity of refractive media, so these eight mice were not counted. The success rate of mice with clear refractive media was 75% (54/72). There were no adverse effects in the anterior chamber after intracameral injection (such as endophthalmitis, keratitis, corneal neovascularization, corneal opacities, incision leakage, cataracts, and ulceration). There were 82 mice which consist of 10 mice of the control group and 72 mice of the COH group during the process of the whole experimental period. In order to reduce the statistical error, 6 mice in the control group and 18 mice in the hydrogel injection group were used for the value of IOP analysis. The preoperative IOP was similar between the hydrogel-injected eyes and the control group (9.5 ± 1.0 and 9.8 ± 0.9 mmHg, $p = 0.4994$). The mean IOP of the hydrogel-injected eyes and the control group was 19.3 ± 4.1 and 9.5 ± 0.8 mmHg, respectively (this value is the average of 240 IOP measurements in the entire experimental period, $p < 0.0001$). In the operation group, IOP decreased slowly from the first measurement, remained relatively stable at the third week after the operation, and was sustained for at least 8 weeks compared with the control group. The difference between the hydrogel-injected eyes and the control group appeared significant at every time point after the intracameral injection (**Table 2**). The above results suggested that the injection of cross-linking hydrogel can induce IOP elevation successfully (**Figure 2**).

TABLE 2 | Summary of IOP measurements preoperation and postoperation in mice.

Time		Group ($n = 24$)	IOP (mmHg) (mean ± SD)	Significance (p) vs. control
Preoperation		Control	9.8 ± 0.9	–
		COH	9.5 ± 1.0	0.4994
Postoperation	Day 3	Control	9.5 ± 1.0	–
		COH	26.9 ± 4.5	<0.0001
	Week 1	Control	9.8 ± 0.8	–
		COH	21.4 ± 4.0	<0.0001
	Week 2	Control	10.1 ± 0.8	–
		COH	20.3 ± 2.5	<0.0001
	Week 3	Control	9.5 ± 1.0	–
		COH	19.0 ± 2.9	<0.0001
	Week 4	Control	9.2 ± 1.0	–
		COH	17.8 ± 2.1	<0.0001
	Week 5	Control	9.3 ± 0.5	–
		COH	17.3 ± 1.8	<0.0001
	Week 6	Control	9.5 ± 0.5	–
		COH	16.5 ± 1.7	<0.0001
	Week 7	Control	9.2 ± 0.8	–
		COH	17.4 ± 1.6	<0.0001
	Week 8	Control	9.2 ± 0.8	–
		COH	16.6 ± 1.3	<0.0001

The 24 mice include 6 mice of the control group and 18 mice of the COH group. Data were analyzed using two-tailed independent-samples t test followed by Bonferroni test.

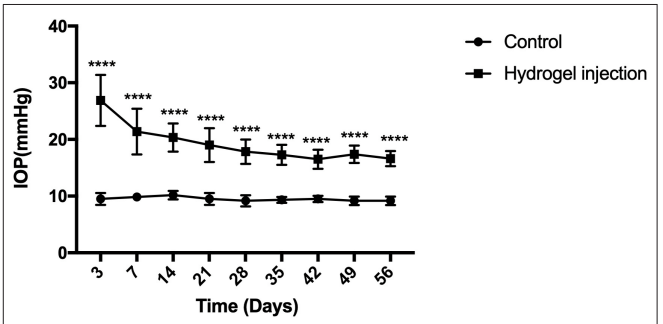

FIGURE 2 | Elevation of intraocular pressure (IOP) after intracameral injection of cross-linking hydrogel. The IOP of hydrogel injection eyes decreased slowly from the first measurement and then processed into a relatively stable phase of ocular hypertension for at least 8 weeks (average, 19.3 ± 4.1 mmHg). The control group presented a stable level of IOP throughout the whole period of the experiment (average, 9.5 ± 0.8 mmHg). There was statistical difference between the two groups ($p < 0.0001$). Data were analyzed using two-tailed independent-samples *t* test followed by Bonferroni test (****$p < 0.0001$, the group with injection of cross-linking hydrogel vs. the control group). $N = 24$ mice (control group: 6 mice; hydrogel injection group: 18 mice). Bars represent mean ± SD.

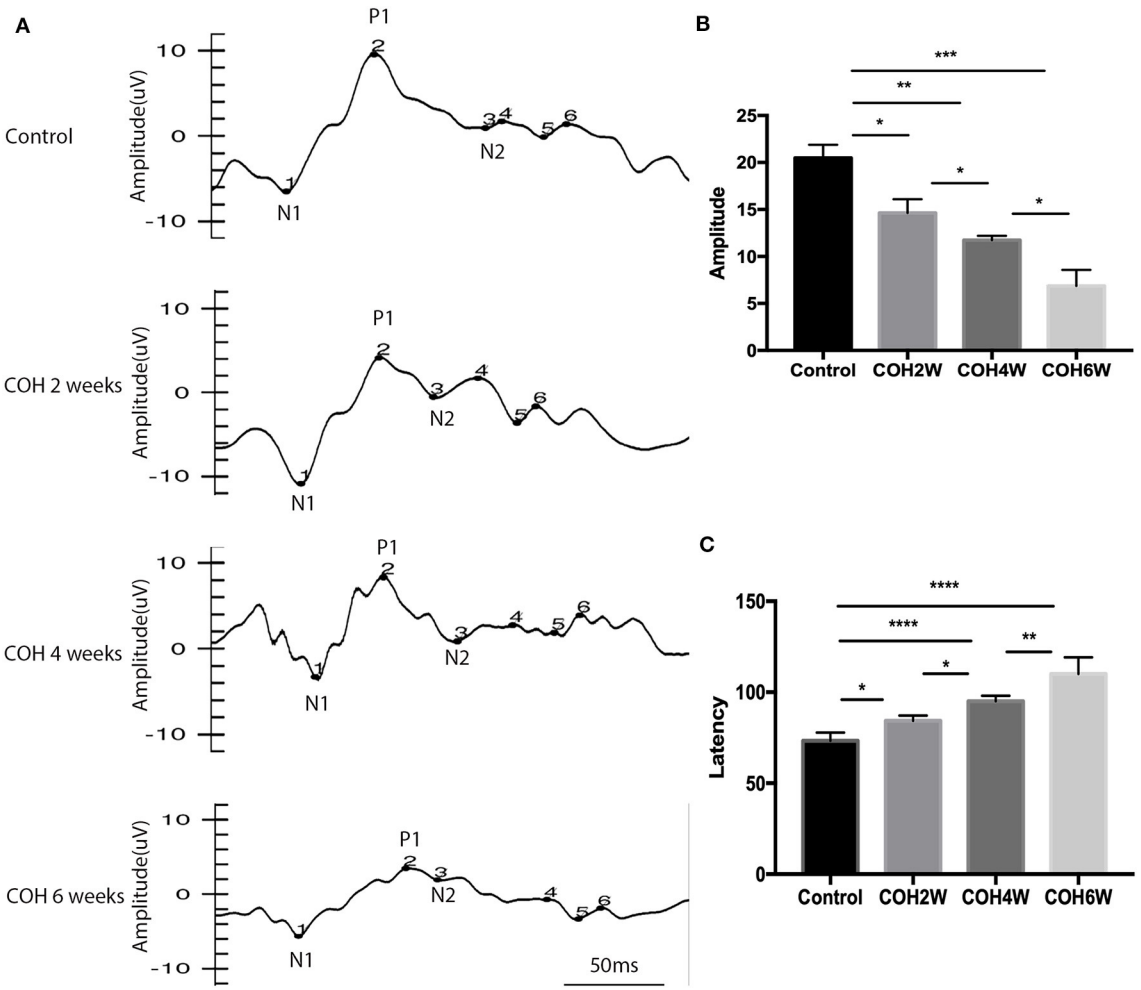

FIGURE 3 | Flash visual evoked potential (F-VEP) test result of C57BL/6J mice. **(A)** The F-VEP test was measured before and 2, 4, and 6 weeks after IOP elevation induced by intracameral injection of hydrogel. **(B)** The amplitudes of P1 were significantly reduced in the hydrogel-injected eyes compared with those in the control group. **(C)** The latent periods of P1 were significantly prolonged in mice at 2, 4, and 6 weeks of COH compared with those in the control group. Data were analyzed using one-way ANOVA followed by Tukey's *post hoc* test (*$p < 0.05$, **$p < 0.01$, ***$p < 0.001$, and ****$p < 0.0001$). $N = 24$ mice (control group: 6 mice; hydrogel injection group: 18 mice). Bars represent mean ± SD.

Flash Visual Evoked Potential

F-VEP was examined in mice preoperatively, and mice were subjected to 2, 4, and 6 weeks of COH. The average amplitude of P1 in the control group was 20.5 ± 3 μV, and the average amplitudes of P1 in mice at 2, 4, and 6 weeks of COH were 14.6 ± 1.5, 11.7 ± 0.5, and 6.9 ± 1.7 μV, respectively. There was a significant difference between the eyes after intracameral injection of cross-linking hydrogel and the control group ($p = 0.0149$, 0.0012, and 0.0009 at 2, 4, and 6 weeks after COH vs. the control group, respectively). The average latent period of N1 in the control group was 73.3 ± 4.5 ms, and the latent periods of P1 in mice at 2, 4, and 6 weeks of COH were 84.3 ± 2.9, 95.0 ± 3.0, and 110.0 ± 9.2 ms, respectively. A significant difference in the latent period was noted between the eyes with elevated IOP induced by cross-linking hydrogel and the control group ($p = 0.0239$, <0.0001, and <0.0001 vs. 2, 4, and 6 weeks of COH vs. the control group, respectively) (**Figure 3**).

Expression of Inflammatory Factors After Intracameral Injection of Cross-Linking Hydrogel

Western blotting showed that retinal tumor necrosis factor alpha (TNF-α), interleukin (IL)-1β, and IL-17A protein expression in COH mice generally increased over time (**Figure 4A**). At the second week after COH, TNF-α protein expression was increased compared with the control group by 14.9% ($p < 0.0001$). At the fourth and sixth weeks after COH, TNF-α protein expression increased by 17.5 and 39.7%, respectively ($p < 0.0001$ at each group vs. the control group). At the fourth week after COH, TNF-α protein expression showed no significant difference

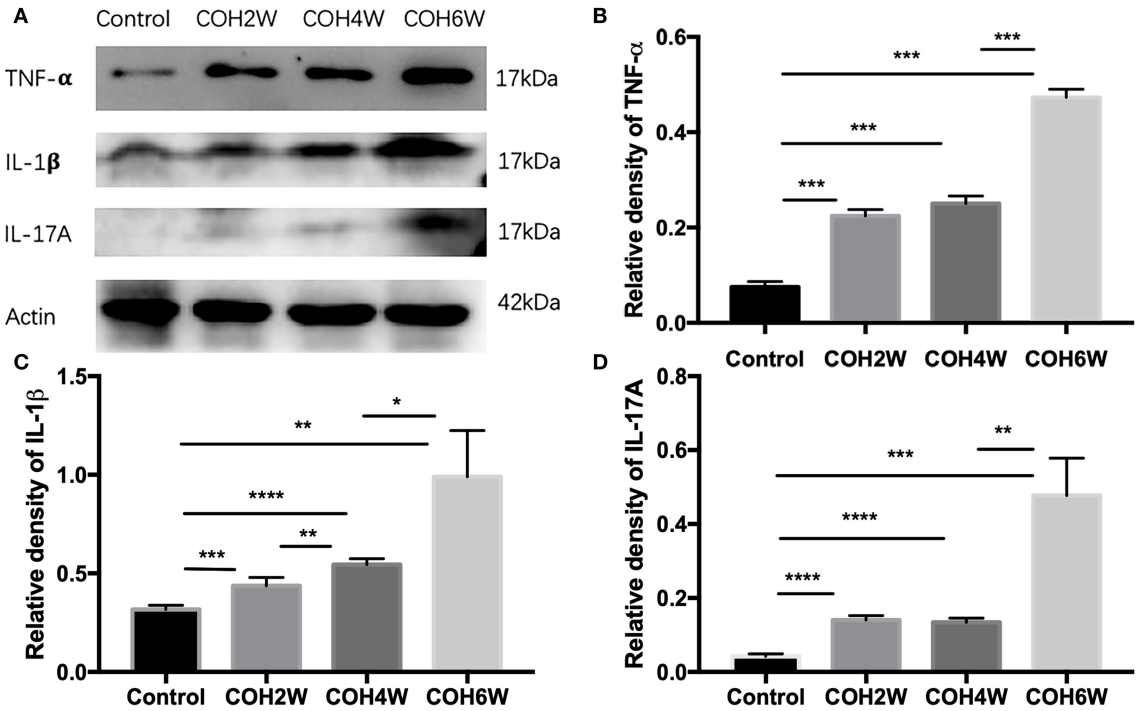

FIGURE 4 | Western blotting of retinal expressions of inflammatory factors. **(A)** Bands of western blotting. **(B–D)** Quantitative analysis of western blotting gray values; TNF-α, IL-1β, and IL-17A protein expression increased gradually from the second week to the sixth week after COH. Data were analyzed using one-way ANOVA followed by Tukey's *post hoc* test (*$p < 0.05$, **$p < 0.01$, ***$p < 0.001$, and ****$p < 0.0001$). $N = 20$ mice (control group: 5 mice; hydrogel injection group: 15 mice). Bars represent mean ± SD.

from the second week after COH (**Figure 4B**). IL-1β protein expression was increased by 11.9, 22.8, and 67.2% at the second, fourth, and sixth weeks after COH, respectively ($p = 0.0006$, $p < 0.0001$, and 0.0028 vs. the control group, respectively) (**Figure 4C**). IL-17A protein expression was increased by 9.8, 9.1, and 43.5% at the second, fourth, and sixth weeks after COH, respectively ($p < 0.0001$, <0.0001, and 0.0005 vs. the control group, respectively) (**Figure 4D**). However, no significant difference in IL-17A protein expression was noted between 2 and 4 weeks after COH.

Increase in Microglial Cell Activation Under IOP Elevation

Immunofluorescent images showed microglial cell activation early in the COH group. The number of Iba-1+ microglial cells in the control group and in mice at 2, 4, and 6 weeks of COH was 75.3 ± 3.5, 149.4 ± 19.3, 268.0 ± 20.7, and 429 ± 74.1/mm^2, respectively. Compared with the control group, the number of microglial cells in the retina of the COH group was significantly increased ($p = 0.0258$, <0.001, and <0.001 vs. the control group, respectively) (**Figure 5B**). The cell morphology became rounder, and the processes were thicker (**Figure 5A**). Western blotting results also demonstrated that retinal Iba-1 and CD68 protein expression levels were both markedly upregulated in the COH group (**Figure 6A**). Iba-1 protein expression increased by 32.6, 37.9, and 56.0% at the second, fourth, and sixth weeks after COH, respectively. A significant difference was noted between the COH mice and the control group ($p = 0.0005$, 0.0002, and <0.0001, respectively). CD68 protein expression was increased by 3.1, 25.1, and 53.4% at the second, fourth, and sixth weeks after COH, respectively. A significant difference was noted in mice between the fourth and sixth weeks of COH and the control group ($p = 0.0099$ and 0.0356, respectively) (**Figures 6B,C**).

Decrease of RGCs After Intracameral Injection of Cross-Linking Hydrogel

The double label of Brn3a and the TUNEL assay were used to evaluate the apoptosis of RGCs in the retinas of mice after intracameral injection of cross-linking hydrogel. The TUNEL assay showed that RGC apoptosis was obvious in mice after 2, 4, and 6 weeks of COH (**Figure 7A**). The proportion of TUNEL-positive neurons in the GCL was 2.0 ± 0.8, 33.3 ± 9.5, 60.6 ± 11.3, and 78.6 ± 6.3% of the control group and of mice after 2, 4, and 6 weeks of COH, respectively ($p = 0.0061$, 0.0012, <0.0001, and 0.0371 vs. the control group, respectively) (**Figure 7B**), indicating that elevated IOP induced by cross-linking hydrogel injection can lead to RGC apoptosis.

Immunofluorescence staining with Brn3a in retinal whole mounts was performed in mice 2, 4, 6, and 8 weeks following intracameral injection of the hydrogel and in the control group. In the control group, the number of RGCs was 1,369.0 ± 77.4/mm^2 in 1/6 retinal radius, 1,046.0 ± 175.3/mm^2 in 3/6

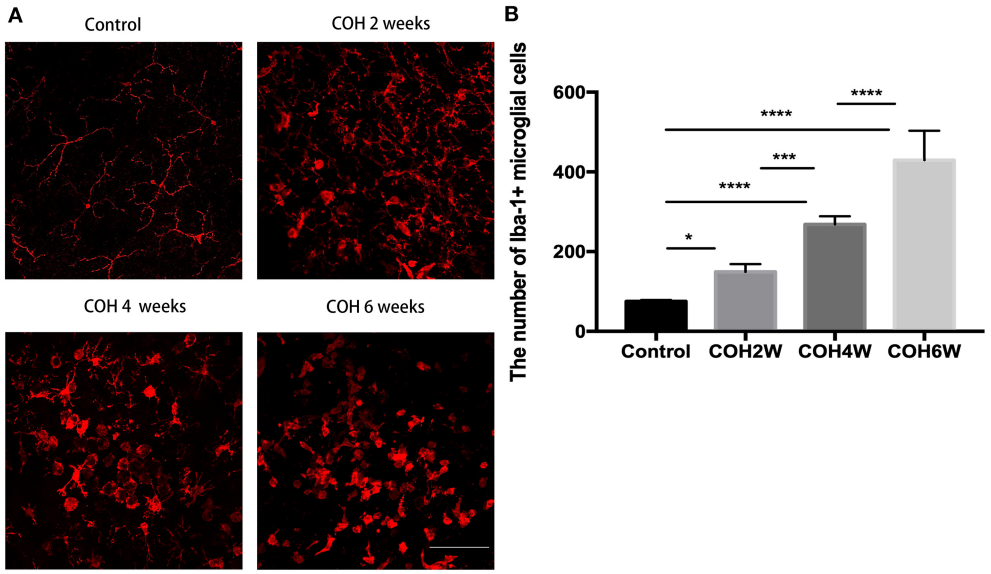

FIGURE 5 | Activation of microglial cells induced by COH. **(A)** Immunofluorescence staining of Iba-1 proteins in retinal whole mounts. In the group of COH, microglial cell showed amoeba morphological change (magnification ×200, scale bar = 50 μm). **(B)** The number of Iba-1+ microglial cells in COH mice. The number and activation of microglial cell increased with the prolonged duration of COH. Data were analyzed using one-way ANOVA followed by Tukey's *post hoc* test (*$p < 0.05$, ***$p < 0.001$, and ****$p < 0.0001$). $N = 16$ mice (control group: 4 mice; hydrogel injection group: 12 mice). Bars represent mean ± SD.

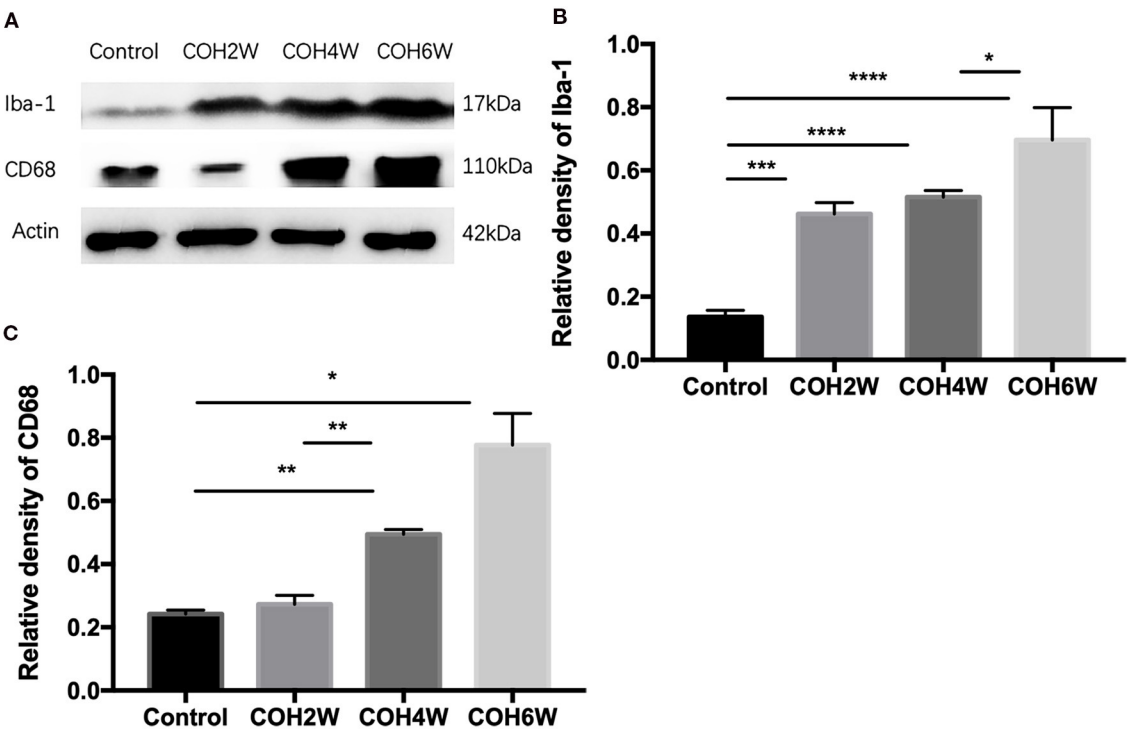

FIGURE 6 | Western blotting of retinal expressions of Iba-1 and CD68. **(A)** Bands of western blotting. **(B,C)** Quantitative analysis of western blotting gray values. The expression of Iba-1 and CD68 increased after the second week of COH. Data were analyzed using one-way ANOVA followed by Tukey's *post hoc* test (*$p < 0.05$, **$p < 0.01$, ***$p < 0.001$, and ****$p < 0.0001$). $N = 20$ mice (control group: 5 mice; hydrogel injection group: 15 mice). Bars represent mean ± SD.

retinal radius, and 795.0 ± 43.8/mm^2 in 5/6 retinal radius, respectively. In the COH group, the RGC density decreased significantly in all three retinal positions compared with the control group (**Figure 8**). The number of RGCs in the COH 2-week group (1,213.0 ± 61.4/mm^2 in 1/6 retinal radius, 888.2 ± 100.6/mm^2 in 3/6 retinal radius, and 710.6 ± 21.1/mm^2 in 5/6

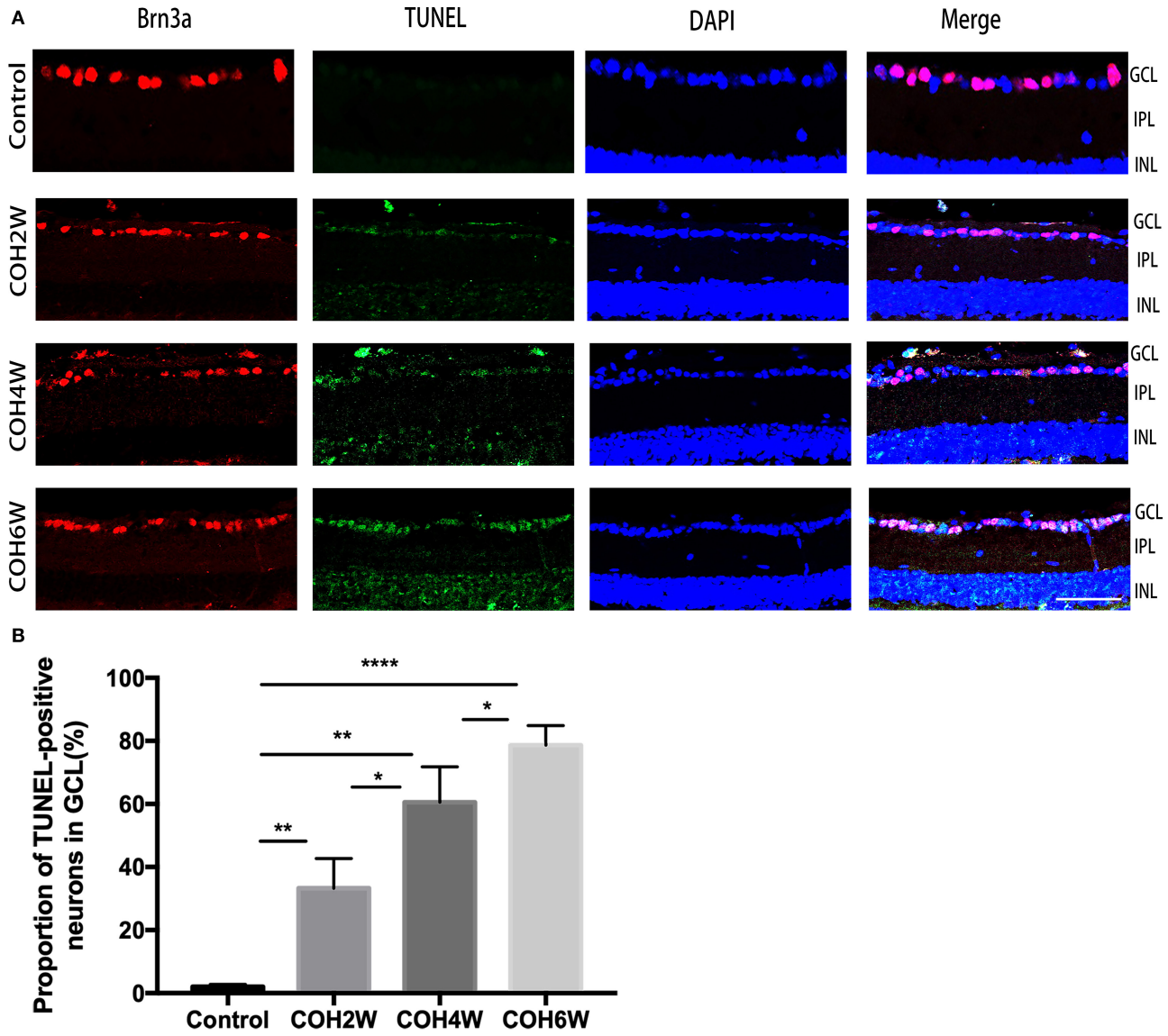

FIGURE 7 | Apoptosis of neurons in the ganglion cell layer (GCL) was obvious after intracameral injection of cross-linking hydrogel. **(A)** Representative images of TUNEL (green fluorescence) and Brn3a (red fluorescence) double-staining for apoptosis evaluation of neurons in the GCL of different groups (magnification ×200, scale bar = 50 μm). Cell nuclei were marked with DAPI (blue). **(B)** Quantitative analysis of proportions of TUNEL-positive cells to Brn3a-positive cells in the GCL (*p < 0.05, **p < 0.01, and ****p < 0.0001). Data were analyzed using one-way ANOVA followed by Tukey's *post hoc* test. N = 24 mice (control group: 6 mice; hydrogel injection group: 18 mice). Bars represent mean ± SD.

retinal radius, respectively) decreased markedly in comparison with the control group (p = 0.0366, 0.0495, and 0.0181, respectively). The number of RGCs in the COH 4-week group (1,027.0 ± 10.5/mm^2 in 1/6 retinal radius, 841 ± 86.9/mm^2 in 3/6 retinal radius, and 606.6 ± 38.0/mm^2 in 5/6 retinal radius, respectively), the COH 6-week group (916.6 ± 43.4/mm^2 in 1/6 retinal radius, 756.6 ± 78.7/mm^2 in 3/6 retinal radius, and 530.8 ± 32.5/mm^2 in 5/6 retinal radius, respectively), and the COH 8-week group (728.6 ± 33.5/mm^2 in 1/6 retinal radius, 636.6 ± 49.7/mm^2 in 3/6 retinal radius, and 436.5 ± 52.5/mm^2 in 5/6 retinal radius, respectively) further decreased in comparison with the control group, respectively (COH 4 weeks, p = 0.0037, 0.0310, and <0.0001 vs. the control group, respectively; COH 6 weeks, p = 0.0037, 0.0187, and <0.0001 vs. the control group, respectively; COH 8 weeks, p = 0.0038, 0.0187, and<0.0001 vs. the control group, respectively). In mice at 8 weeks of COH, the rates of RGC loss were 46.8% in 1/6 retinal radius, 39.2% in 3/6 retinal radius, and 45.1% in 5/6 retinal radius, respectively (**Figure 9**).

Optic Nerve Axon Loss After Intracameral Injection of Cross-Linking Hydrogel

To analyze the loss of optic nerve axons in mice with intracameral injection of cross-linking hydrogel, immunofluorescence

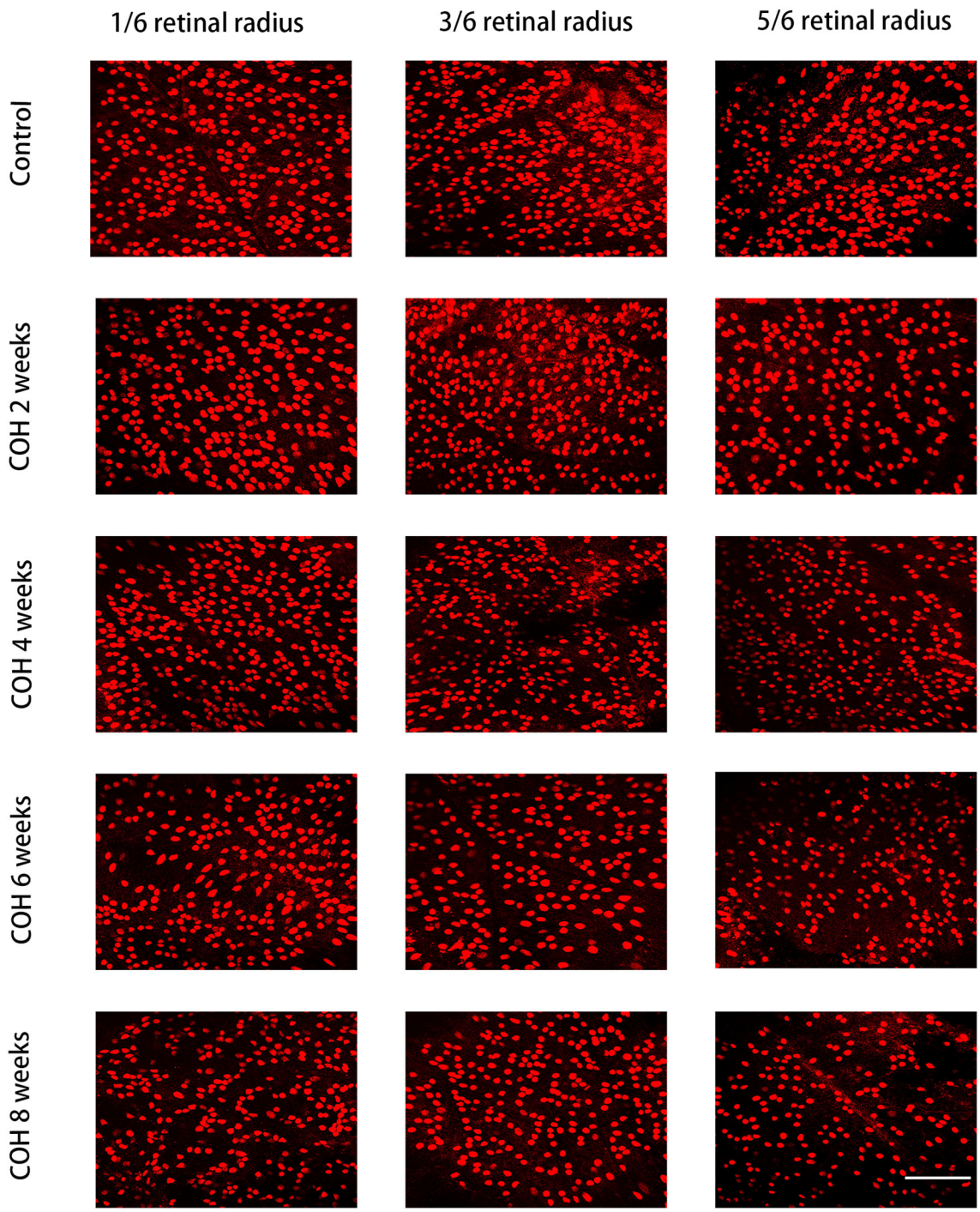

FIGURE 8 | Density of retinal ganglion cells (RGCs) in the control group and COH mice. The label of RGCs with Brn3a in 1/6, 3/6, and 5/6 retinal radius in mice at 2, 4, 6, and 8 weeks of COH (magnification ×200, scale bar = 50μm). $N = 12$ mice (control group: 3 mice; hydrogel injection group: 9 mice).

staining with neurofilament heavy polypeptide (NEFH) was performed in optic nerve cross-sections of the control group and COH mice. The mean fluorescence intensity of NEFH in the control mice was 133.6 ± 26.7. The mean fluorescence intensity (MFI) of NEFH was significantly reduced in mice at 2, 4, and 6 weeks of COH compared with that of the control group ($p = 0.0095$, 0.0002, and <0.0001 vs. the control group, respectively) (**Figure 10A**). The MFI of NEFH in mice at 2 weeks of COH was 93.9 ± 6.3; in mice at 4 weeks of COH, it was 62.4 ± 5.0; and in mice at 6 weeks of COH, it was 40.7 ±

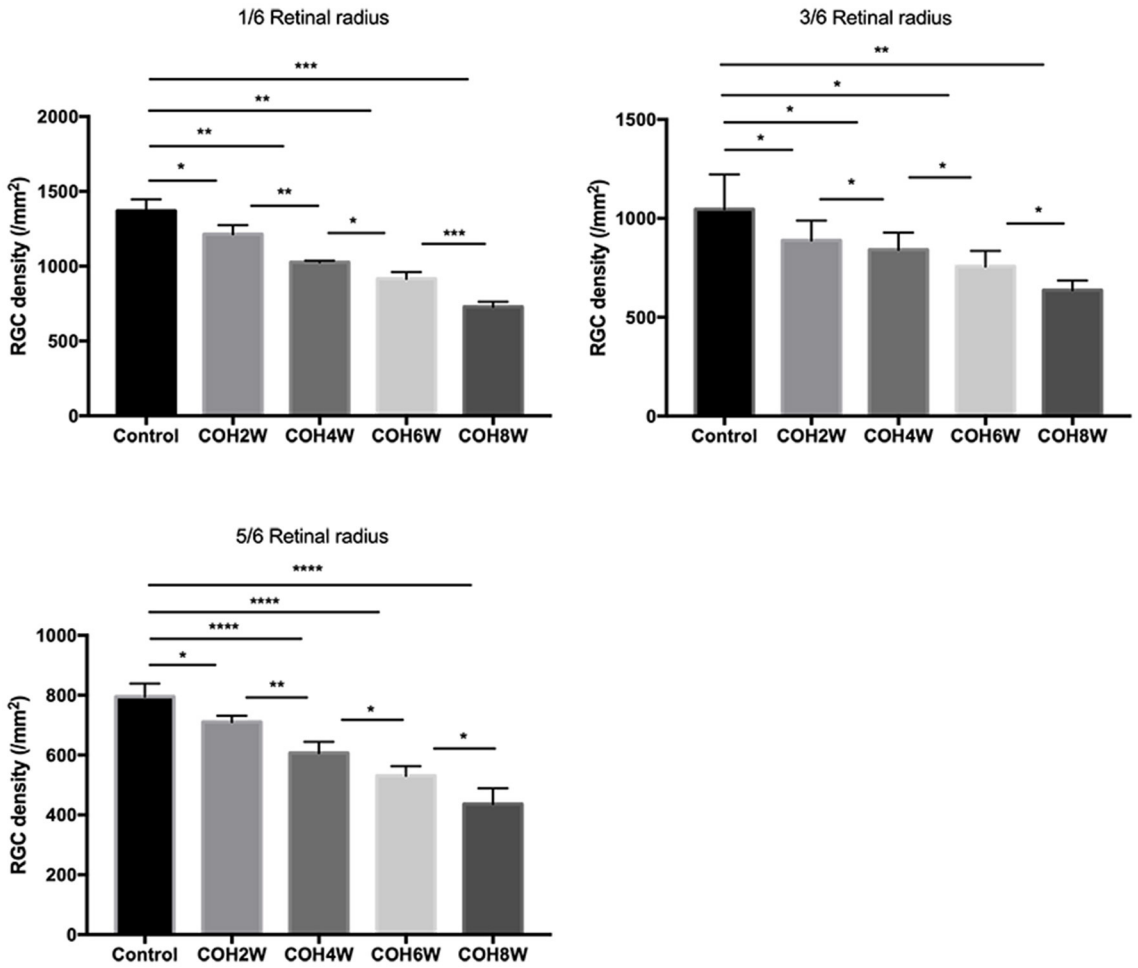

FIGURE 9 | Quantitative analysis of surviving RGCs after COH. Two, 4, 6, and 8 weeks following the induction of COH, the RGC density in 1/6, 3/6, and 5/6 retinal radius was significantly lower than that in the control group. Data were analyzed using one-way ANOVA followed by Tukey's *post hoc* test (*$p < 0.05$, **$p < 0.01$, ***$p < 0.001$, and ****$p < 0.0001$). $N = 12$ mice (control group: 3 mice; hydrogel injection group: 9 mice). Bars represent mean ± SD.

1.7 (**Figure 10B**). The rate of optic nerve axon loss was 69.5% at 6 weeks of COH.

DISCUSSION

Glaucoma is a group of diseases characterized by the loss of the visual field and progressive damage to RGCs and axons, which eventually lead to irreversible blindness (1). The pathological core is the chronic neurodegeneration. At present, the mechanism of glaucoma optic nerve degeneration is not completely understood. Glaucoma is considered to be an optic neurodegenerative disease caused by multiple factors, including mechanical damage of elevated IOP, neurotrophic factor deprivation, ischemia or reperfusion injury, oxidative stress injury, excitatory glutamate toxicity, and abnormal immune inflammatory response (17–19). Therefore, it is very important to construct an effective animal model of ocular hypertension for future glaucoma research.

In our study, we used a cross-linking hydrogel for intracameral injection to induce COH in mice and to study chronic degeneration of the RGCs and visual function in experimental glaucoma. Intracameral injection of cross-linking hydrogel effectively increased the IOP in mice for at least 8 weeks. In the operation group, IOP decreased slowly from the first measurement and remained relatively stable at the third week after the operation. The postoperative mean IOP was 19.3 ± 4.1 mmHg. The IOP of the cross-linked hydrogel-injected eyes was significantly increased compared with that of the control group. Immunofluorescent images and western blotting showed that the expression of inflammatory mediators, such as IL-17A, was increased, and microglial cells were active in our glaucoma model. F-VEP results showed that the visual function of mice decreased gradually after intracameral injection of the cross-linking hydrogel. The latent period of F-VEP in mice with COH was longer, and the amplitude was reduced compared with that in the control group. Our model shows a chronic neurodegeneration in RGCs and significant loss of optic

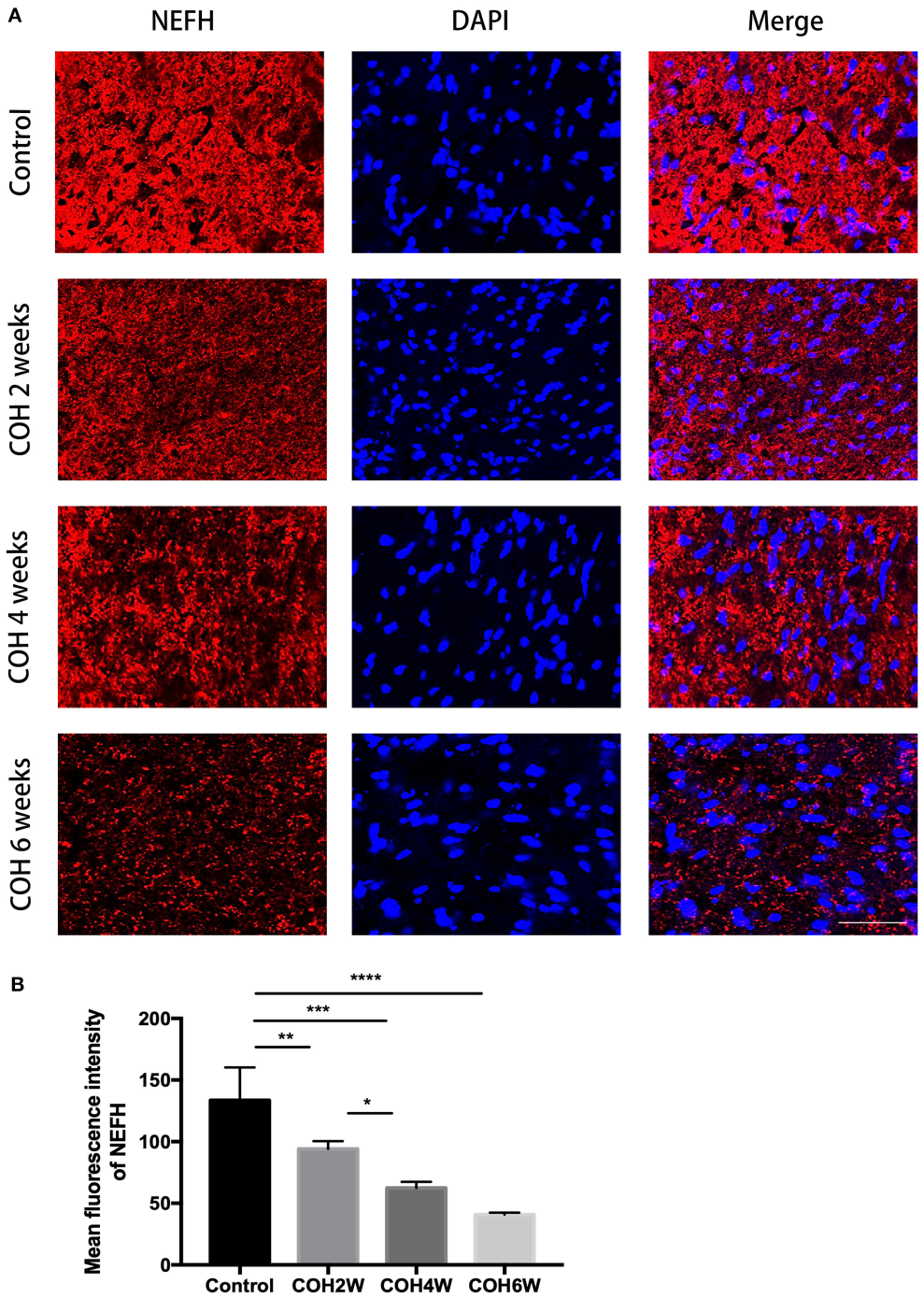

FIGURE 10 | Quantitative analysis of axon loss after COH. **(A)** Optic nerve slices were stained with NEFH (red fluorescence) and cell nuclei were marked with DAPI (blue fluorescence) (magnification ×200, scale bar = 50 μm). **(B)** Quantitative analysis of mean fluorescence intensity of NEFH in the control group and the COH mice. COH mice showed a significant decrease of NEFH compared with the control group. Data were analyzed using one-way ANOVA followed by Tukey's *post hoc* test (*$p < 0.05$, **$p < 0.01$, ***$p < 0.001$, and ****$p < 0.0001$). $N = 12$ mice (control group: 3 mice; hydrogel injection group: 9 mice). Bars represent mean ± SD. NEFH, neurofilament heavy polypeptide.

nerve axons. The positive rate of the RGC TUNEL assay in mice with COH was significantly increased compared with that in control mice.

As a biocompatible and multifunctional material, the cross-linked hydrogels have presented flexible characteristics for various applications in the clinical practice of ophthalmology,

including ocular surface treatment, contact lenses of drug delivery systems for glaucoma treatment, and substitutes for vitreous (20–22). Cross-linking hydrogels, such as thiol-modified hyaluronic acid, have the advantage of *in situ* gelling by premix-separating components in different proportions at appropriate time points to control gelation (23). In addition, to induce the IOP elevation successfully, the cross-linking hydrogel should be able to gel rapidly immediately after intracameral injection or be diluted by the aqueous humor. Our study showed that the IOP elevation was induced by injection of the cross-linking hydrogel at a ratio of 4:1 and the cross-linking hydrogel gel *in situ* for ∼5 min. The elevated IOP is stable, and a high success rate of induction of IOP elevation is observed (the success rate is 68%). Hydrogels can be retained in the eye for a long time due to their good biocompatibility and non-degradable properties. Hyaluronic acid (HA) is the main component of cross-linking hydrogels, and it is highly biocompatible. *In vitro* studies have shown that *in situ* gelation and gel incubation of HA are not toxic to eye cells. *In vivo* studies have shown that *in situ* cross-linked hydrogels injected into the eyes of non-human primates and rats have good biocompatibility and no obvious adverse reactions (24–26). The mechanism of COH induced by intracameral injection of cross-linking hydrogel is the blocking of the outflow pathway of aqueous humor. The gel droplets formed by injecting the cross-linking hydrogel into the anterior chamber exhibit a physical blocking effect, which can prevent the outflow pathway of aqueous humor and achieve long-term stable maintenance of COH. In terms of operation, we used a corneal long tunnel incision that can self-seal after surgery. In addition, after the cross-linked hydrogel was completely injected into the anterior chamber, the syringe was stopped *in situ* for 5 min, and the syringe was pulled out after *in situ* cross-linked gelation to further prevent liquid leakage and ensure the effect of increasing and maintaining the intraocular pressure of our model.

Many types of animal models for IOP elevation have been described. In some models, glaucoma is caused by blocking outflow of aqueous humor, including injection of microbeads and hyaluronic acid into the anterior chamber, injection of hypertonic saline into the episcleral veins or limbal vessels, occlusion of the episcleral veins by cauterization or suture ligation, and laser photocoagulation of the trabecular meshwork at the limbus (9–11, 27). In addition, DBA/2J mice have also been studied as glaucoma models. However, in existing models, there have always been technical challenges in maintaining a clear optical media to facilitate the study of the structural and functional integrity of RGCs. For laser photocoagulation and episcleral vein cauterization or ligation, maintaining the clarity of the cornea is typically not easy to achieve (12). Laser photocoagulation typically requires 60–80 photocoagulated spots on the trabecular meshwork and scleral surface veins of the mouse eye, which is very difficult and requires repeated operations. Due to the small size of the mouse eye, it requires high technical requirements for the operator and special laser equipment (28). The success rate of laser photocoagulation-induced COH ranged from 80 to 90% for a single laser treatment lasting for 4 to 8 weeks (29, 30). Superior scleral vein burning or ligation can significantly increase IOP, and the mechanism may be caused by congestion in the uveal vascular system. This method is simple to perform. However, the method also blocks the outflow of blood in the eye, resulting in congestion and ischemic changes in the eye, which makes the injury factors more complicated. The blood return flow in the unoccluded superior scleral vein in the experimental eye may be increased to compensate, and the phenomena of occluded paravenous angiogenesis and recanalization are also noted. These changes may lead to a decrease in IOP, resulting in the failure of the model and a low success rate. Zhao et al. (31) reported the success rate was 50%, and the duration of IOP elevation was 12 weeks. The procedure has a high rate of complications. Hyphema occurred in 71% of the mice, and suture breaks occurred in 29% of the mice (31). For the intracameral injection of microbeads, a second injection is always required, which means an additional invasive operation and possible side effects (such as inflammation and infection) (32). It was reported that a single injection of microbeads resulted in a 30% success rate in elevating IOP and persisted for more than 3 weeks (27). Intracameral injection of hyaluronic acid requires repeated injection to maintain a high IOP because hyaluronic acid is easily metabolized, degraded, and absorbed in the eye. Thus, there was local corneal edema and severe inflammation around the injection site. A single injection of elevated IOP lasted for up to 7 days (33). In DBA/2J mice, IOP began to spontaneously increase from 7 to 8 months after birth. The increase in IOP was due to mutations in two genes GPNMB and TyrPL in mice. These mutations led to the depigmentation of the iris, and the shed pigment and cell debris blocked the outflow of atrial fluid, thus causing high IOP. By 10 to 12 months after birth, IOP begins to decrease again due to lesions in the ciliary epithelial cells. However, the DBA/2J experimental glaucoma model showed variability in expression, and 22% of the animals developed major systemic complications (34). This feature makes it difficult to assess disease progression and study the structure and function of RGCs in glaucoma. Episcleral vein injection of hypertonic saline can cause the sclerosis of the aqueous humor outflow system in mice, which increases the resistance of aqueous humor outflow and leads to an increase in IOP. Kipfer-Kauer et al. (35) reported that in the case of reintervention, the success rate was 100% and the elevated IOP was sustained for 6 weeks. However, this model is difficult to operate, and a special microsyringe equipment is needed, which requires higher operating skills for the operator. Chan et al. (12) reported the use of a homemade cross-linking hydrogel for intracameral injection to induce COH in mice. The daily mean IOP ranged between 14 ± 3 and 24 ± 3 mmHg, which was similar to our study. They reported that the elevated IOP was sustained for 4 weeks. In our study, our model preserves the clarity of optical media. The IOP elevation induced by the cross-linking hydrogel could be sustained for at least 8 weeks with only one injection, which helped to avoid the risk of inflammatory responses caused by additional operations. In addition, we used commercial hydrogels to ensure the stability of the hydrogel products. Therefore, the model has strong operability.

In recent years, increasing attention has been given to the role of the immune inflammatory response in glaucoma optic nerve damage (36). Retinal microglial cells are one of the main cells involved in the immune inflammatory response in the retina and optic nerve. During retinal and optic nerve injury, microglial cells play a neuroprotective role by morphologically changing,

proliferating, and migrating to the damaged site to phagocytose and eliminate microbes, protein aggregates, and dead cells (6). However, excessive activation of microglial cells leads to damage of the nerve tissue by releasing a series of toxic substances (such as TNF-α, IL-1β, etc.) (6). Studies have shown that microglial cells are involved in the pathological process of glaucoma. Neufeld (37) found that microglial cells were activated in the optic papilla of glaucoma patients, and cell morphology and distribution were changed. Wang et al. (38) found that in an animal model of glaucoma, activated microglial cells appeared in the RGC layer only 2 h after IOP elevation. CD68 is an activation marker of microglial cells. In our study, CD68 expression was observed after 2 weeks of COH and microglial cells have a transition from slender branching to globular amoeboid morphology. The number of microglial cells and Iba-1 and CD68 protein levels increased in COH mice over time. Some studies have analyzed the microglial activation in glaucoma models in mice at different times after ocular hypertension induction. CD68 and MHC-II expression were observed in the nerve fiber layer–ganglion cell layer after 15 days of unilateral laser-induced experimental glaucoma model (13). These findings were similar to those in our study. Others reported that the number of Iba-1+ microglial cells was increased in laser-induced ocular hypertension eyes compared with control eyes at 3, 5, 8, and 15 days, and the peak number of Iba-1+ microglial cells occurred at 3 days (39).

IL-17A is a cytokine that is secreted mainly by activated CD4+ T cells (Th17 cells). The IL-17 family is composed of six structurally similar cytokines (IL-17A∼IL-17F) and five receptors (IL-17RA∼IL-17RE) (40). These cytokines are dimeric molecules with sizes of 23∼36 kDa composed of 163∼202 amino acids (40). IL-17a, a well-studied cytokine in the IL-17 family, plays an important role in the immune inflammatory response, angiogenesis, and the occurrence and development of tumors (41). Studies have shown that IL-17A is involved in the pathogenesis of CNS neurodegenerative diseases. In recent years, some researchers have studied IL-17A levels in patients with glaucoma. The frequency of IL-17A-secreting cells and IL-17A+ CD4 T cells is significantly higher in patients with glaucoma compared with controls (42). In our study, the protein levels of IL17, TNF-α, and IL-1β were upregulated from 2 to 4 weeks postelevated IOP and then further increased at 6 weeks postelevated IOP. Various cells have been reported to produce IL-17A, one of which is microglial cells (43). In our model, IL-17A, TNF-α, and IL-1β may be produced by activated microglial cells during COH. Elevated IL-17A and retinal nerve injury caused by COH further could activate microglial cells and astrocytes and could transform microglia into an M1- or M2-like phenotype and astrocytes into an A1- or A2-type phenotype, respectively. Microglial cells often undergo a dynamic process during injury, which is characterized by the mixing or conversion between the M1 and M2 phenotype (44). Classical M1-like microglial cells produce high levels of proinflammatory cytokines (such as TNF-α and IL-1β). In addition, activated astrocytes and microglial cells recruit monocytes, macrophages, and T cells to cross the blood–eye barrier into the retina and increase the secretion of proinflammatory cytokines. Elevated levels of TNF-α, IL-1β, and IL-17A further stimulate microglia and astrocytes and increase their activity. Proinflammatory cytokines and glial cells in the retina form a tight positive feedback loop. As the disease progresses, the levels of proinflammaroy cytokines increase (45). To our knowledge, we are the first to report increased IL-17A expression in an experimental glaucoma model. Further research is needed.

VEP refers to the cortical electrical activity recorded after visual stimulation. The electrophysiological signal is generated in the striatum and extrastriate cortex (46). VEP provides a useful tool for assessing the functional retina and cortex and the state of visual pathways from the retina to the cortex. In an animal model of glaucoma, alteration of the inner retinal circuitry was found to precede RGC degeneration and optic nerve atrophy (46). Thus, VEP contributes to characterizing the progression of glaucoma. In DBA/2J mice with ocular hypertension, the amplitude of VEP was clearly reduced (47). In our study, the amplitude and latent period of mice at 2, 4, and 6 weeks of COH were significantly different compared with those in the control group.

In acute IOP elevation, RGC loss was induced in the first week of injury but not thereafter (48). In an animal model of laser photocoagulation-induced intraocular hypertension, the rate of RGC loss was 20–30% at 8 weeks (49) and the rate of axon loss was 59% at 24 weeks (50). Zhu et al. (51) reported that the rate of RGC loss was 30% at 11 weeks and 8% at 12 weeks by Zhao et al. (31) in the model of episcleral vein cauterization and circumlimbal suture. Chan et al. (12) reported that the survival rate of RGCs was 37% in mice at 4 weeks of COH. In our study, we found that RGCs and optic nerve axons were gradually lost over time in the eyes after IOP elevation. The rates of RGC loss were 46.8% in 1/6 retinal radius, 39.2% in 3/6 retinal radius, and 45.1% in 5/6 retinal radius at 8 weeks of COH, respectively. The rate of optic nerve axon loss was 69.5% at 6 weeks of COH. In different animal models of ocular hypertension, the number of RGC in control mice was significantly different. Liu et al. (52) reported that in the model of circumlimbal suture, the number of RGC was 3,098 ± 189/mm^2 (×20 magnification). However, in the same animal model by Zhu et al. (51), the number of RGC was approximately 720/mm^2 in peripheral retina (×200 magnification). In our model, the number of RGCs was 1,369.0 ± 77.4/mm^2 in 1/6 retinal radius, 1,046.0 ± 175.3/mm^2 in 3/6 retinal radius, and 795.0 ± 43.8/mm^2 in 5/6 retinal radius of the control group, respectively (×200 magnification). The difference in the number of RGC may be caused by different magnifications. Together, these results support that intracameral injection of cross-linking hydrogel damaged the inner retina and is an efficient model to study the functional degeneration of the RGCs.

In summary, we established a new COH model induced by intracameral injection of the cross-linking hydrogel. The model worked efficiently to demonstrate the features simulating glaucoma. Therefore, we provide a new, effective, and simple animal model for glaucoma research.

DATA AVAILABILITY STATEMENT

The raw data supporting the conclusions of this article will be made available by the authors, without undue reservation.

ETHICS STATEMENT

The animal study was reviewed and approved by Ruijin Hospital, Shanghai Jiao Tong University School of Medicine Animal Care and Use Committee.

AUTHOR CONTRIBUTIONS

JC wrote and edited the manuscript. JS provided pictures of some of the results. HY, PH, and YZ edited the manuscript. All authors read and approved the final manuscript.

FUNDING

This work was supported by the National Nature Science Foundation of China (Nos. 82070953, 81870652, and 82000885) and Shanghai Municipal Commission of Health and Family Planning Project Foundation (Nos. 2020LP034 and 2018JP008).

SUPPLEMENTARY MATERIAL

The Supplementary Material for this article can be found online at: https://www.frontiersin.org/articles/10.3389/fmed.2021.643402/full#supplementary-material

REFERENCES

1. Tian K, Shibata-Germanos S, Pahlitzsch M, Cordeiro MF. Current perspective of neuroprotection and glaucoma. *Clin Ophthalmol.* (2015) 9:2109–18. doi: 10.2147/opth.s80445
2. Tham YC, Li X, Wong TY, Quigley HA, Aung T, Cheng CY. Global prevalence of glaucoma and projections of glaucoma burden through 2040: a systematic review and meta-analysis. *Ophthalmology.* (2014) 121:2081–90. doi: 10.1016/j.ophtha.2014.05.013
3. Gordon MO, Beiser JA, Brandt JD, Heuer DK, Higginbotham EJ, Johnson CA, et al. The Ocular Hypertension Treatment Study: baseline factors that predict the onset of primary open-angle glaucoma. *Arch Ophthalmol.* (2002) 120:714–20; discussion 829–30. doi: 10.1001/archopht.120.6.714
4. Chen H, Cho KS, Vu THK, Shen CH, Kaur M, Chen G, et al. Commensal microflora-induced T cell responses mediate progressive neurodegeneration in glaucoma. *Nat Commun.* (2018) 9:3209. doi: 10.1038/s41467-018-05681-9
5. Williams PA, Marsh-Armstrong N, Howell GR. Neuroinflammation in glaucoma: a new opportunity. *Exp Eye Res.* (2017) 157:20–7. doi: 10.1016/j.exer.2017.02.014
6. Chidlow G, Ebneter A, Wood JP, Casson RJ. Evidence Supporting an Association Between Expression of Major Histocompatibility Complex II by Microglia and Optic Nerve Degeneration During Experimental Glaucoma. *J Glaucoma.* (2016) 25:681–91. doi: 10.1097/ijg.0000000000000447
7. Tezel G, Wax MB. The immune system and glaucoma. *Curr Opin Ophthalmol.* (2004) 15:80–4. doi: 10.1097/00055735-200404000-00003
8. Libby RT, Anderson MG, Pang IH, Robinson ZH, Savinova OV, Cosma IM, et al. Inherited glaucoma in DBA/2J mice: pertinent disease features for studying the neurodegeneration. *Vis Neurosci.* (2005) 22:637–48. doi: 10.1017/s0952523805225130
9. WoldeMussie E, Ruiz G, Wijono M, Wheeler LA. Neuroprotection of retinal ganglion cells by brimonidine in rats with laser-induced chronic ocular hypertension. *Invest Ophthalmol Vis Sci.* (2001) 42:2849–55.
10. Bayer AU, Danias J, Brodie S, Maag KP, Chen B, Shen F, et al. Electroretinographic abnormalities in a rat glaucoma model with chronic elevated intraocular pressure. *Exp Eye Res.* (2001) 72:667–77. doi: 10.1006/exer.2001.1004
11. Vidal-Sanz M, Galindo-Romero C, Valiente-Soriano FJ, Nadal-Nicolás FM, Ortin-Martinez A, Rovere G, et al. Shared and Differential Retinal Responses against Optic Nerve Injury and Ocular Hypertension. *Front Neurosci.* (2017) 11:235.doi: 10.3389/fnins.2017.00235
12. Chan KC, Yu Y, Ng SH, Mak HK, Yip YWY, van der Merwe Y, et al. Intracameral injection of a chemically cross-linked hydrogel to study chronic neurodegeneration in glaucoma. *Acta Biomater.* (2019) 94:219–31. doi: 10.1016/j.actbio.2019.06.005
13. Rojas B, Gallego BI, Ramírez AI, Salazar JJ, de Hoz R, Valiente-Soriano FJ, et al. Microglia in mouse retina contralateral to experimental glaucoma exhibit multiple signs of activation in all retinal layers. *J Neuroinflammation.* (2014) 11:133. doi: 10.1186/1742-2094-11-133
14. Huang S, Huang P, Liu X, Lin Z, Wang J, Xu S, et al. Relevant variations and neuroprotecive effect of hydrogen sulfide in a rat glaucoma model. *Neuroscience.* (2017) 341:27–41. doi: 10.1016/j.neuroscience.2016.11.019
15. Wiemann S, Reinhard J, Reinehr S, Cibir Z, Joachim SC, Faissner A. Loss of the Extracellular Matrix Molecule Tenascin-C Leads to Absence of Reactive Gliosis and Promotes Anti-inflammatory Cytokine Expression in an Autoimmune Glaucoma Mouse Model. *Front Immunol.* (2020) 11:566279. doi: 10.3389/fimmu.2020.566279
16. Odom JV, Bach M, Brigell M, Holder GE, McCulloch DL, Mizota A, et al. ISCEV standard for clinical visual evoked potentials: (2016 update). *Doc Ophthalmol.* (2016) 133:1–9. doi: 10.1007/s10633-016-9553-y
17. Burgoyne CF. A biomechanical paradigm for axonal insult within the optic nerve head in aging and glaucoma. *Exp Eye Res.* (2011) 93:120–32. doi: 10.1016/j.exer.2010.09.005
18. Rieck J. The pathogenesis of glaucoma in the interplay with the immune system. *Invest Ophthalmol Vis Sci.* (2013) 54:2393–409. doi: 10.1167/iovs.12-9781
19. KriŽaj D, Ryskamp DA, Tian N, Tezel G, Mitchell CH, Slepak VZ, et al. From mechanosensitivity to inflammatory responses: new players in the pathology of glaucoma. *Curr Eye Res.* (2014) 39:105–19. doi: 10.3109/02713683.2013.836541
20. Jung HJ, Abou-Jaoude M, Carbia BE, Plummer C, Chauhan A. Glaucoma therapy by extended release of timolol from nanoparticle loaded silicone-hydrogel contact lenses. *J Control Release.* (2013) 165:82–9. doi: 10.1016/j.jconrel.2012.10.010
21. Williams DL, Mann BK. Efficacy of a crosslinked hyaluronic acid-based hydrogel as a tear film supplement: a masked controlled study. *PLoS ONE.* (2014) 9:e99766. doi: 10.1371/journal.pone.0099766
22. Tao Y, Tong X, Zhang Y, Lai J, Huang Y, Jiang YR, et al. Evaluation of an in situ chemically crosslinked hydrogel as a long-term vitreous substitute material. *Acta Biomater.* (2013) 9:5022–30. doi: 10.1016/j.actbio.2012.09.026
23. Zarembinski TI, Doty NJ, Erickson IE, Srinivas R, Wirostko BM, Tew WP. Thiolated hyaluronan-based hydrogels crosslinked using oxidized glutathione: an injectable matrix designed for ophthalmic applications. *Acta Biomater.* (2014) 10:94–103. doi: 10.1016/j.actbio.2013.09.029
24. Yu Y, Lin X, Wang Q, He M, Chau Y. Long-term therapeutic effect in nonhuman primate eye from a single injection of anti-VEGF controlled release hydrogel. *Bioeng Transl Med.* (2019) 4:e10128. doi: 10.1002/btm2.10128
25. Yu Y, Lau LC, Lo AC, Chau Y. Injectable Chemically Crosslinked Hydrogel for the Controlled Release of Bevacizumab in Vitreous: A 6-Month In Vivo Study. *Transl Vis Sci Technol.* (2015) 4:5. doi: 10.1167/tvst.4.2.5
26. Yu H, Zhong H, Chen J, Sun J, Huang P, Xu X, et al. Efficacy, Drug Sensitivity, and Safety of a Chronic Ocular Hypertension Rat Model Established Using a Single Intracameral Injection of Hydrogel into the Anterior Chamber. *Med Sci Monit.* (2020) 26:e925852. doi: 10.12659/msm.925852
27. Sappington RM, Carlson BJ, Crish SD, Calkins DJ. The microbead occlusion model: a paradigm for induced ocular hypertension in rats and mice. *Invest Ophthalmol Vis Sci.* (2010) 51:207–16. doi: 10.1167/iovs.09-3947

28. Johnson TV, Tomarev SI. Rodent models of glaucoma. *Brain Res Bull.* (2010) 81:349–58. doi: 10.1016/j.brainresbull.2009.04.004
29. Gross RL, Ji J, Chang P, Pennesi ME, Yang Z, Zhang J, et al. A mouse model of elevated intraocular pressure: retina and optic nerve findings. *Trans Am Ophthalmol Soc.* (2003) 101:163–9; discussion 69–71.
30. Grozdanic SD, Betts DM, Sakaguchi DS, Allbaugh RA, Kwon YH, Kardon RH. Laser-induced mouse model of chronic ocular hypertension. *Invest Ophthalmol Vis Sci.* (2003) 44:4337–46. doi: 10.1167/iovs.03-0015
31. Zhao D, Nguyen CT, Wong VH, Lim JK, He Z, Jobling AI, et al. Characterization of the Circumlimbal Suture Model of Chronic IOP Elevation in Mice and Assessment of Changes in Gene Expression of Stretch Sensitive Channels. *Front Neurosci.* (2017) 11:41. doi: 10.3389/fnins.2017.00041
32. Chen H, Wei X, Cho KS, Chen G, Sappington R, Calkins DJ, et al. Optic neuropathy due to microbead-induced elevated intraocular pressure in the mouse. *Invest Ophthalmol Vis Sci.* (2011) 52:36–44. doi: 10.1167/iovs.09-5115
33. Moreno MC, Marcos HJ, Oscar Croxatto J, Sande PH, Campanelli J, Jaliffa CO, et al. A new experimental model of glaucoma in rats through intracameral injections of hyaluronic acid. *Exp Eye Res.* (2005) 81:71–80. doi: 10.1016/j.exer.2005.01.008
34. Turner AJ, Vander Wall R, Gupta V, Klistorner A, Graham SL. DBA/2J mouse model for experimental glaucoma: pitfalls and problems. *Clin Exp Ophthalmol.* (2017) 45:911–22. doi: 10.1111/ceo.12992
35. Kipfer-Kauer A, McKinnon SJ, Frueh BE, Goldblum D. Distribution of amyloid precursor protein and amyloid-beta in ocular hypertensive C57BL/6 mouse eyes. *Curr Eye Res.* (2010) 35:828–34. doi: 10.3109/02713683.2010.494240
36. Tsai T, Reinehr S, Maliha AM, Joachim SC. Immune Mediated Degeneration and Possible Protection in Glaucoma. *Front Neurosci.* (2019) 13:931. doi: 10.3389/fnins.2019.00931
37. Neufeld AH. Microglia in the optic nerve head and the region of parapapillary chorioretinal atrophy in glaucoma. *Arch Ophthalmol.* (1999) 117:1050–6. doi: 10.1001/archopht.117.8.1050
38. Wang X, Tay SS, Ng YK. An immunohistochemical study of neuronal and glial cell reactions in retinae of rats with experimental glaucoma. *Exp Brain Res.* (2000) 132:476–84. doi: 10.1007/s002210000360
39. Ramírez AI, de Hoz R, Fernández-Albarral JA, Salobrar-Garcia E, Rojas B, Valiente-Soriano FJ, et al. Time course of bilateral microglial activation in a mouse model of laser-induced glaucoma. *Sci Rep.* (2020) 10:4890. doi: 10.1038/s41598-020-61848-9
40. Gaffen SL. Recent advances in the IL-17 cytokine family. *Curr Opin Immunol.* (2011) 23:613–9. doi: 10.1016/j.coi.2011.07.006
41. Kuwabara T, Ishikawa F, Kondo M, Kakiuchi T. The Role of IL-17 and Related Cytokines in Inflammatory Autoimmune Diseases. *Mediators Inflamm.* (2017) 2017:3908061. doi: 10.1155/2017/3908061
42. Ren Y, Qi Y, Su X. Th17 cells in glaucoma patients promote Ig production in IL-17A and IL-21-dependent manner. *Clin Exp Pharmacol Physiol.* (2019) 46:875–82. doi: 10.1111/1440-1681.13141
43. Chen J, Liu X, Zhong Y. Interleukin-17A: The Key Cytokine in Neurodegenerative Diseases. *Front Aging Neurosci.* (2020) 12:566922. doi: 10.3389/fnagi.2020.566922
44. Cherry JD, Olschowka JA, O'Banion MK. Neuroinflammation and M2 microglia: the good, the bad, and the inflamed. *J Neuroinflammation.* (2014) 11:98. doi: 10.1186/1742-2094-11-98
45. Wei X, Cho KS, Thee EF, Jager MJ, Chen DF. Neuroinflammation and microglia in glaucoma: time for a paradigm shift. *J Neurosci Res.* (2019) 97:70–6. doi: 10.1002/jnr.24256
46. Cerri E, Fabiani C, Criscuolo C, Domenici L. Visual Evoked Potentials in Glaucoma and Alzheimer's Disease. *Methods Mol Biol.* (2018) 1695:69–80. doi: 10.1007/978-1-4939-7407-8_7
47. Domenici L, Origlia N, Falsini B, Cerri E, Barloscio D, Fabiani C, et al. Rescue of retinal function by BDNF in a mouse model of glaucoma. *PLoS ONE.* (2014) 9:e115579. doi: 10.1371/journal.pone.0115579
48. Leung CK, Lindsey JD, Chen L, Liu Q, Weinreb RN. Longitudinal profile of retinal ganglion cell damage assessed with blue-light confocal scanning laser ophthalmoscopy after ischaemic reperfusion injury. *Br J Ophthalmol.* (2009) 93:964–8. doi: 10.1136/bjo.2008.150482
49. Feng L, Chen H, Suyeoka G, Liu X. A laser-induced mouse model of chronic ocular hypertension to characterize visual defects. *J Vis Exp.* (2013). doi: 10.3791/50440
50. Yun H, Lathrop KL, Yang E, Sun M, Kagemann L, Fu V, et al. A laser-induced mouse model with long-term intraocular pressure elevation. *PLoS ONE.* (2014) 9:e107446. doi: 10.1371/journal.pone.0107446
51. Zhu Y, Zhang L, Schmidt JF, Gidday JM. Glaucoma-induced degeneration of retinal ganglion cells prevented by hypoxic preconditioning: a model of glaucoma tolerance. *Mol Med.* (2012) 18:697–706. doi: 10.2119/molmed.2012.00050
52. Liu HH, Flanagan J. A mouse model of chronic ocular hypertension induced by circumlimbal suture. *Invest Ophthalmol Vis Sci.* (2017) 58:353–61. doi: 10.1167/iovs.16-20576

Conflict of Interest: The authors declare that the research was conducted in the absence of any commercial or financial relationships that could be construed as a potential conflict of interest.

frontiers in Medicine

CORRECTION
published: 30 April 2021
doi: 10.3389/fmed.2021.687339

Corrigendum: Evaluation of the Effectiveness of a Chronic Ocular Hypertension Mouse Model Induced by Intracameral Injection of Cross-Linking Hydrogel

Junjue Chen[1†], *Jun Sun*[1†], *Huan Yu*[1], *Ping Huang*[2*] *and Yisheng Zhong*[1*]

[1] Department of Ophthalmology, Ruijin Hospital, Shanghai Jiao Tong University School of Medicine, Shanghai, China, [2] Shanghai Key Laboratory for Bone and Joint Diseases, Shanghai Institute of Traumatology and Orthopedics, Ruijin Hospital Affiliated Medical School, Shanghai Jiaotong University, Shanghai, China

Keywords: glaucoma, animal model, mice, cross-linking hydrogel, intracameral injection

OPEN ACCESS

Approved by:
Frontiers Editorial Office, Frontiers Media SA, Switzerland

***Correspondence:**
Yisheng Zhong
yszhong68@126.com
Ping Huang
pinghpingh@126.com

[†]These authors have contributed equally to this work and share first authorship

Specialty section:
This article was submitted to Ophthalmology, a section of the journal Frontiers in Medicine

Received: *29 March 2021*
Accepted: *30 March 2021*
Published: *30 April 2021*

Citation:
Chen J, Sun J, Yu H, Huang P and Zhong Y (2021) Corrigendum: Evaluation of the Effectiveness of a Chronic Ocular Hypertension Mouse Model Induced by Intracameral Injection of Cross-Linking Hydrogel. Front. Med. 8:687339. doi: 10.3389/fmed.2021.687339

A Corrigendum on

Evaluation of the Effectiveness of a Chronic Ocular Hypertension Mouse Model Induced by Intracameral Injection of Cross-Linking Hydrogel
by Chen, J., Sun, J., Yu, H., Huang, P., and Zhong, Y. (2021). Front. Med. 8:643402. doi: 10.3389/fmed.2021.643402

In the original article, there was an error. The corresponding author's email was incorrectly spelled as "yszhong@126.com." The correct email is yszhong68@126.com.

The authors apologize for this error and state that this does not change the scientific conclusions of the article in any way. The original article has been updated.

frontiers in Medicine

ORIGINAL RESEARCH
published: 29 April 2021
doi: 10.3389/fmed.2021.625487

Development and Validation of Automated Visual Field Report Extraction Platform Using Computer Vision Tools

Murtaza Saifee[1], *Jian Wu*[1,2], *Yingna Liu*[1], *Ping Ma*[1,3], *Jutima Patlidanon*[1,4], *Yinxi Yu*[5], *Gui-Shuang Ying*[5] *and Ying Han*[1,6*]

[1] Department of Ophthalmology, University of California, San Francisco, San Francisco, CA, United States, [2] Beijing Ophthalmology and Visual Science Key Lab, Beijing Tongren Eye Center, Beijing Tongren Hospital, Beijing Institute of Ophthalmology, Capital Medical University, Beijing, China, [3] Department of Ophthalmology, Shandong Provincial Hospital, Shandong First Medical University, Jinan, China, [4] Department of Ophthalmology, Bhumibol Adulyadej Hospital, Bangkok, Thailand, [5] Center for Preventive Ophthalmology and Biostatistics, Perelman School of Medicine, University of Pennsylvania, Philadelphia, PA, United States, [6] Ophthalmology Section, Surgical Service, San Francisco Veterans Affairs Medical Center, San Francisco, CA, United States

Purpose: To introduce and validate hvf_extraction_script, an open-source software script for the automated extraction and structuring of metadata, value plot data, and percentile plot data from Humphrey visual field (HVF) report images.

Methods: Validation was performed on 90 HVF reports over three different report layouts, including a total of 1,530 metadata fields, 15,536 value plot data points, and 10,210 percentile data points, between the computer script and four human extractors, compared against DICOM reference data. Computer extraction and human extraction were compared on extraction time as well as accuracy of extraction for metadata, value plot data, and percentile plot data.

Results: Computer extraction required 4.9-8.9 s per report, compared to the 6.5-19 min required by human extractors, representing a more than 40-fold difference in extraction speed. Computer metadata extraction error rate varied from an aggregate 1.2-3.5%, compared to 0.2-9.2% for human metadata extraction across all layouts. Computer value data point extraction had an aggregate error rate of 0.9% for version 1, <0.01% in version 2, and 0.15% in version 3, compared to 0.8-9.2% aggregate error rate for human extraction. Computer percentile data point extraction similarly had very low error rates, with no errors occurring in version 1 and 2, and 0.06% error rate in version 3, compared to 0.06-12.2% error rate for human extraction.

Conclusions: This study introduces and validates hvf_extraction_script, an open-source tool for fast, accurate, automated data extraction of HVF reports to facilitate analysis of large-volume HVF datasets**,** and demonstrates the value of image processing tools in facilitating faster and cheaper large-volume data extraction in research settings.

Keywords: glaucoma, visual field, neuroophthalmogy, optical character reader, computer vision and image processing

OPEN ACCESS

Edited by:
Soosan Jacob,
Dr. Agarwal's Eye Hospital, India

Reviewed by:
Haotian Lin,
Sun Yat-sen University, China
Saif Aldeen AlRyalat,
The University of Jordan, Jordan

***Correspondence:**
Ying Han
ying.han@ucsf.edu

Specialty section:
This article was submitted to Ophthalmology, a section of the journal Frontiers in Medicine

Received: *03 November 2020*
Accepted: *31 March 2021*
Published: *29 April 2021*

Citation:
Saifee M, Wu J, Liu Y, Ma P, Patlidanon J, Yu Y, Ying G-S and Han Y (2021) Development and Validation of Automated Visual Field Report Extraction Platform Using Computer Vision Tools. Front. Med. 8:625487. doi: 10.3389/fmed.2021.625487

INTRODUCTION

Within ophthalmology, large volume data analysis requires structured data to perform. Data extraction and structuring are often a critical and overlooked aspect of such projects. Especially with the advent of machine learning and other "large data" processing techniques, there is a strong need for fast, cheap, and reliable data extraction to develop large databases for analysis and academic research, for data such as automated perimetry reports or ophthalmic imaging data (1). Indeed, some of the data can be extracted *via* manufacture-provided licensed software (2), but they are often expensive and can be cost prohibitive for many institutions and practices. Alternatively, study data can be manually transcribed by trained researchers, but this is costly and tedious with high risk for human error (3–5), which limits the types and scope of research projects that can be done.

Static automated perimetry exemplifies this issue well. Perimetry data involves large volume of quantitative data for each location tested, often done serially to track longitudinal progression in conditions such as glaucoma or neuro-ophthalmic disease. Such data can be analyzed using a variety of analysis techniques with both global and localized metrics (6, 7). One challenge in managing the large volume of perimetry data is obtaining accurate and detailed data points from each test (8). Therefore, most recent studies rely on small and single institution datasets containing hundreds of eyes (9). Few studies examining automated perimetry have datasets up to 2,000-3,000 eyes or more, with one study requiring the development of an in-house data extraction software system (10, 11). These studies indicate that there is an unmet need to develop methods to automatically and accurately extract large volume of perimetry studies, which is critical to building massive perimetry datasets for future detection and progression study in the ophthalmology field.

To solve this need in the field of automated perimetry, we have developed and validated a software platform for extraction of Humphrey® Visual Field (HVF) reports, a form of static automated perimetry used widely in clinical environments. Our aim in developing this platform was to automate HVF report data extraction in a fast, accurate way to facilitate (1) development of large-volume datasets for clinical research and (2) novel methodologies in computational analysis of perimetry data.

METHODS

Description and Development of Platform

The software platform was developed by the author (MS) using Python 3.6.4 (12). The software leverages OpenCV 3.4.3 (13), an open source computer vision library, for image processing and figure detection, Tesseract 4.1.1 (14), an open source optical character recognition library, for metadata extraction, and Fuzzywuzzy (15), a fuzzy regular expression library for text matching. DICOM file reading was done using PyDICOM, an open-source DICOM reading package (16). Development and testing was performed on a MacBook Air (mid-2013) running Catalina 10.15.2 (Apple Inc, Cupertino, CA, USA).

In broad detail, this software platform takes as input HVF report image files, "extracts" data from the report image, and outputs structured, digital data represented in that report (**Figure 1**). The data on the HVF report image is categorized into three data types: metadata, value plot data, and percentile plot data.

Metadata is defined as any data to be extracted not included within visual field plots. Within HVF reports, 17 fields are identified to be extracted by the platform:

1. Name
2. ID
3. Date of birth
4. Test date
5. Laterality (right or left)
6. Foveal sensitivity
7. False positive rate
8. False negative rate
9. Fixation loss rate
10. Test duration
11. Field size
12. Test strategy
13. Pupil diameter
14. Refraction used
15. Mean deviation
16. Pattern standard deviation
17. Visual Field Index (VFI).

To extract the data, the software first crops the image containing the metadata of interest and applies optical character recognition (OCR) using Tesseract. The resulting text data is then processed using regular expressions and string matching to structure and standardize the text data into the expected metadata fields.

Value plots are defined as plots with numerical perimetry data, that is, raw sensitivity plot data, total deviation value plot data, and pattern deviation value plot data (**Figure 1**). To extract data, the software locates the plot by identifying the plot axes and subsequently crops the plot image. It then aligns the plot to a 10 $\times$ 10 grid, and each cell is processed using a custom-built optical character recognition system (based on template matching) in order to determine and extract the value of the cell.

Percentile plots were defined as plots percentile sensitivity data values, that is, total deviation percentile plot data and pattern deviation percentile plot data (**Figure 1**). Percentile plots are processed in an identical fashion to value plots, but each cell is processed using a separate template-matching based system to determine the icon of the cell.

Data processed by the platform is represented and stored in an object-oriented format and can be used for further processing within the Python environment.

In addition to HVF report images, the software platform can also accept other types of input such as ophthalmic visual field (OPV) DICOM files containing HVF data and text serialization files in Javascript Object Notation (JSON) format that have been outputted by the software platform. An example of the output text file is shown in **Figure 2**.

The perimetry data processed by the platform can be analyzed and processed internally within the Python environment, output as a JSON text file (e.g., to be re-imported and processed by the

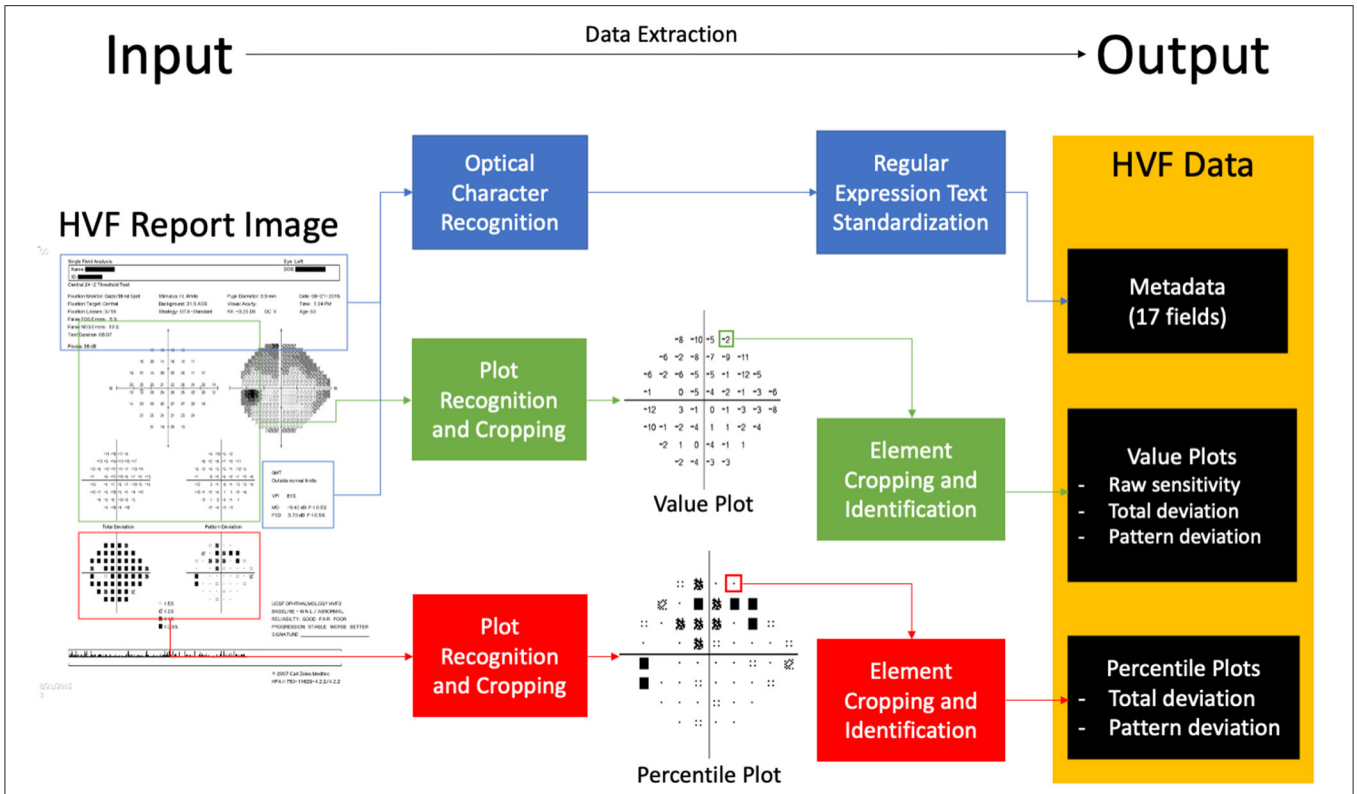

FIGURE 1 | Block diagram of extraction software. An input visual field report identifies areas of metadata, value plots and percentile plots, processes and extracts data, and outputs structured data.

software platform at a different time) or output as a tab-delimited file to be imported into a spreadsheet processing software.

The software scripting platform was open-sourced under the GPL 3.0 license (17).

Extraction Platform Validation

This study was compliant with the Health Insurance Portability and Accountability Act and the Declaration of Helsinki for research involving human participants. Institutional Review Board approval was obtained from the University of California, San Francisco Human Research Protection Program.

Visual Field Testing

All VF examinations and reports were done by a Humphrey VF analyzer (HFA2 or HFA3) (Carl Zeiss Ophthalmic Systems, Inc., Dublin, CA) on a 10-2, 24-2 or 30-2 test pattern, size III white stimulus, with a Swedish Interactive Threshold Algorithm (SITA) strategy. Reports were exported as a.PNG image to the ophthalmology department picture archiving and communication system (PACS) server and downloaded from the server.

HVF Report Dataset Collection—Selection, Inclusion, and Exclusion Criteria

Three different types of HVF report resolution/layout formats (version 1, 2, and 3 layouts) present in the PACS system of our institution were identified. Examples of these layouts are shown in **Figure 3**. Image dimensions for these layouts are:

Version 1: 650 pixels by 938 pixels (HFA2, low resolution)
Version 2: 2,400 pixels by 3,180 pixels (HFA2, high resolution)
Version 3: 3,726 pixels by 5,262 pixels (HFA3, high resolution)

A total of 90 HVF report images, with 30 HVFs for each layout version, was collected for validation. The sample size was determined by preliminary extraction tests to ensure valid statistical comparisons. Based on preliminary extraction runs, a human extraction accuracy of 98% and a computer extraction accuracy of 99.3% was assumed. At an alpha level of 0.05 and a power of 90%, assuming a 1:1 study ratio, sample size calculations determined a minimum of 1,808 data points was needed to detect a statistically significant difference; this equates to a minimum of 18 visual field reports. A set size of 30 was chosen to meet and exceed this minimum requirement.

All HVF reports were collected from patients seen at the University of California, San Francisco Ophthalmology Visual Field Testing Clinic. For version 1 layout, 30 historical HVF reports were taken from consecutive patients 2014 or prior. For version 2 layout, 30 HVF reports were selected from consecutive patients seen from March 4, 2019 to March 5, 2019. For version 3, 30 HVF reports taken from consecutive patients seen from August 30, 2019 onward.

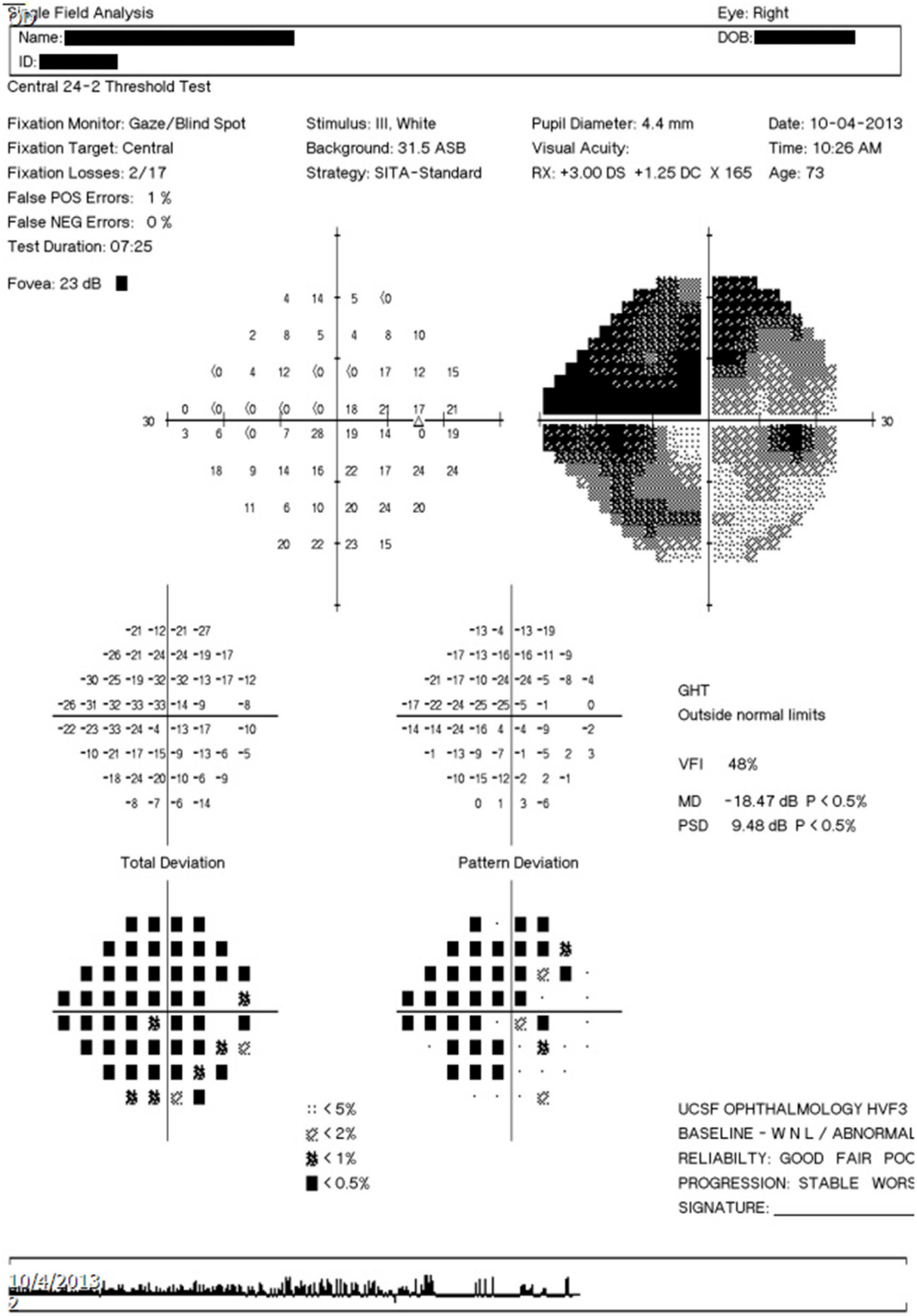

FIGURE 2 | Example output text file. Example output text file corresponding to the image report seen in **Figure 3C**.

A maximum of two HVFs per patient were selected (one for each eye). Only HVFs with strategy SITA-Standard, SITA-Fast or SITA-Faster were included; HVFs performed with a Full-Threshold strategy or any other strategy were excluded. There was no inclusion or exclusion criteria based on patient diagnosis, reliability indices, mean deviation, or type of defect noted.

Data Extraction and Accuracy Measurements

Four human extractors, all ophthalmologists familiar with reading HVF reports, were selected. Each extractor manually recorded the data from each HVF report into a spreadsheet, as well as time required for extraction. Each extractor was allowed to perform extraction independently, without proctoring, in an environment they selected as optimal. In addition to manual human extraction, each HVF report image was processed using the data extraction software script.

Each set of extracted data (from human extractors and software extractions script) was compared against data obtained from the DICOM OPV file representing the report of interest, obtained from the Humphrey Field Analyzer device. A custom testing platform, written in Python, was developed to compare these outputs.

Metadata fields were compared on a per-field basis; field were considered correct if the computer image extraction matched exactly to the DICOM reference. Two types of inaccuracy were determined by a masked grader who was blind to human or software data extraction (YH). Formatting inconsistencies were defined as when the extracted data was different from the DICOM reference in a minor way, such that the data still provided correct information; examples include case inconsistencies, whitespace differences, and differences in date reporting. True errors were defined as all other field inequalities that did not represent the correct data.

A

JSON Example.txt


```
{
    "id": "<Deleted>",
    "name": "<Deleted>",
    "dob": "<Deleted>",
    "test_date": "Apr 09, 2019",
    "laterality": "Left",
    "fovea": "34",
    "fixation_loss": "0/16",
    "false_pos": "0%",
    "false_neg": "0%",
    "field_size": "24-2",
    "strategy": "SITA Standard",
    "test_duration": "06:43",
    "pupil_diameter": "3.9",
    "rx": "+0.75DS",
    "md": "-6.51",
    "psd": "7.21",
    "vfi": "85%",
    "raw_value_plot": [
        "   |   |   |   |   |   |   |   |   |   ",
        "   |   |   |  3| 14| 13| 20|   |   |   ",
        "   |   |  0| 25| 26| 24| 27| 19|   |   ",
        "   |  8| 10| 18| 27| 26| 28| 27| 24|   ",
        "   | <0| 15| 28| 30| 25| 30| 31| 28| 22",
        "   | <0| <0| 27| 30| 26| 30| 29| 26| 18",
        "   | 24| 30| 29| 24| 20| 27| 25| 22|   ",
        "   |   | 27| 28| 24| 25| 27| 29|   |   ",
        "   |   |   | 26| 18| 17| 22|   |   |   ",
        "   |   |   |   |   |   |   |   |   |   "
    ],
    "absolute_value_plot": [
        "   |   |   |   |   |   |   |   |   |   ",
        "   |   |   |-23|-13|-13| -7|   |   |   ",
        "   |   |-27| -3| -3| -5| -2|-10|   |   ",
        "   |-20|-19|-12| -3| -5| -2| -3| -4|   ",
        "   |-31|   | -3| -2| -7| -1|  0| -1| -4",
        "   |-32|   | -4| -2| -7| -2| -2| -4| -9",
        "   | -5| -1| -2| -7|-12| -5| -5| -7|   ",
        "   |   | -3| -2| -6| -6| -3| -1|   |   ",
        "   |   |   | -4|-11|-12| -6|   |   |   ",
        "   |   |   |   |   |   |   |   |   |   "
    ]
```


FIGURE 3 | Continued

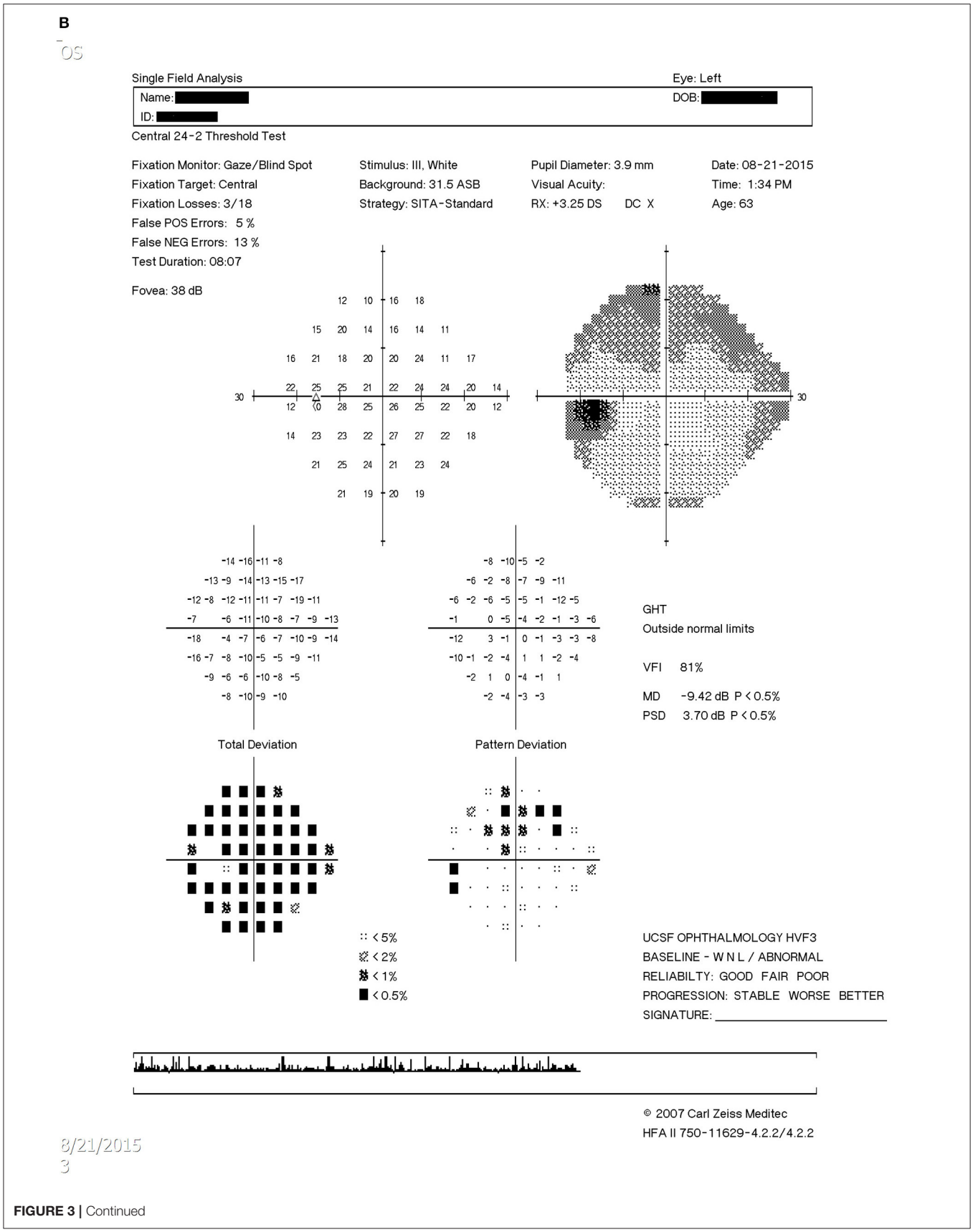

FIGURE 3 | Continued

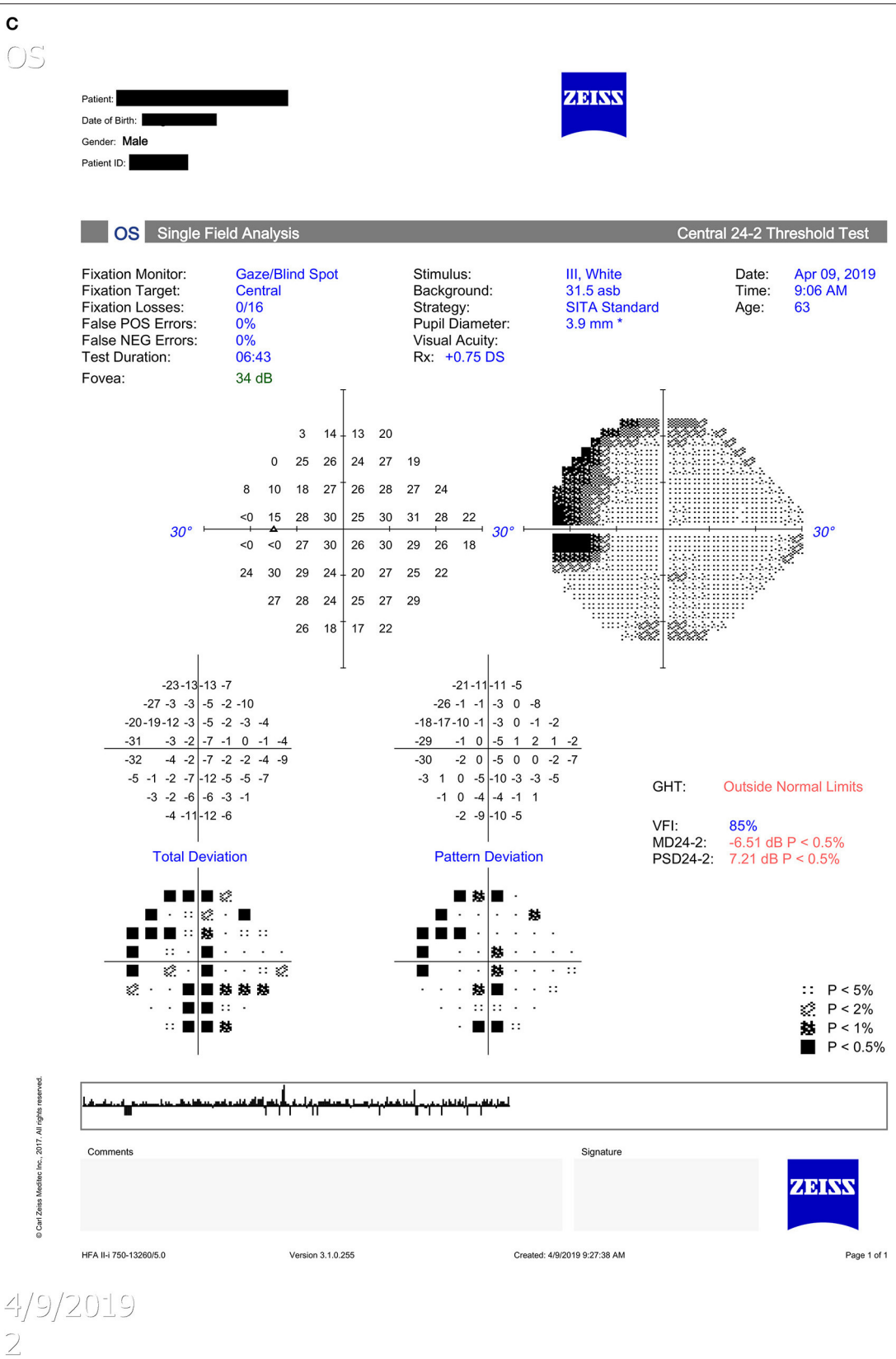

FIGURE 3 | Humphrey Visual Field report layout types. **(A)** Version 1 layout. **(B)** Version 2 layout. **(C)** Version 3 layout.

Data points from value plots and percentile plots were compared on a per data point basis, among all non-empty value data points within value plots. Data points were considered correct if the value from the extraction exactly matched the DICOM reference value.

Statistical Analysis

For each HVF record, we calculated the total number of errors for extracting metadata, value plot data, percentile plot by using computer script, and four human extractors. We summarized the errors using total number of errors from all records of each HVF layout (e.g., aggregate errors), aggregate error rate (calculated as aggregate errors divided by the total number of fields tested) and its 95% binomial confidence intervals, and median (interquartile) of number of errors in each HVF record. For each of HVF layout, we compared between computer script and each of four human extractors in the mean time used for data extraction using repeated measures one-way analysis of variance and in the number of errors per HVF record using Friedman's Chi-Square test due to skewed distribution. All the statistical analyses were performed in SAS v9.4 (SAS Institute Inc., Cary, NC), and two-sided $p < 0.05$ was considered to be statistically significant.

TABLE 1 | Characteristics of validation set visual field reports.

	V1 Layout ($n = 30$)	V2 Layout ($n = 30$)	V3 Layout ($n = 30$)
Number of patients	16	16	17
Number of eyes	15	14	13
Right			
Left	15	16	17
Field Size	21	24	22
24-2			
30-2	8	4	6
10-2	1	2	2
Average mean deviation (dB)	−4.81	−3.45	−2.44
>-6.0	24	26	28
−6.0 to −12.0	3	2	1
< −12.0	3	2	1
Average pattern standard deviation (dB)	4.50	2.74	3.43
Total number of metadata fields tested	510	510	510
Total number of value plot data points tested	5,263	5,045	5,228
Total number of percentile plot data points tested	3,453	3,309	3,448

RESULTS

The HVF extraction program was developed in line with the specifications outlined in the Methods section. It is available free for access and usage at https://pypi.org/project/hvf-extraction-script/. Its source code can be found at https://github.com/msaifee786/hvf_extraction_script.

Characteristics of the HVF reports for each layout version is shown in **Table 1**. A total of 1,530 metadata fields, 15,536 value plot data points, and 10,210 percentile data points were tested over three layout version groups. Each group included a similar number of right and left eyes and included at least one report from each field size test. There was representation from each severity of visual field defect based on mean deviation magnitude.

Validation was performed between the computer extraction and human extraction for each HVF layout, measuring extraction times (**Table 2**), metadata error rates (**Table 3A**) and format inconsistencies (**Table 3B**), value plot error rates (**Table 4**) and percentile plot error rates (**Table 5**). Notably, minor post-processing editing was done on the human extraction datasets in order to standardized formatting prior to validation testing. Human extractor P2 mislabeled three files in the V1 layout data due to a skip in the sequential numbering; this was corrected prior to the validation comparison. Human extractor P4 skipped a column field in the extracted dataset, which was added in (with blank values) to standardized format prior to validation comparison. Lastly, datasets for P3 and P4 required trivial substitutions of characters (e.g., upper to lower case conversion).

Extraction Times

Average extraction time for the computer platform varied from 4.9 to 8.9 s, with minimal variation between the different layouts (**Table 2**). The highest resolution V3 layout had the longest average computer extraction time. Human extractors had average extraction times varying from 394 to 1,190 s for all three versions, with a statistically significant longer time in comparison to computer extraction ($p < 0.001$). There was no clear difference in human extraction time among different versions. In general, the computer platform performed extractions on the order of 50-100 times faster than human extractions.

Metadata Extraction

Within the computer extraction group, there were a total of 32 metadata extraction errors across all three layouts, with a per-layout error rate varying from 1.2-3.5%, with the highest error rate occurring the V1 layout group (**Table 3A**). The highest frequency of extraction errors was due to incorrect character recognition (seven errors). Among all four human extractors, the average per-layout error rate varied from 2.5-4.4%. Examples of metadata extraction errors that occurred in this study are shown in **Table 6**.

Computer extraction overall performed similarly to human extraction for metadata. In V1 layout, there was no difference between the computer and human extractors. Computer had a lower number of metadata errors than P2 and P3 in V2 layout and P3 in V3 layout, while P4 had less metadata errors than computer in V2 and V3 layouts. There was nearly no significant difference between format inconsistencies between the computer and human extractions in any version layout (**Table 3B**).

Value Plot Extraction

For every layout, value plot extraction errors were less for computer extraction than every human extractor (**Table 4**). These comparisons were statistically significant in layouts V2 and V3.

TABLE 2 | Extraction times for each resolution layout.

Extraction Time per report (secs)	Computer program (*N* = 30)	Human 1 (*N* = 30)	Human 2 (*N* = 30)	Human 3 (*N* = 30)	Human 4 (*N* = 30)
V1 layout					
Mean (SD)	6.0 (0.7)	598.0 (187.4)	1,190.0 (274.8)	886.0 (281.7)	966.0 (228.0)
P-value	Reference	<0.001	<0.001	<0.001	<0.001
V2 layout					
Mean (SD)	4.9 (0.6)	440.0 (53.0)	846.0 (137.7)	768.0 (201.4)	748.0 (173.1)
P-value	Reference	<0.001	<0.001	<0.001	<0.001
V3 layout					
Mean (SD)	8.9 (0.8)	394.0 (62.4)	808.0 (150.1)	728.3 (196.2)	708.0 (192.6)
P-value	Reference	<0.001	<0.001	<0.001	<0.001

Extraction times from the computer program was used as reference for all statistical comparisons within each layout.

TABLE 3A | Comparison between computer program and human metadata extraction (Metadata errors).

Metadata errors	Computer program (*N* = 30)	Human 1 (*N* = 30)	Human 2 (*N* = 30)	Human 3 (*N* = 30)	Human 4 (*N* = 30)
V1 layout					
Total errors	18	10	16	24	9
Percentage of total error %*	3.5 (2.1-5.5)	2.0 (0.9-3.6)	3.1 (1.8-5.0)	4.7 (3.0-6.9)	1.8 (0.8-3.3)
Median (Q1, Q3) error per report**	0 (0, 1)	0 (0, 1)	0 (0, 1)	1 (0, 1)	0 (0, 0)
P-value	Reference	0.80	0.56	0.09	0.41
V2 layout					
Total errors	6	6	32	47	4
Percentage of total error %*	1.2 (0.4-2.5)	1.2 (0.4-2.5)	6.3 (4.3-8.7)	9.2 (6.9-12.1)	0.8 (0.2-2.0)
Median (Q1, Q3) error per report**	0 (0, 0)	0 (0, 0)	1 (0, 2)	1 (1, 2)	0 (0, 0)
P-value	Reference	0.01	0.001	<0.001	0.046
V3 layout					
Total errors	8	7	10	33	1
Percentage of total error %*	1.6 (0.7-3.1)	1.4 (0.6-2.8)	2.0 (0.9-3.6)	6.5 (4.5-9.0)	0.2 (0.0-1.1)
Median (Q1, Q3) error per report **	0 (0, 0)	0 (0, 0)	0 (0, 1)	1 (1, 2)	0 (0, 0)
P-value	Reference	1.00	0.62	<0.001	0.03

**Numbers in parenthesis indicate 95% confidence interval.*
***Q1, Q3 refer to first and third quartile, respectively.*

The highest number of value plot errors among human extractors were due to P2 and P4; a large number of these errors occurred due to a frame shift error for all left eyes. Examples of value plot errors that occurred in this study are shown in **Table 6**.

Computer extraction value plot errors occurred predominantly within the V1 layout extraction; most of the errors occurred as a misidentification between 4, 6, and 8, as well as between 1 and 7 (**Table 6**). Majority of these occurred in the raw value plot, while the remaining errors occurred in the total deviation value plot. These errors occurred in scattered parts of the plot with no association to a specific location. In the V2 and V3 layout value plot extraction, all errors occurred in the raw value plot along the horizontal midline in the temporal field (i.e., corresponding to the area of the physiologic blind spot). Almost uniformly for these errors, the areas had a reduced sensitivity value (often "0" or "<0") and an adjacent open triangle icon (or fragment thereof) near the value.

Percentile Plot Extraction

Overall, percentile plot extraction errors occurred rarely in the computer extraction (**Table 5**). No computer extraction percentile plot extraction errors occurred in the V1 and V2 layout. Two errors occurred in the V3 layout in total deviation percentile plots. The computer performed nominally lower than every human extractor for every layout; all but two of these comparisons (P3 in V1 and P1 in V3) were statistically significant.

DISCUSSION

To our knowledge, this is the first open-source data extraction software script for perimetry output in the literature. The main purpose of the development of this platform is to improve our ability to research and analyze perimetry data and ultimately to better guide treatment of vision-threatening diseases. To that

TABLE 3B | Comparison between computer program and human metadata extraction (format inconsistencies).

Metadata format inconsistencies	Computer Program (*N* = 30)	Human 1 (*N* = 30)	Human 2 (*N* = 30)	Human 3 (*N* = 30)	Human 4 (*N* = 30)
V1 layout					
Total number	8	7	7	8	10
Percentage of total inconsistency %*	1.6 (0.7-3.1)	1.3 (0.6-2.8)	1.3 (0.6-2.8)	1.6 (0.7-3.1)	2.0 (0.9-3.6)
Median (Q1, Q3) inconsistencies per report**	0 (0, 1)	0 (0, 0)	0 (0, 0)	0 (0, 1)	0 (0, 1)
P-value	Reference	0.56	0.56	1.00	0.41
V2 layout					
Total number	4	2	6	5	9
Percentage of total inconsistency %*	0.8 (0.2-2.0)	0.4 (0.1-1.4)	1.2 (0.4-2.5)	1.0 (0.3-2.3)	1.8 (0.8-3.3)
Median (Q1, Q3) number of inconsistencies per report**	0 (0, 0)	0 (0, 0)	0 (0, 0)	0 (0, 0)	0 (0, 1)
P-value	Reference	0.16	0.41	0.32	0.03
V3 layout					
Total number	3	0	5	4	7
Percentage of total inconsistency %*	0.6 (0.1-1.7)	0 (0.0-0.7)	1.0 (0.3-2.3)	0.8 (0.2-2.0)	1.4 (0.6-2.8)
Median (Q1, Q3) number of inconsistencies per report**	0 (0, 0)	0 (0, 0)	0 (0, 0)	0 (0, 0)	0 (0, 0)
P-value	Reference	0.08	0.32	0.56	0.16

**Numbers in parenthesis indicate 95% confidence interval.*
***Q1, Q3 refer to first and third quartile, respectively.*

TABLE 4 | Comparison between computer program and human on value plot extraction errors.

Value plot errors	Computer program (*N* = 30)	Human 1 (*N* = 30)	Human 2 (*N* = 30)	Human 3 (*N* = 30)	Human 4 (*N* = 30)
V1 layout					
Total errors	46	197	603	47	563
Percentage of total error %*	0.9 (0.6-1.2)	3.7 (3.3-4.3)	11.5 (10.6-12.4)	0.9 (0.7-1.2)	10.7 (9.9-11.6)
Median (Q1, Q3) errors per report**	1.5 (1, 2)	3.5 (2, 8)	2.5 (0, 53)	1 (0, 2)	1.5 (0, 52)
P-value	Reference	<0.001	0.16	0.30	0.69
V2 layout					
Total errors	2	155	730	48	760
Percentage of total error %*	0.0 (0-0.1)	3.1 (2.6-3.6)	14.5 (13.5-15.5)	1.0 (0.7-1.3)	15.1 (14.1-16.1)
Median (Q1, Q3) errors per report**	0 (0, 0)	1 (0, 3)	4.5 (0, 54)	1 (0, 2)	2.5 (0, 54)
P-value	Reference	<0.001	<0.001	<0.001	<0.001
V3 layout					
Total errors	8	118	768	97	653
Percentage of total error %*	0.2 (0.1-0.3)	2.3 (1.9-2.7)	14.7 (13.7-15.7)	1.9 (1.5-2.3)	12.5 (11.6-13.4)
Median (Q1, Q3) errors per report**	0 (0, 1)	2 (1, 5)	3 (1, 53)	0.5 (0, 3)	2 (0, 52)
P-value	Reference	<0.001	<0.001	0.04	<0.001

**Numbers in parenthesis indicate 95% confidence interval.*
***Q1, Q3 refer to first and third quartile, respectively.*

end, this code has been made available through the Python Package Index (PyPi), and its source code has been published as open source, available through GitHub. We encourage anyone to utilize this program, scrutinize its effectiveness, improve upon it and adapt it for their own uses.

The method employed to extract data from HVF perimetry reports in this script is optical character recognition (OCR) technology, which has been available since the 1950s (18). Recently, this technology has improved significantly with improved image processing techniques and the advent of neural networks. In the literature, studies that have specifically used OCR technology for medical data exaction tasks mostly focus on scanned reports for clinical laboratory tests, with reasonably high accuracy (19–21). Adamo et al. utilized Tesseract OCR (the same OCR platform as used in our script) to achieve an accuracy of 95% in their extraction system (19). Another team was able to achieve a similar accuracy of 92.3-95.8% using a custom neural network model on multilingual reports containing Chinese and

TABLE 5 | Comparison between computer program and human on percentile plot extraction errors.

Percentile plot errors	Computer program (*N* = 30)	Human 1 (*N* = 30)	Human 2 (*N* = 30)	Human 3 (*N* = 30)	Human 4 (*N* = 30)
V1 layout					
Total errors	0	54	302	9	289
Percentage of total error %*	0 (0-0.1)	1.6 (1.2-2.0)	8.8 (7.8-9.7)	0.2 (0.1-0.5)	8.4 (7.5-9.3)
Median (Q1, Q3) errors per report**	0 (0, 0)	0 (0, 3)	5 (0, 21)	0 (0, 0)	1.5 (0, 24)
P-value	Reference	0.003	<0.001	0.08	<0.001
V2 layout					
Total errors	0	26	356	38	372
Percentage of total error %*	0 (0-0.1)	0.8 (0.5-1.2)	10.8 (9.7-11.9)	1.2 (0.8-1.6)	11.2 (10.2-12.4)
Median (Q1, Q3) errors per report**	0 (0, 0)	0 (0, 0)	4 (0, 22)	0 (0, 0)	9 (0, 22)
P-value	Reference	0.008	<0.001	0.01	<0.001
V3 layout					
Total errors	2	2	435	55	273
Percentage of total error %*	0.1 (0.0-0.2)	0.1 (0.0-0.2)	12.6 (11.5-13.8)	1.6 (1.2-2.1)	7.9 (7.0-8.9)
Median (Q1, Q3) errors per report**	0 (0, 0)	0 (0, 0)	10 (0, 23)	0 (0, 1)	1 (0, 20)
P-value	Reference	1.00	<0.001	0.02	0.002

**Numbers in parenthesis indicate 95% confidence interval.*
***Q1, Q3 refer to first and third quartile, respectively.*

TABLE 6 | Examples of extraction errors.

Field	Extracted Value	True Value	Type of Error
Computer Extractions			
Metadata			
Test Duration	06:54	06:543	Erroneous extra value
Mean Deviation	0.47	−0.47	Dropped minus sign
Refraction Used	−0.75DS +1.26DC X 88	−0.75DS +1.25DC X 88	Incorrect character recognition
Pupil Diameter	4.1	4.7	Incorrect character recognition
Value Plot			
	24	28	Incorrect character recognition
	21	27	Incorrect character recognition
Human Extractions			
Metadata			
Mean Deviation	−0.3	−0.39	Missed digit
Test Duration	06:15	06:16	Incorrect character recognition
Refraction Used	−1.5DS DC X	−2.00DS +3.00DC X 175	Incorrect field extracted
Strategy	SITA Standard	SITA Fast	Incorrect field extracted
ID	43150443	34150443	Transposed characters
Date of Birth	11-15-1941	11-16-1941	Incorrect character recognition
Value Plot			
	<0	0	Incorrect character recognition
	17	21	Incorrect field extracted

Latin characters (20, 21). Our script shows a nominally higher accuracy rate than these systems; this is likely due to our study utilizing standardized digital report images rather than scanned documents. Nonetheless, these studies highlight the value of computer vision and OCR tools in the data extraction of medical reports.

Our script offers specific value in ophthalmology, especially in the field of glaucoma, by facilitating access to structured perimetry data. Static automated perimetry is an integral component in the management and monitoring of glaucoma, and numerous studies in the literature have examined various perimetry metrics in search of an optimal marker of diagnosis

or progression (22). In recent years, machine learning and neural networks have also been used in perimetry research (9); these algorithms are heavily dependent on well-categorized, large volume datasets. Thus, developing new perimetry metrics is an important focus of research in glaucoma (23), and access to structured perimetry is critical in facilitating this research (23). Our program was designed to offer a versatile option to generate structured HVF data for analysis from DICOM files or images files (such as JPG or PNG formats). With this, the program can serve as an avenue to several opportunities for perimetry data analysis. Additionally, this platform can potentially be used in conjunction with other analysis platforms such as the R package visualField (an open source module for analysis of visual field data), with the appropriate software to interface the two systems (24). Our platform has been used in a published study on HVFs in glaucoma patients undergoing glaucoma tube shunt implantation (25). Other research teams have performed studies with large volumes of HVFs for metric analysis and machine learning using in-house extraction software (6, 11); however, their script was not published and validation cannot be compared with ours.

One of the main strengths of computer extraction is the speed of extraction. Not only does the computer script offer more than a 50-fold increase in extraction speed, but also allows the extraction process to be automated for a large number of reports. Thus, the computer script can free up researchers for other tasks, and overall help reduce the cost and effort of data extraction. In institutions where structured digital perimetry data are not easily available straight from the acquisition devices, the computer extraction script offers an effective alternative to costly human extraction.

The validation results show an overall low error rate for the computer extraction data. Most errors occurred in metadata extraction, which has the most variability in the type and structure of the extracted data fields. As expected, the error rate increases with lower resolution images; this is due to the nature of image detection and OCR technology, which we used heavily in metadata extraction. Despite this correlation, metadata error rates remain low and similar to human extraction error rates, regardless of resolution of input image.

The error rate for computer extracted value and percentile data was very low and were statistically significantly better than human extraction except for value plot extractions in the low-resolution layout V1. Misidentification of similar appearing numbers in low-resolution images and interference of the open triangle icon in the area of the physiologic blind spot within the raw sensitivity plot were the main reasons for errors. The accuracy of the computer script in value and percentile plot data shows one of its main strengths, especially in the face of significant error rates in human extraction.

A notable result in our validation study is the high frequency of errors that arises from manual, human data extraction. Data errors in medical research have been studied in the past; one study showed error rates ranging from 2.3-26.9% in separately maintained clinical research databases at a single institution, due to a combination of presumed transcription and cognitive errors (26). This compares similarly to our study, with human extraction error rates as high as 10-15% in some categories. The substantially high error rate among human extraction in our study is possibly related to the display of plot data within HVF reports, which contain a high density of values within an area. This is supported by prior studies that show that displaying a high volume of data in the source document is correlated with transcription errors (4). Additionally, human extraction data tends to be variably formatted, especially when several different people contribute to the extracted datasets; this variability of data often requires standardization prior to further processing. Overall, understanding the relative strengths and weaknesses of human vs. computer extraction is important to improving research data integrity.

Lastly, it should be noted that while the computer program extraction is faster and more accurate than human extraction, it does not have 100% accuracy. Human validation of the extracted data may be needed to correct any computer errors. Understanding the limitations of computer data extraction and common areas of errors can help guide human validation of the data to speed up the process.

There are a few limitations of this validation study. First, the report layouts were limited to three distinct resolutions; while the different resolutions demonstrate the correlation of accuracy with resolution, the limited resolution layouts may not capture the full spectrum of image resolutions in use in the community. The limited number of reports per trial and selection methodology may not fully represent the spectrum of visual field defects possible, which may limit the generalizability of the error rates to specific HVF reports.

In summary, in this paper we introduce and validate a computer program for the extraction of HVF data from report images. In comparison to human extraction, computer extraction is faster and more accurate; however, human validation of the computer extraction data may be necessary for situations that require high fidelity of data. Overall, this program can help reduce the cost of data analysis for research institutions where HVF data is otherwise inaccessible.

DATA AVAILABILITY STATEMENT

The original contributions presented in the study are included in the article/supplementary material, further inquiries can be directed to the corresponding author/s.

ETHICS STATEMENT

This study was compliant with the Health Insurance Portability and Accountability Act and the Declaration of Helsinki for research involving human participants. Institutional Review Board approval was obtained from the University of California, San Francisco Human Research Protection Program.

AUTHOR CONTRIBUTIONS

MS developed software platform and contributed to study design, data collection, and analysis. JW, YL, PM,

and JP contributed to data collection and analysis. YY and G-SY contributed to data analysis and statistical calculations. YH contributed to study design, data analysis, and statistical calculations. All authors contributed to manuscript preparation.

FUNDING

NEI EY028747-01 funding to YH, NEI P30 EY002162 Core Grant for Vision Research, and an unrestricted grant from Research to Prevent Blindness, New York, NY.

REFERENCES

1. Armstrong GW, Lorch AC. A(eye): a review of current applications of artificial intelligence and machine learning in ophthalmology. *Int Ophthalmol Clin.* (2020) 60:57-71. doi: 10.1097/IIO.0000000000000298
2. Carl Zeiss Meditec AG. *DICOM Conformance Statement - Forum Version 3.2*. Available online at: https://www.zeiss.com/content/dam/Meditec/downloads/pdf/DICOM/DICOM_Conformance_Statement_FORUM_v3.2.pdf (accessed November 3, 2020).
3. Norman DA. Design rules based on analyses of human error. *Commun ACM.* (1983) 26:254-8. doi: 10.1145/2163.358092
4. Soboczenski F. *The Effect of Interface Elements on Transcription Tasks to Reduce Number-Entry Errors.* (2014). Availble online at: http://etheses.whiterose.ac.uk/11775/1/thesis.pdf (accessed November 3, 2020).
5. Thimbleby H, Cairns P. Reducing number entry errors: solving a widespread, serious problem. *J R Soc Interface.* (2010) 7:1429-39. doi: 10.1098/rsif.2010.0112
6. Saeedi OJ, Elze T, D'Acunto L, Swamy R, Hegde V, Gupta S, et al. Agreement and predictors of discordance of 6 visual field progression algorithms. *Ophthalmology.* (2019) 126:822-8. doi: 10.1016/j.ophtha.2019.01.029
7. Nouri-Mahdavi K, Caprioli J. Measuring rates of structural and functional change in glaucoma. *Br J Ophthalmol.* (2015) 99:893-8. doi: 10.1136/bjophthalmol-2014-305210
8. Zheng C, Johnson TV, Garg A, Boland MV. Artificial intelligence in glaucoma. *Curr Opin Ophthalmol.* (2019) 30:97-103. doi: 10.1097/ICU.0000000000000552
9. Mursch-Edlmayr AS, Ng WS, Diniz-Filho A, Sousa DC, Arnold L, Schlenker MB, et al. Artificial intelligence algorithms to diagnose glaucoma and detect glaucoma progression: translation to clinical practice. *Transl Vis Sci Technol.* (2020) 9:55. doi: 10.1167/tvst.9.2.55
10. Yousefi S, Kiwaki T, Zheng Y, Sugiura H, Asaoka R, Murata H, et al. Detection of longitudinal visual field progression in glaucoma using machine learning. *Am J Ophthalmol.* (2018) 193:71-9. doi: 10.1016/j.ajo.2018.06.007
11. Wen JC, Lee CS, Keane PA, Xiao S, Rokem AS, Chen PP, et al. Forecasting future Humphrey visual fields using deep learning. *PLoS ONE.* (2019) 14:e0214875. doi: 10.1371/journal.pone.0214875
12. Welcome to python.org. Available online at: https://www.python.org/ (accessed November 3, 2020).
13. OpenCV. Available online at: https://opencv.org/ (accessed November 3, 2020).
14. tesseract-ocr/tesseract: Tesseract Open Source OCR Engine (main repository). Available online at: https://github.com/tesseract-ocr/tesseract (accessed November 3, 2020).
15. seatgeek/fuzzywuzzy: Fuzzy String Matching in Python. Available online at: https://github.com/seatgeek/fuzzywuzzy (accessed November 3, 2020).
16. pyDICOM. Available online at: https://github.com/pydicom/pydicom (accessed November 3, 2020).
17. The GNU General Public License v3.0 - GNU Project - Free Software Foundation. Available online at: https://www.gnu.org/licenses/gpl-3.0.en.html (accessed November 3, 2020).
18. Chaudhuri A, Mandaviya K, Badelia P, Ghosh KS. Optical Character Recognition Systems. In: *Optical Character Recognition System for Different Languages With Soft Computing, Studies in Fuzziness and Soft Computing.* Cham: Springer (2017). doi: 10.1007/978-3-319-50252-6_2
19. Adamo F, Attivissimo F, Di Nisio A, Spadavecchia M. An automatic document processing system for medical data extraction. *Meas J Int Meas Confed.* (2015) 61:88-99. doi: 10.1016/j.measurement.2014.10.032
20. Xue W, Li Q, Zhang Z, Zhao Y, Wang H. Table analysis and information extraction for medical laboratory reports. In: *Proc - IEEE 16th Int Conf Dependable, Auton Secur Comput IEEE 16th Int Conf Pervasive Intell Comput IEEE 4th Int Conf Big Data Intell Comput IEEE 3.* Athens (2018) 200-7. Available online at: https://ieeexplore.ieee.org/document/8511886
21. Xue W, Li Q, Xue Q. Text detection and recognition for images of medical laboratory reports with a deep learning approach. *IEEE Access.* (2020) 8:407-16. doi: 10.1109/ACCESS.2019.2961964
22. Nouri-Mahdavi K, Nassiri N, Giangiacomo A, Caprioli J. Detection of visual field progression in glaucoma with standard achromatic perimetry: a review and practical implications. *Graefe's Arch Clin Exp Ophthalmol.* (2011) 249:1593-1616. doi: 10.1007/s00417-011-1787-5
23. Brusini P, Johnson CA. Staging functional damage in glaucoma: review of different classification methods. *Surv Ophthalmol.* (2007) 52:156-79. doi: 10.1016/j.survophthal.2006.12.008
24. Marín-Franch I, Swanson WH. The visualFields package : a tool for analysis and visualization of visual fields. *J Vis.* (2013) 13:1-12. doi: 10.1167/13.4.10
25. Liu Q, Saifee M, Yu Y, Ying G-S, Li S, Zhong H, et al. Evaluation of long-term visual field function in patients undergoing glaucoma drainage device implantation. *Am J Ophthalmol.* (2020) 216:44-54. doi: 10.1016/j.ajo.2020.03.025
26. Goldberg SI, Niemierko A, Turchin A. Analysis of data errors in clinical research databases. *AMIA Annu Symp Proc.* (2008) 2008:242-6.

Conflict of Interest: The authors declare that the research was conducted in the absence of any commercial or financial relationships that could be construed as a potential conflict of interest.

frontiers in Medicine

ORIGINAL RESEARCH
published: 14 May 2021
doi: 10.3389/fmed.2021.680823

Low-Contrast High-Pass Visual Acuity Might Help to Detect Glaucoma Damage: A Structure-Function Analysis

*Yun Wen[1], Zidong Chen[1], Chengguo Zuo[1], Yangfan Yang[1], Jiangang Xu[1], Yang Kong[2], Hui Cheng[3] and Minbin Yu[1]**

[1] State Key Laboratory of Ophthalmology, Zhongshan Ophthalmic Center, Sun Yat-sen University, Guangzhou, China, [2] School of Electronics and Communication Engineering, Sun Yat-sen University, Shenzhen, China, [3] School of Computer Science and Engineering, Sun Yat-sen University, Guangzhou, China

Purpose: The conventional visual acuity (VA) test is not sensitive enough to detect glaucoma macular damage. We aimed to investigate whether VA measurements using low-contrast high-pass optotypes are more sensitive to macular dysfunction in glaucoma and to find the potential structural basis of this difference.

Methods: A total of 147 subjects were recruited, including 118 patients with glaucoma (mean age: 46.08 ± 14.64 years) and 29 healthy controls (mean age: 39.83 ± 9.81 years). For each participant, monocular best-corrected VA was measured using a conventional chart and six high-pass charts at 100, 50, 10, 5, 2.5, and 1.25% contrast levels, respectively. The macular retinal thickness and circumpapillary retinal nerve fiber layer (cpRNFL) thickness of all the glaucoma patients were obtained by spectral-domain optical coherence tomography (SD-OCT).

Results: Compared with healthy subjects, glaucoma patients with normal vision demonstrated worse VAs in high-pass acuity measurements (0.22–0.93 vs. 0.28–1.08, $p < 0.05$). Receiver operating characteristic curve (ROC) showed that 1.25% low-contrast high-pass VA was optimal for discriminating between the controls and glaucoma patients (AUC: 0.918, $p < 0.001$; sensitivity: 77.33%; specificity: 96.55%). Compared with conventional VA, 1.25% high-pass VA correlated better with nasal-side macular retinal ganglion cell (RGC)-related parameters ($r = -0.419$ to -0.446 vs. $r = -0.538$ to -0.582; Fisher's Z transformation, $p_Z < 0.05$). There was no difference in the strength of correlations between the VAs measured using different charts and cpRNFL thickness (Fisher's Z transformation; $p_Z > 0.05$).

Conclusions: VA measurement taken with low-contrast (1.25%) high-pass acuity chart is more sensitive in detecting central visual loss in glaucoma than that taken with the conventional chart. Macular RGC damage appears to be associated with low-contrast (1.25%) high-pass visual loss in glaucomatous eyes.

Keywords: low-contrast visual acuity, high-pass optotypes, glaucoma, macular damage, optical coherence tomography

OPEN ACCESS

Edited by:
Michele Lanza, University of Campania Luigi Vanvitelli, Italy

Reviewed by:
Andreas Ebneter, Roche Innovation Center, Switzerland
Roger Anderson, Ulster University, United Kingdom
Alessio Martucci, University of Rome Tor Vergata, Italy

***Correspondence:**
Minbin Yu
yuminbin@mail.sysu.edu.cn

Specialty section:
This article was submitted to Ophthalmology, a section of the journal Frontiers in Medicine

Received: *15 March 2021*
Accepted: *19 April 2021*
Published: *14 May 2021*

Citation:
Wen Y, Chen Z, Zuo C, Yang Y, Xu J, Kong Y, Cheng H and Yu M (2021) Low-Contrast High-Pass Visual Acuity Might Help to Detect Glaucoma Damage: A Structure-Function Analysis. Front. Med. 8:680823. doi: 10.3389/fmed.2021.680823

INTRODUCTION

Glaucoma is the most frequent cause of irreversible blindness and visual impairment worldwide. It has been projected to affect around 112 million people by 2040 (1). The common features of glaucoma are loss of RGCs, thinning of the cpRNFL, cupping of the optic disc and visual field (VF) defects (1, 2). Glaucoma has traditionally been regarded as an insidious disease that features progressive loss of peripheral vision and sparing of macular vision until late in the process of the disease (3). This perception was based on the VA test, the most common clinical measurement used to assess macular visual function (3). This subjective and rough method evaluates only the resolution ability of the eye at a fixed high contrast. However, resolving power is only one aspect of the very complex central visual perception pathway. Many glaucoma patients have complaints regarding central vision despite normal VA (4, 5).

Accumulating evidence shows that macular involvement occurs earlier in glaucomatous eyes than once thought (6–8). Studies investigating reading speed (9) and facial recognition (10) have reported that the macular vision of glaucomatous eyes is significantly compromised. Other studies have confirmed that spatial contrast sensitivity (CS) declines in glaucoma patients, even those with normal VA, specifically at the high spatial frequency end (11). However, it is important to have a functional test that is sensitive to glaucoma macular damage that can be conveniently conducted in busy clinical practices and easily understood by patients.

There are two distinct visual thresholds regarding the conventional black-on-white letters, specifically the detection threshold and the recognition threshold (12). Significant differences in the low spatial frequency content of the conventional letters make them more identifiable at a much greater distance than the actual resolution required (12). Thus, this discrepancy between detection and resolution thresholds can help to achieve superior levels of VA. Howland et al. have devised a special type of optotype called high-pass spatial frequency letters (13). The special design of these stimuli make the low spatial frequencies removed and appear as letters with a black core and a white outline (or vice versa) with their mean luminance equal to that of the gray background. In healthy eyes, the detection threshold almost coincides with the resolution threshold under foveal viewing.

VA measured by high-pass filtered optotypes demonstrated higher sensitivity to neural limitations of age-related macular degeneration (AMD) damage than conventional black-on-white letters (14). However, it is reasonable to speculate that undersampling as a result of RGC loss around the fovea in glaucomatous eyes may cause discrepancies between detection and resolution thresholds, resulting in acuity loss for high-pass filtered letters.

Previous studies on patients with multiple sclerosis and optic neuritis confirmed that acuity charts with a set of variable contrasts provide qualitatively similar diagnostic information to that provided by the sinusoidal gratings of different contrast and different spatial frequencies in CS tests (15, 16). Patients with glaucoma also exhibited visual loss in the low-contrast acuity test (17). However, VA tests using high-pass filtered optotype settings at various contrasts have not yet been performed in glaucoma patients. Do these charts offer simple and more sensitive ways of detecting macular dysfunction in glaucoma? To answer this question, we compared the test results of various contrast high-pass VA charts between glaucoma patients and healthy participants and explored the structure-function relationships between OCT parameters and VA results in glaucoma patients.

MATERIALS AND METHODS

Patients

This study was performed according to the tenets of the Declaration of Helsinki and was approved by the ethics committee of the Zhongshan Ophthalmic Center (NO.2019KYPJ115). Written informed consent was obtained from all participants prior to the experiment. The subjects were recruited from the Glaucoma Clinic at Zhongshan Ophthalmic Center.

The patients with glaucoma in the current study met the following criteria: (1) a diagnosis of primary open-angle glaucoma (POAG) or normal tension glaucoma (NTG) in one or both eyes as determined by at least two glaucoma specialists (2); In the current study, glaucoma was diagnosed based on characteristic optic nerve damage on stereoscopic imaging, cpRNFL thinning on SD-OCT, open anterior chamber angles on gonioscopy and absence of other known explanations of progressive glaucomatous optic nerve change. (2) A best-corrected visual acuity (BCVA) better than or equal to 0.20 logMAR (Early Treatment Diabetic Retinopathy Study logMAR chart, ETDRS chart) in the eye; (3) spherical equivalents between −6.0 diopters (D) and +3.00 D and cylinder correction within ±3D; (4) no N2 or worse nuclear sclerotic cataract graded by the Lens Opacities Classification System III criteria (18) or any posterior subcapsular or cortical lenticular changes in the lens; (5) no severe dry eye or other ophthalmic surface diseases; and (6) no ocular or systemic disease that could affect the optic nerve, macula, or VF results. Finally, a total of 147 subjects were recruited, including 118 patients with glaucoma (110 patients with POAG and 8 patients with NTG; mean age 46.08 ± 14.64 years) and 29 age-similar healthy controls (mean age 39.83 ± 9.81 years) with BCVA equal to or better than 0.00 logMAR on ETDRS acuity chart.

To determine the best-corrected refractive correction and the BCVA of each enrolled eye, a cycloplegic refraction was done on each participant within a week before the experiment. Objective refraction was measured by autorefraction (NIDEK ARK-1) first. Then subjective refinements to achieve the best VA and optimum optical correction were performed using a phoropter (NIDEK RT-5100). The contemplated prescription was then used in a trial frame for monocular VA measurements performed with the ETDRS illuminator cabinets (Precision Vision, Inc., USA; illuminance, 160 cd/m^2) at a distance of 4 m.

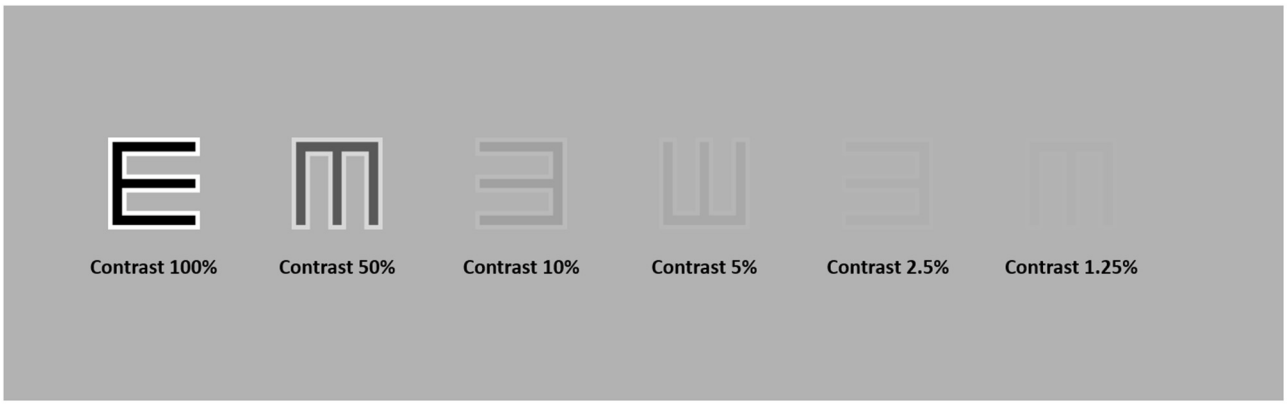

FIGURE 1 | High-pass letter "E" at six different contrast levels, namely, 100, 50, 10, 5, 2.5, and 1.25%. The contrast was defined as Michelson Contrast.

VA and Contrast Testing

Apparatus

High-pass VA was measured using specially designed electronic charts (e-charts) generated by MATLAB (MathWorks, Inc., Natick, MA) with the Psychophysics Toolbox for Windows 10, administered on a laptop computer. The e-charts were displayed on a liquid crystal display monitor (DELL, P2415Q, 23.8 inches, resolution: 3,840 × 2,160, refresh rate: 60 Hz). Luminance of the display monitor was made linear after gamma correction using a TES-1330A Digital Light Meter (TES Electrical Electronic Corp., Taipei, Taiwan). The values of the properties for the display of stimuli in the current study were specified in pixels. The brightness of the screen and the surround luminance was kept consistent. The screen brightness was set at 100%. The room lights were turned off on the side of the screen, ensuring a stable ambient illumination of 8 lux, while the lights on the side of the subjects remained on, providing a luminance of 160 cd/m^2. Participants were seated on a chair with a vertical back 4 meters away from the front of the screen.

Stimuli

The e-charts employed the same layout as the current standard ETDRS chart, with optotype sizes ranging from 58.18 to 2.92 mm, providing a test range from 1.0 logMAR to −0.3 logMAR at a 4 m distance. We used the 5 × 5 letter "E" with a lighter edge (luminance: 228 cd/m^2) and a darker core (luminance: 3 cd/m^2), which formed a constant ratio of 1:2:1 (edge: core: edge), as the optotype design (high-pass design). The mean luminance of the strokes was consistent with the luminance of the gray background (luminance: 112 cd/m^2). The contrast was defined as Michelson contrast (see **Figure 1**). During the test, the visual chart went line by line on the center of the screen. In each line, there were five optotypes with interval spaces as one letter width. The high-pass "E" was presented randomly in four directions: left, right, up, and down.

Test Procedure

The best-corrected refractive correction was used for each participant before the tests. For each VA test in the current study, participants were required to identify every optotype in each row by a forced choice procedure. They were instructed to identify the orientations of the high-pass "E"s by pressing direction buttons on a Bluetooth keyboard. Testing time was not restricted. Once the participants were unsure of an optotype, they were encouraged to guess. The tests automatically stopped when four or more errors occurred in a row. Then, the final VA score was calculated using the method described by Ferris et al. (19). When a participant could not correctly read at least 4 letters of the top row at 4 m, the test distance was reduced to 1 m. In this case, only the top 6 rows were required, and a +0.75DS was added to the prescription in the trial frame as the refractive compensation for the distance reduction. In the current study, VA was scored as logMAR values on a by-letter basis. High-pass VAs were measured at contrast settings of 100, 50, 10, 5, 2.5, and 1.25%. Participants were allowed to take a 5-min break between tests to minimize the effects of fatigue.

For comparison, the conventional VA test was also conducted using the same set of apparatuses. The black-on-white VA chart followed the design of the current standard ETDRS chart. The test procedure and scoring rules were all in accordance with the high-pass VA tests.

SD-OCT Scan

Macular retinal layer thickness of each enrolled eye was acquired by a well-trained ophthalmic photographer using SD-OCT (Spectralis, Heidelberg Engineering GmbH, Heidelberg, Germany). The macular images were generated using the "Dense" protocol in high-resolution volume scan mode with an automatic real-time mean value of 15. The imaging covered a 6 × 6 mm area of the macula centered on the fovea. The thickness of each layer was segmented and calculated by the automatic segmentation algorithms of the built-in software (Version 6.3.4). Scans were acquired with 49 B-scans consisting of 1,024 A-scans. All scans were reviewed, and any scan with a quality score <20 dB or segmentation error was excluded from analysis. The ganglion cell complex (GCC) layer thickness was the sum of the thickness of the retinal nerve fiber layer (RNFL), ganglion cell layer (GCL), and inner plexiform layer (IPL); the

ganglion cell inner plexiform layer (GCIPL) thickness was the combination of the GCL and IPL (see **Figure 2A**). The average retinal thickness and retinal volume were divided into nine subfields according to the ETDRS grid, specifically a central subfield (diameter 1 mm), the inner ring (radius 0.5 mm and radius 2 mm) and the outer ring (radius 3 mm). The inner ring and outer ring were automatically divided into four quadrants by in-build software: superior, nasal, inferior and temporal (see **Figure 2A**).

The cpRNFL protocol was also conducted, in which 3.4-mm-diameter circle scans were acquired. Sectoral cpRNFL thicknesses, specifically the global average of the circle scan (G), nasal (N), superonasal (NS), superotemporal (TS), temporal (T), inferotemporal (TI), and inferonasal (NI) quadrants, provided by the built-in software were read (see **Figure 2B**).

Data Analysis

We first compared the VA data between glaucomatous eyes with normal vision ($N = 75$) and healthy controls ($N = 29$). Here, normal vision was defined as BCVA equal to or better than 0.00 logMAR on the ETDRS VA chart. The normality of the data was checked using the Shapiro-Wilk test. Bland-Altman plots (20) were used to display the comparison results for the different charts in the glaucoma group and healthy control group. Regression analysis was used to quantify any potential proportional bias. The discrimination performance of the VA

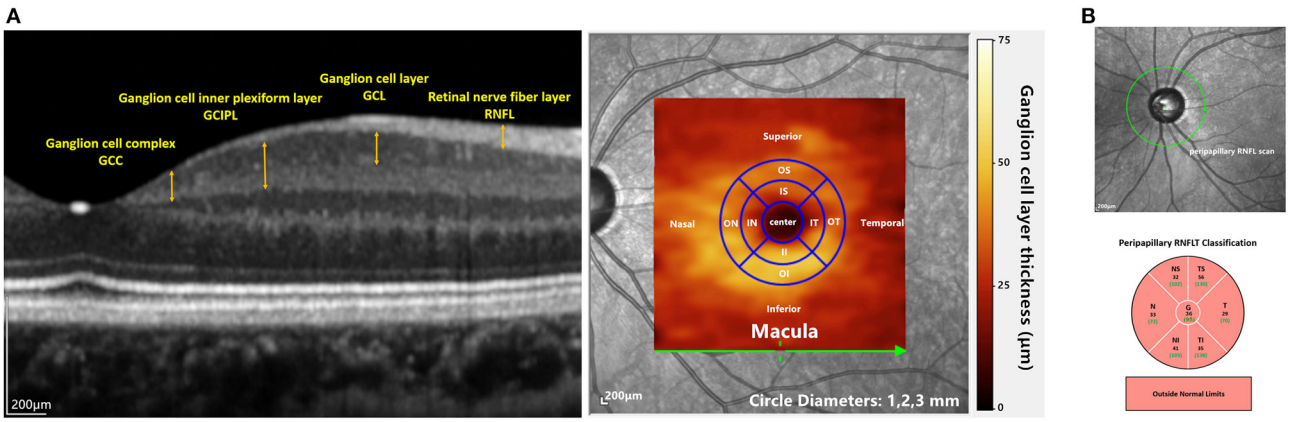

FIGURE 2 | OCT imaging in the current study: **(A)** the left image shows macular layers that were used for analyzing the structure-function relationships in this study. The right panel shows the overlay of the GCL thickness heat map on a fundus image. The inner and outer annuli were divided into four quadrants (IS, IT, II, IN and OS, OT, OI, ON) according to the ETDRS map. **(B)** the upper image shows the cpRNFL scan. The lower picture shows the sectoral cpRNFL thicknesses classification, specifically the global average of the circle scan (G) and N, NS, TS, T, TI, and NI quadrants.

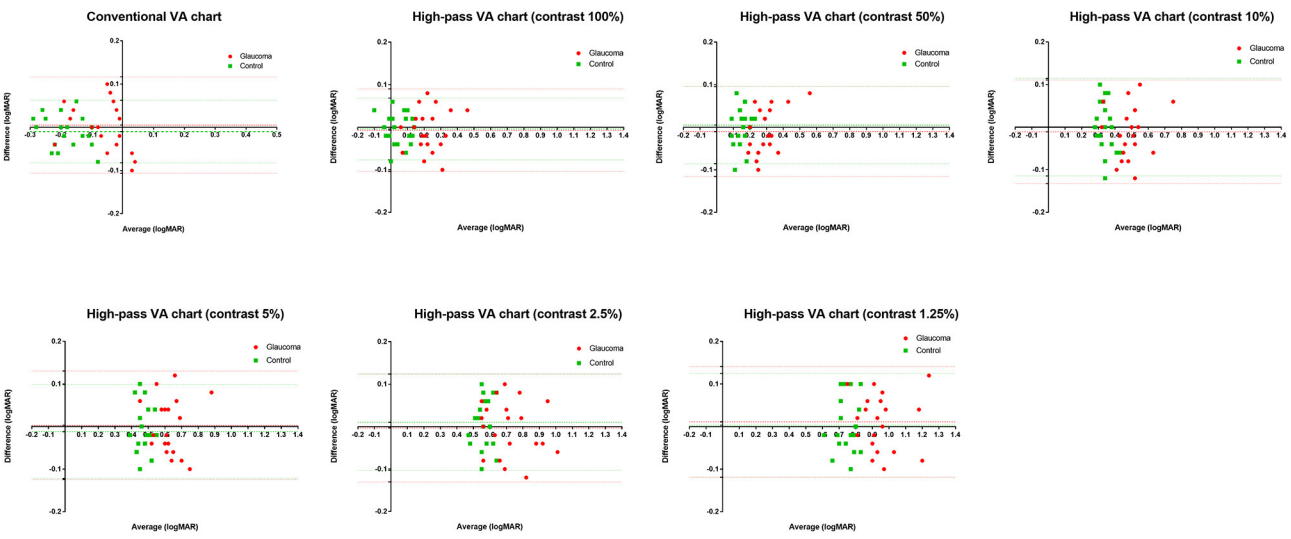

FIGURE 3 | Bland-Altman plots for test-retest measurements for the conventional chart (1st test vs. 2nd test) and the high-pass charts (1st test vs. 2nd test) with data for the 20 healthy controls plotted in green (squares) and the 20 glaucoma patients in red (dots). The mean difference of the two tests and 95% Limits of Agreements are also shown in the plots (dotted lines).

tests in glaucoma damage was assessed by ROC curve analysis. Areas under the curves (AUCs) were calculated to compare the discriminative value of each VA test. The optimal cutoff value was obtained according to Youden index analysis as the points with the best sensitivity-specificity balance.

Then, the correlations between multiple OCT parameters and VA results were evaluated by Pearson's partial correlation analysis after adjusting for age and spherical equivalent (SE) in all glaucoma participants ($N = 118$). Then Fisher's Z transformation was conducted for comparisons of the correlations.

Statistical analysis was conducted using SPSS for Windows (version 20.0; SPSS, Inc., Chicago, IL, USA), the GraphPad Prism statistical analysis package (version 7.00; GraphPad Software, Inc., La Jolla, California, USA) and MedCalc statistical software (version 19.0.4; MedCalc Software Ltd, Ostend, Belgium).

RESULTS

The Test-Retest Reliability of the Conventional Chart and the High-Pass Charts

In this part, 20 glaucoma patients with BCVA equal to or better than 0.00 logMAR on ETDRS chart and 20 healthy controls underwent VA tests under the same conditions at two different points in time. The test-retest reliability was analyzed using Bland-Altman plots (see **Figure 3**).

The mean difference between the two tests (the 1st test and the 2nd test) and the 95% limits of agreement (LoA) of each VA chart were calculated separately (see **Table 1**).

TABLE 1 | Test-retest reliability of the conventional chart and the novel high-pass charts.

	Mean difference of 1st and 2nd test	TRV, 95% Limits of agreement
Conventional chart		
Healthy control	−0.010 ± 0.037	−0.083 to 0.063
Glaucoma	0.005 ± 0.057	−0.107 to 0.117
High-pass chart (contrast 100%)		
Healthy control	−0.004 ± 0.037	−0.077 to 0.069
Glaucoma	−0.007 ± 0.050	−0.104 to 0.090
High-pass chart (contrast 50%)		
Healthy control	0.005 ± 0.046	−0.086 to 0.096
Glaucoma	−0.010 ± 0.054	−0.116 to 0.096
High-pass chart (contrast 10%)		
Healthy control	0.000 ± 0.058	−0.114 to 0.115
Glaucoma	−0.011 ± 0.062	−0.133 to 0.111
High-pass chart (contrast 5%)		
Healthy control	−0.012 ± 0.056	−0.122 to 0.098
Glaucoma	0.003 ± 0.065	−0.123 to 0.130
High-pass chart (contrast 2.5%)		
Healthy control	0.010 ± 0.058	−0.103 to 0.123
Glaucoma	−0.003 ± 0.065	−0.130 to 0.124
High-pass chart (contrast 1.25%)		
Healthy control	0.003 ± 0.062	−0.119 to 0.125
Glaucoma	0.011 ± 0.066	−0.119 to 0.141

TRV, Test-retest variability.

Visual Acuity Measured Using Conventional Chart and High-Pass Charts in Glaucomatous Eyes With Normal Vision

In this section, we tried to determine whether low-contrast high-pass charts are more sensitive for detecting central visual dysfunction in glaucomatous eyes. Thus, we compared the VA data between glaucoma patients with normal vision and healthy controls. A total of 75 glaucomatous eyes with BCVA equal to or better than 0.00 logMAR and 29 healthy eyes were included in the analysis. The characteristics of the participants are summarized in **Table 2**. VAs measured using conventional chart and high-pass charts at 100, 50, 10, 5, 2.5, and 1.25% contrast levels among the two group of participants are shown in **Figure 4**.

TABLE 2 | Characteristics of the glaucoma patients with normal vision and the healthy controls.

	Glaucoma patients with normal vision ($N = 75$)	Healthy controls ($N = 29$)	*P*-value
Age, years	43.19 ± 13.98	39.83 ± 9.81	0.239
Gender, F/M	32/43	16/13	0.251
Spherical equivalents, diopters	−2.02 ± 2.59	−2.24 ± 2.28	0.683
MD of 30-2 VF, dB	−10.48 ± 7.82	−1.74 ± 1.30	<0.001
BCVA, logMAR	−0.09 ± 0.08	−0.17 ± 0.07	<0.001

P-value was obtained from independent sample t-test, except gender data was compared using Chi-squared Test.
F/M, female/male; MD, mean deviation; VF, visual field; BCVA, best-corrected visual acuity; logMAR, the logarithm of the minimum angle of resolution.

The differences in VAs measured using conventional chart and each high-pass chart in the glaucoma group and healthy control group are summarized in **Table 3**. The difference between conventional VA and high-pass VA at any one of the contrast levels was significantly different between the two groups of participants ($p_{100\%} = 0.004$, $p_{50\%} = 0.014$, $p_{10\%} = 0.007$, $p_{5\%} < 0.0001$, $p_{2.5\%} < 0.0001$, $p_{1.25\%} < 0.0001$).

Figure 5 displays the difference in VAs measured using conventional chart and high-pass charts between the glaucoma group with normal vision (in red) and the healthy controls (in green). We can see that there was a greater level of disagreement at the worse acuity end on the pattern form by the data from glaucoma patients. Regression analysis confirmed that these proportional biases were statistically significant ($p_{100\%} = 0.0021$, $p_{50\%} = 0.0081$, $p_{10\%} = 0.0012$, $p_{5\%} < 0.0001$, $p_{2.5\%} < 0.0001$, $p_{1.25\%} < 0.0001$). As the contrast decreased, the difference between VAs became larger. At the 1.25% contrast level, the slope of the regression line reached −0.88. When we looked at the pattern formed by the data from healthy controls, the difference was relatively constant throughout, and the regression analysis showed no statistical significance ($p_{100\%} = 0.9992$, $p_{50\%} = 0.0585$, $p_{10\%} = 0.1702$, $p_{5\%} = 0.2828$, $p_{2.5\%} = 0.8431$, $p_{1.25\%} = 0.8294$).

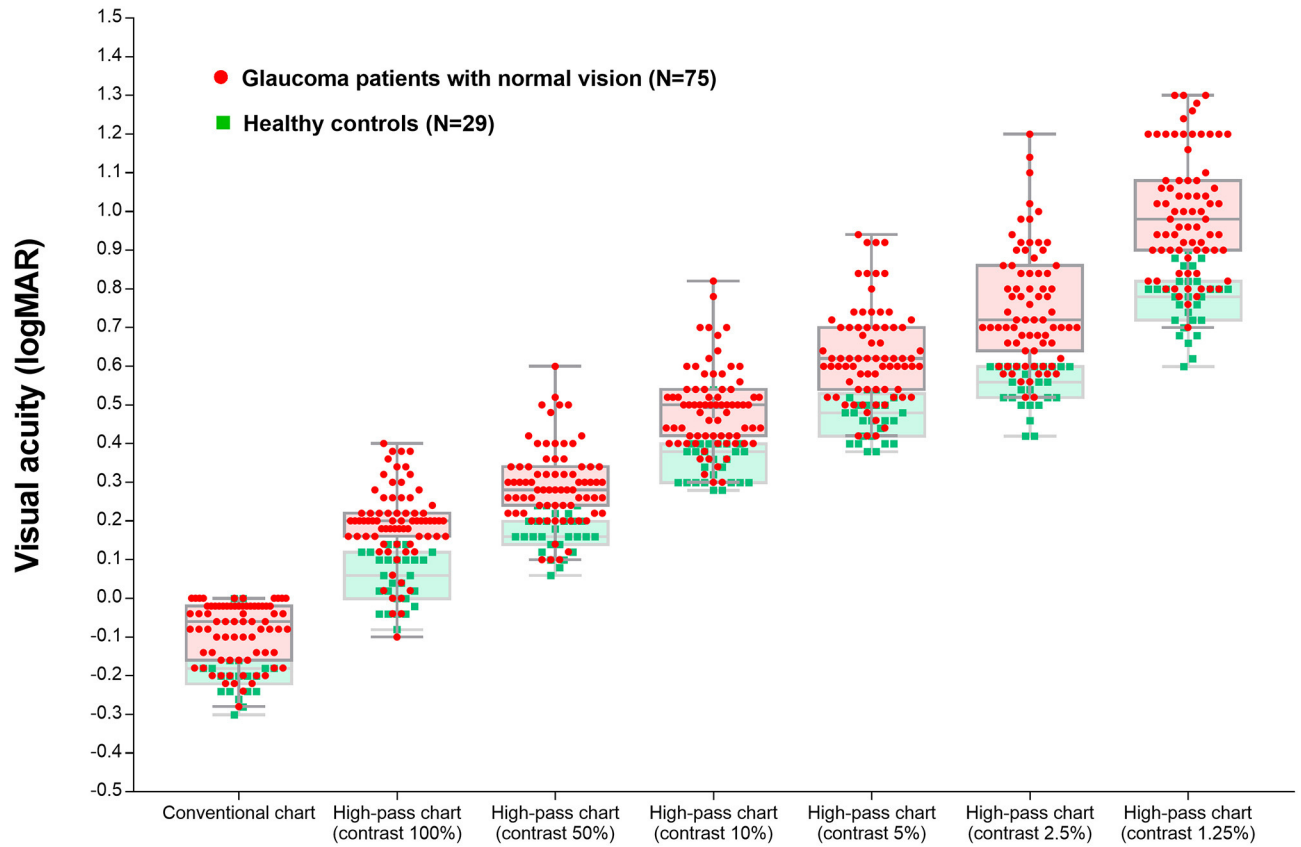

FIGURE 4 | Visual acuity measured using the conventional chart and high-pass charts at 100, 50, 10, 5, 2.5, and 1.25% contrast levels among glaucoma patients with normal vision and the healthy controls.

TABLE 3 | Differences in visual acuities measured using conventional chart and high-pass charts in glaucoma patients with normal vision ($N = 75$) and the healthy controls ($N = 29$).

Reference: Conventional VA	Differences, Mean ± SD (95% CI)		*P*-value (two-tailed)
	Healthy controls ($N = 29$)	Glaucoma patients ($N = 75$)	
High-pass VA (contrast 100%)	0.22 ± 0.08 (0.19–0.26)	0.28 ± 0.07 (0.26–0.29)	0.004
High-pass VA (contrast 50%)	0.33 ± 0.06 (0.31–0.36)	0.38 ± 0.08 (0.36–0.39)	0.014
High-pass VA (contrast 10%)	0.53 ± 0.05 (0.50–0.55)	0.57 ± 0.08 (0.55–0.59)	0.007
High-pass VA (contrast 5%)	0.64 ± 0.06 (0.62–0.67)	0.71 ± 0.09 (0.69–0.74)	<0.0001
High-pass VA (contrast 2.5%)	0.73 ± 0.05 (0.71–0.75)	0.84 ± 0.12 (0.81–0.86)	<0.0001
High-pass VA (contrast 1.25%)	0.93 ± 0.07 (0.90–0.96)	1.08 ± 0.13 (1.05–1.11)	<0.0001

P-value was obtained from independent sample t-test; VA, visual acuity.

ROC curve analysis was performed to determine the optimal method for discriminating glaucomatous eyes from healthy eyes (**Figure 6**). The AUCs of the high-pass charts were larger than that of the conventional chart, with the highest figure peaking at 0.918 (95% CI: 0.847–0.963), showing at 1.25% contrast level (**Figure 6**). In addition, the optimal cutoff point of each VA test was obtained from the Youden index with the best sensitivity-specificity balance (**Table 4**).

Structure-Function Relationship Between Visual Acuity and Retinal Thickness Measured by SD-OCT in Glaucoma Patients

In this section, data from a total of 118 glaucomatous eyes were analyzed. The BCVA was −0.02 ± 0.11 logMAR and the mean deviation (MD) of 30-2 VF was −13.05 ± 8.60 dB. The correlations between OCT parameters and the VAs were examined by Pearson's partial correlation adjusted for age and SE. There were significant correlations between VAs and the overall RGC-related parameters (GCL, GCIPL, and GCC) of macular scans (**Figure 7**). Among all the VAs, high-pass VA with the 1.25% contrast setting showed the higher correlations with most of the macular scan parameters, especially RGC-related parameters of the nasal (−0.538 to −0.582, $p < 0.001$) and superior subfields ($r = -0.472$ to -0.528, $p < 0.001$). Fisher's Z transformation confirmed that high-pass VA at 100, 50, and

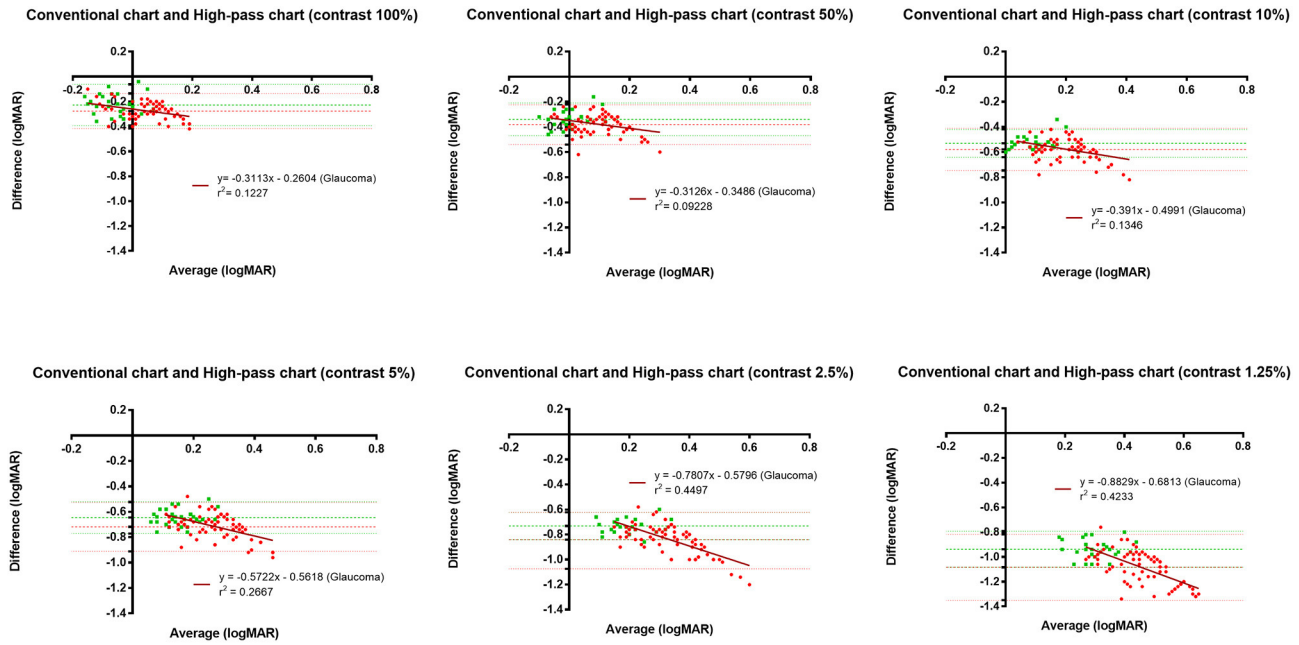

FIGURE 5 | Bland-Altman plots displaying the differences in VAs measured using the conventional chart and high-pass charts in glaucomatous eyes with normal vison ($n = 75$) and healthy controls ($n = 29$). The red dots represent data from glaucoma patients, whereas the green squares represent data for healthy controls. The horizontal lines represent the bias of the tests and 95% limits of agreement. The dark red lines represent the best linear fit to the data from glaucoma patients.

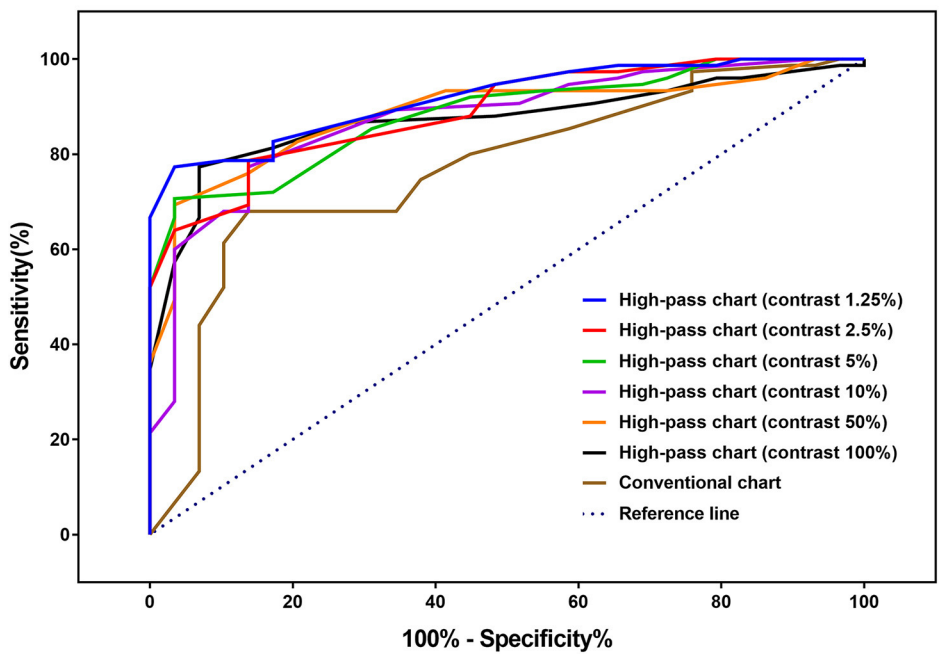

FIGURE 6 | Receiver operating characteristic (ROC) curve for each VA test to detect glaucoma damage.

TABLE 4 | Receiver operating characteristic curve analysis of visual acuities between glaucoma patients with normal vison ($N = 75$) and healthy controls ($N = 29$).

	AUC (95% CI)	*P*-value	Cutoff value	Sensitivity	Specificity	Youden index
Conventional chart	0.768 (0.675–0.845)	<0.0001	−0.12	68.00	86.21	0.5421
High-pass chart						
Contrast 100%	0.872 (0.792–0.929)	<0.0001	0.14	77.33	93.10	0.7044
Contrast 50%	0.883 (0.806– 0.938)	<0.0001	0.24	69.33	96.55	0.6589
Contrast 10%	0.874 (0.794–0.931)	<0.0001	0.40	77.33	86.21	0.6354
Contrast 5%	0.883 (0.805–0.937)	<0.0001	0.56	70.67	96.55	0.6722
Contrast 2.5%	0.889 (0.812–0.942)	<0.0001	0.60	78.67	86.21	0.6487
Contrast 1.25%	0.918 (0.847–0.963)	<0.0001	0.88	77.33	96.55	0.7389

AUC, area under the ROC curve; CI, confidence interval.

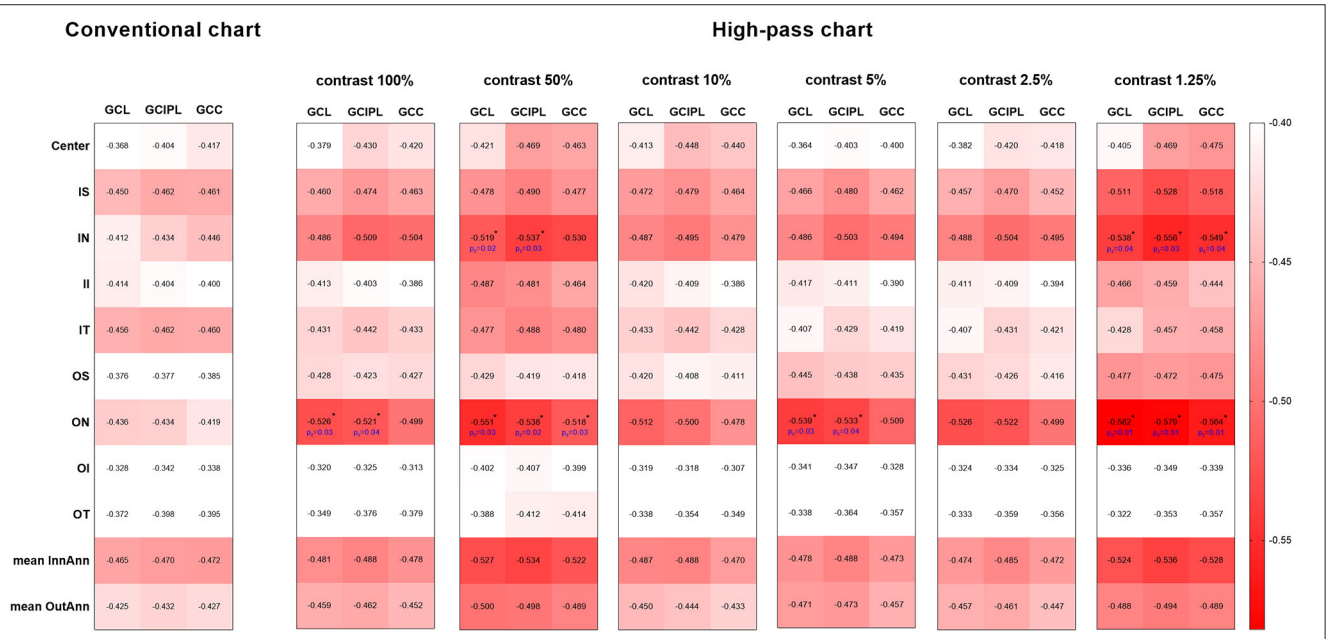

FIGURE 7 | Heat map demonstrates the correlations between each parameter of the macular scan and VA data (Pearson's partial correlation analysis). The red-scale strength range of the correlation coefficients are shown on the right side of the plots. The correlations shown above were all statistically significant at the level of 0.01. The values marked with asterisks are statistically significant at $p < 0.05$ level (one-tailed) in Fisher's Z transformation and represent stronger structure-function correlations than those between structure parameters and conventional VA. GCL, ganglion cell layer; GCIPL, ganglion cell inner plexiform layer; GCC, ganglion cell complex; IS, inner superior; IN, inner nasal; II, inner inferior; IT, inner temporal; OS, outer superior; ON, outer nasal; OI, outer inferior; OT, outer temporal; InnAnn, inner annulus; OutAnn, outer annulus.

5% contrast level demonstrated slightly stronger correlations with some of the nasal-side parameters when compared with that of conventional VA (one-tailed p_z, < 0.05), and 1.25% low-contrast high-pass VA demonstrated stronger structure-function relationships with all of the nasal-side RGC-related parameters (Fisher's Z transformation; one-tailed $p_{z,} < 0.05$).

The correlations between cpRNFL parameters and the VAs are summarized in **Table 5**. Temporal-side RNFL thickness had the strongest correlations with the low-contrast high-pass VAs at 10, 5, 2.5, and 1.25% contrast settings ($r = -0.367$ to -0.439, $p_r < 0.05$). The conventional VA and high-pass VAs at 100 and 50% contrast settings showed slightly better correlations with the global average cpRNFL thickness ($r = -0.347$, -0.403, and -0.399, respectively; $p_r < 0.05$). However, Fisher's Z transformation confirmed that there is no difference in the strength of correlations between VAs measured using different charts and cpRNFL thickness (Fisher's Z transformation; two-tailed $p_z > 0.05$).

DISCUSSION

Glaucoma has gradually become known as a condition that has macular involvement in the early stage even with well-preserved VA (6, 7, 21), and this macular damage greatly affects vision-related quality of life among glaucoma patients (10, 22). Various visual function tests have been studied for the early detection of macular damage, such as VF tests (23), CS tests (11), and letter recognition tasks (24). Although these tests are

TABLE 5 | Correlations between cpRNFL thickness and visual acuity results.

	Conventional chart, r	High-pass charts, *r*					
		Contrast 100%	Contrast 50%	Contrast 10%	Contrast 5%	Contrast 2.5%	Contrast 1.25%
TS	−0.320	−0.360	−0.338	−0.313	−0.330	−0.315	−0.310
T	−0.340	−0.378	−0.363	−0.367	−0.397	−0.367	−0.439
TI	−0.259	−0.267	−0.295	−0.200	−0.240	−0.215	−0.205
NI	−0.231	−0.249	−0.259	−0.212	−0.218	−0.163*	−0.166*
N	−0.085*	−0.175*	−0.125*	−0.049*	−0.077*	−0.026*	−0.012*
NS	−0.300	−0.332	−0.334	−0.297	−0.270	−0.242	−0.240
Global average	−0.347	−0.402	−0.399	−0.340	−0.369	−0.328	−0.343

The correlations showed above were statistically significant at the level of 0.05, except for those marked. cpRNFL, circumpapillary retinal nerve fiber layer; TS, superotemporal; T, temporal; TI, inferotemporal; NI, inferonasal; N, nasal; NS, superonasal.*

workable for glaucoma discrimination, the VA test is still the most convenient and simplest test to apply in clinical practice. However, there have been limited studies regarding VA in glaucoma patients.

Shah et al. confirmed that in foveal viewing, while conventional letters are good stimuli for detecting defocus, high-pass filtered letters were less vulnerable to optical defocus and more sensitive to neural limitations in conditions such as AMD (14, 25). A significant difference between the detection and resolution thresholds of high-pass letters, owing to undersampling as a result of photoreceptor loss, may be responsible for the VA loss measured by the high-pass letter chart (14, 25). As in the case of glaucoma, undersampling resulting from RGC damage may also affect the resolution threshold of high-pass letters in the fovea condition. Moreover, as contrast-sensitive neurons, RGCs play an important role in detecting differences in contrast (24, 26). Previous studies have shown that the low-contrast letter test could detect visual loss in patients with ocular hypertension and glaucoma, even when conventional VA was normal (17). Kwon et al. also pointed out an elevated contrast requirement for letter recognition in central vision (24).

In the present study, we sought to measure the effect of both a high-pass design and a low-contrast setting on the pattern resolution of glaucomatous eyes under foveal viewing. We wanted to first confirm whether low-contrast high-pass optotypes could better serve as stimuli for glaucoma detection and then to assess the structure-function relationships between retinal thicknesses measured by SD-OCT and VAs to find the potential structural basis that undermined central pattern vision in glaucomatous eyes.

In agreement with previous studies (14, 25), the recognition thresholds for high-pass optotypes were significantly higher than those for conventional letters in fovea viewing. As the contrast decreased, even higher thresholds were shown (**Figure 4**). Given that most of the low-frequency information was extracted from the stimuli, increasing letter size was obliged to turn the higher spatial frequencies into lower spatial frequencies so that the visual system could resolve the content. When the low contrast setting was superimposed, an even larger size was required. However, compared with healthy control eyes, glaucomatous eyes showed a greater level of disagreement between conventional VA and high-pass VA (**Figure 5**). Even at the 100% contrast level, there is a significant difference between the two VAs. Part of this might be explained by the slightly lopsided VA level between the glaucoma patients with normal vision and the healthy controls (-0.09 ± 0.08 logMAR vs. -0.17 ± 0.07 logMAR). However, the peculiar property of high-pass design may also account for this. We also notice that the lower the contrast was, the larger this difference was. Among glaucoma patients, conventional VA measurements were nearly 3 lines (0.28 logMAR) better than 100% high-pass acuity measurements compared with a figure of 2 lines (0.22 logMAR) in the healthy control group. For the data between the 1.25% high-pass VA and conventional VA, the disparity enlarged to 11 lines (1.08 logMAR) vs. 9 lines (0.93 logMAR). However, while the findings of low-contrast high-pass VA charts are potentially clinical meaningful, their value will be greatly diminished if large test-retest variabilities (TRVs) exists. **Figure 3** graphically displays the results of repeated measurements for each VA chart among glaucoma patients with normal vision and healthy controls separately. We found that TRV for each VA chart were similar in both groups. In line with previous studies, the TRV for the high-pass VA chart at 100% contrast setting are lower than that for the conventional VA chart (27). Poorer TRVs were showed in glaucoma patients both for high-pass VA charts and conventional VA chart. TRVs for high-pass VA charts with lower contrast settings were even higher (TRV values varying from $\pm$ 0.10 to $\pm$ 0.14 logMAR). However, here TRVs were measured only in 20 glaucoma patients and 20 normal subjects with these charts. Future work is require to explore this issue in a larger sample size. We can also see from **Figure 5** that the significant regression slopes indicated that the difference between conventional VA and high-pass VA was greater in glaucoma subjects with worse acuity. This suggests that the high-pass charts are able to detect functional loss as a result of glaucoma damage when conventional VA is still normal. In addition, 1.25% low-contrast high-pass VA had the highest sensitivity and specificity of these techniques.

Kim et al. pointed out that only weak structure-function relationships were shown between macular mGCC parameters and conventional VA ($r = -0.363$ to -0.410), and the global average cpRNFL thickness showed the highest correlation with

coefficient value of −0.447 (28). Our findings showed that most of the RGC-related parameters from macular SD-OCT scans correlated better with high-pass VAs, particularly the 1.25% low-contrast high-pass VAs. The 1.25% low-contrast high-pass VA showed stronger structure-function correlations with nasal-side RGC-related thickness than conventional VA with statistical significance. However, there were only weak-to-moderate correlations between cpRNFL and VAs. These results are different from those in the study by Kim et al., which may be due to the different spectrum of glaucomatous damage involved. Here, we focused on the population with relatively good VA (BCVA equal to or better than 0.20 logMAR on ETDRS chart) but no requirement for VF defects. Given that the RNFL contains not merely nerve fibers but also non-neural or glial tissues, it is readily comprehensible that macular thickness parameters, especially RGC-related ones, are supposed to demonstrate stronger structure-function relationships than cpRNFL parameters with functional parameters that are sensitive to glaucoma damage.

We acknowledge that our study has some major limitations. First, our study is failed to make comparisons between conventional chart and high-pass chart at equal contrast levels. We hold the view that it is better to have a standard reference, like ETDRS chart used in the current study, for the multi-contrast comparisons. However, these have already been integrated within the scope of our further study. Second, as one of the main purposes of this study was to investigate whether low-contrast high-pass acuity charts were able to detect functional loss as a result of glaucoma damage when conventional VA was still quite good, we only included glaucoma patients with ETDRS logMAR VA equal to or better than 0.20 logMAR, which does not cover the full spectrum of glaucomatous damage. Third, no longitudinal investigations were conducted to determine RGC damage and high-pass VA loss over time, which prevents the study from indicating the ability of high-pass stimuli to detect glaucomatous progression. Fourth, the participants included were relatively young generally, therefore the findings are not applicable for the older population with glaucoma in whom cataract and macular degeneration are common.

To summarize, VA measurements taken with low-contrast high-pass acuity charts appear to be more sensitive in detecting central visual loss in glaucoma than those taken with conventional charts. Nasal-side macular GCL thinning appears to be associated with low-contrast high-pass visual loss in glaucomatous eyes.

DATA AVAILABILITY STATEMENT

The raw data supporting the conclusions of this article will be made available by the authors, without undue reservation.

ETHICS STATEMENT

The studies involving human participants were reviewed and approved by the ethics committee of the Zhongshan Ophthalmic Center (NO.2019KYPJ115). The patients/participants provided their written informed consent to participate in this study.

AUTHOR CONTRIBUTIONS

YW, ZC, and MY conceived and designed the study. ZC, YK, and HC conducted the coding and programming. YW, ZC, CZ, YY, JX, and MY analyzed and interpreted the patient data. YW analyzed the data and was a major contributor in writing the manuscript. All authors provided critical appraisal and final approval of the manuscript.

FUNDING

This study was supported by the Space Medical Experiment Project of China Manned Space Program (HYZHXM01015) and the Natural Science Foundation Team Project of Guangdong Province Grant (2015A030312016) to MY, and National Natural Science Foundation for Young Scientists to ZC (81600761).

REFERENCES

1. Jonas JB, Aung T, Bourne RR, Bron AM, Ritch R, Panda-Jonas S. Glaucoma. *Lancet*. (2017) 390:2183–93. doi: 10.1016/S0140-6736(17)31469-1
2. Prum BE Jr, Rosenberg LF, Gedde SJ, Mansberger SL, Stein JD, Moroi SE, et al. Primary open-angle glaucoma preferred practice pattern(®) guidelines. *Ophthalmology*. (2016) 123:41–111. doi: 10.1016/j.ophtha201510053
3. Stamper RL. The effect of glaucoma on central visual function. *Trans Am Ophthalmol Soc*. (1984) 82:792–826.
4. Tanna AP. Growing evidence of the importance of the macula in glaucoma. *JAMA Ophthalmol*. (2017) 135:747–8. doi: 10.1001/jamaophthalmol20171379
5. Hu CX, Zangalli C, Hsieh M, Gupta L, Williams AL, Richman J, et al. What do patients with glaucoma see? Visual symptoms reported by patients with glaucoma. *Am J Med Sci*. (2014) 348:403–9. doi: 10.1097/MAJ0000000000000319
6. Hood DC, Slobodnick A, Raza AS, de Moraes CG, Teng CC, Ritch R. Early glaucoma involves both deep local, and shallow widespread, retinal nerve fiber damage of the macular region. *Invest Ophthalmol Vis Sci*. (2014) 55:632–49. doi: 10.1167/iovs13-13130
7. Hood DC, Raza AS, de Moraes CG, Liebmann JM, Ritch R. Glaucomatous damage of the macula. *Prog Retin Eye Res*. (2013) 32:1–21. doi: 10.1016/j.preteyeres201208003
8. Senger C, da Silva MJL, De Moraes CG, Messias A, Paula JS. Spatial correlation between localized decreases in exploratory visual search performance and areas of glaucomatous visual field loss. *Graefes Arch Clin Exp Ophthalmol*. (2019) 257:153–60. doi: 10.1007/s00417-018-4164-9
9. Rubin GS, Legge GE. Psychophysics of reading. VI-The role of contrast in low vision. *Vision Res*. (1989) 29:79–91. doi: 10.1016/0042-6989(89)90175-2
10. Hirji SH, Liebmann JM, Hood DC, Cioffi GA, Blumberg DM. Macular damage in glaucoma is associated with deficits in facial recognition. *Am J Ophthalmol*. (2020) 217:1–9. doi: 10.1016/j.ajo202004032
11. Ichhpujani P, Thakur S, Spaeth GL. Contrast sensitivity and glaucoma. *J Glaucoma*. (2020) 29:71–5. doi: 10.1097/IJG0000000000001379
12. Frisén L. Vanishing optotypes. New type of acuity test letters. *Arch Ophthalmol*. (1986) 104:1194. doi: 10.1001/archopht198601050200100060
13. Howland B, Ginsburg A, Campbell F. High-pass spatial frequency letters as clinical optotypes. *Vision Res*. (1978) 18:1063–6. doi: 10.1016/0042-6989(78)90036-6

14. Shah N, Dakin SC, Dobinson S, Tufail A, Egan CA, Anderson RS. Visual acuity loss in patients with age-related macular degeneration measured using a novel high-pass letter chart. *Br J Ophthalmol*. (2016) 100:1346–52. doi: 10.1136/bjophthalmol-2015-307375
15. Balcer LJ, Frohman EM. Evaluating loss of visual function in multiple sclerosis as measured by low-contrast letter acuity. *Neurology*. (2010) 74:S16–23. doi: 10.1212/WNL0b013e3181dbb664
16. Park SH, Park CY, Shin YJ, Jeong KS, Kim NH. Low contrast visual acuity might help to detect previous optic neuritis. *Front Neurol*. (2020) 11:602193. doi: 10.3389/fneur2020602193
17. Regan D, Neima D. Low-contrast letter charts in early diabetic retinopathy, ocular hypertension, glaucoma, and Parkinson's disease. *Br J Ophthalmol*. (1984) 68:885–9. doi: 10.1136/bjo6812885
18. Chylack LT Jr, Wolfe JK, Singer DM, Leske MC, Bullimore MA, Bailey IL, et al. The lens opacities classification system III. *Arch Ophthalmol*. (1993) 111:831–6. doi: 10.1001/archopht199301090060119035
19. Ferris FL III, Kassoff A, Bresnick GH, Bailey I. New visual acuity charts for clinical research. *Am J Ophthalmol*. (1982) 94:91–6. doi: 10.1016/0002-9394(82)90197-0
20. Bland JM, Altman DG. Statistical methods for assessing agreement between two methods of clinical measurement. *Lancet*. (1986) 1:307–10. doi: 10.1016/S0140-6736(86)90837-8
21. Hood DC. Improving our understanding, and detection, of glaucomatous damage: An approach based upon optical coherence tomography (OCT). *Prog Retin Eye Res*. (2017) 57:46–75. doi: 10.1016/j.preteyeres2016 12002
22. Prager AJ, Hood DC, Liebmann JM, De Moraes CG, Al-Aswad LA, Yu Q, et al. Association of glaucoma-related, optical coherence tomography-measured macular damage with vision-related quality of life. *JAMA Ophthalmol*. (2017) 135:783–8. doi: 10.1001/jamaophthalmol20171659
23. Ohkubo S, Higashide T, Udagawa S, Sugiyama K, Hangai M, Yoshimura N, et al. Focal relationship between structure and function within the central 10 degrees in glaucoma. *Invest Ophthalmol Vis Sci*. (2014) 55:5269–77. doi: 10.1167/iovs14-14153
24. Chien L, Liu R, Girkin C, Kwon M. Higher contrast requirement for letter recognition and macular RGC+ layer thinning in glaucoma patients and older adults. *Invest Ophthalmol Vis Sci*. (2017) 58:6221–31. doi: 10.1167/iovs17-22621
25. Shah N, Dakin SC, Anderson RS. Effect of optical defocus on detection and recognition of vanishing optotype letters in the fovea and periphery. *Invest Ophthalmol Vis Sci*. (2012) 53:7063–70. doi: 10.1167/iovs12-9864
26. Liu R, Kwon M. Increased equivalent input noise in glaucomatous central vision: is it due to undersampling of retinal ganglion cells? *Invest Ophthalmol Vis Sci*. (2020) 61:10. doi: 10.1167/iovs61810
27. Nilpa S, Dakin SC, Whitaker HL, Anderson RS. Effect of scoring and termination rules on test-retest variability of a novel high-pass letter acuity chart. *Invest Ophthalmol Vis Sci*. (2014) 55:1386–92. doi: 10.1167/iovs13-13340
28. Kim JH, Lee HS, Kim NR, Seong GJ, Kim CY. Relationship between visual acuity and retinal structures measured by spectral domain optical coherence tomography in patients with open-angle glaucoma. *Invest Ophthalmol Vis Sci*. (2014) 55:4801–11. doi: 10.1167/iovs13-13052

Conflict of Interest: The authors declare that the research was conducted in the absence of any commercial or financial relationships that could be construed as a potential conflict of interest.

frontiers in Medicine

ORIGINAL RESEARCH
published: 04 June 2021
doi: 10.3389/fmed.2021.684676

Extended Ganglion Cell Layer Thickness Deviation Maps With OCT in Glaucoma Diagnosis

Paul Lehmann[†], *Bettina Hohberger*[†], *Robert Lämmer and Christian Mardin*[*]

Department of Ophthalmology, University of Erlangen-Nürnberg, Friedrich-Alexander-University of Erlangen-Nürnberg, Erlangen, Germany

OPEN ACCESS

Edited by:
Michele Lanza, University of Campania Luigi Vanvitelli, Italy

Reviewed by:
Brent Siesky, Icahn School of Medicine at Mount Sinai, United States
Christoph Faschinger, Private Practitioner, Graz, Austria
Huiyuan Hou, University of California, San Diego, United States
Feng Wen, Sun Yat-sen University, China

***Correspondence:**
Christian Mardin
christian.mardin@uk-erlangen.de

[†]*These authors have contributed equally to this work and share first authorship*

Specialty section:
This article was submitted to Ophthalmology, a section of the journal Frontiers in Medicine

Received: *23 March 2021*
Accepted: *30 April 2021*
Published: *04 June 2021*

Citation:
Lehmann P, Hohberger B, Lämmer R and Mardin C (2021) Extended Ganglion Cell Layer Thickness Deviation Maps With OCT in Glaucoma Diagnosis. Front. Med. 8:684676. doi: 10.3389/fmed.2021.684676

Purpose: The aim of the present study was to investigate the diagnostic power of RGCL in the macula quantitatively and qualitatively by using a conventional and extended elliptic grid with deviation maps.

Subjects and Methods: Thickness of RGCL was measured using SPECTRALIS® OCT (Heidelberg Engineering, Heidelberg, Germany) in 150 eyes of 150 subjects of the Erlangen Glaucoma Registry (EGR; NTC00494923): 26 ocular hypertension (OHT), 39 pre-perimetric open-angle glaucoma (pre-OAG), 19 normal tension glaucoma (NTG), 34 primary open-angle glaucoma (POAG), 16 secondary open-angle glaucoma (SOAG), and 16 controls. Analysis of RGCL was done quantitatively (global value, GV) and qualitatively (qualitative total value, QTV) by using a color-coded point score for data of the common elliptic macular grid of deviation maps. Furthermore, qualitative analysis of RGCL was done for an extended elliptic macula grid (extended qualitative total value, eQTV). Receiver operating characteristic (ROC) curves were calculated for the conventional and the enlarged macular grid for all subjects' groups.

Results: GV of RGCL thickness differed significantly between pre-OAG ($p < 0.05$), NTG ($p < 0.001$), POAG ($p < 0.001$), SOAG ($p < 0.001$), yet not OHT ($p > 0.05$) and controls, respectively. Quantitative ROC analysis of GV showed AUC of 0.965 (SOAG), 0.942 (POAG), 0.916 (NTG), 0.772 (pre-OAG), and 0.526 (OHT). QTV differed significantly between pre-POAG ($p < 0.05$), NTG ($p < 0.001$), POAG ($p < 0.001$), SOAG ($p < 0.001$), yet not OHT ($p > 0.05$) and controls, respectively. Qualitative ROC analysis of QTV showed AUCs of 0.908 (NTG) 0.914 (POAG), 0.930 (SOAG), 0.734 (pre-POAG), and 0.519 (OHT). Implementation of eQTV yielded even higher AUCs for NTG (0.919), POAG (0.969), and SOAG (0.973) compared to GV. Similar AUCs of eQTV and GV were observed for OHT (0.514) and pre-OAG (0.770).

Conclusion: The results of the present study showed that quantitative and qualitative analysis of RGCL thickness yielded similar diagnostic impacts compared to RNFL. Qualitative analysis might be a quick and easy useable tool for clinical all-day life. The present data suggest that analysis of an extended macula region might improve its diagnostic impact.

Keywords: retinal ganlion cell, OCT, spectralis, glaucoma, GRID

INTRODUCTION

Glaucoma is one of the most common causes of blindness worldwide. The health burden caused by glaucoma increased in the last 25 years (1, 2). Several risk factors are involved in the multifactorial pathogenesis of this neurodegenerative disease (3) including advanced age, positive family history, severe myopia, and its main risk factor an elevated intraocular pressure (IOP) (4, 5). It is assumed that high IOP triggers retinal ganglion cell (RGC) loss (6). Loss of RGCs occurs before functional abnormalities can be seen in a patient's perimetry (7).

Optical coherence tomography (OCT) offers the ability to examine characteristics of the retina and optic nerve head of glaucoma patients in an objective and non-invasive way (8). Thereby, scan quality reaches to the level of histological images. It seems to be more precisely than perimetry for diagnosing the progression of glaucoma in earlier stages (9). Next to measurement of the peripapillary retinal nerve fiber layer (RNFL), RGC layer (RGCL) thickness can be quantified (10). The RNFL thinning decreases in speed while glaucoma disease continues to progress. In contrast, RGCL thickness continued to decrease constantly with glaucoma progression (9). Thus, analysis of RGCL thickness might offer an additional diagnostic parameter for revealing progression of glaucoma from early to advanced stages. In eyes with early pre-perimetric glaucoma average RGCL thickness and especially the inferior region of the macula RGCL were observed to be the most appropriate ones for diagnostics (7). Implementation of enlarged grids for RGCL analysis, enabling analysis of larger macula regions, lead to an enhanced diagnostic power, as temporal quadrants of larger macular grids reached highest AUC value (11).

Most of the recent studies analyzed the ganglion cell complex (GCC), consisting of the inner plexiform layer (IPL), ganglion cell layer (GCL), and retinal nerve fiber layer (RNFL) (12) or GCIPL (i.e., GCL and IPL) (13, 14). To best of our knowledge, we did not find a study in literature focusing on single RGCL thickness in patients with different types of glaucoma. However, a finer analysis of macular retinal layers could identify distinct alterations of retinal ganglion cells. Thus, by analyzing single RGCL thickness, very fine changes in RGCL could be detected at even earlier stages of disease. The aim of the present study was to investigate the diagnostic power of only RGCL in the macula quantitatively and qualitatively by using a conventional and extended elliptic grid in patients with ocular hypertension (OHT), pre-perimetric open-angle glaucoma (pre-OAG), normal tension glaucoma (NTG), primary open-angle glaucoma (POAG), and secondary open-angle glaucoma (SOAG) compared to controls. In addition, RGCL data were compared to RNFL in patients' groups.

MATERIALS AND METHODS

Patients

One hundred fifty eyes of 150 patients of the Erlangen Glaucoma Registry (EGR; NTC00494923) of the Department of Ophthalmology of the University of Erlangen-Nürnberg were analyzed retrospectively: 26 ocular hypertension (OHT), 39 pre-perimetric open-angle glaucoma (pre-OAG), 19 normal tension glaucoma (NTG), 34 primary open-angle glaucoma (POAG), 16 secondary open-angle glaucoma (SOAG), and 16 controls. The EGR is a longitudinal follow-up study under therapy, including subjects with manifest glaucoma, glaucoma suspects, and a control group. All patients received an ophthalmic examination, including slit lamp microscopy, fundoscopy, and gonioscopy. IOP was measured by Goldmann applanation tonometry. Visual field was tested using white-on-white Octopus perimetry (mean defect, MD; Octopus 500, 900; program G1, Interzeag, Schlieren, Schweiz, Peridata Software). Demographic data of all subjects can be seen in **Table 1**.

TABLE 1 | Classification of perimetric glaucoma patients (NTG, POAG, SOAG) into subgroups based on mean defect (MD, Octopus perimetry): mild, moderate, and advanced; ratio represents percentage of disease severity in all perimetric glaucoma eyes.

Severity	Total ratio %	NTG	POAG	SOAG
Mild MD $\leq$ 6 dB	30.4	5	11	5
Moderate MD $>$ 6 dB and $\leq$ 12 dB	33.3	10	9	4
Advanced MD $>$ 12 dB	36.2	4	14	7

Diagnosis was done according to the following criteria:

OHT

Diagnosis of OHT was based on an increased IOP $>$ 21 mmHg (repeated twice). Optic nerve head and visual fields showed no pathological alterations.

Pre-OAG

Pre-OAG showed an increased IOP $>$ 21 mmHg (repeated twice), alterations of the optic nerve head, classified according to Jonas et al. (15) Visual field was normal.

POAG

Diagnosis of POAG was based on an increased IOP $>$ 21 mmHg (repeated twice), alterations of the optic nerve head, classified according to Jonas et al. Visual field defects were detected according to the following criteria: Scotomas with $\geq$3 neighboring test points on the pattern deviation map with a probability of $<$5%, $\geq$2 adjacent test points on the pattern deviation map with a probability of $<$1% and MD $>$ 2.8 dB. These perimetric defects had to be located at the same side in at least 2 consecutive examinations.

NTG

Diagnosis of NTG was as for POAG (see above), yet IOP was within normal ranges $\leq$21 mmHg.

SOAG

Patients meeting criteria of POAG and additionally were affected by pseudoexfoliation syndrome (7) or melanin dispersion (9) were classified as SOAG.

If both eyes met the inclusion criteria, one eye of each person was selected randomly for the present analysis. Glaucoma

TABLE 2 | Demographic data: median and quartiles [of all subgroups (OHT, pre-OAG, POAG, NTG, SOAG, controls); Gender [m/f]], Age [years], BCVA, IOP [mmHg], MD [dB], and RNFL [μm].

	Gender [m/f]	Age [years]	BCVA	IOP [mmHg]	MD [dB]	Global RNFL [μm]
OHT	13/13	60.0 (49.8–71.3)	0.8 (0.8–1.0)	17.0 (15.0–19.0)	2.18 (0.9–3.4)	94.0 (88.0–103.3)
Pre-OAG	20/19	66.0 (60.0–75.0)	1.0 (0.8–1.0)	14.0 (12.0–17.0)	2.5 (1.1–4.4)	76.0 (64.0–84.0)
NTG	6/13	75.0 (66.0–80.0)	0.7 (0.5–0.9)	10.0 (10.0–13.0)	9.1 (4.5–12.0)	62.0 (55.0–73.0)
POAG	15/19	71.0 (65.5–78.0)	0.8 (0.6–0.9)	13.0 (11.8–15.0)	9.65 (4.4–13.9)	55.5 (48.0–72.8)
SOAG	10/6	66.0 (56.0–75.3)	0.63 (0.5–1.0)	12.5 (10.0–14.8)	9.7 (5.1–17.1)	59.0 (49.3–67.3)
Controls	5/11	57.5 (51.3–66.5)	0.95 (0.8–1.0)	13.5 (12.0–16.0)	1.33 (0.2–2.7)	90.0 (87.0–96.0)

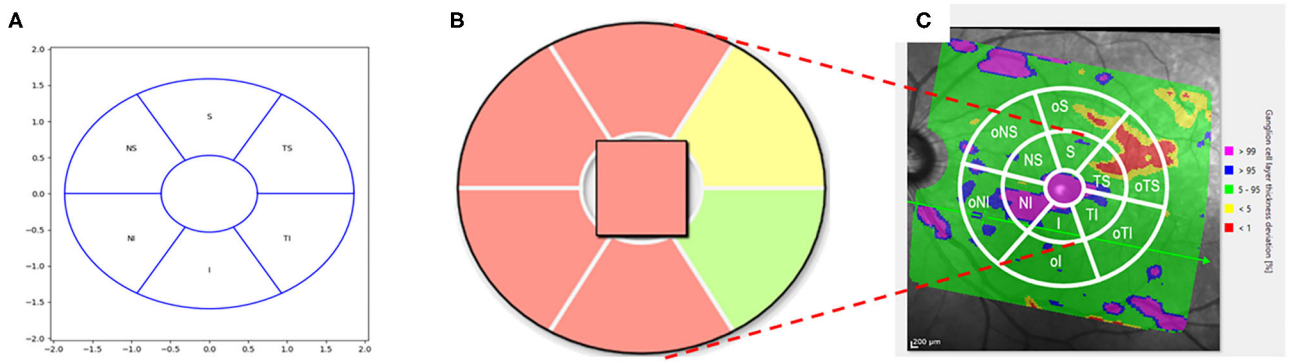

FIGURE 1 | Schematic scetch of the conventional macular grid **(A)** with color coding **(B)** and extended version **(C)**. **(A)** Conventional Macular Grid: The macular grid was defined by an elliptical ring: the inner radius was 0.618 mm in the horizontal axis and the inner radius of the vertical axis was 0.531 mm. The outer radius of the elliptical ring was 1.857 mm horizontally and 1.590 mm vertically. The elliptical ring was divided into 6 sectors with angles of 60°. These 6 sectors of the macular grid corresponded to the superior (S), inferior (I), temporal-superior (TS), temporal-inferior (TI), nasal-superior (NS), and nasal-inferior (NI) macular region. **(B)** Macular Grid color-coding: The sectors of the macular grid were color-coded according to percentiles: A sector is marked with green if the thickness of the RGCL in this sector is >5th percentile of a healthy reference population. If a sector is colored yellow, the value of the average RGCL thickness < 5th percentile, yet > 1st percentile of the reference database. A red colored sector represented data which were < 1st percentile. In the qualitative analysis, a green sector was counted with one point, a yellow sector with 2 and a red sector with 3 points. (C) Extended Macular Grid: An enlarged elliptical ring was added to the pre-existing macular grid (extended macular grid): 3.714 mm horizontally and 3.18 mm vertically (i.e., doubled outer radii of the conventional macular grid, respectively). This resulted in 6 new outer sectors (o). The outer sectors were called outer superior (oS), outer inferior (oI), outer temporal-superior (oTS), outer temporal-inferior (oTI), outer nasal-superior (oNS), and outer nasal-inferior (oNI).

patients were classified into 3 groups based on the severity of visual field defect in Octopus perimetry. Mild glaucoma was defined as MD ≤ 6 dB. Moderate glaucoma was present when the patient's MD was >6 dB and ≤12 dB. Advanced glaucoma was allocated when MD was >12 dB. Classification of patients with mild, moderate and advanced glaucoma can be seen in **Table 2**.

Controls

Control eyes showed an IOP within normal ranges ≤21 mmHg, no alterations of the optic nerve head and a normal visual field. MD was ≤2.8 dB. Less than 3 adjacent test points on the pattern deviation map with a probability of <5% and <2 adjacent test points on the pattern deviation map with a probability of <1%.

Thickness of the retinal ganglion cell layer (RGCL) and global retinal nerve fiber layer thickness (gRNFL) were measured using SPECTRALIS® optical coherence tomography (Heidelberg Engineering, Heidelberg, Germany). "Macular grid" was used to study the region of the macula lutea. On the basis of a 30°×25° volume scan of the macula the macular grid is defined by an elliptical ring (**Figure 1A**): the inner radius was 0.618 mm in the horizontal axis and the inner radius of the vertical axis was 0.531 mm. Outer radius of the elliptical ring was 1.857 mm horizontally and 1.590 mm vertically. The elliptical ring was divided into 6 sectors with angles of 60°. These 6 sectors of the macula grid corresponded to the superior (S), inferior (I), temporal-superior (TS), temporal-inferior (TI), nasal-superior (NS), and nasal-inferior (NI) macular region. Macular grid is normalized to the axis between the center of Bruch's membrane opening of the disc and the foveola (Anatomic Positioning System, APS).

Thickness of RGCL was measured (μm) by Spectralis II (Heidelberg, Germany). Sectorial and global mean (*global value "GV"*) were presented, respectively. The sectors of the macular grid in so-called deviation maps were color-coded according to percentiles (**Figure 1B**): A sector is marked with green if thickness of the RGCL in this sector is >5th percentile of a healthy reference population (16). If a sector is colored yellow, the value of the average RGCL thickness < 5th percentile, yet > 1st percentile of the reference database. A red colored sector represented data which were < 1st percentile. The

TABLE 3 | Global and sectorial RGCL thickness (median, quartiles; μm) of all subgroups (OHT, pre-OAG, NTG, POAG, SOAG, controls); GV, global value; TS, temporal superior; S, superior; NS, nasal superior; NI, nasal inferior; I, inferior; TI, temporal inferior; p-values (p) for comparison of each subgroup with controls for quantitative RGCL thickness ([μm], Bonferroni-corrected).

	OHT	Pre-OAG	POAG
GV	51.5 (47.0–55.0) $p > 0.05$	45.0 (37.0–49.0) $p < 0.05$	35.0 (27.8–40.0) $p < 0.001$
TS	48.5 (43.6–52.0) $p > 0.05$	38.0 (29.0–47.0) $p < 0.05$	29.0 (21.0-41.0) $p < 0.001$
S	53.0 (48.8–56.3) $p > 0.05$	45.0 (35.0–51.0) $p < 0.05$	39.5 (30.0–45.3) $p < 0.001$
NS	52.0 (48.0–56.0) $p > 0.05$	47.0 (41.0–52.0) $p < 0.05$	39.5 (30.8–47.5) $p < 0.001$
NI	52.5 (48.8–56.0) $p > 0.05$	48.0 (41.0–52.0) $p > 0.05$	41.0 (32.8–44.8) $p < 0.001$
I	52.5 (49.0–54.0) $p > 0.05$	48.0 (40.0–51.0) $p < 0.05$	32.5 (24.8–42.3) $p < 0.001$
TI	51.5 (47.0–53.0) $p > 0.05$	45.0 (35.0–50.0) $p < 0.05$	27.0 (19.8–40.0) $p < 0.001$
	NTG	**SOAG**	**Controls**
GV	38.0 (29.0–42.0) $p < 0.001$	29.0 (24.3–38.3) $p < 0.001$	52.0 (48.3–53.0) 47.5 (44.0–50.0)
TS	31.0 (24.0–39.0) $p < 0.001$	23.5 (20.3–31.8) $p < 0.001$	53.0 (48.8–54.8) 53.5 (48.5–55.0)
S	40.0 (29.0–50.0) $p < 0.001$	29.0 (25.3–37.3) $p < 0.001$	53.0 (49.3–55.8) 52.0 (51.0–54.8)
NS	43.0 (35.0–52.0) $p < 0.001$	35.5 (26.3–44.0) $p < 0.001$	51.0 (47.5–52.8)
NI	45.0 (31.0–50.0) $p < 0.01$	33.0 (23.0–44.8) $p < 0.001$	
I	34.0 (24.0–45.0) $p < 0.001$	28.5 (24.0–38.8) $p < 0.001$	
TI	24.0 (18.0–40.0) $p < 0.001$	23.5 (18.8–34.3) $p < 0.001$	

SPECTRALIS® retinal thickness reference database is based on data of 255 eyes of 255 healthy patients of European origin. Data in this database were corrected due for age and the distance between fovea and BMO center using a multiple linear regression model. The study was done in accordance with the Helsinki Declaration and was approved by the ethics committee of the University of Erlangen-Nürnberg.

Extended Macular Grid

The SPECTRALIS® software measures a much larger retinal section than the central macular grid covers for RGCL analysis and these thickness deviation maps are also color-coded. Yet, only qualitative, no quantitative data of RGCL are available for this "extended" region.

An enlarged elliptical ring was added to the pre-existing macular grid (extended macular grid, **Figure 1C**): 3.714 mm horizontally and 3.18 mm vertically (i.e., doubled outer radii of the original macular grid, respectively). This resulted in 6 new outer sectors (o). The outer sectors were called outer superior (oS), outer inferior (oI), outer temporal-superior (oTS), outer temporal-inferior (oTI), outer nasal-superior (oNS), and outer nasal-inferior (oNI). Combing each original macular grid sector with its corresponding outer sector (for example eS = S + oS), extended sectors were created: extended superior (eS), extended inferior (eI), extended temporal-superior (eTS), extended temporal-inferior (eTI), extended nasal-superior (eNS), and extended nasal-inferior (eNI) sector.

Statistical Analysis

Statistical analysis was done using the SPSS Version 24.0. A non-parametric test (Mann-Whitney-U-Test) was used. All results were corrected according to Bonferroni considering multiple testing. A quantitative and qualitative analysis of the RGCL thickness were done. A self-developed point score was designed for qualitative analysis (see below). To compare statistical power of different ROCs, sensitivity, and specificity were calculated. When calculating sensitivity and specificity, cut-off was selected as the point where Youden index had its maximum (i.e., optimum sensitivity and specificity) (17).

Quantitative Analysis

Quantitative analysis measured the absolute RGCL thickness [μm] for each sector, respectively. In addition, mean of all sectors was calculated (i.e., global value; GV). Receiver Operating Characteristic (ROC) curves were performed considering each sector individually and GV.

Qualitative Analysis

For the qualitative analysis of the RGCL a point scoring was allocated to each sector of the macula grid (**Figure 1B**):

- red: 3 points
- yellow: 2 points
- green: 1 point

This point scoring of all sectors was summed up (i.e., qualitative total value; QTV). ROC curves were done for each sector of the macula grid and QTV.

Qualitative Analysis of the Extended Macular Grid

For the qualitative analysis of the RGCL thickness of the extended macular grid (**Figure 1C**) an additional point scoring was established. The following points were allocated for each of the 12 sectors (there had to be a cluster of at least 3 pixels to be counted valid):

- Only green (complete sector): 0 points
- Only yellow and ≤50% of the area in one sector: 1 point
- Only yellow and >50% of the area in one sector: 2 points
- Yellow and red and ≤50% of the area in one sector: 3 points
- Yellow and red and >50% of the area in one sector: 4 points
- Only red (complete sector): 5 points

The points of an extended sector were obtained by summing up the points from the outer sector with its corresponding sector from the original macular grid (for example points eS = points S + points oS). This point scoring of all extended sectors was summed up (i.e., extended qualitative total value; eQTV). ROC curves were done for each extended sector of the extended macula grid and eQTV.

TABLE 4 | AUC of ROC analysis of quantitative RGCL thickness for each subgroup (OHT, pre-OAG, NTG, POAG, SOAG vs. controls, respectively): global (GV, global value) and sectorial (TS, temporal superior; S, superior; NS, nasal superior; NI, nasal inferior; I, inferior; TI, temporal inferior).

		TS	S	NS	NI	I	TI	GV
OHT-controls	AUC	0.561	0.525	0.534	0.513	0.523	0.512	0.526
Pre-OAG-controls	AUC	0.748	0.763	0.742	0.708	0.78	0.795	0.772
NTG-controls	AUC	0.88	0.9	0.859	0.845	0.883	0.882	0.916
POAG-controls	AUC	0.903	0.926	0.886	0.884	0.937	0.945	0.942
SOAG-controls	AUC	0.977	0.959	0.936	0.918	0.965	0.947	0.965

RESULTS

Quantitative Analysis

Median and quartiles of RGCL thickness for GV and each sector can be seen in **Table 3**. In addition, **Table 3** shows *p*-values for all comparison groups. GV differed significantly between pre-OAG, NTG, POAG, SOAG, and controls ($p < 0.05$), respectively. Yet, no significant difference was observed between OHT and controls ($p > 0.05$).

ROC analysis of quantitative RGCL thickness is shown in **Table 4**. GV yielded highest AUCs for SOAG, POAG, and NTG vs. controls, respectively (>0.9). Sectorial analysis for these subgroups ranged between 0.882 and 0.977. AUCs of OHT vs. controls showed values between 0.5 and 0.6.

Qualitative Analysis

Median and quartiles of RGCL thickness score can be found in **Table 5**. *P*-values for all comparison groups are shown in **Table 5**. QTV of RGCL thickness score differed significantly between pre-OAG, NTG, POAG, SOAG, and controls ($p < 0.05$), respectively. Yet, not significant difference was observed between OHT and controls ($p > 0.05$).

ROC analysis of qualitative RGCL thickness score is shown in **Table 6**. QTV showed highest AUC for SOAG, POAG and NTG vs. controls, respectively (>0.9).

TABLE 5 | Total and sectorial RGCL thickness score (median, quartiles) of all subgroups (OHT, pre-OAG, NTG, POAG, SOAG, controls): QTV, qualitative total value; TS, temporal superior; S, superior; NS, nasal superior; NI, nasal inferior; I, inferior; TI, temporal inferior; p-values (p) for comparison of each subgroup with controls (Bonferroni-corrected).

	OHT	Pre-OAG	POAG
QTV	0.0 (0.0–0.0) $p > 0.05$	1.0 (0.0–7.0) $p < 0.05$	8.0 (4.0–11.0) $p < 0.001$
TS	0.0 (0.0–0.0) $p > 0.05$	0.0 (0.0–2.0) $p < 0.05$	2.0 (0.0–2.0) $p < 0.001$
S	0.0 (0.0–0.0) $p > 0.05$	0.0 (0.0–2.0) $p < 0.05$	1.5 (0.0–2.0) $p < 0.001$
NS	0.0 (0.0–0.0) $p > 0.05$	0.0 (0.0–1.0) $p > 0.05$	1.0 (0.0–2.0) $p < 0.001$
NI	0.0 (0.0–0.0) $p > 0.05$	0.0 (0.0–1.0) $p > 0.05$	1.0 (0.0–2.0) $p < 0.001$
I	0.0 (0.0–0.0) $p > 0.05$	0.0 (0.0–1.0) $p > 0.05$	2.0 (0.0–2.0) $p < 0.001$
TI	0.0 (0.0–0.0) $p > 0.05$	0.0 (0.0–2.0) $p < 0.05$	2.0 (0.8–2.0) $p < 0.001$
	NTG	**SOAG**	**Controls**
QTV	6.0 (3.0–12.0) <0.001	11.5 (6.0–12.0) $p < 0.001$	(0.0–0.0) (0.0–0.0)
TS	2.0 (0.0–2.0) $p < 0.05$	2.0 (2.0–2.0) $p < 0.001$	(0.0–0.0) (0.0–0.0)
S	1.0 (0.0–2.0) >0.05	2.0 (2.0–2.0) $p < 0.001$	(0.0–0.0) (0.0–0.0)
NS	0.0 (0.0–2.0) >0.05	2.0 (0.0–2.0) <0.01	0.0 (0.0–0.0)
NI	0.0 (0.0–2.0) >0.05	2.0 (0.0–2.0) <0.05	
I	2.0 (0.0-2.0) <0.05	2.0 (1.3–2.0) $p < 0.001$	
TI	2.0 (1.0–2.0) <0.05	2.0 (1.3–2.0) $p < 0.001$	

Comparison Quantitative vs. Qualitative Analysis

Comparing ROC curves of QTV and GV yielded similar AUC for each subgroup analysis (**Figure 2**). Mean difference between AUC of GV and QTV (Δ_{GV-QTV}) was 0.02 ± 0.016 for the total cohort. Subgroup analysis showed a Δ_{GV-QTV} of 0.007 (OHT vs. control), 0.043 (pre-OAG vs. controls), 0.008 (NTG vs. controls), 0.028 (POAG vs. controls), and 0.035 (SOAG vs. controls). Δ_{GV-QTV} plotted against their corresponding average can be seen in **Figure 3** for each subgroup, respectively.

Qualitative Analysis of Extended Macular Grid

Median and quartiles of extended RGCL thickness score is shown in **Table 7**. *P*-values for all comparison groups can be seen in **Table 7**. EQTV differed significantly between pre-OAG, NTG, POAG, SOAG, and controls ($p < 0.05$), respectively. Yet, not significant difference was observed between OHT and controls ($p > 0.05$).

ROC analysis of extended macular grid is shown in **Table 8**. EQTV yielded highest AUCs for SOAG, POAG, and NTG vs. controls, respectively (>0.9). Also, sectorial analysis reached high AUC values (**Table 8**).

Comparison of Quantitative (Macular Grid) Analysis vs. Extended Qualitative Analysis (Using Extended Macular Grid) and Global RNFL

Comparing ROC curves of GV and eQTV it can be noticed that eQTV yielded higher AUCs than GV in the comparison groups

TABLE 6 | AUC of ROC analysis of qualitative RGCL thickness score for each subgroup (OHT, pre-OAG, NTG, POAG, SOAG vs. controls, respectively): total (QTV, qualitative total value) and sectorial (TS, temporal superior; S, superior; NS, nasal superior; NI, nasal inferior; I, inferior; TI, temporal inferior).

		TS	S	NS	NI	I	TI	QTV
OHT-controls	AUC	0.528	0.51	0.538	0.508	0.531	0.519	0.519
Pre-OAG-controls	AUC	0.711	0.683	0.654	0.629	0.616	0.667	0.729
NTG-controls	AUC	0.857	0.747	0.737	0.692	0.832	0.895	0.908
POAG-controls	AUC	0.81	0.832	0.794	0.806	0.826	0.882	0.914
SOAG-controls	AUC	0.932	0.9	0.81	0.799	0.93	0.938	0.93

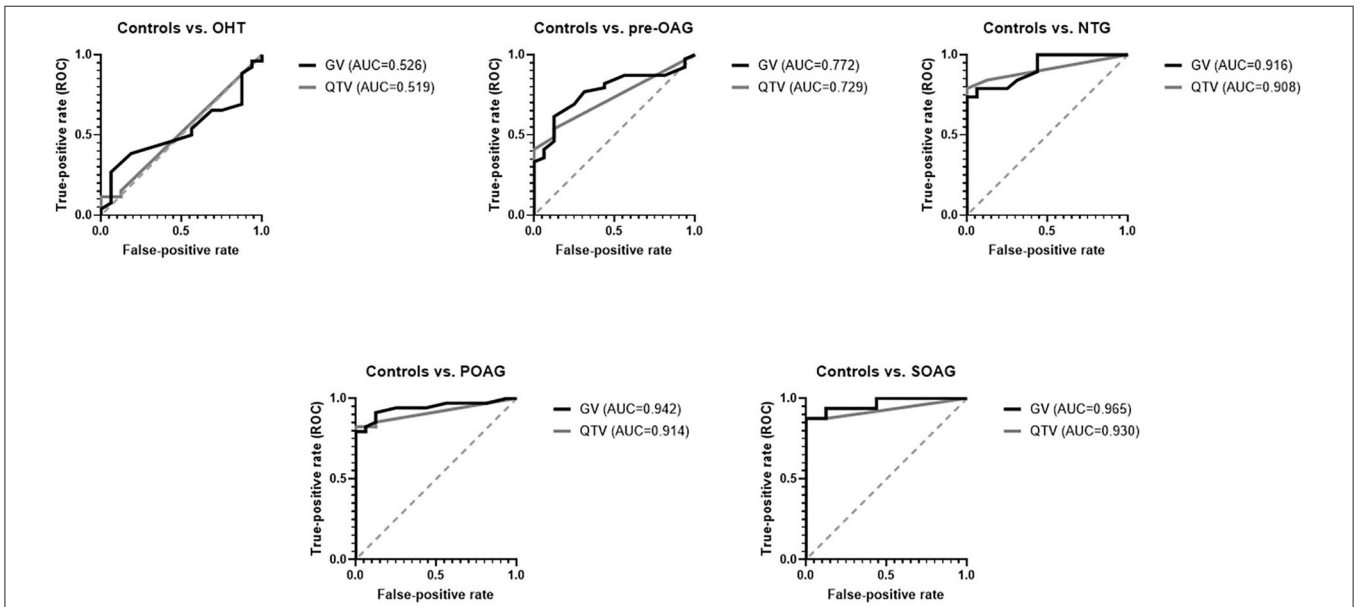

FIGURE 2 | ROC curves for GV and QTV for each subgroup (controls, OHT, Pre-OAG, NTG, POAG, SOAG): GV and QTV yielded similar AUCs.

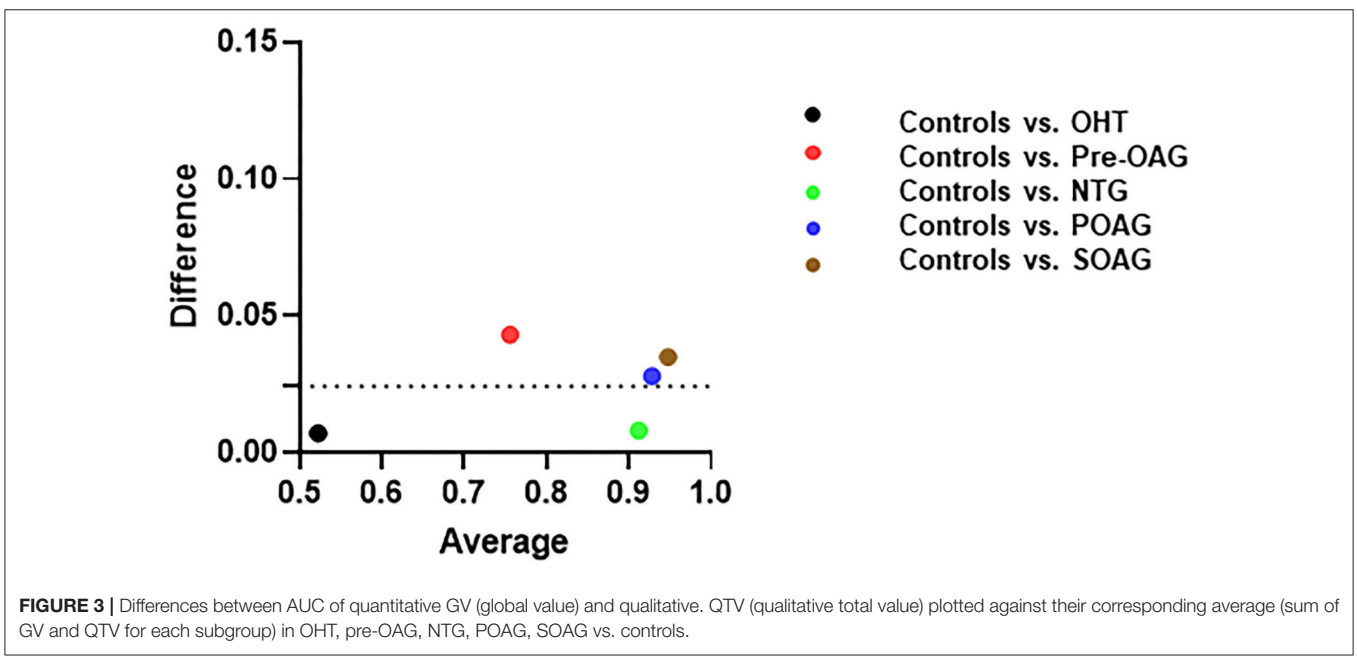

FIGURE 3 | Differences between AUC of quantitative GV (global value) and qualitative. QTV (qualitative total value) plotted against their corresponding average (sum of GV and QTV for each subgroup) in OHT, pre-OAG, NTG, POAG, SOAG vs. controls.

TABLE 7 | Extended QTV (qualitative total value) and extended sector scoring of RGCL thickness (median, quartiles) of all subgroups (OHT, pre-OAG, NTG, POAG, SOAG, controls); eQTV, extended qualitative total value; eTS, extended temporal superior; eS, extended superior; eNS, extended nasal superior; eNI, extended nasal inferior; eI, extended inferior; eTI, extended temporal inferior; p-values (p) for comparison of each subgroup with controls (Bonferroni-corrected).

	OHT	**Pre-OAG**	**POAG**
eQTV	5.0 (3.0–12.3) >0.05	20.0 (8.0–42.0) <0.01	40.0 (31.8–46.3) <0.001
eTS	1.0 (0.0–3.0) >0.05	5.0 (1.0–7.0) <0.01	7.0 (4.8–8.0) <0.001
eS	1.0 (0.0–3.0) >0.05	4.0 (1.0–7.0) <0.01	7.5 (4.0–8.0) <0.001
eNS	1.0 (0.0–2.3) >0.05	4.0 (0.0–7.0) >0.05	7.0 (4.0–7.0) <0.001
eNI	0.0 (0.0–3.0) >0.05	2.0 (1.0–7.0) >0.05	7.0 (6.0–7.0) <0.001
eI	0.0 (0.0–1.0) >0.05	3.0 (0.0–7.0) >0.05	7.0 (3.8–8.0) <0.001
eTI	0.0 (0.0–3.0) >0.05	4.0 (0.0–7.0) <0.05	8.0 (6.8–8.0) <0.001
	NTG	**SOAG**	**Controls**
eQTV	40.0 (32.0–45.0) <0.001	11.5 (6.0–12.0) <0.001	43.5 (35.5–47.0) 8.0 (7.0–8.0)
eTS	7.0 (4.8–8.0) <0.001	2.0 (2.0–2.0) <0.001	8.5 (7.0–8.0) 7.0 (4.5–8.0)
eS	7.5 (4.0–8.0) <0.001	2.0 (2.0–2.0) <0.001	7.0 (5.3–7.0) 7.0 (5.5–8.0)
eNS	7.0 (4.0–7.0) <0.05	2.0 (0.0–2.0) <0.01	8.0 (7.0–8.0)
eNI	7.0 (6.0–7.0) <0.001	2.0 (0.0–2.0) <0.05	
eI	7.0 (3.8–8.0) <0.001	2.0 (1.3–2.0) <0.001	
eTI	8.0 (6.8–8.0) <0.001	2.0 (1.3–2.0) <0.001	

SOAG, POAG, and NTG vs. controls, respectively (**Figure 4**). At fixed specificity of 100% GV and eQTV had the same sensitivity in SOAG vs. controls; in NTG vs. controls sensitivity of eQTV was even higher (**Table 9**). In the two remaining subgroups (OHT, pre-OAG), the AUCs of eQTV and GV behaved similarly (**Figure 4** and **Table 9**). In SOAG vs. controls, AUC of global RNFL behaved similarly to AUC of eQTV and GV. Sensitivity and specificity in this subgroup were the same for GV, eQTV, and global RNFL (**Table 9**). In POAG vs. controls, AUC of global RNFL was smaller than GV and eQTV. In NTG, pre-OAG, and OHT vs. controls, respectively, global RNFL had the highest AUC (**Table 9**).

DISCUSSION

By 2040, the number of patients with glaucoma will have risen to 111.8 million worldwide, visualizing the impact of glaucoma disease (18). Glaucoma is a multifactorial disease with an elevated IOP as most important risk factor, known until now (19). Several studies showed that an increased IOP leads to RGC loss (20–25). One molecular mechanism might be seen in the presence of mechanosensitive Piezo channels within the GCL (26). Piezo channels enable cells to convert a mechanical force into a molecular signaling by detection of e.g., shear stress. After activation of Piezo channels a non-selective influx of cations into the cell generates membrane depolarization and activation of different signaling pathways (Ca^{2+} dependent) (27). Interestingly, the number of retinal Piezo 2 channels within the RGCL was increased after elevating IOP in an animal model (mice) (26). Morphometric measurements of RGCL seem to be prior compared to functional tests (28). It was shown that macular thickness measured by OCT can be considered as a surrogate indicator of RGC loss (29). Especially, in myopic eyes macular GCC thickness measurement performed better than RNFL (30). The present study showed that even looking at the qualitative analysis of RGCL data, yielded a similar diagnostic impact as quantitative data. This has a very practical impact in everyday clinical work where areas of ganglion cell layer thinning can immediately be noticed by an examiner. In addition, implementation of an enlarged macular grid in RGCL analysis was very well-suited to distinguish healthy from glaucoma subjects. It is notable that purely qualitative analysis of the enlarged macular grid—using a point score—yielded higher or at least similar good AUCs compared to the quantitative analysis of conventional smaller macular grid.

Data from earlier studies showed that there is a significant difference in macular thickness volume between healthy subjects and those with glaucoma. However, the diagnostic power did not approach that of the RNFL (31, 32). The diagnostic power was increased by introduction of macular segmentation algorithms, showing similar diagnostic value to RNFL (33, 34). To the best of our knowledge, the present study is the first one, investigating single macular RGCL thickness with the conventional SPECTRALIS® grid and enlarged grid in deviation maps in different types of glaucoma. All recent studies aimed on analysis of the ganglion cell complex (i.e., IPL, GCL, and RNFL) or GCIPL (ganglion cell–inner plexiform layer, i.e., RGCL and IPL) (7, 12, 13). Analyzing average macular GCIPL thickness AUCs of 0.590 (glaucoma suspects vs. controls), 0.668 (early glaucoma vs. controls), and 0.614 (glaucoma suspect and early glaucoma vs. controls) were observed, measured by Cirrus HD-OCT (Carl Zeiss Meditec, Inc., Dublin, CA) (12). AUCs of 0.806 and 0.929 were presented for GCC data, based on measurements with RTVue-100 (Optovue Inc., Fremont, CA) when comparing early glaucoma and advanced glaucoma vs. controls, respectively (35). Next to the differences in measurement of the retinal layers, different grids were used by the two devices: Cirrus HD-OCT measures GCIPL within an elliptical annulus centered on the fovea within an area of 14.13 mm^2 in six sectors (superotemporal, superior, superonasal, inferonasal, inferior, inferotemporall) and calculates an average value for the whole grid (7, 13). RTVue-100 measures GCC by a square grid of 7 × 7 mm located on the central macula. Quantitative data given by the software include the average thickness and hemifield thickness (superior and inferior) of GCC. Furthermore, the software gives two additional parameters: focal loss volume (FLV) (i.e., average amount of focal GCC loss divided by map area) and global loss volume (GLV) (i.e., sum of all negative

TABLE 8 | AUC of ROC analysis of extended qualitative RGCL thickness score for each subgroup (OHT, pre-OAG, NTG, POAG, SOAG vs. controls, respectively): total (eQTV, extended qualitative total value) and sectorial (eTS, extended temporal superior; eS, extended superior; eNS, extended nasal superior; eNI, extended nasal inferior; eI, extended inferior; eTI, extended temporal inferior).

		eTS	eS	eNS	eNI	eI	eTI	eQTV
OHT-controls	AUC	0.516	0.581	0.594	0.52	0.553	0.519	0.514
Pre-OAG-controls	AUC	0.788	0.765	0.667	0.691	0.685	0.744	0.77
NTG-controls	AUC	0.901	0.929	0.793	0.890	0.908	0.933	0.919
POAG-controls	AUC	0.925	0.910	0.931	0.943	0.938	0.96	0.969
SOAG-controls	AUC	0.949	0.98	0.891	0.924	0.924	0.969	0.973

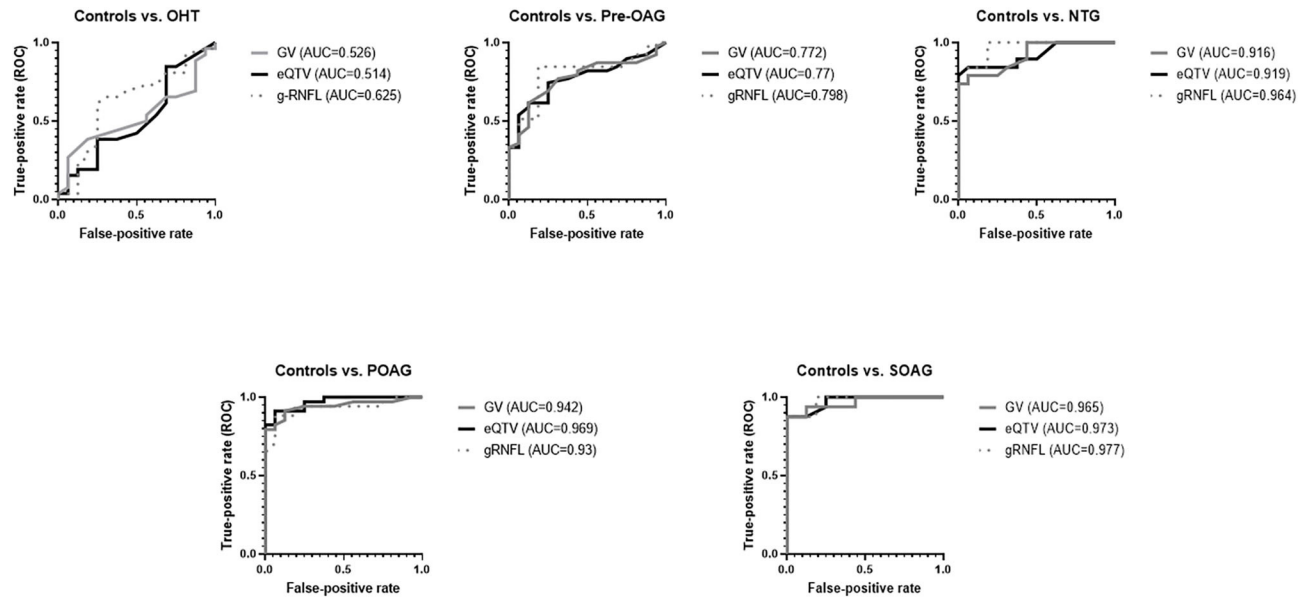

FIGURE 4 | ROC curves for GV, eQTV, and global RNFL (gRNFL) for each subgroup (OHT, Pre-OAG, NTG, POAG, SOAG vs. controls, respectively): In comparison to GV, eQTV yielded higher or similar AUCs.

fractional deviations within the whole area of the map) (36). Especially, data of the inferior hemifield yielded highest AUCs: AUC 0.75 (pre-OAG vs. controls) (37), AUC of 0.815 (pre-OAG vs. controls) (35), AUC of 0.715 (early glaucoma vs. OHT/controls) (38), and AUC of 0.827 (POAG vs. controls). (38) These results are in accordance with the quantitative data of the macular RGCL thickness in the present study. Highest AUCs were observed in sector TI (AUC = 0.795) and sector I (AUC = 0.78) for controls vs. pre-OAG. In the extended grid sector eTS and eQTV yielded the highest AUCs (0.788, 0.77) for this subgroup. Contrary, the superior hemifield of GCC was observed to be the best for diagnosing glaucoma in eyes with pre-POAG (AUC 0.84 and 0.76) in only one previous study (39).

As an increased IOP induced RGC loss (20–25), devices, investigating thickness of single RGC layer, might improve the diagnostic value of GCC/GCIPL. SPECTRALIS® offers the possibility of analysis of single GCL layer in a defined macular region with different grids. For one special grid an automatic deviation map is generated for each single measurement enabling simultaneously quantitative and qualitative (color-coded) analysis. This macular grid is defined by an elliptic ring consisting of six sectors [superior (S), inferior (I), temporal-superior (TS), temporal-inferior (TI), nasal-superior (NS), and nasal-inferior (NI)]. To best of our knowledge, up to know there is no study available on GCL data of the deviation map and only one study on GCL analysis in eyes with NTG measured by SPECTRALIS® (40). An enhanced stratification of the retina might offer an improved and even finer analysis of pathological alterations. Thus, affections of RGCL might be observed in even earlier stages of disease. Data of the only recent study showed that macular RGCL was significantly thinner in patients with NTG compared to healthy controls (1, 3, 6 mm ETDRS grid). The highest AUC value was reached in superior outer macula sector (0.863), confirming data of the present study (0.9). It is notable that outer sectors yielded generally higher AUC values (0.863, 0.837) than inner sectors (0.747, 0.747) in a previous (1, 3, 6 mm ETDRS grid) (40)

TABLE 9 | Sensitivity, specificity and AUCs of ROC for GV [μm], QTV, eQTV, and global RNFL [μm] for OHT, pre-OAG, NTG, POAG, and SOAG vs. controls, respectively.

		Cut-off	Sensitivity %	Specificity %	AUC
OHT vs. controls	GV	54.5	26.9	93.8	0.526
	QTV	2.5	11.5	100	0.519
	eQTV	2.5	84.6	31.3	0.514
	global RNFL	93.5	61.5	75.0	0.625
Pre-OAG vs. controls	GV	47.5	61.5	87.5	0.772
	QTV	0.5	53.8	87.5	0.729
	eQTV	8.5	74.4	75.0	0.77
	global RNFL	86.5	84.6	81.3	0.798
NTG vs. controls	GV	40.5	73.7	100	0.916
	QTV	2.5	78.9	100	0.908
	eQTV	31	78.9	100	0.919
	global RNFL	86.5	100	81.3	0.964
POAG vs. controls	GV	40.5	79.4	100	0.942
	QTV	2.5	82.4	100	0.914
	eQTV	18	91.2	93.8	0.969
	global RNFL	76.5	88.2	93.8	0.930
SOAG vs. controls	GV	40.5	87.5	100	0.965
	QTV	3.5	87.5	100	0.93
	eQTV	31	87.5	100	0.973
	global RNFL	69.5	87.5	100	0.977

The cut-off was selected as the point where Youden index had its maximum in each ROC curve (i.e. optimum for sensitivity and specificity).

and present study [macular grid; eTI (0.933), eQTV (0.919)]. In addition, the outer superior sector of the ETDRS grid yielded the best AUC for differentiating between eyes with primary open-angle glaucoma and controls (AUC = 0.840) (41). Even analysis of macula GCC thickness showed that enlarged grids improved discrimination between glaucoma subjects and controls compared to a smaller standard grid (11). Using the enlarged macular grid, qualitative analysis yielded highest AUCs for sector TI (0.96) and eQTV (0.969; POAG vs. controls) and for sector eS (0.98) and eQTV (0.973, SOAG vs. controls) for the present study cohort. This may reflect the observation that in high-tension open-angle glaucoma loss of ganglion cells are found more to the peripheral macula. In normal-tension glaucoma GCL and visual field defects tend to be more located in the perifoveolar area. This observation may be reflected by our finding that GV an eQTV yielded similar AUC values (0.916 vs. 0.919, respectively).

The study is not without limitations. Patients' cohort is rather small, yet all patients were well-known study participants of the Erlangen Glaucoma Registry and had a follow-up for several years. So, there was no doubt about their clinical classification of disease severity. Furthermore, the extended grid could only be evaluated semi-quantitatively and analysis could not be analyzed in comparison to absolute values. Nevertheless, we used the color-coded information to show, that there is much more information in the whole macular scan than in software's central, standard grid. Color-coded information has the great advantage for clinical examiners to detect deviation of topographic RGCL thickness measurements from normal in a glance. We could show that this clinically comprehensive, qualitative approach showed similar discrimination in the central grid as the absolute, quantitative values. Thirdly, in the analysis the total area of the deviation map was not considered. Probably there would have been even more information on RGCL thickness deviation from normal, in doing so, but we tried to standardize the area of investigation using an extended circle with a fixed prolongation of the software's central, standard grid.

CONCLUSION

The results indicate that analysis of RGCL thickness could represent a valuable parameter in glaucoma diagnosis, being comparable to analysis of RNFL. Quantitative analysis showed that AUCs of 0.772 to even 0.965 can be obtained. Analysis of an extended macular region might improve its diagnostic impact. Furthermore, qualitative analysis using the standard macular grid yielded even similar diagnostic impacts compared to quantitative analysis. Clinical practitioners might use this quantitative analysis in their clinical all-day life.

DATA AVAILABILITY STATEMENT

The original contributions presented in the study are included in the article/supplementary material, further inquiries can be directed to the corresponding authors.

ETHICS STATEMENT

The studies involving human participants were reviewed and approved by the study was approved by the ethics committee of the University of Erlangen-Nürnberg. The patients/participants provided their written informed consent to participate in this study.

AUTHOR CONTRIBUTIONS

PL: data analysis and writing of the draft of the manuscript. BH: supervision, revision of the manuscript, and clinical study. RL: clinical study. CM: supervision, revision of the manuscript, and clinical study.

FUNDING

The Erlangen Glaucoma Registry was funded by the German Research Society (DFG) from 1991 to 2009, NCT00494923; no specific funding was received for the present study.

ACKNOWLEDGMENTS

The present work was performed in fulfillment of the requirements for obtaining the degree Dr. med. for PL. The Department of Ophthalmology is part of the University of Erlangen-Nürnberg, Friedrich-Alexander-Universität Erlangen-Nürnberg (FAU), Germany.

REFERENCES

1. Flaxman SR, Bourne RRA, Resnikoff S, Ackland P, Braithwaite T, Cicinelli MV, et al. Global causes of blindness and distance vision impairment 1990-2020: a systematic review and meta-analysis. *Lancet Glob Health.* (2017) 5:e1221–34. doi: 10.1016/S2214-109X(17)30393-5
2. Wang W, He M, Li Z, Huang W. Epidemiological variations and trends in health burden of glaucoma worldwide. *Acta Ophthalmol.* (2019) 97:e349–55. doi: 10.1111/aos.14044
3. Jutley G, Luk SM, Dehabadi MH, Cordeiro MF. Management of glaucoma as a neurodegenerative disease. *Neurodegener Dis Manag.* (2017) 7:157–72. doi: 10.2217/nmt-2017-0004
4. Jonas JB, Aung T, Bourne RR, Bron AM, Ritch R, Panda-Jonas S. Glaucoma. *Lancet*. (2017) 390:2183–93. doi: 10.1016/S0140-6736(17)31469-1
5. Bertaud S, Aragno V, Baudouin C, Labbe A. [Primary open-angle glaucoma]. *Rev Med Interne.* (2019) 40:445–52. doi: 10.1016/j.revmed.2018.12.001
6. Joachim SC, Jehle T, Boehm N, Gramlich OW, Lagreze WA, Pfeiffer N, et al. Effect of ischemia duration on autoantibody response in rats undergoing retinal ischemia-reperfusion. *Ophthalmic Res*. (2012) 48:67–74. doi: 10.1159/000335965
7. Scuderi G, Fragiotta S, Scuderi L, Iodice CM, Perdicchi A. Ganglion cell complex analysis in glaucoma patients: what can it tell us? *Eye Brain.* (2020) 12:33–44. doi: 10.2147/EB.S226319
8. Iorga RE, Moraru A, Ozturk MR, Costin D. The role of optical coherence tomography in optic neuropathies. *Rom J Ophthalmol.* (2018) 62:3–14. doi: 10.22336/rjo.2018.2
9. Zhang X, Dastiridou A, Francis BA, Tan O, Varma R, Greenfield DS, et al. Comparison of glaucoma progression detection by optical coherence tomography and visual field. *Am J Ophthalmol.* (2017) 184:63–74. doi: 10.1016/j.ajo.2017.09.020
10. Ng DS, Gupta P, Tham YC, Peck CF, Wong TY, Ikram MK, et al. Repeatability of perimacular ganglion cell complex analysis with spectral-domain optical coherence tomography. *J Ophthalmol.* (2015) 2015:605940. doi: 10.1155/2015/605940
11. Kim HJ, Park KH, Kim YK, Jeoung JW. Evaluation of layer-by-layer segmented ganglion cell complex thickness for detecting early glaucoma according to different macular grids. *J Glaucoma.* (2017) 26:712–7. doi: 10.1097/IJG.0000000000000709
12. Aquino LG, Aquino NM. Evaluation of macular ganglion cell layer thickness vs peripapillary retinal nerve fiber layer thickness for glaucoma detection using spectral-domain optical coherence tomography in a tertiary Philippine hospital. *J Curr Glaucoma Pract*. (2020) 14:50–6. doi: 10.5005/jp-journals-10078-1278
13. Hwang YH, Jeong YC, Kim HK, Sohn YH. Macular ganglion cell analysis for early detection of glaucoma. *Ophthalmology*. (2014) 121:1508–15. doi: 10.1016/j.ophtha.2014.02.019
14. Alshareef RA, Dumpala S, Rapole S, Januwada M, Goud A, Peguda HK, et al. Prevalence and distribution of segmentation errors in macular ganglion cell analysis of healthy eyes using cirrus HD-OCT. *PLoS ONE*. (2016) 11:e0155319. doi: 10.1371/journal.pone.0155319
15. Jonas JB, Gusek GC, Naumann GO. Optic disc morphometry in chronic primary open-angle glaucoma. II. Correlation of the intrapapillary morphometric data to visual field indices. *Graefes Arch Clin Exp Ophthalmol*. (1988) 226:531–8. doi: 10.1007/BF02169200
16. Chauhan BC, Danthurebandara VM, Sharpe GP, Demirel S, Girkin CA, Mardin CY, et al. Bruch's membrane opening minimum rim width and retinal nerve fiber layer thickness in a normal white population: a multicenter study. *Ophthalmology*. (2015) 122:1786–94. doi: 10.1016/j.ophtha.2015.06.001
17. Carter JV, Pan J, Rai SN, Galandiuk S. ROC-ing along: evaluation and interpretation of receiver operating characteristic curves. *Surgery*. (2016) 159:1638–45. doi: 10.1016/j.surg.2015.12.029
18. Tham YC, Li X, Wong TY, Quigley HA, Aung T, Cheng CY. Global prevalence of glaucoma and projections of glaucoma burden through 2040: a systematic review and meta-analysis. *Ophthalmology*. (2014) 121:2081–90. doi: 10.1016/j.ophtha.2014.05.013
19. Quigley HA, Broman AT. The number of people with glaucoma worldwide in 2010 and 2020. *Br J Ophthalmol.* (2006) 90:262–7. doi: 10.1136/bjo.2005.081224
20. Chen H, Wei X, Cho KS, Chen G, Sappington R, Calkins DJ, et al. Optic neuropathy due to microbead-induced elevated intraocular pressure in the mouse. *Invest Ophthalmol Vis Sci.* (2011) 52:36–44. doi: 10.1167/iovs.09-5115
21. Wei X, Yu Z, Cho KS, Chen H, Malik MT, Chen X, et al. Neuroglobin is an endogenous neuroprotectant for retinal ganglion cells against glaucomatous damage. *Am J Pathol.* (2011) 179:2788–97. doi: 10.1016/j.ajpath.2011.08.015
22. Aptel F, Bron AM, Lachkar Y, Schweitzer C. Change in visual field progression following treatment escalation in primary open-angle glaucoma. *J Glaucoma*. (2017) 26:875–80. doi: 10.1097/IJG.0000000000000748
23. Samsel PA, Kisiswa L, Erichsen JT, Cross SD, Morgan JE. A novel method for the induction of experimental glaucoma using magnetic microspheres. *Invest Ophthalmol Vis Sci.* (2011) 52:1671–5. doi: 10.1167/iovs.09-3921
24. Urcola JH, Hernandez M, Vecino E. Three experimental glaucoma models in rats: comparison of the effects of intraocular pressure elevation on retinal ganglion cell size and death. *Exp Eye Res.* (2006) 83:429–37. doi: 10.1016/j.exer.2006.01.025
25. Biswas S, Wan KH. Review of rodent hypertensive glaucoma models. *Acta Ophthalmol*. (2019) 97:e331–40. doi: 10.1111/aos.13983
26. Morozumi W, Inagaki S, Iwata Y, Nakamura S, Hara H, Shimazawa M. Piezo channel plays a part in retinal ganglion cell damage. *Exp Eye Res.* (2020) 191:107900. doi: 10.1016/j.exer.2019.107900
27. Parpaite T, Coste B. Piezo channels. *Curr Biol.* (2017) 27:R250–2. doi: 10.1016/j.cub.2017.01.048
28. Kerrigan-Baumrind LA, Quigley HA, Pease ME, Kerrigan DF, Mitchell RS. Number of ganglion cells in glaucoma eyes compared with threshold visual field tests in the same persons. *Invest Ophthalmol Vis Sci.* (2000) 41:741–8.
29. Greenfield DS, Bagga H, Knighton RW. Macular thickness changes in glaucomatous optic neuropathy detected using optical

coherence tomography. *Arch Ophthalmol*. (2003) 121:41–6. doi: 10.1001/archopht.121.1.41
30. Wang WW, Wang HZ, Liu JR, Zhang XF, Li M, Huo YJ, et al. Diagnostic ability of ganglion cell complex thickness to detect glaucoma in high myopia eyes by Fourier domain optical coherence tomography. *Int J Ophthalmol.* (2018) 11:791–6. doi: 10.18240/ijo.2018.05.12
31. Lederer DE, Schuman JS, Hertzmark E, Heltzer J, Velazques LJ, Fujimoto JG, et al. Analysis of macular volume in normal and glaucomatous eyes using optical coherence tomography. *Am J Ophthalmol*. (2003) 135:838–43. doi: 10.1016/S0002-9394(02)02277-8
32. Ojima T, Tanabe T, Hangai M, Yu S, Morishita S, Yoshimura N. Measurement of retinal nerve fiber layer thickness and macular volume for glaucoma detection using optical coherence tomography. *Jpn J Ophthalmol*. (2007) 51:197–203. doi: 10.1007/s10384-006-0433-y
33. Tan O, Li G, Lu AT, Varma R, Huang D, Advanced Imaging for Glaucoma Study G. Mapping of macular substructures with optical coherence tomography for glaucoma diagnosis. *Ophthalmology*. (2008) 115:949–56. doi: 10.1016/j.ophtha.2007.08.011
34. Tan O, Chopra V, Lu AT, Schuman JS, Ishikawa H, Wollstein G, et al. Detection of macular ganglion cell loss in glaucoma by Fourier-domain optical coherence tomography. *Ophthalmology*. (2009) 116:2305–14.e1-2. doi: 10.1016/j.ophtha.2009.05.025
35. Arintawati P, Sone T, Akita T, Tanaka J, Kiuchi Y. The applicability of ganglion cell complex parameters determined from SD-OCT images to detect glaucomatous eyes. *J Glaucoma*. (2013) 22:713–8. doi: 10.1097/IJG.0b013e318259b2e1
36. Kim NR, Lee ES, Seong GJ, Kim JH, An HG, Kim CY. Structure-function relationship and diagnostic value of macular ganglion cell complex measurement using Fourier-domain OCT in glaucoma. *Invest Ophthalmol Vis Sci.* (2010) 51:4646–51. doi: 10.1167/iovs.09-5053
37. Rao HL, Addepalli UK, Chaudhary S, Kumbar T, Senthil S, Choudhari NS, et al. Ability of different scanning protocols of spectral domain optical coherence tomography to diagnose preperimetric glaucoma. *Invest Ophthalmol Vis Sci.* (2013) 54:7252–7. doi: 10.1167/iovs.13-12731
38. Barua N, Sitaraman C, Goel S, Chakraborti C, Mukherjee S, Parashar H. Comparison of diagnostic capability of macular ganglion cell complex and retinal nerve fiber layer among primary open angle glaucoma, ocular hypertension, and normal population using Fourier-domain optical coherence tomography and determining their functional correlation in Indian population. *Indian J Ophthalmol.* (2016) 64:296–302. doi: 10.4103/0301-4738.182941
39. Na JH, Lee K, Lee JR, Baek S, Yoo SJ, Kook MS. Detection of macular ganglion cell loss in preperimetric glaucoma patients with localized retinal nerve fibre defects by spectral-domain optical coherence tomography. *Clin Exp Ophthalmol.* (2013) 41:870–80. doi: 10.1111/ceo.12142
40. Lin JP, Lin PW, Lai IC, Tsai JC. Segmental inner macular layer analysis with spectral-domain optical coherence tomography for early detection of normal tension glaucoma. *PLoS ONE*. (2019) 14:e0210215. doi: 10.1371/journal.pone.0210215
41. Morales-Fernandez L, Jimenez-Santos M, Martinez-de-la-Casa JM, Sanchez-Jean R, Nieves M, Saenz-Frances F, et al. Diagnostic capacity of SD-OCT segmented ganglion cell complex versus retinal nerve fiber layer analysis for congenital glaucoma. *Eye*. (2018) 32:1338–44. doi: 10.1038/s41433-018-0077-4

Conflict of Interest: The authors declare that the research was conducted in the absence of any commercial or financial relationships that could be construed as a potential conflict of interest.

frontiers in Medicine

SYSTEMATIC REVIEW
published: 01 July 2021
doi: 10.3389/fmed.2021.696004

Optical Coherence Tomography Evaluation of Peripapillary and Macular Structure Changes in Pre-perimetric Glaucoma, Early Perimetric Glaucoma, and Ocular Hypertension: A Systematic Review and Meta-Analysis

Yuxin Tong[1,2†], *Tiantian Wang*[3†], *Xinyu Zhang*[1,2], *Yi He*[4] *and Bing Jiang*[1,2*]

[1] Department of Ophthalmology, Second Xiangya Hospital, Central South University, Changsha, China, [2] Hunan Clinical Research Center of Ophthalmic Disease, Changsha, China, [3] Department of Ophthalmology, Xiangya Hospital, Central South University, Changsha, China, [4] Department of Neurosurgery, Xiangya Hospital, Central South University, Changsha, China

OPEN ACCESS

Edited by:
Michele Lanza,
University of Campania Luigi Vanvitelli, Italy

Reviewed by:
Je Hyun Seo,
Pusan National University, South Korea
Christian Mardin,
University of Erlangen Nuremberg, Germany

***Correspondence:**
Bing Jiang
drjiangb@csu.edu.cn

[†]These authors have contributed equally to this work

Specialty section:
This article was submitted to Ophthalmology, a section of the journal Frontiers in Medicine

Received: 15 April 2021
Accepted: 28 May 2021
Published: 01 July 2021

Citation:
Tong Y, Wang T, Zhang X, He Y and Jiang B (2021) Optical Coherence Tomography Evaluation of Peripapillary and Macular Structure Changes in Pre-perimetric Glaucoma, Early Perimetric Glaucoma, and Ocular Hypertension: A Systematic Review and Meta-Analysis. Front. Med. 8:696004. doi: 10.3389/fmed.2021.696004

Background: This study aimed to assess the differences in the average and sectoral peripapillary retinal nerve fiber layer (pRNFL), macular ganglion cell plus inner plexiform layer (mGCIPL), and macular ganglion cell complex (mGCC) thickness using optical coherence tomography (OCT) in patients with pre-perimetric glaucoma (PPG) compared to those with early perimetric glaucoma (EG) and ocular hypertension (OHT).

Methods: A comprehensive literature search of the PubMed database, the Cochrane Library, and Embase was performed from inception to March 2021. The weighted mean difference (WMD) with the 95% confidence interval (CI) was pooled for continuous outcomes.

Results: Twenty-three cross-sectional studies comprising 2,574 eyes (1,101 PPG eyes, 1,233 EG eyes, and 240 OHT eyes) were included in the systematic review and meta-analysis. The pooled results demonstrated that the average pRNFL (WMD = 8.22, 95% CI = 6.32–10.12, $P < 0.00001$), mGCIPL (WMD = 4.83, 95% CI = 3.43–6.23, $P < 0.00001$), and mGCC (WMD = 7.19, 95% CI = 4.52–9.85, $P < 0.00001$) were significantly thinner in patients with EG than in those with PPG. The sectoral thickness of pRNFL, mGCIPL, and mGCC were also significantly lower in the EG eyes. In addition, the average pRNFL and mGCC were significantly thinner in the PPG eyes than those in the OHT eyes (pRNFL: WMD = −8.57, 95% CI = −9.88 to −7.27, $P < 0.00001$; mGCC: WMD = −3.23, 95% CI = −6.03 to −0.44, $P = 0.02$). Similarly, the sectoral pRNFL and mGCC were also significantly thinner in the PPG eyes than those in the OHT eyes.

Conclusion: OCT-based measurements of peripapillary and macular structural alterations can be used to distinguish PPG from EG and OHT, which can help understand the pathophysiology of glaucoma at earlier stages. Studies that employ clock hour classification methods and longitudinal studies are needed to verify our findings.

Systematic Review Registration:
https://www.crd.york.ac.uk/prospero/display_record.php?RecordID=239798
CRD42021239798

Keywords: pre-perimetric glaucoma, early perimetric glaucoma, ocular hypertension, optical coherence tomography, retinal nerve fiber layer, ganglion cell plus inner plexiform layer, ganglion cell complex

INTRODUCTION

Glaucoma is a group of neurodegenerative diseases that is characterized by the progressive loss of retinal ganglion cells (RGCs) and axons, followed by the irreversible visual field (VF) deterioration (1). Glaucoma is one of the leading causes of blindness, and ∼111.8 million people worldwide are expected to suffer from glaucomatous optic neuropathy through 2040. This imposes a huge burden on public health systems (2). Elevated intraocular pressure (IOP) is believed to be one of the major risk factors of glaucoma. Patients that have increased IOP with normal appearance of the optic disc can have about nine times the risk of developing glaucoma and are regarded as ocular hypertension (OHT) individuals or glaucoma suspects (3). Currently, reducing the IOP is the only effective method for glaucoma treatment (4, 5). However, since glaucoma has an insidious onset and obscure symptoms especially at the earlier stages, such as pre-perimetric glaucoma (PPG) and early perimetric glaucoma (EG), patients are usually diagnosed at an advanced stage with severe VF defects (2, 6). Thus, early detection of glaucomatous damage is crucial for hypotensive therapies to slow glaucoma progression and ameliorate the quality of life (7, 8).

Several methods have been utilized for the diagnosis of glaucoma, and of these, standard automated perimetry-based VF examination is the gold standard for evaluating the severity of glaucomatous damage (9). Nevertheless, studies have shown that ganglion cell loss can precede VF defects in glaucoma (10–18) indicating that morphological changes occur earlier than functional damage. Since severe functional damage is closely related to the central region of the VF, it is difficult to solely rely on poor patient performance in standard automated perimetry (19). Moreover, the VF test is occasionally unreliable, which impairs its diagnostic efficacy. Therefore, more objective and reproducible methods are required for assessing the peripapillary and macular structure changes in glaucoma.

Optical coherence tomography (OCT) is a quantitative and non-invasive method of enhanced-depth visualization of the optic nerve head (ONH) and retina with high imaging quality and scanning speed, which enables clinicians to monitor morphological changes of the ONH and retina in glaucoma (20–24). Several studies using OCT have reported that the attenuation of the peripapillary retinal nerve fiber layer (pRNFL), macular ganglion cell plus inner plexiform layer (GCIPL), and macular ganglion cell complex (mGCC) could be hallmark features of glaucoma (20, 22, 24, 25). Although some investigations have revealed the continuum of glaucoma from mild to advanced stages, studies have shown inconsistencies regarding the diagnostic values of OCT indicators in differentiating PPG from EG (26–44) and in differentiating PPG from OHT (39, 43, 45–48).

Thus, we conducted this systematic review and meta-analysis to facilitate a better understanding of glaucomatous progression form OHT without apparent ONH configuration changes to the pre-perimetric stage with structural deterioration, and from the pre-perimetric to the early perimetric stage with impaired VF in view of the peripapillary and macular structural alterations, and to enable ophthalmologists to discriminate PPG from EG, and PPG from OHT.

METHODS

This systematic review and meta-analysis adhered to the Preferred Reporting Items for Systematic Reviews and Meta-analysis (PRISMA) statement methodology and the Meta-analysis of Observational Studies in Epidemiology (MOOSE) guidelines (49, 50). Three investigators (YT, TW, and YH) independently performed the literature search, data extraction, and quality assessment based on the same standard. The study was registered in PROSPERO (CRD42021239798).

Literature Search

We performed a comprehensive literature search of the PubMed database, Embase, and the Cochrane Library from inception to March 2021 using the following strategy with the combination of free text terms and Medical Subject Headings (MeSH): "preperimetric"[All Fields] AND ("glaucoma"[MeSH Terms] OR "glaucoma"[All Fields] OR "glaucomas"[All Fields]) AND ("ocular hypertension"[MeSH Terms] OR ("ocular"[All Fields] AND "hypertension"[All Fields]) OR "ocular hypertension"[All Fields] OR ("suspect"[All Fields] OR "suspected"[All Fields] OR "suspecting"[All Fields] OR "suspects"[All Fields]) OR "early"[All Fields] OR "mild"[All Fields] OR ("hypertense"[All Fields] OR "hypertension"[MeSH Terms] OR "hypertension"[All Fields] OR "hypertension s"[All Fields] OR "hypertensions"[All Fields] OR "hypertensive"[All Fields] OR "hypertensive s"[All Fields] OR "hypertensives"[All Fields])) AND ("tomography, optical coherence"[MeSH Terms] OR ("tomography"[All Fields] AND "optical"[All Fields] AND "coherence"[All Fields]) OR "optical coherence tomography"[All Fields] OR ("optical"[All Fields] AND "coherence"[All Fields] AND "tomography"[All Fields]) OR "OCT"[All Fields]). We modified search strategies according to the different requirements of the different databases. Full-text screening was conducted to include potentially applicable studies.

Inclusion and Exclusion Criteria

Eligible studies were included if they fulfilled the following criteria: (1) original article; (2) inclusion of PPG and (EG or

OHT) with the same diagnostic standard: for PPG, patients had to demonstrate characteristic glaucomatous optic nerve damage (i.e., neuroretinal rim thinning, excavation, or notching) without a reproducible VF; for EG, in addition to the typical glaucomatous optic disc changes (i.e., neuroretinal rim thinning, excavation, or notching), the mean deviation (MD) of the VF defect had to exceed −6 dB based on the Hodapp-Anderson-Parrish VF severity grading scale (51); for OHT, patients with an elevated IOP > 21 mmHg but with normal optic disc appearance and VF were included; and (3) inclusion of at least one of the following quantitative indicators measured by OCT – pRNFL, mGCIPL, or mGCC thickness.

The exclusion criteria were: (1) animal experiments, reviews, case reports, and conference abstracts; (2) non-inclusion of PPG, EG and OHT; (3) lack of information regarding pRNFL, mGCIPL, or mGCC thickness; (4) different diagnostic standards; and (5) studies with unextractable data.

Data Extraction

The following details were extracted with regard to the studies: title, first author, publication year, study type, region, source of patients, number of patients and eyes, mean age of patients, female/male ratios, type of spectral domain OCT (SD-OCT) or time domain OCT (TD-OCT) devices, type of glaucoma, diagnostic standards, average and sectoral pRNFL, mGCIPL and mGCC thickness, scan area and protocol of the ONH and macular region, and MD of the VF. Disagreements were resolved through consensus after discussion among all authors.

Quality Assessment

The Agency for Healthcare Research and Quality (AHRQ) methodology checklist was used to evaluate the quality of the included cross-sectional studies.

Statistical Analyses

All statistical analyses were conducted using Review Manager V5.4.1 (Cochrane Collaboration, London, United Kingdom) and Stata V12.0 (StataCorp LLC, Texas, America). We employed the weighted mean difference (WMD) with the 95% confidence interval (CI) to pool the mean differences of OCT parameters between the PPG and EG groups, and between the PPG and OHT groups. A *P*-value of <0.05 was considered to be statistically significant. Heterogeneity was estimated using Cochrane's Q test and I^2 statistics. A fixed-effects model was used when I^2 < 50% (52); otherwise, a random-effects model (Der Simonian-Laird method) was used. We performed subgroup analyses according to the type of glaucoma, type of OCT device, and macular scan area. Subgroups with less than two included studies were excluded to prevent further discrepancy. "Leave-one-out" sensitivity analyses were performed to validate the stability and

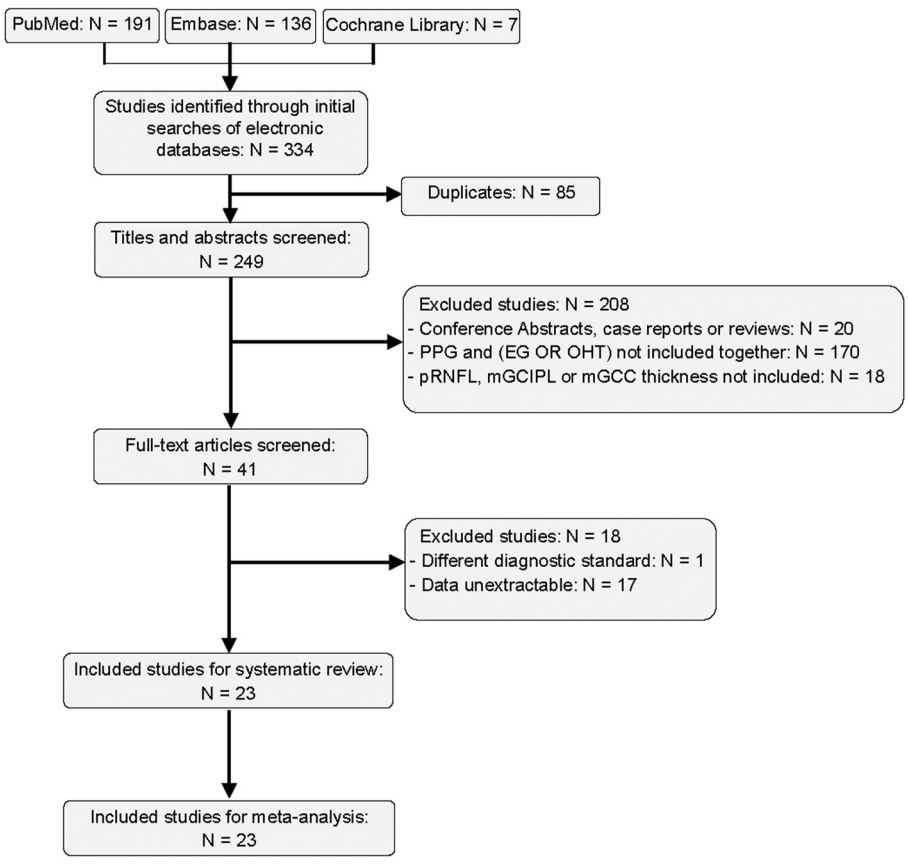

FIGURE 1 | Flow diagram of included studies.

TABLE 1 | Characteristics of included studies.

Study	Year	Region	No. eyes			Mean age ± SD (yrs)			Gender (F/M)			Device (OCT)	Glaucoma types	Main outcome	Scan area (mm^2 or mm^3)	
			PPG	EG	OHT	PPG	EG	OHT	PPG	EG	OHT				ONH	Macular region
Wang et al. (44)	2020	China	26	22		36.9 ± 11.1	41.4 ± 13.9		6/16	7/12		RTVue	POAG	pRNFL, GCC		6 × 6
Sarigül Sezenöz et al. (43)	2020	Turkey	28	31	18	66.71 ± 11.33	68.20 ± 9.12	66.61 ± 10.44	N/A	N/A	N/A	Heidelberg	Mixed	pRNFL, GCC, total retina thickness, G/T ratio		
Lu et al. (42)	2020	China	44	42		43 ± 11	46 ± 11		17/27	20/22		RTVue	POAG	pRNFL, GCC	4.5 × 4.5	6 × 6
Hou et al. (41)	2019	USA	68	162		68.4 ± 10.8	68.4 ± 8.6		30/25	60/61		RTVue Spectralis	POAG	pRNFL, GCC		3 × 3
Kim et al. (40)	2017	Korea	26	26		52.08 ± 11.77	55.65 ± 13.36		16/10	16/10		Cirrus Spectralis	OAG	mRNFL, GCIPL, GCL, IPL		6 × 6
Aydogan et al. (39)	2017	Turkey	94	66	77	53.2 ± 11.1	59.4 ± 9.5	52.8 ± 8.2	57/37	36/30	62/15	RTVue	Mixed	pRNFL, GCC, TR, OR	3.45-mm circle	7 × 7
Akil et al. (38)	2017	USA	20	20		63.13 ± 16.43	65.375 ± 5.2		10/10	8/12		Cirrus	POAG	pRNFL	3.4-mm circle	
Kumar et al. (37)	2016	India	28	83		57.04 ± 2.78	61.2 ± 1.34		N/A	N/A		RTVue	Mixed	pRNFL, GCC	3.45-mm circle	6 × 6
Cennamo et al. (36)	2016	Italy	66	41		64.86 ± 7.12	63.78 ± 11.70		30/36	25/16		RTVue	OAG	pRNFL, GCC	3.45-mm circle	7 × 7
Park et al. (35)	2015	Korea	50	106		58.2 ± 13.7	56.0 ± 12.7		26/24	66/40		Cirrus	Mixed	pRNFL, GCIPL, TNM ratio	3.46-mm circle	6 × 6 × 2
Kim et al. (34)	2015	Korea	79	83		54.6 ± 11.8	57.5 ± 11.6		40/39	43/40		Cirrus	Mixed	pRNFL, GCIPL	Optic disc Cube 200 × 200	Macular Cube 512 × 128
Hwang et al. (33)	2015	Korea	48	110		51.7 ± 13.8	51.6 ± 12.7		N/A	N/A		Cirrus	Mixed	GCIPL		6 × 6
Yamada et al. (32)	2014	Japan	30	31		56.9 ± 14.7	61.8 ± 11.5		13/17	19/12		Spectralis	Mixed	mRNFL, GCC, GCL, TR		30 × 15 degreed macular area
Sung et al. (31)	2014	Korea	37	70		54.22 ± 12.70	53.97 ± 12.36		20/17	29/41		Cirrus	Mixed	pRNFL, GCIPL	3.46-mm circle	14.13 mm^2 elliptical annulus area
Kim et al. (30)	2014	Korea	68	72		53.12 ± 10.69	56.83 ± 12.73		N/A	N/A		3D OCT-2000	OAG	pRNFL, mRNFL, GCIPL, GCC	3.46-mm circle	6 × 6

(Continued)

TABLE 1 | Continued

Study	Year	Region	No. eyes			Mean age ± SD (yrs)			Gender (F/M)			Device (OCT)	Glaucoma types	Main outcome	Scan area (mm^2 or mm^3)	
			PPG	EG	OHT	PPG	EG	OHT	PPG	EG	OHT				ONH	Macular region
Kim et al. (29)	2014	Korea	103	111		57.2 ± 11.8.	56.8 ± 11.4		52/51	52/59		Cirrus	OAG	pRNFL, GCIPL	3.46-mm circle	Macular Cube 200 × 200
Holló et al. (48)	2014	Hungary	33		28	56.2 ± 12.1		50.7 ± 15.6	N/A		N/A	RTVue	Mixed	pRNFL, GCC, total retina thickness, G/T ratio	4-mm circle	
Arintawati et al. (28)	2013	Japan	32	81		58.94 ± 12.15	60.16 ± 16.77		18/14	45/36		RTVue	Mixed	pRNFL, GCC, FLV, GLV	3.5-mm circle	7 × 7
Pomorska et al. (47)	2012	Poland	33		27	61.0 ± 9.6		57.8 ± 11.2	17/16		18/9	Sratus	Mixed	pRNFL	3.4-mm circle	
Morooka et al. (27)	2012	Japan	23	24		56.8 ± 9.4	51.9 ± 12.2		16/7	13/11		RS3000	Mixed	pRNFL, GCC	3.45-mm circle	9 × 9
Horn et al. (26)	2011	Germany	77	52		59.2 ± 10.0	60.8 ± 10.5		41/36	27/25		Sepctralis	OAG	pRNFL	3.4-mm circle	
Garas et al. (46)	2011	Hungary	46		36	57.6 ± 11.8		51.5 ± 16.5	N/A		N/A	RTVue	Mixed	pRNFL, GCC, FLV	4-mm circle	
Taliantzis et al. (45)	2009	Greece	42		54	58.1 ± 11.6		56.7 ± 13.2	20/22		25/29	Stratus	Mixed	pRNFL	3.4-mm circle	

PPG, pre-perimetric glaucoma; EG, early perimetric glaucoma; OHT, ocular hypertension; OAG, open-angle glaucoma; POAG, primary open-angle glaucoma; Mixed, unclassified glaucoma or more than one types of glaucoma; pRNFL, peripapillary retinal nerve fiber layer; mRNFL, macular retinal nerve fiber layer; GCIPL, ganglion cell plus inner plexiform layer; GCL, ganglion cell layer; IPL, inner plexiform layer; GCC, ganglion cell complex; G/T ratio, macular GCC to total retinal thickness; TR, macular total retinal parameters; OR, macular outer retinal parameters; FLV, focal loss volume; GLV, global loss volume; TNM ratio, temporal to nasal macular GCIPL thickness ratio; F/M, female/male; ONH, optic nerve head.

reliability of the results. Publication bias was evaluated by the combination of Begg's funnel plot and Egger's test (53, 54).

In some articles, the eight-quadrant classification method was used to display sectoral thickness while other studies employed the four-quadrant classification method. Since most of the studies used the four-quadrant classification (only one study used the eight-quadrant classification, which we included for the combined analysis regarding the pRNFL thickness), we transformed the eight-quadrant data to four-quadrant data to reduce heterogeneity using the following formula to combine the means and standard deviations of the two groups:

$$\bar{x}_{12} = \frac{N_1 \cdot \bar{x}_1 + N_2 \cdot \bar{x}_2}{N_1 + N_2}$$

$$\sigma_{12} = \sqrt{\frac{(N_1 - 1) \cdot \sigma_1^2 + (N_2 - 1) \cdot \sigma_2^2 + \frac{N_1 \cdot N_2}{N_1 + N_2} \cdot \left(\bar{x}_1^2 + \bar{x}_2^2 - 2\bar{x}_1 \cdot \bar{x}_2\right)}{N_1 + N_2 - 1}}$$

$\bar{x}_1$ and $\bar{x}_2$ are the mean pRNFL or mGCIPL or mGCC thickness of the two adjacent sections in the eight-quadrant classification. σ_1 and σ_2 are the standard deviations of the two groups. N_1 and N_2 are number of the eyes in the two sections. $\bar{x}_{12}$ and σ_{12} are the combined mean and standard deviation (i.e., $\bar{x}_1$ and σ_1 refer to parameters of the temporal superior quadrant, $\bar{x}_2$ and σ_2 refer to parameters of the temporal inferior quadrant, and $\bar{x}_{12}$ and σ_{12} refer to combined parameters of the temporal superior and inferior quadrants).

RESULTS

Literature Search

A total of 334 studies were retrieved in our screening, of which 85 duplicates were removed and 208 articles were excluded by titles and abstracts. We further excluded 17 studies with unextractable data and 1 study that used a different diagnostic standard. Finally, 23 studies were integrated into the qualitative and quantitative analyses (26–48). The flow diagram of literature search is shown in **Figure 1**.

TABLE 2 | Methodological quality of included studies.

Study	11-item check list recommended by AHRQ												
	i	ii	iii	iv	v	vi	vii	viii	ix	x	xi	Score	Quality
Wang et al. (44)	★	★	★			★		★		★		6	M
Sarigül Sezenöz et al. (43)	★	★	★			★		★				5	M
Lu et al. (42)	★	★	★			★		★		★		6	M
Hou et al. (41)	★	★	★			★		★		★		6	M
Kim et al. (40)	★	★	★			★		★		★		6	M
Aydogan et al. (39)	★	★	★			★		★		★		6	M
Akil et al. (38)	★	★	★			★	★	★		★		7	M
Kumar et al. (37)	★	★	★			★	★	★		★		7	M
Cennamo et al. (36)	★	★	★				★	★		★		6	M
Park et al. (35)	★	★	★		★	★	★	★		★		8	H
Kim et al. (34)	★	★	★			★	★	★		★		7	M
Hwang et al. (33)	★	★				★		★		★		5	M
Yamada et al. (32)	★	★	★		★	★	★	★		★		8	H
Sung et al. (31)	★	★	★			★	★	★		★		7	M
Kim et al. (30)	★	★	★		★	★	★	★		★		8	H
Kim et al. (29)	★	★	★			★		★		★		6	M
Holló et al. (48)	★	★	★			★		★		★		6	M
Arintawati et al. (28)	★	★	★					★		★		5	M
Pomorska et al. (47)	★	★	★			★	★			★		6	M
Morooka et al. (27)	★	★	★		★	★		★		★		7	M
Horn et al. (26)	★	★	★			★		★		★		6	M
Garas et al. (46)	★	★	★			★	★	★		★		7	M
Taliantzis et al. (45)	★	★	★			★				★		5	M

AHRQ, Agency for Healthcare Research and Quality; H, high quality; M, moderate quality; L, low quality; high quality (score: 8–11); moderate quality (score: 4–7); low quality (score: 0–3). i, Define the source of information; ii, List inclusion and exclusion criteria for exposed and unexposed subjects (cases and controls) or refer to previous publications; iii, Indicate time period used for identifying patients; iv, Indicate whether or not subjects were consecutive if not population-based; v, Indicate if evaluators of subjective components of study were masked to other aspects of the status of the participants; vi, Describe any assessments undertaken for quality assurance purposes; vii, Explain any patient exclusions from analysis; viii, Describe how confounding was assessed and/or controlled; ix, If applicable, explain how missing data were handled in the analysis; x, Summarize patient response rates and completeness of data collection; xi, Clarify what follow-up, if any, was expected and the percentage of patients for which incomplete data or follow-up was obtained. ★means the study meets the requirements of the corresponding items.

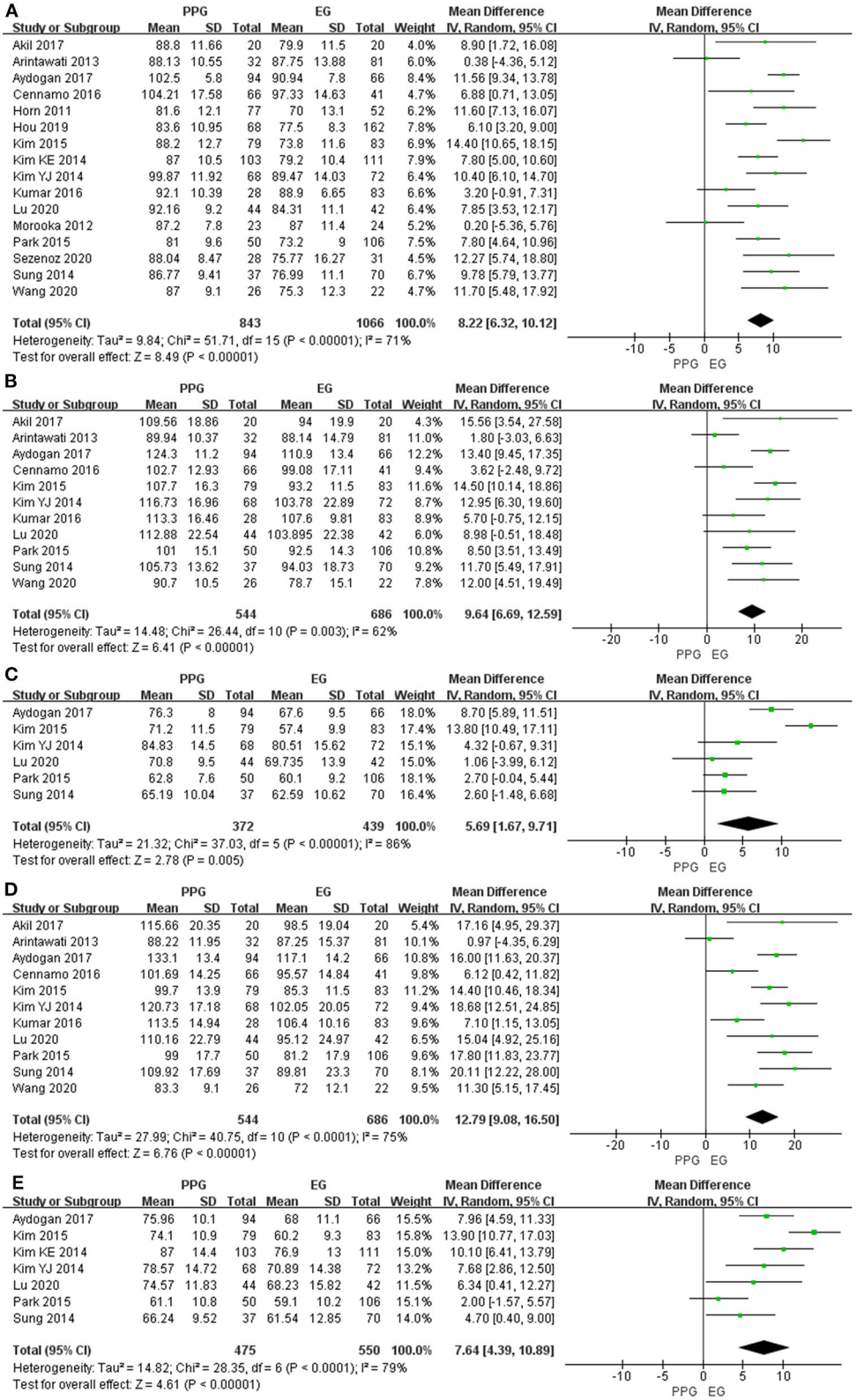

FIGURE 2 | pRNFL thickness in patients with PPG and EG. **(A)** Average. **(B)** Superior. **(C)** Nasal. **(D)** Inferior. **(E)** Temporal.

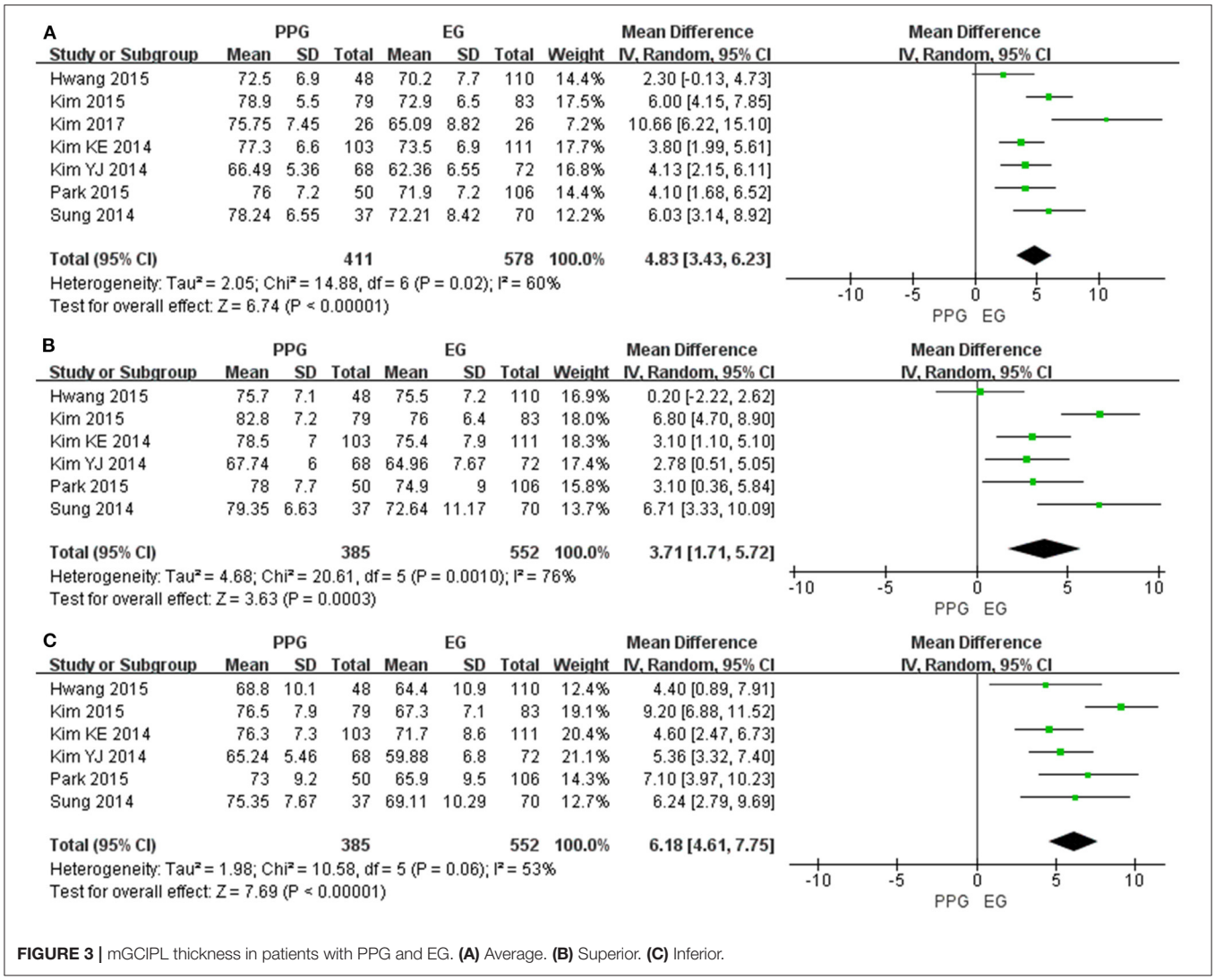

FIGURE 3 | mGCIPL thickness in patients with PPG and EG. **(A)** Average. **(B)** Superior. **(C)** Inferior.

Characteristics of Included Studies

According to our eligibility criteria, 23 cross-sectional studies comprising 2,574 eyes (1,101 PPG eyes, 1,233 EG eyes, and 240 OHT eyes) were included in the systematic review and the meta-analysis. Detailed characteristics of the included studies are summarized in **Table 1**. The AHRQ checklist scores of all the included cross-sectional studies were not <5, demonstrating that the studies were of good quality. Details are presented in **Table 2**.

PPG vs. EG

Peripapillary RNFL Thickness

Sixteen studies evaluating pRNFL thickness showed significant heterogeneity ($I^2 > 50\%$); thus, the random-effects model was used. The pooled results demonstrated a significant decrease in the average and quadrant pRNFL thickness in the EG eyes compared with the PPG eyes (average: WMD = 8.22, 95% CI = 6.32–10.12, $P < 0.00001$, **Figure 2A**; superior: WMD = 9.64, 95% CI = 6.69–12.59, $P < 0.00001$, **Figure 2B**; nasal: WMD = 5.69, 95% CI = 1.67–9.71, $P = 0.005$, **Figure 2C**; inferior: WMD = 12.79, 95% CI = 9.08–16.50, $P < 0.00001$, **Figure 2D**; temporal: WMD = 7.64, 95% CI = 4.39–10.89, $P < 0.00001$, **Figure 2E**).

Macular GCIPL Thickness

Seven of the included studies assessed the average mGCIPL thickness and six studies assessed superior and inferior mGCIPL thickness with significant heterogeneity ($I^2 > 50\%$). The pooled results indicated the average mGCIPL thickness was significantly less in the EG eyes than in the PPG eyes (WMD = 4.83, 95% CI = 3.43–6.23, $P < 0.00001$, **Figure 3A**). Likewise, the superior and inferior mGCIPL were also significantly thinner in patients with EG than in those with PPG (superior: WMD = 3.71, 95% CI = 1.71–5.72, $P = 0.0003$, **Figure 3B**; inferior: WMD = 6.18, 95% CI = 4.61–7.75, $P < 0.00001$, **Figure 3C**).

Macular GCC Thickness

Ten studies measured the average mGCC thickness and seven studies assessed quadrant mGCC thickness with $I^2 > 50\%$. All the pooled mGCC thickness values were significantly

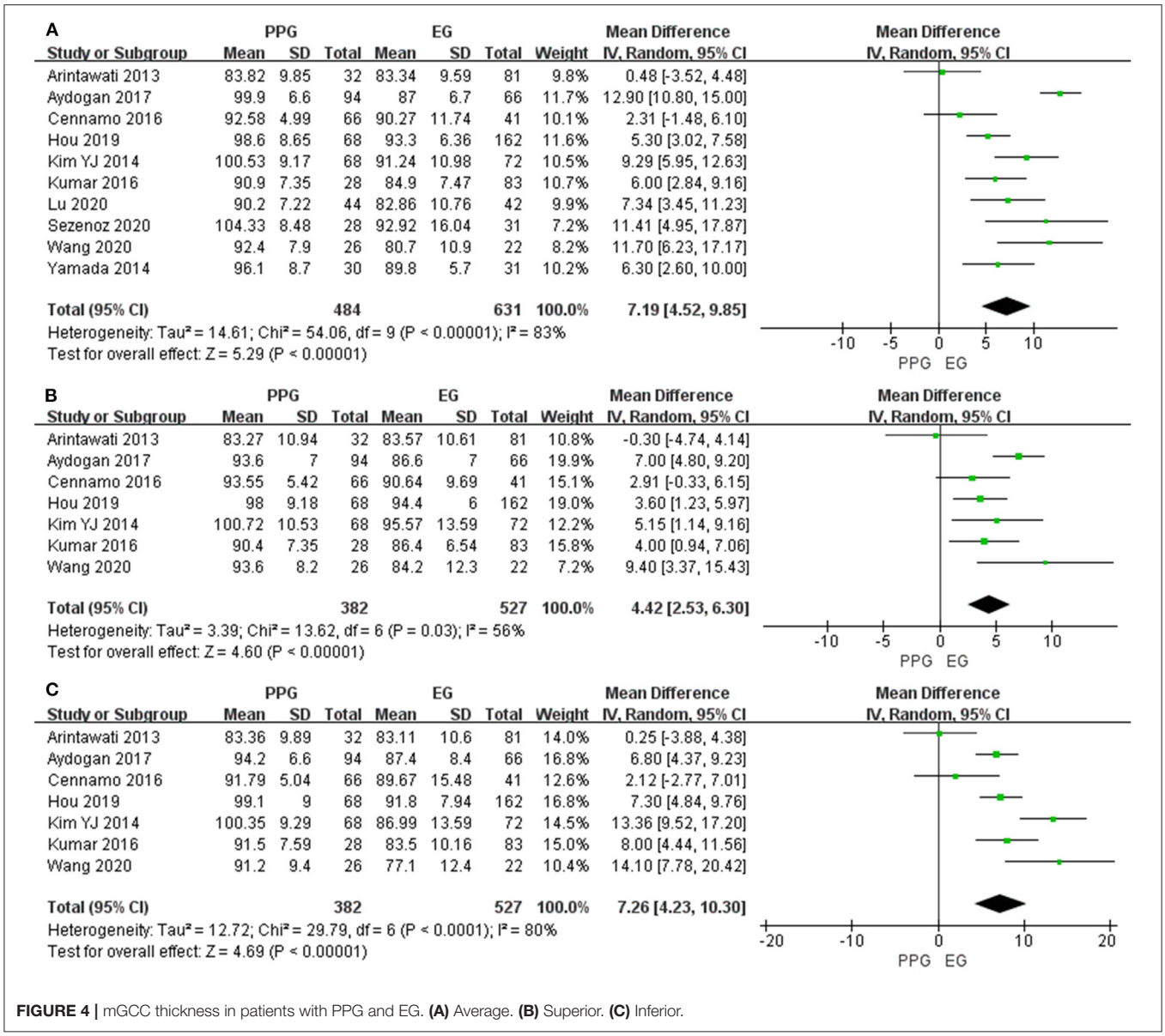

FIGURE 4 | mGCC thickness in patients with PPG and EG. **(A)** Average. **(B)** Superior. **(C)** Inferior.

reduced in the EG eyes compared to the PPG eyes (average: WMD = 7.19, 95% CI = 4.52–9.85, $P < 0.00001$, **Figure 4A**; superior: WMD = 4.42, 95% CI = 2.53–6.30, $P < 0.00001$, **Figure 4B**; inferior: WMD = 7.26, 95% CI = 4.23–10.30, $P < 0.00001$, **Figure 4C**).

Subgroup Analyses

The stratified subgroup analysis according to the type of glaucoma (**Table 3**) showed a similar decreased trend of pRNFL and mGCIPL thickness in EG compared with PPG except for the superior quadrant of pRNFL in the open-angle glaucoma subgroup (WMD = 8.19, 95% CI = −0.95 to 17.33, $P = 0.08$). However, unlike the combined pooled data, in the subgroup of the open-angle glaucoma in terms of the average and inferior mGCC thickness, there was no difference between the EG and PPG eyes (average: WMD = 5.86, 95% CI = −0.98 to 12.70, $P = 0.09$; inferior: WMD = 7.85, 95% CI = −3.17 to 18.86, $P = 0.16$).

In addition, considering the different types of OCT (**Table 4**), the average and quadrant pRNFL thickness were significantly lower in the EG eyes than in the PPG eyes regardless of the kind of OCT that was used except for the nasal quadrant of pRNFL in the Cirrus SD-OCT subgroup (WMD = 6.38, 95% CI = −1.02 to 13.78, $P = 0.09$).

The subgroup analysis regarding the scan area of the macular region (**Table 5**) revealed that the average and sectoral mGCC thickness were significantly lower in patients with EG than in those with PPG in the 6 × 6 mm subgroup, whereas no difference was found in 7 × 7 mm subgroup (average: WMD = 5.36, 95% CI = −3.27 to 13.99, $P = 0.22$; superior: WMD = 3.54, 95% CI =

TABLE 3 | Subgroup analysis of average and sectoral pRNFL, mGCIPL and mGCC thickness according to the type of glaucoma in patients with PPG and EG.

Subgroup	No.	Heterogeneity		WMD (95% CI)	Overall effect	
		I^2	*P*		Z	*P*
1. pRNFL						
POAG						
Average	4	0%	0.42	7.45 (5.30, 9.59)	6.81	<0.00001
Superior	3	0%	0.70	11.75 (6.47, 17.04)	4.36	<0.0001
Inferior	3	0%	0.64	13.07 (8.24, 17.89)	5.31	<0.00001
OAG						
Average	4	0%	0.41	8.99 (7.02, 10.96)	8.94	<0.00001
Superior	2	76%	0.04	8.19 (−0.95, 17.33)	1.76	**0.08**
Inferior	2	88%	0.003	12.34 (0.03, 24.65)	1.97	0.05
Mixed						
Average	8	84%	<0.00001	7.60 (4.13, 11.07)	4.29	<0.0001
Superior	6	75%	0.001	9.41 (5.29, 13.53)	4.48	<0.00001
Inferior	6	83%	<0.0001	12.47 (6.41, 18.52)	4.03	<0.0001
2. mGCIPL						
OAG						
Average	3	75%	0.02	5.44 (2.57, 8.31)	3.72	0.0002
Superior	2	0%	0.84	2.96 (1.46, 4.46)	3.87	0.0001
Inferior	2	0%	0.61	5.00 (3.52, 6.47)	6.65	<0.00001
Mixed						
Average	4	55%	0.08	4.63 (2.87, 6.40)	5.14	<0.00001
Superior	4	84%	0.0003	4.16 (0.87, 7.45)	2.48	0.01
Inferior	4	46%	0.13	7.32 (5.84, 8.80)	9.66	<0.00001
3. mGCC						
POAG						
Average	3	58%	0.09	7.38 (4.09, 10.67)	4.40	<0.0001
Superior	2	68%	0.08	5.81 (0.29, 11.33)	2.06	0.04
Inferior	2	74%	0.05	10.05 (3.51, 16.59)	3.01	0.003
OAG						
Average	2	86%	0.007	5.86 (−0.98, 12.70)	1.68	**0.09**
Superior	2	0%	0.39	3.79 (1.27, 6.32)	2.95	0.003
Inferior	2	92%	0.0004	7.85 (−3.17, 18.86)	1.40	**0.16**
Mixed						
Average	5	89%	<0.00001	7.37 (2.64, 12.11)	3.05	0.002
Superior	3	78%	0.01	3.96 (0.12, 7.80)	2.02	0.04
Inferior	3	78%	0.01	5.23 (1.14, 9.32)	2.51	0.01

PPG, pre-perimetric glaucoma; EG, early perimetric glaucoma; POAG, primary open-angle glaucoma; OAG, open-angle glaucoma; Mixed, unclassified glaucoma or more than one types of glaucoma; pRNFL, peripapillary retinal nerve fiber layer; mGCIPL, macular ganglion cell plus inner plexiform layer; mGCC, macular ganglion cell complex; WMD, weighted mean difference; CI, confidence interval; I^2, I-square heterogeneity statistic; Z, Z-statistic. The bold values refer to the studies with a P value > 0.05.

−0.64 to 7.72, $P = 0.10$; inferior: WMD = 3.35, 95% CI = −1.08 to 7.79, $P = 0.14$).

PPG vs. OHT

Peripapillary RNFL Thickness

Six studies evaluated average pRNFL thickness in patients with PPG and OHT with $I^2 < 50\%$; thus, fixed-effects model was used. The pooled results demonstrated that the average and quadrant pRNFL thickness were significantly lower in patients with PPG than in those with OHT (average: WMD = −8.57, 95% CI = −9.88 to −7.27, $P < 0.00001$, **Figure 5A**; superior: WMD = −12.43, 95% CI = −15.00 to −9.86, $P < 0.00001$, **Figure 5B**; inferior: WMD = −11.02, 95% CI = −13.81 to −8.23, $P < 0.00001$, **Figure 5C**).

Macular GCC Thickness

Four studies measured average mGCC thickness with $I^2 > 50\%$, and three studies assessed sectoral mGCC thickness with $I^2 < 50\%$. The average and sectoral mGCC were significantly thinner in the PPG eyes than those in the OHT eyes (average: WMD

TABLE 4 | Subgroup analysis of average and sectoral pRNFL thickness according to the type of OCT in patients with PPG and EG.

Subgroup	No.	Heterogeneity		WMD (95% CI)	Overall effect	
		I^2	*P*		Z	*P*
RTVue SD-OCT						
Average	6	81%	<0.0001	6.96 (2.96, 10.95)	3.42	0.0006
Superior	6	71%	0.004	7.51 (2.98, 12.04)	3.25	0.001
Nasal	2	0%	1.00	8.70 (6.72, 10.68)	8.60	<0.00001
Inferior	6	77%	0.0006	9.18 (4.13, 14.22)	3.56	0.0004
Temporal	2	0%	0.64	7.56 (4.64, 10.49)	5.06	<0.00001
Cirrus SD-OCT						
Average	5	56%	0.06	9.67 (7.09, 12.25)	7.35	<0.00001
Superior	4	14%	0.32	12.04 (8.91, 15.17)	7.53	<0.00001
Nasal	3	93%	0.00001	6.38 (-1.02, 13.78)	1.69	**0.09**
Inferior	4	0%	0.56	16.18 (13.24, 19.13)	10.77	<0.00001
Temporal	4	89%	<0.00001	7.74 (2.20, 13.29)	2.74	0.006

PPG, pre-perimetric glaucoma; EG, early perimetric glaucoma; pRNFL, peripapillary retinal nerve fiber layer; OCT, optical coherence tomography; SD-OCT, spectral domain OCT; WMD, weighted mean difference; CI, confidence interval; I^2, I-square heterogeneity statistic; Z, Z-statistic. The bold value refers to the study with a P value > 0.05.

TABLE 5 | Subgroup analysis of average and sectoral mGCC thickness according to the macular scan area (mm^2) in patients with PPG and EG.

Subgroup	No.	Heterogeneity		WMD (95% CI)	Overall effect	
		I^2	*P*		Z	*P*
6 × 6						
Average	4	25%	0.26	8.09 (5.91, 10.27)	7.27	<0.00001
Superior	3	18%	0.29	5.28 (2.69, 7.86)	4.00	<0.0001
Inferior	3	61%	0.08	11.44 (7.38, 15.50)	5.53	<0.00001
7 × 7						
Average	3	95%	<0.00001	5.36 (−3.27, 13.99)	1.22	**0.22**
Superior	3	80%	0.006	3.54 (−0.64, 7.72)	1.66	**0.10**
Inferior	3	76%	0.01	3.35 (−1.08, 7.79)	1.48	**0.14**

PPG, pre-perimetric glaucoma; EG, early perimetric glaucoma; mGCC, macular ganglion cell complex; WMD, weighted mean difference; CI, confidence interval; I^2, I-square heterogeneity statistic; Z, Z-statistic. The bold values refer to the studies with a P value > 0.05.

= −3.23, 95% CI = −6.03 to −0.44, $P = 0.02$, **Figure 6A**; superior: WMD = −5.78, 95% CI = −7.25 to −4.31, $P < 0.00001$, **Figure 6B**; inferior: WMD = −6.14, 95% CI = −7.54 to −4.73, $P < 0.00001$, **Figure 6C**).

Subgroup Analysis

The subgroup analysis demonstrated that the average pRNFL thickness was significantly lower in patients with PPG than in those with OHT, regardless of the type of OCT (SD-OCT: WMD = −9.04, 95% CI = −10.62 to −7.46, $P < 0.00001$; TD-OCT: WMD = −7.56, 95% CI = −9.88 to −5.24, $P < 0.00001$, **Supplementary Figure 1**).

Publication Bias

No significant publication bias was shown according to the results of Egger's and Begg's tests ($P > 0.05$, **Table 6**), and no obvious asymmetry or correlation between study and effect size was observed in the funnel plot in terms of pRNFL and mGCC thickness (**Supplementary Figures 2–5**). However, slight asymmetry was noted in the funnel plot of average mGCIPL thickness (**Supplementary Figure 6A**), but not in those of superior and inferior mGCIPL thickness (**Supplementary Figures 6B,C**).

Sensitivity Analyses

There was no obvious change in the results after "leave-one-out" sensitivity analyses, indicating the reproducibility and stability of our results (**Supplementary Figures 7–11**). However, the sensitivity analysis of average mGCIPL thickness in patients with PPG and EG indicated that the study by Kim et al. (40) contributed mostly to the heterogeneity (**Table 7**). After excluding this study, heterogeneity was largely reduced (I^2 = 34%, **Supplementary Figure 12**) and the funnel plot became symmetrical (**Table 6** and **Supplementary Figure 13**, *P*-value of Egger's test increased from 0.195 to 0.745). In addition, the sensitivity analysis of average mGCC thickness in PPG

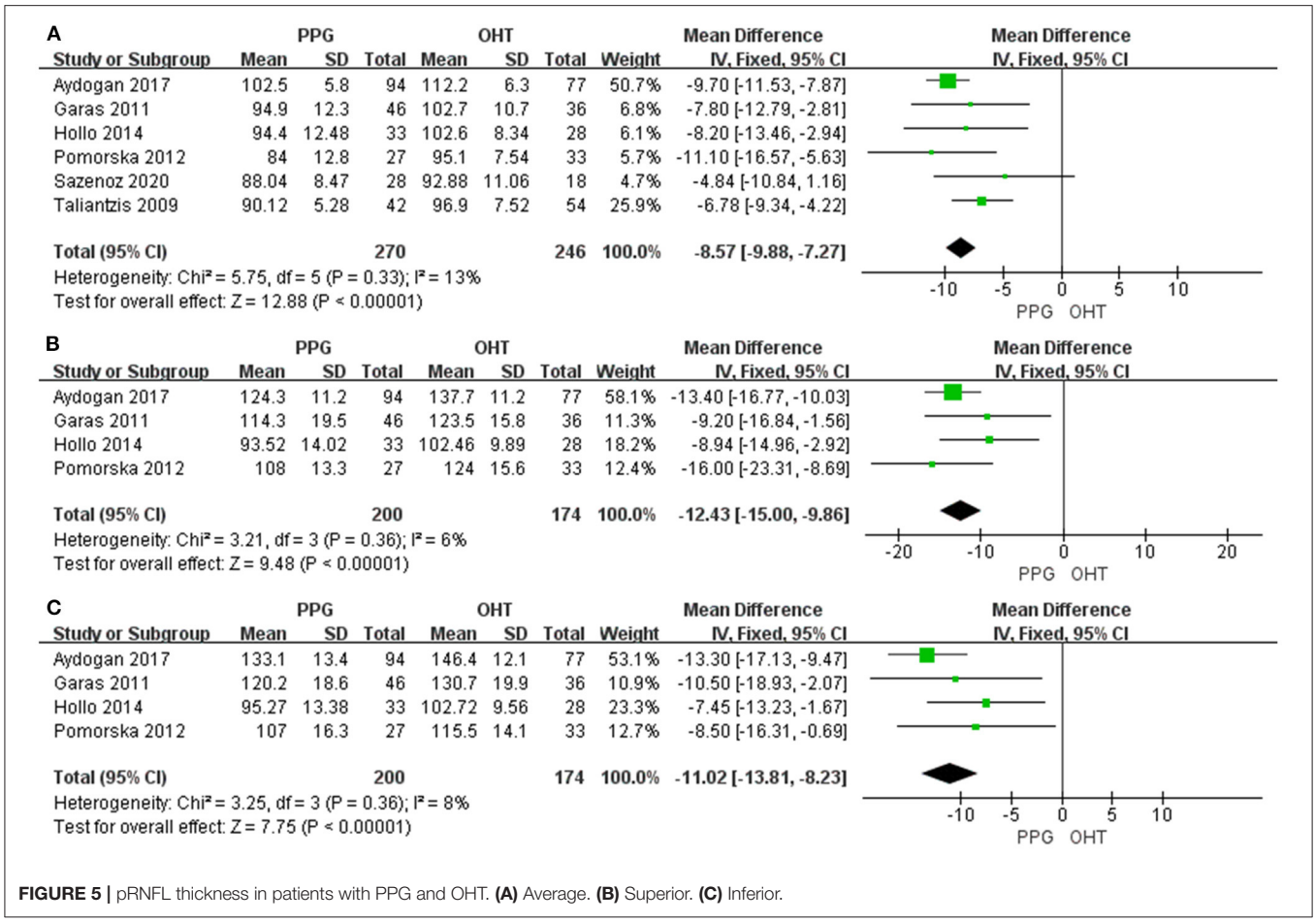

FIGURE 5 | pRNFL thickness in patients with PPG and OHT. **(A)** Average. **(B)** Superior. **(C)** Inferior.

eyes and EG eyes demonstrated that the study by Aydogan et al. (39) was the major source of the heterogeneity (**Table 8**). After excluding this study, the I^2 decreased from 83% to 64% (**Supplementary Figure 14**). In the sensitivity analysis of average mGCC thickness in the PPG eyes and OHT eyes, the study by Aydogan et al. (39) was also shown to introduce the heterogeneity mostly (**Table 9**). After excluding this study, no heterogeneity was noted ($I^2 = 0\%$, **Supplementary Figure 15**).

DISCUSSION

In the present study, we first pooled the average and sectoral pRNFL, mGCIPL, and mGCC thickness in patients with PPG and EG. Our results demonstrated that the average and sectoral pRNFL, mGCIPL, and mGCC were significantly thinner in the EG eyes than in the PPG eyes. These findings were consistent across several studies (26, 29, 34, 38–41, 43, 44), whereas the results of eight studies were not significantly different in terms of the average or sectoral pRNFL thickness (27, 28, 30, 31, 35–37, 42); two studies reported there was no significant difference in the EG eyes compared to the PPG eyes concerning mGCC thickness (28, 36), and one study did not demonstrate a significant reduction in the EG eyes regarding the average and superior mGCIPL thickness (33). Currently, the exact biomechanisms of glaucomatous neurodegeneration remain poorly understood (1, 55). Nevertheless, continuous and progressive glaucomatous damage may lead to configuration changes in retinal ganglion cell dendrites, soma, and axons (56, 57), causing the attenuation of thickness in corresponding residing sites, inner plexiform layer, ganglion cell layer and RNFL (20). Our pooled results of pRNFL, mGCIPL, and mGCC thickness suggested that more serious structural damage occurred in EG than in PPG.

To explore the source of heterogeneity across the included studies, we performed subgroup analyses according to the different types of glaucoma. Our findings did not show a significant decrease in the superior quadrant of pRNFL ($P = 0.08$), and the average, as well as the inferior mGCC thickness in the EG eyes when patients with open-angle glaucoma were enrolled (average: $P = 0.09$; inferior quadrant: $P = 0.16$). This was probably mainly due to the relatively small sample size in the subgroup of OAG regarding the pRNFL and the mGCC thickness ($N = 2$), because of which heterogeneity could not be excluded. Another reason was that no quality assurance step was taken in the study of Cennamo et al. (36). Since only a single OCT examination was performed to evaluate each parameter by one experienced ophthalmologist, ensuring the reproducibility and reliability of the examination results was difficult.

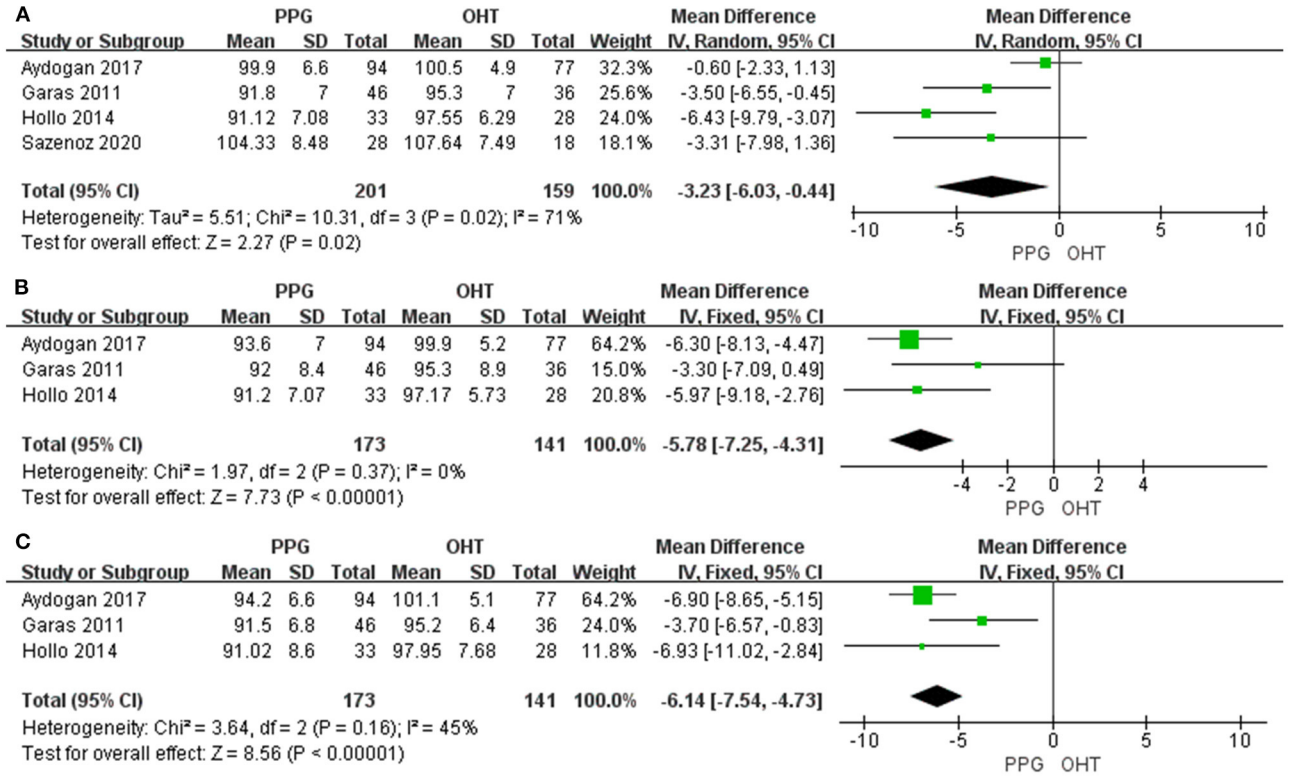

FIGURE 6 | mGCC thickness in patients with PPG and OHT. **(A)** Average. **(B)** Superior. **(C)** Inferior.

Based on the anatomy of retina, ∼30–50% RGCs are centered within the 4.5-mm-circle region of the fovea (44, 58–60); thus, using a relatively small scan area of 3 × 3 mm may not allow the differentiation of EG from PPG or suspected glaucoma (41, 61). For this reason, we also performed a subgroup analysis of the macular scan area. Interestingly, our pooled data showed that when the 6 × 6 mm scan protocol was used, there was a significant decrease in mGCC thickness in the EG eyes compared with the PPG eyes, whereas there was no difference when the 7 × 7 mm scan protocol was used. One reason for the different diagnostic performances between these two scan protocols may be the decreased signal-to-noise ratio. Although the enlarged scan area could cover the region with the most abundant RGCs, the concomitant decrease in signal-to-noise ratio and increase in test-retest variability (62) may have undervalued the assessment of GCC thickness measured by SD-OCT. Another explanation was the strict inclusion criteria by Arintawati et al. (28). In this study, investigators only accepted subjects with all the typical glaucomatous changes observed in fundus photographs to avoid false-positive cases. Consequently, patients with higher severity may have been enrolled; thus, showing a minimal difference between the PPG and EG groups. Unfortunately, because of the small sample size ($N = 3$), we were unable to include other scan areas and protocols, introducing difficulties in the overall evaluation of the diagnostic values regarding different macular scan protocols. In addition, sensitivity analysis demonstrated that the study of Aydogan et al. (39) contributed mostly to the heterogeneity of average mGCC thickness. The main reason was that the age was not well-matched among PPG and EG groups ($P < 0.001$), which may induce potential bias since glaucoma is an age-related optic neuropathy (55). However, after excluding this study, the heterogeneity decreased (I^2 decreased from 83 to 64%).

Recently, in addition to OCT, several studies have focused on the macular microvasculature changes in PPG and EG via OCT angiography, revealing the progression patterns of glaucoma with respect to microvascular dysregulation (41, 42, 44, 63, 64). Although macular vessel density (VD) was reported to significantly decrease both in PPG and EG, one study demonstrated that mGCC thickness, unlike macular VD, could serve as a tool to discriminate PPG from EG (41). The study also showed that the percentage loss of mGCC thickness was significantly higher than that of macular VD both in PG and EG. Another study reported that both inferotemporal and superotemporal pRNFL thickness were significantly decreased in EG eyes compared to PPG eyes whereas only the inferotemporal sector of the radial peripapillary capillary VD experienced a significant decrease (42). Considering previous OCT studies that suggest that structural deterioration usually occurs before functional loss (10–18), these findings consolidate the results of our study, which indicate that the OCT

TABLE 6 | Begg's and Egger's tests results for the evaluation of publication bias.

Outcome indicators	No.	Begg's test		Egger's test	
		z	Pr > |z|	*t*	*P* > |*t*|
1. PPG vs. EG					
pRNFL					
Average	16	0.23	0.822	−0.55	0.589
Superior	11	0.62	0.533	−0.53	0.606
Nasal	6	0.00	1.000	−1.21	0.292
Inferior	11	1.71	0.087	−0.76	0.465
Temporal	7	0.30	0.764	−0.60	0.573
mGCC					
Average	10	1.07	0.283	0.20	0.849
Superior	7	0.00	1.000	0.04	0.973
Inferior	7	0.00	1.000	−0.11	0.920
mGCIPL					
Average	7	1.20	0.230	1.50	0.195
Superior	6	0.38	0.707	0.26	0.806
Inferior	6	0.00	1.000	0.36	0.735
2. PPG vs. OHT					
pRNFL					
Average	6	1.13	0.260	2.71	0.053
Superior	4	−0.34	1.000	0.85	0.487
Inferior	4	0.34	0.734	3.32	0.08
mGCC					
Average	4	0.34	0.734	−1.84	0.206
Superior	3	0.00	1.000	0.51	0.700
Inferior	3	0.00	1.000	1.10	0.471

PPG, pre-perimetric glaucoma; EG, early perimetric glaucoma; OHT, ocular hypertension; pRNFL, peripapillary retinal nerve fiber layer; mGCC, macular ganglion cell complex; mGCIPL, macular ganglion cell plus inner plexiform layer.

TABLE 7 | Sensitivity analysis of average mGCIPL thickness in patients with PPG and EG.

Study excluded	Fixed-effects model		Random-effects model		Heterogeneity
	WMD (95% CI)	*P*	WMD (95% CI)	*P*	I^2
Kim et al. (40)	**4.40 (3.53, 5.27)**	**<0.00001**	**4.39 (3.30, 5.47)**	**<0.00001**	**34%**
Park et al. (35)	4.71 (3.80, 5.63)	<0.00001	5.00 (3.35, 6.65)	<0.00001	66%
Kim et al. (34)	4.26 (3.30, 5.23)	<0.00001	4.60 (3.02, 6.18)	<0.00001	59%
Hwang et al. (33)	4.97 (4.05, 5.88)	<0.00001	5.21 (3.80, 6.62)	<0.00001	54%
Sung et al. (31)	4.50 (3.60, 5.40)	<0.00001	4.68 (3.12, 6.24)	<0.00001	64%
Kim et al. (30)	4.75 (3.80, 5.70)	<0.00001	5.03 (3.32, 6.73)	<0.00001	66%
Kim et al. (29)	4.87 (3.90, 5.85)	<0.00001	5.10 (3.41, 6.78)	<0.00001	64%

PPG, pre-perimetric glaucoma; EG, early perimetric glaucoma; mGCIPL, macular ganglion cell plus inner plexiform layer; WMD, weighted mean difference; CI, confidence interval; I^2, I-square heterogeneity statistic. The bold values refer to the study that has contributed mostly to the heterogeneity.

evaluation of macular structure changes could help to clarify the pathophysiological mechanisms of glaucoma and differentiate PPG from EG.

In a subgroup analysis of pRNFL thickness according to the type of SD-OCT, the pooled results were generally consistent with the combined pooled data except for the nasal quadrant in the Cirrus SD-OCT subgroup. The main reason was that Kim et al. (34) utilized the optic disc Cube 200 × 200 scanning protocol, whereas the other two studies focused on a 3.46-mm-diameter circle region of the ONH (31, 35). Although all types of SD-OCT could detect characteristic glaucomatous damage patterns of pRNFL thickness, different algorithms, software, and parameters may have induced subtle differences in diagnostic performance (65). However, our pooled results demonstrate the important diagnostic value of SD-OCT in evaluating the severity of the glaucomatous damage of the ONH.

TABLE 8 | Sensitivity analysis of average mGCC thickness in patients with PPG and EG.

Study excluded	Fixed-effects model		Random-effects model		Heterogeneity
	WMD (95% CI)	*P*	WMD (95% CI)	*P*	I^2
Wang et al. (44)	7.51 (6.46, 8.56)	<0.00001	6.78 (3.98, 9.58)	<0.00001	85%
Sarigül Sezenöz et al. (43)	7.56 (6.52, 8.61)	<0.00001	6.85 (4.06, 9.65)	<0.00001	85%
Lu et al. (42)	7.69 (6.61, 8.76)	<0.00001	7.17 (4.23, 10.11)	<0.00001	85%
Hou et al. (41)	8.27 (7.11, 9.43)	<0.00001	7.44 (4.43, 10.45)	<0.00001	84%
Aydogan et al. (39)	**5.98 (4.80, 7.17)**	**<0.00001**	**6.28 (4.20, 8.37)**	**<0.00001**	**64%**
Kumar et al. (37)	7.86 (6.77, 8.95)	<0.00001	7.33 (4.36, 10.31)	<0.00001	85%
Cennamo et al. (36)	8.09 (7.02, 9.16)	<0.00001	7.73 (5.00, 10.45)	<0.00001	83%
Yamada et al. (32)	7.78 (6.70, 8.85)	<0.00001	7.29 (4.35, 10.23)	<0.00001	85%
Kim et al. (30)	7.49 (6.40, 8.57)	<0.00001	6.95 (3.98, 9.91)	<0.00001	85%
Arintawati et al. (28)	8.17 (7.10, 9.24)	<0.00001	7.90 (5.34, 10.46)	<0.00001	80%

PPG, pre-perimetric glaucoma; EG, early perimetric glaucoma; mGCC, macular ganglion cell complex; WMD, weighted mean difference; CI, confidence interval; I^2, I-square heterogeneity statistic. The bold values refer to the study that has contributed mostly to the heterogeneity.

TABLE 9 | Sensitivity analysis of average mGCC thickness in patients with PPG and OHT.

Study excluded	Fixed-effects model		Random-effects model		Heterogeneity
	WMD (95% CI)	*P*	WMD (95% CI)	*P*	I^2
Sarigül Sezenöz et al. (43)	−2.16 (−3.53,−0.79)	0.002	−3.28 (−6.75, 0.19)	0.06	80%
Aydogan et al. (39)	**−4.54 (−6.57, −2.51)**	**<0.0001**	**−4.54 (−6.57, −2.51)**	**<0.0001**	**0%**
Holo et al. (48)	−1.49 (−2.92, −0.06)	0.04	−1.93 (−4.05, 0.19)	0.08	39%
Garas et al. (46)	−1.96 (−3.42, −0.51)	0.008	−3.52 (−7.20, 0.69)	0.11	79%

PPG, pre-perimetric glaucoma; OHT, ocular hypertension; mGCC, macular ganglion cell complex; WMD, weighted mean difference; CI, confidence interval; I^2, I-square heterogeneity statistic. The bold values refer to the study that has contributed mostly to the heterogeneity.

Apart from this, studies have shown that individuals with OHT are at higher risk of developing glaucoma than others (3, 4, 66); however, there is no optimal IOP cut-off that possesses both reasonable sensitivity and specificity (3), which may delay the early diagnosis until patients are found to have apparent optic disc structural deterioration. Although the widely used cut-off of 21 mmHg has high sensitivity, it can decrease the specificity to 44% (67). In addition, spectrum bias usually occurs when studies inappropriately include the control groups without any suspicious symptoms of the disease, which can impair the diagnostic efficacy when clinically non-relevant individuals are enrolled (68–70). Thus, we also pooled the average and sectoral pRNFL and mGCC thickness in patients with PPG and OHT.

The pooled results revealed that the pRNFL and mGCC were significantly thinner in the PPG eyes than those in the OHT eyes, which were consistent with several investigations (45, 47, 48). However, two studies reported that there was no difference in patients with PPG and OHT in terms of the average mGCC thickness (39, 43); one study demonstrated that the average pRNFL thickness could not serve as a valued indicator for differential diagnosis (43), and another study showed that no difference was noted in the PPG eyes and OHT eyes regarding the superior mGCC thickness (46).

Similar to the investigation of exploring the heterogeneity across different OCT parameters for the differential diagnosis of PPG and EG, we also performed subgroup analysis of average pRNFL thickness according to the type of OCT. However, no difference was noted in the pooled results with either SD-OCT or TD-OCT. Compared to the traditional TD-OCT, SD-OCT is the latest generation of OCT with ultra-high scanning speed and retinal image resolutions, and is reported to have higher diagnostic abilities in terms of sectoral pRNFL and macular thickness. However, both SD-OCT and TD-OCT showed comparable reproducibility regarding the mean pRNFL (71). This was consistent with our finding. In the sensitivity analysis, the study of Aydogan et al. (39) also contributed mostly to the heterogeneity of mGCC thickness in patients with PPG and OHT. This may be due to usage of the different macular scanning protocol.

Despite the strengths of our study, some of its limitations should be considered. First, mild asymmetry was shown in the funnel plot of average mGCIPL thickness (**Supplementary Figure 6A**), suggesting potential publication bias. To elucidate the source of the bias, we performed a "leave-one-out" sensitivity analysis (**Table 7**). The results showed that the study by Kim et al. (40) contributed mostly to the heterogeneity in average mGCIPL thickness, wherein some problems of automated segmentation software occurred, although measures were taken to minimize the consequence of the segmentation error. Therefore, after

excluding this study, low heterogeneity ($I^2 = 34\%$) was noted (**Supplementary Figure 12**), and the funnel plot became symmetrical (**Supplementary Figure 13**). Second, regarding the subgroup analysis of the macular scan area, due to the relatively small sample size, we did not include other scan protocols apart from the 6 × 6 mm and 7 × 7 mm scan protocols. Further, the small sample size may have also introduced heterogeneity in the analysis of mGCC thickness, although sensitivity analyses proved the reliability of our results. Further studies should be included to comprehensively evaluate the influence of scan area and protocols on the assessment of macular structure changes in PPG, EG, and OHT. Moreover, the heterogeneity was high regarding many of our findings, indicating that the results should be cautiously interpreted.

CONCLUSION

The OCT-based assessment of peripapillary and macular structural changes could be potentially utilized to discriminate PPG from EG and OHT. This facilitates a better understanding of the pathophysiology of glaucoma and provides references for ophthalmologists to manage individuals suspected to have glaucoma and glaucoma patients according to the extent of severity in a non-invasive way. Further studies that employ clock hour classification methods that can monitor the configuration alterations in a narrower range and longitudinal studies are needed to verify our findings.

DATA AVAILABILITY STATEMENT

The original contributions presented in the study are included in the article/**Supplementary Material**, further inquiries can be directed to the corresponding author/s.

AUTHOR CONTRIBUTIONS

YT, TW, XZ, and BJ: conceptualization and design. YT, TW, and YH: literature search, data extraction, quality assessment, and data analysis. YT, TW, XZ, YH, and BJ: manuscript writing and editing. BJ: supervision. All authors approved the final version of the manuscript.

FUNDING

This study was supported by the Natural Science Foundation of China (NSFC 82070967 and 81770930 to BJ), Natural Science Foundation of Hunan Province Grant (2020jj4788 to BJ), China Hunan Provincial Science and Technology Department (No. 2020SK2086). The sponsors did not participate in the design or implementation of this study.

SUPPLEMENTARY MATERIAL

The Supplementary Material for this article can be found online at: https://www.frontiersin.org/articles/10.3389/fmed.2021.696004/full#supplementary-material

REFERENCES

1. Weinreb RN, Aung T, Medeiros FA. The pathophysiology and treatment of glaucoma: a review. *JAMA.* (2014) 311:1901–11. doi: 10.1001/jama.2014.3192
2. Tham YC, Li X, Wong TY, Quigley HA, Aung T, Cheng CY. Global prevalence of glaucoma and projections of glaucoma burden through 2040: a systematic review and meta-analysis. *Ophthalmology.* (2014) 21:2081–90. doi: 10.1016/j.ophtha.2014.05.013
3. San Laureano J. When is glaucoma really glaucoma? *Clin Exp Optom.* (2007) 90:376–85. doi: 10.1111/j.1444-0938.2007.00175.x
4. Kass MA, Heuer DK, Higginbotham EJ, Johnson CA, Keltner JL, Miller JP, et al. The ocular hypertension treatment study: a randomized trial determines that topical ocular hypotensive medication delays or prevents the onset of primary open-angle glaucoma. *Arch Ophthalmol.* (2002) 120:701–13. Discussion 829-30. doi: 10.1001/archopht.120.6.701
5. Boland MV, Ervin AM, Friedman DS, Jampel HD, Hawkins BS, Vollenweider D, et al. Comparative effectiveness of treatments for open-angle glaucoma: a systematic review for the U.S. Preventive Services Task Force. *Ann Intern Med.* (2013) 158:271–9. doi: 10.7326/0003-4819-158-4-201302190-00008
6. Heijl A, Bengtsson B, Oskarsdottir SE. Prevalence and severity of undetected manifest glaucoma: results from the early manifest glaucoma trial screening. *Ophthalmology.* (2013) 120:1541–5. doi: 10.1016/j.ophtha.2013.01.043
7. Quigley HA. Number of people with glaucoma worldwide. *Br J Ophthalmol.* (1996) 80:389–93. doi: 10.1136/bjo.80.5.389
8. Shiga Y, Aizawa N, Tsuda S, Yokoyama Y, Omodaka K, Kunikata H, et al. Preperimetric glaucoma prospective study (PPGPS): predicting visual field progression with basal optic nerve head blood flow in normotensive PPG eyes. *Transl Vis Technol.* (2018) 7:11. doi: 10.1167/tvst.7.1.11
9. Camp AS, Weinreb RN. Will perimetry be performed to monitor glaucoma in 2025? *Ophthalmology.* (2017) 124:S71–5. doi: 10.1016/j.ophtha.2017.04.009
10. Quigley HA, Miller NR, George T. Clinical evaluation of nerve fiber layer atrophy as an indicator of glaucomatous optic nerve damage. *Arch Ophthalmol.* (1980) 98:1564–71. doi: 10.1001/archopht.1980.01020040416003
11. Airaksinen PJ, Drance SM, Douglas GR, Mawson DK, Nieminen H. Diffuse and localized nerve fiber loss in glaucoma. *Am J Ophthalmol.* (1984) 98:566–71. doi: 10.1016/0002-9394(84)90242-3
12. Sommer A, Katz J, Quigley HA, Miller NR, Robin AL, Richter RC, et al. Clinically detectable nerve fiber atrophy precedes the onset of glaucomatous field loss. *Arch Ophthalmol.* (1991) 109:77–83. doi: 10.1001/archopht.1991.01080010079037
13. Quigley HA, Katz J, Derick RJ, Gilbert D, Sommer A. An evaluation of optic disc and nerve fiber layer examinations in monitoring progression of early glaucoma damage. *Ophthalmology.* (1992) 99:19–28. doi: 10.1016/S0161-6420(92)32018-4
14. Harwerth RS, Carter-Dawson L, Shen F, Smith EL 3rd, Crawford ML. Ganglion cell losses underlying visual field defects from experimental glaucoma. *Invest Ophthalmol Vis Sci.* (1999) 40:2242–50.
15. Asrani S, Challa P, Herndon L, Lee P, Stinnett S, Allingham RR. Correlation among retinal thickness, optic disc, and visual field in glaucoma patients and suspects: a pilot study. *J Glaucoma.* (2003) 12:119–28. doi: 10.1097/00061198-200304000-00006
16. Ajtony C, Balla Z, Somoskeoy S, Kovacs B. Relationship between visual field sensitivity and retinal nerve fiber layer thickness as measured by optical coherence tomography. *Invest Ophthalmol Vis Sci.* (2007) 48:258–63. doi: 10.1167/iovs.06-0410
17. Cho JW, Sung KR, Lee S, Yun SC, Kang SY, Choi J, et al. Relationship between visual field sensitivity and macular ganglion cell complex thickness as measured by spectral-domain optical coherence tomography. *Invest Ophthalmol Vis Sci.* (2010) 51:6401–7. doi: 10.1167/iovs.09-5035
18. Cvenkel B, Sustar M, Perovšek D. Ganglion cell loss in early glaucoma, as assessed by photopic negative response, pattern electroretinogram, and

spectral-domain optical coherence tomography. *Doc Ophthalmol.* (2017) 135:17–28. doi: 10.1007/s10633-017-9595-9
19. Blumenthal EZ, Sapir-Pichhadze R. Misleading statistical calculations in far-advanced glaucomatous visual field loss. *Ophthalmology.* (2003) 110:196–200. doi: 10.1016/S0161-6420(02)01297-6
20. Tan O, Chopra V, Lu AT, Schuman JS, Ishikawa H, Wollstein G, et al. Detection of macular ganglion cell loss in glaucoma by Fourier-domain optical coherence tomography. *Ophthalmology.* (2009) 116:2305–14.e1-2. doi: 10.1016/j.ophtha.2009.05.025
21. Savini G, Carbonelli M, Barboni P. Spectral-domain optical coherence tomography for the diagnosis and follow-up of glaucoma. *Curr Opin Ophthalmol.* (2011) 22:115–23. doi: 10.1097/ICU.0b013e3283437222
22. Hood DC, Raza AS, de Moraes CG, Johnson CA, Liebmann JM, Ritch R. The nature of macular damage in glaucoma as revealed by averaging optical coherence tomography data. *Transl Vis Technol.* (2012) 1:3. doi: 10.1167/tvst.1.1.3
23. Eladawi N, Elmogy MM, Ghazal M, Helmy O, Aboelfetouh A, Riad A, et al. Classification of retinal diseases based on OCT Images. *Front Biosci.* (2018) 23:247–64. doi: 10.2741/4589
24. Hood DC, Raza AS. On improving the use of OCT imaging for detecting glaucomatous damage. *Br J Ophthalmol.* (2014) 98 (Suppl. 2):ii1–9. doi: 10.1136/bjophthalmol-2014-305156
25. Kim MJ, Jeoung JW, Park KH, Choi YJ, Kim DM. Topographic profiles of retinal nerve fiber layer defects affect the diagnostic performance of macular scans in preperimetric glaucoma. *Invest Ophthalmol Vis Sci.* (2014) 55:2079–87. doi: 10.1167/iovs.13-13506
26. Horn FK, Mardin CY, Bendschneider D, Jünemann AG, Adler W, Tornow RP. Frequency doubling technique perimetry and spectral domain optical coherence tomography in patients with early glaucoma. *Eye.* (2011) 25:17–29. doi: 10.1038/eye.2010.155
27. Morooka S, Hangai M, Nukada M, Nakano N, Takayama K, Kimura Y, et al. Wide 3-dimensional macular ganglion cell complex imaging with spectral-domain optical coherence tomography in glaucoma. *Invest Ophthalmol Vis Sci.* (2012) 53:4805–12. doi: 10.1167/iovs.12-9870
28. Arintawati P, Sone T, Akita T, Tanaka J, Kiuchi Y. The applicability of ganglion cell complex parameters determined from SD-OCT images to detect glaucomatous eyes. *J Glaucoma.* (2013) 22:713–8. doi: 10.1097/IJG.0b013e318259b2e1
29. Kim KE, Park KH, Jeoung JW, Kim SH, Kim DM. Severity-dependent association between ganglion cell inner plexiform layer thickness and macular mean sensitivity in open-angle glaucoma. *Acta Ophthalmol.* (2014) 92:e650–6. doi: 10.1111/aos.12438
30. Kim YJ, Kang MH, Cho HY, Lim HW, Seong M. Comparative study of macular ganglion cell complex thickness measured by spectral-domain optical coherence tomography in healthy eyes, eyes with preperimetric glaucoma, and eyes with early glaucoma. *Jpn J Ophthalmol.* (2014) 58:244–51. doi: 10.1007/s10384-014-0315-7
31. Sung MS, Yoon JH, Park SW. Diagnostic validity of macular ganglion cell-inner plexiform layer thickness deviation map algorithm using cirrus HD-OCT in preperimetric and early glaucoma. *J Glaucoma.* (2014) 23:e144–51. doi: 10.1097/IJG.0000000000000028
32. Yamada H, Hangai M, Nakano N, Takayama K, Kimura Y, Miyake M, et al. Asymmetry analysis of macular inner retinal layers for glaucoma diagnosis. *Am J Ophthalmol.* (2014) 158:1318–29.e3. doi: 10.1016/j.ajo.2014.08.040
33. Hwang YH, Ahn SI, Ko SJ. Diagnostic ability of macular ganglion cell asymmetry for glaucoma. *Clin Exp Ophthalmol.* (2015) 43:720–6. doi: 10.1111/ceo.12545
34. Kim YK, Yoo BW, Kim HC, Park KH. Automated detection of hemifield difference across horizontal raphe on ganglion cell–inner plexiform layer thickness map. *Ophthalmology.* (2015) 122:2252–60. doi: 10.1016/j.ophtha.2015.07.013
35. Park JW, Jung HH, Heo H, Park SW. Validity of the temporal-to-nasal macular ganglion cell-inner plexiform layer thickness ratio as a diagnostic parameter in early glaucoma. *Acta Ophthalmol.* (2015) 93:e356–65. doi: 10.1111/aos.12666
36. Cennamo G, Montorio D, Romano MR, Cardone DM, Minervino C, Reibaldi M, et al. Structure-functional parameters in differentiating between patients with different degrees of glaucoma. *J Glaucoma.* (2016) 25:e884–8. doi: 10.1097/IJG.0000000000000491
37. Kumar RS, Anegondi N, Chandapura RS, Sudhakaran S, Kadambi SV, Rao HL, et al. Discriminant function of optical coherence tomography angiography to determine disease severity in glaucoma. *Invest Ophthalmol Vis Sci.* (2016) 57:6079–88. doi: 10.1167/iovs.16-19984
38. Akil H, Huang AS, Francis BA, Sadda SR, Chopra V. Retinal vessel density from optical coherence tomography angiography to differentiate early glaucoma, pre-perimetric glaucoma and normal eyes. *PLoS ONE.* (2017) 12:e0170476. doi: 10.1371/journal.pone.0170476
39. Aydogan T, Akçay BI S, Kardeş E, Ergin A. Evaluation of spectral domain optical coherence tomography parameters in ocular hypertension, preperimetric, and early glaucoma. *Indian J Ophthalmol.* (2017) 65:1143–50. doi: 10.4103/ijo.IJO_157_17
40. Kim EK, Park HL, Park CK. Segmented inner plexiform layer thickness as a potential biomarker to evaluate open-angle glaucoma: dendritic degeneration of retinal ganglion cell. *PLoS ONE.* (2017) 12:e0182404. doi: 10.1371/journal.pone.0182404
41. Hou H, Moghimi S, Zangwill LM, Shoji T, Ghahari E, Penteado RC, et al. Macula vessel density and thickness in early primary open-angle glaucoma. *Am J Ophthalmol.* (2019) 199:120–32. doi: 10.1016/j.ajo.2018.11.012
42. Lu P, Xiao H, Liang C, Xu Y, Ye D, Huang J. Quantitative analysis of microvasculature in macular and peripapillary regions in early primary open-angle glaucoma. *Curr Eye Res.* (2020) 45:629–35. doi: 10.1080/02713683.2019.1676912
43. Sarigül Sezenöz A, Gür Güngör S, Akman A, Öztürk C, Cezairlioglu S, Aksoy M, et al. The diagnostic ability of ganglion cell complex thickness-to-total retinal thickness ratio in glaucoma in a Caucasian population. *Turk J Ophthalomol.* (2020) 50:26–30. doi: 10.4274/tjo.galenos.2019.19577
44. Wang Y, Xin C, Li M, Swain DL, Cao K, Wang H, et al. Macular vessel density versus ganglion cell complex thickness for detection of early primary open-angle glaucoma. *BMC Ophthalmol.* (2020) 20:17. doi: 10.1186/s12886-020-1304-x
45. Taliantzis S, Papaconstantinou D, Koutsandrea C, Moschos M, Apostolopoulos M, Georgopoulos G. Comparative studies of RNFL thickness measured by OCT with global index of visual fields in patients with ocular hypertension and early open angle glaucoma. *Clin Ophthalmol.* (2009) 3:373–9. doi: 10.2147/OPTH.S6150
46. Garas A, Vargha P, Holló G. Diagnostic accuracy of nerve fibre layer, macular thickness and optic disc measurements made with the RTVue-100 optical coherence tomograph to detect glaucoma. *Eye.* (2011) 25:57–65. doi: 10.1038/eye.2010.139
47. Pomorska M, Krzyzanowska-Berkowska P, Misiuk-Hojło M, Zajac-Pytrus H, Grzybowski A. Application of optical coherence tomography in glaucoma suspect eyes. *Clin Exp Optom.* (2012) 95:78–88. doi: 10.1111/j.1444-0938.2011.00654.x
48. Holló G, Naghizadeh F, Vargha P. Accuracy of macular ganglion-cell complex thickness to total retina thickness ratio to detect glaucoma in white Europeans. *J Glaucoma.* (2014) 23:e132–7. doi: 10.1097/IJG.0000000000000030
49. Stroup DF, Berlin JA, Morton SC, Olkin I, Williamson GD, Rennie D, et al. Meta-analysis of observational studies in epidemiology: a proposal for reporting. Meta-analysis of observational studies in epidemiology (MOOSE) group. *JAMA.* (2000) 283:2008–12. doi: 10.1001/jama.283.15.2008
50. Liberati A, Altman DG, Tetzlaff J, Mulrow C, Gøtzsche PC, Ioannidis JP, et al. The PRISMA statement for reporting systematic reviews and meta-analyses of studies that evaluate health care interventions: explanation and elaboration. *J Clin Epidemiol.* (2009) 62:e1–34. doi: 10.1016/j.jclinepi.2009.06.006
51. Parrish RK, 2nd, Gedde SJ, Scott IU, Feuer WJ, Schiffman JC, Mangione CM, et al. Visual function and quality of life among patients with glaucoma. *Arch Ophthalmol.* (1997) 115:1447–55. doi: 10.1001/archopht.1997.01100160617016
52. Higgins JP, Thompson SG, Deeks JJ, Altman DG. Measuring inconsistency in meta-analyses. *BMJ.* (2003) 327:557–60. doi: 10.1136/bmj.327.7414.557
53. Begg CB, Mazumdar M. Operating characteristics of a rank correlation test for publication bias. *Biometrics.* (1994) 50:1088–101. doi: 10.2307/2533446
54. Egger M, Davey Smith G, Schneider M, Minder C. Bias in meta-analysis detected by a simple, graphical test. *BMJ.* (1997) 315:629–34. doi: 10.1136/bmj.315.7109.629

55. Weinreb RN, Khaw PT. Primary open-angle glaucoma. *Lancet.* (2004) 363:1711–20. doi: 10.1016/S0140-6736(04)16257-0
56. Frankfort BJ, Khan AK, Tse DY, Chung I, Pang JJ, Yang Z, et al. Elevated intraocular pressure causes inner retinal dysfunction before cell loss in a mouse model of experimental glaucoma. *Invest Ophthalmol Vis Sci.* (2013) 54:762–70. doi: 10.1167/iovs.12-10581
57. El-Danaf RN, Huberman AD. Characteristic patterns of dendritic remodeling in early-stage glaucoma: evidence from genetically identified retinal ganglion cell types. *J Neurosci.* (2015) 35:2329–43. doi: 10.1523/JNEUROSCI.1419-14.2015
58. Quigley HA, Dunkelberger GR, Green WR. Retinal ganglion cell atrophy correlated with automated perimetry in human eyes with glaucoma. *Am J Ophthalmol.* (1989) 107:453–64. doi: 10.1016/0002-9394(89)90488-1
59. Curcio CA, Allen KA. Topography of ganglion cells in human retina. *J Comp Neurol.* (1990) 300:5–25. doi: 10.1002/cne.903000103
60. Kerrigan-Baumrind LA, Quigley HA, Pease ME, Kerrigan DF, Mitchell RS. Number of ganglion cells in glaucoma eyes compared with threshold visual field tests in the same persons. *Invest Ophthalmol Vis Sci.* (2000) 41:741–8.
61. Triolo G, Rabiolo A, Shemonski ND, et al. Optical coherence tomography angiography macular and peripapillary vessel perfusion density in healthy subjects, glaucoma suspects, and glaucoma patients. *Invest Ophthalmol Vis Sci.* (2017) 58:5713–22. doi: 10.1167/iovs.17-22865
62. Wan KH, Lam AKN, Leung CK. Optical coherence tomography angiography compared with optical coherence tomography macular measurements for detection of glaucoma. *JAMA Ophthalmol.* (2018) 136:866–74.42. doi: 10.1001/jamaophthalmol.2018.1627
63. Poli M, Cornut PL, Nguyen AM, De Bats F, Denis P. Accuracy of peripapillary versus macular vessel density in diagnosis of early to advanced primary open angle glaucoma. *J Fr Ophtalmol.* (2018) 41:619–29. doi: 10.1016/j.jfo.2018.02.004
64. Rolle T, Dallorto L, Tavassoli M, Nuzzi R. Diagnostic ability and discriminant values of OCT-angiography parameters in early glaucoma diagnosis. *Ophthalmic Res.* (2019) 61:143–52. doi: 10.1159/000489457
65. Chen TC, Hoguet A, Junk AK, Nouri-Mahdavi K, Radhakrishnan S, Takusagawa HL, et al. Spectral-domain OCT: helping the clinician diagnose glaucoma: a report by the American Academy of Ophthalmology. *Ophthalmology.* (2018) 125:1817–27. doi: 10.1016/j.ophtha.2018.05.008
66. Jayanetti V, Sandhu S, Lusthaus JA. The latest drugs in development that reduce intraocular pressure in ocular hypertension and glaucoma. *J Exp Pharmacol.* (2020) 12:539–48. doi: 10.2147/JEP.S281187
67. Tielsch JM, Katz J, Singh K, Quigley HA, Gottsch JD, Javitt J, et al. A population-based evaluation of glaucoma screening: the Baltimore Eye Survey. *Am J Epidemiol.* (1991) 134:1102–10. doi: 10.1093/oxfordjournals.aje.a116013
68. Rao HL, Kumbar T, Addepalli UK, Bharti N, Senthil S, Choudhari NS, et al. Effect of spectrum bias on the diagnostic accuracy of spectral-domain optical coherence tomography in glaucoma. *Invest Ophthalmol Vis Sci.* (2012) 53:1058–65. doi: 10.1167/iovs.11-8463
69. Rao HL, Addepalli UK, Chaudhary S, Kumbar T, Senthil S, Choudhari NS, et al. Ability of different scanning protocols of spectral domain optical coherence tomography to diagnose preperimetric glaucoma. *Invest Ophthalmol Vis Sci.* (2013) 54:7252–7. doi: 10.1167/iovs.13-12731
70. Willis BH. Spectrum bias–why clinicians need to be cautious when applying diagnostic test studies. *Fam Pract.* (2008) 25:390–6. doi: 10.1093/fampra/cmn051
71. Schuman JS. Spectral domain optical coherence tomography for glaucoma (an AOS thesis). *Trans Am Ophthalmol Soc.* (2008) 106:426–58.

Conflict of Interest: The authors declare that the research was conducted in the absence of any commercial or financial relationships that could be construed as a potential conflict of interest.

frontiers in Medicine

ORIGINAL RESEARCH
published: 05 July 2021
doi: 10.3389/fmed.2021.701997

Non-invasive Clinical Measurement of Ocular Rigidity and Comparison to Biomechanical and Morphological Parameters in Glaucomatous and Healthy Subjects

Yanhui Ma[1]*, *Sayoko E. Moroi*[1] and *Cynthia J. Roberts*[1,2]

[1] Department of Ophthalmology and Visual Sciences, The Ohio State University Wexner Medical Center, Columbus, OH, United States, [2] Department of Biomedical Engineering, The Ohio State University, Columbus, OH, United States

Purpose: To assess ocular rigidity using dynamic optical coherence tomography (OCT) videos in glaucomatous and healthy subjects, and to evaluate how ocular rigidity correlates with biomechanical and morphological characteristics of the human eye.

Methods: Ocular rigidity was calculated using Friedenwald's empirical equation which estimates the change in intraocular pressure (IOP) produced by volumetric changes of the eye due to choroidal pulsations with each heartbeat. High-speed OCT video was utilized to non-invasively measure changes in choroidal volume through time-series analysis. A control-case study design was based on 23 healthy controls and 6 glaucoma cases. Multiple diagnostic modalities were performed during the same visit including Spectralis OCT for nerve head video, Pascal Dynamic Contour Tonometry for IOP and ocular pulse amplitude (OPA) measurement, Corvis ST for measuring dynamic biomechanical response, and Pentacam for morphological characterization.

Results: Combining glaucoma and healthy cohorts ($n = 29$), there were negative correlations between ocular rigidity and axial length (Pearson $R = -0.53$, $p = 0.003$), and between ocular rigidity and anterior chamber volume ($R = -0.64$, $p = 0.0002$). There was a stronger positive correlation of ocular rigidity and scleral stiffness (i.e., stiffness parameter at the highest concavity [SP-HC]) ($R = 0.62$, $p = 0.0005$) compared to ocular rigidity and corneal stiffness (i.e., stiffness parameter at the first applanation [SP-A1]) ($R = 0.41$, $p = 0.033$). In addition, there was a positive correlation between ocular rigidity and the static pressure-volume ratio (P/V ratio) ($R = 0.72$, $p < 0.0001$).

Conclusions: Ocular rigidity was non-invasively assessed using OCT video and OPA in a clinic setting. The significant correlation of ocular rigidity with biomechanical parameters, SP-HC and P/V ratio, demonstrated the validity of the ocular rigidity measurement. Ocular rigidity is driven to a greater extent by scleral stiffness than corneal stiffness. These *in vivo* methods offer an important approach to investigate the role of ocular biomechanics in glaucoma.

Keywords: ocular rigidity, glaucoma, ocular biomechanics, optical coherence tomography, stiffness parameter, pressure volume relationships

OPEN ACCESS

Edited by:
Michele Lanza, University of Campania Luigi Vanvitelli, Italy

Reviewed by:
Salavat Aglyamov, University of Houston, United States
Eray Atalay, Eskişehir Osmangazi University, Turkey
Henryk Teodor Kasprzak, Wrocław University of Technology, Poland

***Correspondence:**
Yanhui Ma
ma.1634@osu.edu

Specialty section:
This article was submitted to Ophthalmology, a section of the journal Frontiers in Medicine

Received: *28 April 2021*
Accepted: *07 June 2021*
Published: *05 July 2021*

Citation:
Ma Y, Moroi SE and Roberts CJ (2021) Non-invasive Clinical Measurement of Ocular Rigidity and Comparison to Biomechanical and Morphological Parameters in Glaucomatous and Healthy Subjects. Front. Med. 8:701997. doi: 10.3389/fmed.2021.701997

INTRODUCTION

Accumulating clinical and scientific evidence has confirmed the critical roles of biomechanics in ocular health and disease, specifically in glaucoma (1–4). Glaucoma is the second leading cause of blindness worldwide (5), and represents a significant health and financial burden on the economy. Glaucomatous axonal damage initiates at the optic nerve head (ONH) where the retinal nerve fibers (axons of ganglion cell) exit the eye (6, 7). Mathematical modeling and animal studies have suggested that scleral stiffness is a major determinant of the ONH susceptibility to the damage (8–11). Methods for quantifying the pressure-strain response of the sclera focused mainly on *ex vivo* strip testing and inflation testing (12–14). However, *in vivo* evaluation of scleral stiffness remains limited. Assessing the ocular biomechanics in glaucoma, especially in a clinic setting, is imperative to gain a deeper understanding of tissue behavior using newer technologies.

Ocular rigidity describes the change in intraocular pressure (IOP) in response to a change in ocular volume. The ocular volume fluctuates due to the pulsatile vascular filling that occurs with each heartbeat, and for a given volume change, stiffer eyes will have a correspondingly larger increase in IOP, and vice versa for less stiff eyes (15). The pulsatile IOP change, referred as ocular pulse amplitude (OPA), can be easily measured transcorneally with a pneumotonometer or dynamic contour tonometer (DCT). In contrast, assessing the pulsatile volume change is the challenging part in the process of estimating ocular rigidity. Direct invasive methods involve injecting a known volume of saline solution into the anterior chamber, while continually monitoring the IOP (16), which were only applied to subjects undergoing cataract surgery. Retrobulbar anesthesia during the surgery may alter the ocular rigidity (17). Indirect non-invasive methods involve using the anterior-to-posterior expansion of the corneoscleral shell to estimate the volume change (18, 19), which, however, may obfuscate the measurement of ocular rigidity (20), due to confounding variables, such as the preexisting volume of the choroidal circulation and the preexisting IOP level. Thus, a direct measure of the choroidal volume change produced by blood vessel flux with each cardiac cycle is crucial for the reliable non-invasive estimation of ocular rigidity.

Optical coherence tomography (OCT), as a non-invasive imaging tool for visualizing the cross-section of the retina and choroid with micrometer resolution, has become the standard of care in the ophthalmic field. Recent advances in OCT with enhanced depth imaging have brought previously unavailable insights into choroidal anatomy and pathologies. Choroidal-scleral interface (CSI) can be distinguished from high-quality OCT images permitting the thickness of the choroid to be evaluated. At each heartbeat, the pulsatile vascular filling induces a transient change of the choroidal volume. High-speed OCT with dense temporal sampling (up to 153 frames *per second*) enables us to capture the dynamic response and detect the change in the retina and choroid. We have implemented an automated open-source algorithm for CSI segmentation in sequential OCT images with 599 B-scan frames, which allows for the assessment of pulsatile choroidal thickness change deriving the ocular volume change, then the ocular rigidity in conjunction with an independent measurement of OPA.

This study first aimed to evaluate the ocular rigidity in treated glaucoma patients compared to healthy subjects with our *in vivo* non-invasive approach. Note that this approach for *in vivo* estimation of ocular rigidity would not be easily accessible to clinicians for a foreseeable future due to the fact that not all OCT devices provide time series, and also the custom algorithm is currently limited in the generalizability to the real-world setting. Investigation of how ocular rigidity correlates with clinically-measurable parameters may facilitate identifying the surrogates for *in vivo* ocular rigidity. The second aim of this study is to examine the relationship of ocular rigidity with biomechanical and morphological characteristics of the eye.

METHODS

Subject Participants and Ophthalmological Examination

All participants have consented in adherence to the tenets of the Declaration of Helsinki. This study was approved by the Institutional Review Board of The Ohio State University. Subjects with a diagnosis of primary open-angle glaucoma by a glaucoma specialist without a history of intraocular surgery were included in the glaucoma cohort. Healthy controls had an untreated IOP lower than 21 mm Hg, healthy discs, and no ocular pathologies. Exclusion criteria for participants included any history of ocular injury and ocular diseases, such as age-related macular degeneration, diabetic retinopathy, keratoconus, retinal detachment, retinal tear, retinal degeneration, or retinal hole. Participants with spherical equivalent refraction <-6 diopters or more than +6 diopters were also excluded. Any OCT images with significant artifactual components due to blockage of OCT signal by floaters and eyelashes, residual motion artifacts, or other artifacts, were excluded from the study to avoid confounding of quantitative analysis.

Data were acquired on multiple ophthalmic diagnostic devices. All patients underwent a complete ophthalmic examination including the Corvis ST (OCULUS, Wetzlar, Germany), Pentacam (OCULUS, Wetzlar, Germany), Pascal DCT (Ziemer, Port, Switzerland), and Spectralis OCT (Heidelberg Engineering, Heidelberg, Germany) examinations during the same visit. Only one eye (right eye) per subject was included in the analysis. Statistical analyses were conducted using the SAS software (V9.4; SAS Institute Inc., Cary, NC, USA). The normality was checked using the Shapiro-Wilk test. The ocular rigidity in the healthy cohort ($n = 23$) was normally distributed, whereas the distribution of ocular rigidity in the glaucoma cohort ($n = 6$) was not normal, likely due to the small sample size. Thus, non-parametric Mann-Whitney U test (also called Wilcoxon rank sum test) was used to compare the data between glaucoma cases and healthy controls. The correlations of ocular rigidity with biomechanical and morphological characteristics of the eye were evaluated using Pearson correlation with groups of healthy and glaucoma subjects combined ($n = 29$).

Estimation of Ocular Rigidity using Optical Coherence Tomography

Spectralis OCT integrated the active eye-tracking (TruTrack) technology to correct eye motion by reacquisition of OCT images at the same retinal location in a fraction of a second. OCT videos of the posterior eye centered at the ONH consisting of 599 B-scan frames were acquired (**Figure 1A**). Segmentation for the CSI is currently not available on the clinical OCT device that provides time series. Hand-tracing is not only operator-dependent, but also time-consuming and labor-intensive. Herein we have implemented an open-source algorithm for automatically segmenting and quantifying the choroidal layer based on graph search (21). Briefly, graph nodes are defined as the inflection points (where the second derivative changes signs) of the intensity along each depth profile (A-scan). The intensity transition from dark to bright marks the location passing from the choroidal vessel to the sclera. Edge probability was used to compute the weight component for each node (22). Chorioretinal thinning and disruption of the retinal pigment epithelium with the development of peripapillary atrophy (alpha and beta zone of atrophy around the ONH) are more frequently observed in glaucoma (23). It is worth noting that before graph search, each B-scan frame (excluding the central optic nerve region, **Figure 1B**) is flattened with respect to the posterior retinal pigment epithelium to eliminate erroneous paths resultant of the curvature or tilt of the B-scan. Choroidal thickness (ChT) was then calculated as the average location of all searched nodes subtracted by the posterior retinal pigment epithelium depth at each frame.

Compiling the ChTs of all frames presents ChT fluctuation over time. The period of time for acquisition of 599 B-scans varies in the range of 4–7 s depending on the eye's stability as the built-in eye-tracking feature introduces pauses into the acquisition when the scanning beam could not be held in place due to eye movement. Because of this, the ChT points in the time series are not usually equally spaced. A series of signal process techniques are applied to extract the ChT change. First, ChT values that are more than three median absolute deviations are regarded as outliers and discarded from the waveform. Then the non-equally-spaced data are resampled by incorporating an anti-aliasing filter and compensating for the delay introduced by the filter. In order to extract the ChT fluctuations associated mainly with the heart rate, a band-pass filter is applied to only pass frequencies within the range of 0.5 to 3 times the heart rate. The inverse Fourier Transform is used to retrieve the filtered signal, from which average peak-to-valley distance is calculated as the ChT change (denoted as Δt) (**Figure 1C**). Since 85% of total ocular blood flow passes through the choroid (24), fluctuation of the ocular volume is estimated by the choroidal volume change. We simplified the choroid as a thin spherical shell, and its volume change is the difference between the volumes of two spheres: $\frac{4}{3}\pi\ (R+\Delta t)^3 - \frac{4}{3}\pi\ (R)^3$, where R is approximated by half of the axial length based on a spherical eye model. For a small Δt, the ocular volume change is specified as $\Delta V = 4\pi R^2 \Delta t$. Note that the automated segmentation of high-speed OCT imaging was developed by Beaton et al. (22), and we have independently implemented this approach and extended the image analysis to the ONH region with improvement in signal processing for ChT extraction.

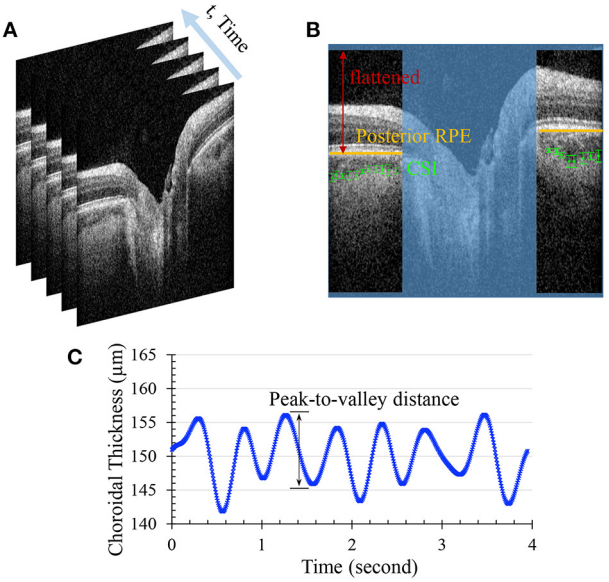

FIGURE 1 | (A) Sequential OCT B-scans of the posterior eye centered at the optic nerve head **(B)** Automated segmentation for the choroidal scleral interface (CSI). The optic nerve region was excluded from the region of interest, and the posterior retinal pigment epithelium (RPE) of each side of the optic nerve was flattened before the graph search for CSI nodes. **(C)** Filtered choroidal thickness waveform. The average peak-to-valley distance was calculated as choroidal thickness change.

In this study, IOP variation within each cardiac cycle was measured by a Pascal DCT immediately before OCT imaging. It has been reported that DCT is relatively independent of corneal biomechanics, generating accurate and reproducible continuous recording of IOP (25, 26). Finally, the ocular rigidity is estimated using Friedenwald's empirical function, as specified by $lnIOP_1 - lnIOP_2 = k\Delta V$, where k denotes the ocular rigidity (15). IOP_1 is the systolic IOP calculated by the sum of IOP reading and OPA from DCT measurement. IOP_2 is the diastolic IOP provided directly by the IOP reading from DCT.

Corneoscleral Biomechanical Response Induced by Air Puff

Dynamic corneal response parameters were measured by Corvis ST which is a novel, non-contact, tonometer coupled with a high-speed Scheimpflug camera that allows investigation of the dynamic reaction of the cornea to an air impulse. The camera acquires 140 sequential images of the central cornea with 8 mm horizontal coverage at over 4,330 frames *per second*. Good repeatability and reproducibility have been shown for dynamic corneal response parameters (27). Stiffness parameters at the first applanation (SP-A1) and highest concavity (SP-HC) were derived from the directly measured dynamic corneal response parameters (28). Specifically, SP-A1 was calculated by $(AP1_{adj} - bIOP)/\delta_{A1}$, where $AP1_{adj}$ is the adjusted air pressure at the time of first applanation, $bIOP$ is biomechanically corrected intraocular

TABLE 1 | Demographic and ocular characteristics of all subjects ($n = 29$).

	Control ($n = 23$)	Glaucoma ($n = 6$)	p-value
Age (*years*)	40.0 ± 12.6	61.5 ± 8.4	**0.002***
Central corneal thickness (μm)	557.90 ± 32.18	544.22 ± 22.93	0.32
Radius of corneal curvature (*mm*)	7.76 ± 0.22	7.65 ± 0.38	0.39
Axial length (*mm*)	24.82 ± 0.89	24.62 ± 1.22	0.65
Anterior Chamber volume (μL)	175.30 ± 30.08	167.72 ± 41.55	0.98
Intraocular pressure (*mmHg*)	16.95 ± 2.00	20.79 ± 6.41	0.07
Ocular pulse amplitude (*mmHg*)	2.46 ± 1.14	3.49 ± 1.51	0.12
Ocular volume change (μL)	9.79 ± 3.29	8.16 ± 1.73	0.35
Ocular rigidity (μL^{-1})	0.015 ± 0.005	0.020 ± 0.010	0.29
SP-A1‡	129.06 ± 14.90	128.04 ± 17.92	0.93
SP-HC‡	15.23 ± 3.41	15.23 ± 5.10	0.70

Differences between healthy and glaucoma subjects were evaluated by using Mann–Whitney U-tests with a significant level of 0.05. Asterisk (*) indicates a significant difference.
‡*Sample size for SP-A1 and SP-HC is 21 for control and 6 for glaucoma.*

pressure (29), and δ_{A1} is the deflection at first applanation. SP-HC was calculated by $(AP1_{adj} - bIOP)/(\delta_{HC} - \delta_{A1})$, where δ_{HC} is the maximum deflection near the highest concavity. In this study, the corneoscleral biomechanical properties characterized from Corvis ST, namely SP-A1 and SP-HC for corneal stiffness and scleral stiffness, respectively, were examined and correlated with ocular rigidity estimated using OCT.

Ocular Characteristics

The Pentacam was used to measure the radius of corneal curvature, central cornea thickness (CCT), and anterior chamber volume (ACV). IOP and OPA were measured with the Pascal DCT. A direct measure of axial length (AL) was not available for all subjects in this study. We therefore derived AL from the Gullstrand-Emsley model (30, 31) using the focus setting (refraction) on Spectralis and the radius of corneal curvature. To validate this approach, a separate group of subjects ($n = 53$ eyes from healthy and pathological subjects) was used that had measurements from both the Spectralis and the ANTERION (Heidelberg Engineering, Heidelberg, Germany). We compared the calculated AL using the Spectralis with that directly reported by the ANTERION using Bland-Altman analysis.

RESULTS

Ocular Characteristics in Healthy Controls vs. Glaucoma Cases

Twenty-nine subjects with processable OCT videos and valid IOP measurements were ultimately included in this study (23 healthy controls and 6 glaucoma cases). Demographics and ocular characteristics for patients with glaucoma cases and healthy eye controls are summarized in **Table 1**. The calculated AL was strongly correlated with the measured AL ($p < 0.00001$, **Figure 2A**), and the paired t-test suggested that there was no statistically significant difference ($p > 0.1$), validating our approach for axial length assessment using the OCT device. Bland-Altman plot for calculated AL and measured AL is shown in **Figure 2B**.

No significant difference was found in CCT, ACV, AL, radius of corneal curvature, ocular volume change, DCT-measured IOP, and OPA between treated glaucoma subjects and healthy controls using non-parametric Mann–Whitney U-test (**Table 1**). The glaucoma cohort was older than subjects in the healthy control cohort (61.5 ± 8.4 years vs. 40.0 ± 12.6 years; $p = 0.002$). Ocular rigidity was not correlated with age in this dataset with $n = 29$ combing healthy and glaucoma cohorts (Pearson $R = 0.06$; $p = 0.75$).

The mean ocular rigidity in the 23 healthy controls was 0.015 μL^{-1} (95% confidence interval, 0.012 to 0.017 μL^{-1}), and the mean ocular rigidity in the 6 glaucoma cases was 0.020 μL^{-1} (95% confidence interval, 0.009 to 0.030 μL^{-1}). Ocular rigidity did not demonstrate a significant difference between the treated glaucoma subjects and healthy controls ($p = 0.29$). The dynamic corneal response parameters measured by Corvis ST were not available in two subjects (out of 23) in the control cohort. The corneoscleral stiffness parameters, namely SP-A1 and SP-HC, were compared between 6 glaucoma and 21 healthy subjects. No significant difference was observed in glaucoma compared to healthy cohorts in terms of the corneoscleral stiffness parameters in this dataset. **Table 1** summarizes the mean value and standard deviation of all the ocular characteristics in the treated glaucoma cohort and healthy cohort, and their comparison p-value using the Mann–Whitney U-test.

Ocular Rigidity vs. Morphological Characteristics and Stiffness Parameters

With glaucoma and healthy cohorts combined ($n = 29$), there were negative correlations between ocular rigidity and AL ($R = -0.53$, $p = 0.003$, **Figure 3A**), and between ocular rigidity and ACV ($R = -0.64$, $p = 0.0002$, **Figure 3B**); while ocular rigidity was not correlated with CCT or radius of corneal curvature. There was a positive correlation between ocular rigidity and OPA ($R = 0.51$, $p = 0.004$); whereas there was no correlation between ocular rigidity and IOP. For the biomechanical parameters, ocular rigidity was shown to be positively correlated with SP-HC ($R = 0.62$, $p = 0.0005$, **Figure 3C**) and SP-A1 ($R = 0.41$, $p = 0.033$, **Figure 3D**). This correlation analysis was determined with the combination of the healthy cohort ($n = 23$) and glaucoma cohort ($n = 6$). When only the healthy cohort was included, the results of correlation analysis were consistent. The parameters that demonstrated a significant correlation with ocular rigidity in the healthy cohorts included AL (negative), ACV (negative), OPA (positive), SP-A1 (positive), and SP-HC (positive). The Pearson correlation coefficients between ocular rigidity and ocular characteristics are tabulated in **Table 2**.

DISCUSSION

The ocular rigidity estimates the change in IOP produced by volumetric changes of the eye due to choroidal pulsations. We have implemented an approach for direct non-invasive

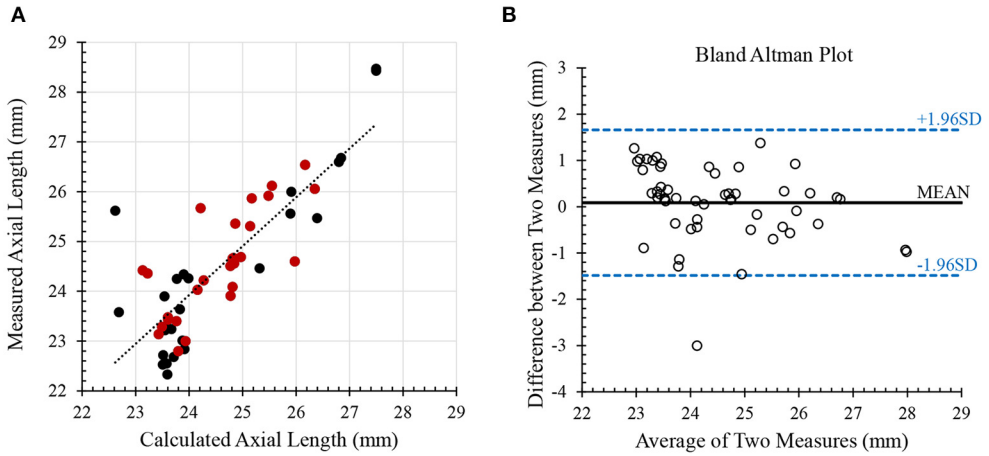

FIGURE 2 | Validation of axial length. **(A)** the calculated axial length from Spectralis was strongly correlated with the measured axial length from ANTERION. Red dots indicate healthy subjects and black dots indicate pathological subjects ($n = 53$; Pearson $R = 0.83$; $p < 0.00001$) **(B)** Bland-Altman plot for comparing calculated and measure axial lengths.

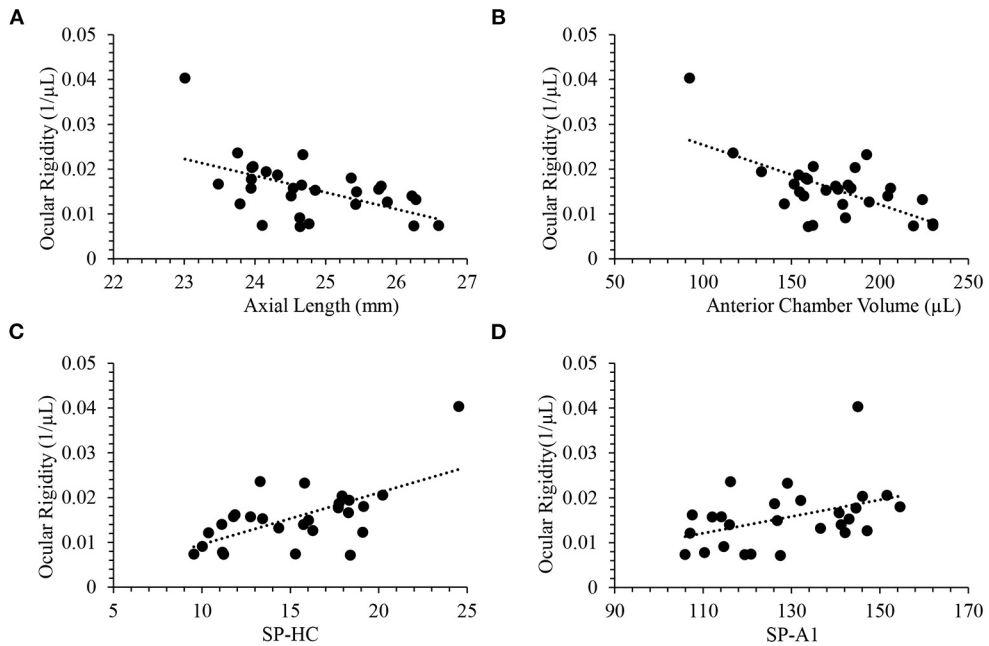

FIGURE 3 | Ocular rigidity was negatively correlated with **(A)** axial length ($R = -0.53$; $p = 0.003$) and **(B)** anterior chamber volume ($R = -0.64$; $p = 0.0002$). Ocular rigidity was positively correlated with **(C)** SP-HC ($R = 0.62$; $p = 0.0005$) and **(D)** SP-A1 ($R = 0.41$; $p = 0.033$).

measurement of choroidal volume change through automated segmentation using high-speed OCT that incorporates time series. To assess the role of ocular rigidity in glaucoma, the OCT videos in this study were taken at the ONH. This non-invasive approach for estimation of choroidal volume change was reported by another group recently that validated using sequential OCT imaging centered at the macula, and the repeatability was found to be good with an intra-session correlation coefficient of 0.96 (22, 32). We have found a statistically significant negative correlation between ocular rigidity and axial length (**Figure 3A**). A previous study that estimated the ocular rigidity invasively by monitoring the IOP change caused by the injection of saline solution also showed the negative correlation between ocular rigidity and axial length (33). Our findings on ocular rigidity determined using a non-invasive approach were in the same range as those reported in early studies using an invasive approach (16, 33). Thus, the consistency between the ocular rigidity measurements determined by an

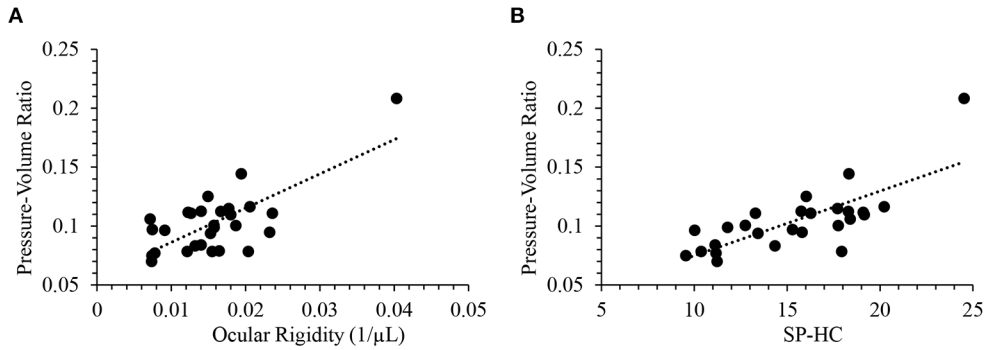

FIGURE 4 | Pressure-volume ratio was positively correlated with **(A)** ocular rigidity ($R = 0.72$; $p < 0.0001$) and **(B)** SP-HC ($R = 0.75$; $p < 0.0001$).

TABLE 2 | Correlation of ocular rigidity with morphological characteristics and stiffness parameters.

	Glaucoma + control ($n = 29$)		Control only ($n = 23$)	
Correlation of ocular rigidity with:	**R**	***p*-value**	**R**	***p*-value**
Central corneal thickness	0.069	0.72	0.083	0.71
Radius of corneal curvature	−0.089	0.65	0.20	0.36
Axial length	−0.53	**0.003***	−0.44	**0.034***
Anterior chamber volume	−0.64	**0.0002***	−0.50	**0.015***
Intraocular pressure	0.079	0.68	−0.070	0.75
Ocular pulse amplitude	0.51	**0.004***	0.41	**0.049***
SP-A1‡	0.41	**0.033***	0.43	**0.050***
SP-HC‡	0.62	**0.0005***	0.48	**0.026***

Asterisk (*) indicates a significant correlation at the level of 0.05. ‡Sample size for SP-A1 and SP-HC is 21 for control and 27 for glaucoma and control combined.

invasive approach and our ocular rigidity data determined by our non-invasive approach provides evidence of the validity of the measurements.

Quantitative characteristics of corneal biomechanical parameters derived from Corvis ST have demonstrated diagnostic power in corneal disease (34). The stiffness parameter at the first applanation SP-A1 is indicative of corneal stiffness (28). A finite-element study on the biomechanical impact of the sclera on displacement amplitude reported that a stiffer sclera limits corneal deformation (35). It was suggested that the stiffness parameter at the highest concavity (SP-HC) is indicative of scleral stiffness, as validated by *ex vivo* experiments, in which SP-HC was found to be significantly higher after scleral stiffening with 4% glutaraldehyde without changes in corneal parameters (36). Thus, SP-HC derived from air-puff induced deformation offers a clinical measure indicating scleral stiffness. Although our results showed no significant difference in SP-HC between healthy and glaucoma subjects due to small *n*, a positive correlation of SP-HC was found with ocular rigidity (**Figure 3C**) despite the small sample size. Note that the ocular rigidity accounts for the properties of both the sclera and cornea. Since the cornea is less stiff than the sclera and the sclera encompasses greater surface area than the cornea, the ocular rigidity is driven to a greater extent by scleral stiffness than corneal stiffness in normal and disease. This statement is supported by the evidence that our data showed a stronger correlation of ocular rigidity with SP-HC than with SP-A1 (**Table 2**, Pearson $R = 0.62$ vs. 0.41). These parameters are analogous to others in combined analyses of controls and glaucoma cases that have been successfully investigated as a continuous quantitative trait in genome-wide association studies that investigated the risk factor for glaucoma, such as CCT (37) and IOP (38).

A previous study has reported a positive correlation between ocular rigidity and age in 79 living human eyes, in which ocular rigidity was determined by cannulating the anterior chamber in patients undergoing cataract surgery (16). In the current study, no correlation between ocular rigidity and age was observed, possibly due to the smaller sample size ($n = 29$) and the different approaches to quantifying ocular rigidity. Inflation tests of human eyes have shown the age-related stiffening in the pressure-strain response in the sclera (39, 40). This observed tissue behavior may be due to a mechanism related to an accumulation of intermolecular non-enzymatic cross-linking (4). As it has been speculated that the scleral stiffness increases with age, the fact that open-angle glaucoma prevalence increase with age may be sharing a mechanism of scleral stiffness as part of the pathogenesis of glaucoma. Computational and *ex vivo* experimental studies have demonstrated that the sclera becomes stiffer with glaucoma (41, 42). Whether or not a stiffer sclera is a risk factor for glaucoma remains unclear and inconclusive. Based on computational models representing generic ONH geometry and material properties (8), higher sclera stiffness was associated with less deformation in ONH tissues. On the other hand, mechanical insult has been hypothesized as an initiating factor and a driving force in the disease process of glaucoma (43, 44), suggesting more ONH deformation may be related to more glaucomatous axonal damage. Lower ocular rigidity was found to be positively correlated to greater glaucomatous damage represented by ganglion cell complex, retinal nerve fiber layer thicknesses, and neuroretinal rim area (45). It must be acknowledged that there are multiple contributing factors to the pathogenesis of glaucoma, and the change of biomechanical

environment could drive connective tissue remodeling, possibly resulting in an alteration of stiffness in the progression of glaucoma (2). In addition, the use of prostaglandin analogs (PGA) for the treatment of glaucoma may lead to changes in the biomechanical properties of the eye (46).

IOP fluctuation over time may be a result of both physiological regulations related to a circadian rhythm of aqueous humor secretion, and progressive damage to the segmental outflow through the trabecular meshwork. The ocular rigidity based on Friedenwald's empirical equation reveals the pressure-volume relationship in the eye that takes the fluctuation into consideration. Ocular compliance defined as $\Delta V/\Delta P$ was previously measured in mice using iPerfusion which also accounts for the dynamic mechanical response of the eye (47). Alternatively, a simple static pressure-volume relationship could be the pressure-volume ratio (P/V ratio) calculated as IOP divided by ACV. There was a strong positive correlation between ocular rigidity and P/V ratio (Pearson R= 0.72; $p < 0.0001$). **Figure 4A** provides a scatterplot of the relationship between ocular rigidity and P/V ratio. In addition, P/V ratio and SP-HC were significantly correlated ($R = 0.75$; $p < 0.0001$, **Figure 4B**). Ocular rigidity estimated from OCT (plus Pascal DCT for IOP measurement), SP-HC quantified from Corvis ST, and P/V ratio characterized by Pentacam (plus DCT) correlated with each other. To the best of our knowledge, our study design is one of the first reports to evaluate the association of different ocular biomechanical parameters measured from multiple ophthalmic devices.

IOP remains the only modifiable and treatable risk factor for the development and progression of glaucoma. Studies have confirmed the benefit of lowering IOP in glaucoma patients, even in those without detectable high IOP (48, 49). PGAs have been used as first-line monotherapies for IOP reduction in adult patients with glaucoma. A recent prospective study evaluated the relationship of IOP and ACV with the use of PGAs in glaucoma patients, and it suggested that P/V ratio before the naïve use of PGA therapy (baseline visit) was significantly correlated with the IOP reduction at visit 2 (1 month after the naïve use of PGA) (46). It reported that the majority of eyes had a decrease in ACV with a decrease in IOP after the use of PGAs. Paradoxically, it also showed that in one-third of treated glaucoma eyes, a mean increase in ACV was accompanied by a mean decrease in IOP (46), suggesting that ocular rigidity is altered after treatment with PGA therapy. The chronic use of PGAs has shown to be associated with a decrease in the collagen type I level (50, 51), which is the main load-bearing constituent of the extracellular matrix existing in human eye tissues, such as cornea and sclera. The mechanism of changing ocular rigidity after the naïve use of PGA therapy warrants further investigation.

Limitations of this study include that the method for choroidal volume change estimation is highly dependent on the image quality of OCT video. Different from the structural OCT image which relies on real-time image averaging of multiple B-scans to enhance signal-noise ratio, no averaging was set for the acquisition of OCT video in the current study. In addition, since the central optic nerve region with no choroid was excluded from the analysis, a relatively small region of the image was available for processing. The simplification of volume change based on the choroidal thickness change, Δt, at a single cross-sectional scan limits its ability to incorporate the possible difference in Δt at different regions, such as macula vs. ONH, nasal-temporal vs. superior-inferior. Peripapillary choroidal volumetric parameters may be impacted by the alpha- and beta-zone around the ONH in glaucoma (23), however, it is unclear if the pulsatile volume change is altered by the peripapillary atrophy. The mathematical model used to extrapolate the pulsatile ocular volume change was based on a spherical eye model, which simplified the process for ocular rigidity estimation, but was limited in accounting for anatomical characteristics of the choroid. Another limitation was the small sample size in the glaucoma cohort. New algorithms for improving the CSI segmentation and choroidal volume change estimation are currently being developed with the objective of processing more OCT videos and increasing the sample size.

In conclusion, non-invasive clinical measurement of ocular rigidity was determined using sequential OCT imaging and OPA measurement. No significant difference in ocular rigidity was detected in the treated glaucoma subjects and healthy controls. As the measured ocular rigidity describes the total response of the eye, it was found to be correlated with ocular morphological and biomechanical characteristics. Specifically, there were negative correlations between ocular rigidity and axial length, and between ocular rigidity and anterior chamber volume. In addition, ocular rigidity significantly increased with increasing corneoscleral stiffness parameters characterized by air-puff induced deformation. The significant correlation of ocular rigidity with SP-HC and pressure-volume ratio demonstrated not only the validity of this measurement, but also the consistency of multiple ophthalmic devices in examining ocular biomechanics. A larger longitudinal study may provide greater insights into the development and progression of glaucoma, and response to treatment.

DATA AVAILABILITY STATEMENT

The datasets presented in this article are not readily available because the datasets will not be available until after the grant concludes. Requests to access the datasets should be directed to Cynthia Roberts, roberts.8@osu.edu.

ETHICS STATEMENT

The studies involving human participants were reviewed and approved by the Institutional Review Board of The Ohio State University. The patients/participants provided their written informed consent to participate in this study.

AUTHOR CONTRIBUTIONS

YM: algorithm implementation and improvement, analysis and interpretation of data, writing, and

revising the manuscript. SM: interpretation of data and critical revision of the manuscript. CR: conception and design, interpretation of data, and critical revision of the manuscript. All authors approved the submitted version.

FUNDING

This work was supported by the National Eye Institute of the National Institutes of Health (NIH; Bethesda, MD, USA) R01 EY027399.

REFERENCES

1. Burgoyne CF, Downs JC, Bellezza AJ, Suh J-KF, Hart RT. The optic nerve head as a biomechanical structure: a new paradigm for understanding the role of IOP-related stress and strain in the pathophysiology of glaucomatous optic nerve head damage. *Prog Retin Eye Res.* (2005) 24:39–73. doi: 10.1016/j.preteyeres.2004.06.001
2. Downs JC, Roberts MD, Sigal IA. Glaucomatous cupping of the lamina cribrosa: a review of the evidence for active progressive remodeling as a mechanism. *Exp Eye Res.* (2011) 93:133–40. doi: 10.1016/j.exer.2010.08.004
3. Ma Y, Pavlatos E, Clayson K, Pan X, Kwok S, Sandwisch T, et al. Mechanical deformation of human optic nerve head and peripapillary tissue in response to acute IOP elevation. *Invest Ophthalmol Vis Sci.* (2019) 60:913–20. doi: 10.1167/iovs.18-26071
4. Boote C, Sigal IA, Grytz R, Hua Y, Nguyen TD, Girard MJA. Scleral structure and biomechanics. *Prog Retin Eye Res.* (2020) 74:100773. doi: 10.1016/j.preteyeres.2019.100773
5. Quigley HA, Broman AT. The number of people with glaucoma worldwide in 2010 and 2020. *Br J Ophthalmol.* (2006) 90:262–7. doi: 10.1136/bjo.2005.081224
6. Quigley HA, Addicks EM, Green WR, Maumenee AE. Optic nerve damage in human glaucoma: II. The site of injury and susceptibility to damage. *Arch Ophthalmol.* (1981) 99:635–49. doi: 10.1001/archopht.1981.03930010635009
7. Nickells RW, Howell GR, Soto I, John SWM. Under pressure: cellular and molecular responses during glaucoma, a common neurodegeneration with axonopathy. *Annu Rev Neurosci.* (2012) 35:153–79. doi: 10.1146/annurev.neuro.051508.135728
8. Sigal IA, Flanagan JG, Ethier CR. Factors influencing optic nerve head biomechanics. *Invest Ophthalmol Vis Sci.* (2005) 46:4189–99. doi: 10.1167/iovs.05-0541
9. Nguyen C, Cone FE, Nguyen TD, Coudrillier B, Pease ME, Steinhart MR, et al. Studies of scleral biomechanical behavior related to susceptibility for retinal ganglion cell loss in experimental mouse glaucoma. *Invest Ophthalmol Vis Sci.* (2013) 54:1767–80. doi: 10.1167/iovs.12-10952
10. Yang H, Downs JC, Girkin C, Sakata L, Bellezza A, Thompson H, et al. 3-D histomorphometry of the normal and early glaucomatous monkey optic nerve head: lamina cribrosa and peripapillary scleral position and thickness. *Invest Ophthalmol Vis Sci.* (2007) 48:4597–607. doi: 10.1167/iovs.07-0349
11. Downs JC, Suh JKF, Thomas KA, Bellezza AJ, Hart RT, Burgoyne CF. Viscoelastic material properties of the peripapillary sclera in normal and early-glaucoma monkey eyes. *Invest Ophthalmol Vis Sci.* (2005) 46:540–6. doi: 10.1167/iovs.04-0114
12. Elsheikh A, Geraghty B, Alhasso D, Knappett J, Campanelli M, Rama P. Regional variation in the biomechanical properties of the human sclera. *Exp Eye Res.* (2010) 90:624–33. doi: 10.1016/j.exer.2010.02.010
13. Pavlatos E, Ma Y, Clayson K, Pan X, Liu J. Regional deformation of the optic nerve head and peripapillary sclera during IOP elevation. *Invest Ophthalmol Vis Sci.* (2018) 59:3779–88. doi: 10.1167/iovs.18-24462
14. Ma Y, Pavlatos E, Clayson K, Kwok S, Pan X, Liu J. Three-dimensional inflation response of porcine optic nerve head using high-frequency ultrasound elastography. *J Biomech Eng.* (2020) 142: doi: 10.1115/1.4045503
15. Friedenwald JS. Contribution to the theory and practice of tonometry. *Am J Ophthalmol.* (1937) 20:985–1024. doi: 10.1016/S0002-9394(37)90425-2
16. Pallikaris IG, Kymionis GD, Ginis HS, Kounis GA, Tsilimbaris MK. Ocular rigidity in living human eyes. *Invest Ophthalmol Vis Sci.* (2005) 46:409–14. doi: 10.1167/iovs.04-0162
17. Friberg TR, Fourman SB. Scleral buckling and ocular rigidity: clinical ramifications. *Arch Ophthalmol.* (1990) 108:1622–7. doi: 10.1001/archopht.1990.01070130124042
18. Hommer A, Fuchsjäger-Mayrl G, Resch H, Vass C, Garhofer G, Schmetterer L. Estimation of ocular rigidity based on measurement of pulse amplitude using pneumotonometry and fundus pulse using laser interferometry in glaucoma. *Invest Ophthalmol Vis Sci.* (2008) 49:4046–50. doi: 10.1167/iovs.07-1342
19. Ebneter A, Wagels B, Zinkernagel MS. Non-invasive biometric assessment of ocular rigidity in glaucoma patients and controls. *Eye.* (2009) 23:606–11. doi: 10.1038/eye.2008.47
20. Silver DM, Farrell RA, Langham ME, O'Brien V, Schilder P. Estimation of pulsatile ocular blood flow from intraocular pressure. *Acta Ophthalmol.* (1989) 67:25–9. doi: 10.1111/j.1755-3768.1989.tb07083.x
21. Mazzaferri J, Beaton L, Hounye G, Sayah DN, Costantino S. Open-source algorithm for automatic choroid segmentation of OCT volume reconstructions. *Sci Rep.* (2017) 7:42112. doi: 10.1038/srep42112
22. Beaton L, Mazzaferri J, Lalonde F, Hidalgo-Aguirre M, Descovich D, Lesk MR, et al. Non-invasive measurement of choroidal volume change and ocular rigidity through automated segmentation of high-speed OCT imaging. *Biomed Opt Express.* (2015) 6:1694–706. doi: 10.1364/BOE.6.001694
23. Jonas JB. Clinical implications of peripapillary atrophy in glaucoma. *Curr Opin Ophthalmol.* (2005) 16:84–8. doi: 10.1097/01.icu.0000156135.20570.30
24. Bill A. Blood circulation and fluid dynamics in the eye. *Physiol Rev.* (1975) 55:383–417. doi: 10.1152/physrev.1975.55.3.383
25. Kotecha A, White E, Schlottmann PG, Garway-Heath DF. Intraocular pressure measurement precision with the Goldmann applanation, dynamic contour, and ocular response analyzer tonometers. *Ophthalmology.* (2010) 117:730–7. doi: 10.1016/j.ophtha.2009.09.020
26. Boehm AG, Weber A, Pillunat LE, Koch R, Spoerl E. Dynamic contour tonometry in comparison to intracameral IOP measurements. *Invest Ophthalmol Vis Sci.* (2008) 49:2472–7. doi: 10.1167/iovs.07-1366
27. Lopes BT, Roberts CJ, Elsheikh A, Vinciguerra R, Vinciguerra P, Reisdorf S, et al. Repeatability and reproducibility of intraocular pressure and dynamic corneal response parameters assessed by the Corvis ST. *J Ophthalmol.* (2017) 2017:8515742. doi: 10.1155/2017/8515742
28. Roberts CJ, Mahmoud AM, Bons JP, Hossain A, Elsheikh A, Vinciguerra R, et al. Introduction of two novel stiffness parameters and interpretation of air Puff–Induced biomechanical deformation parameters with a dynamic scheimpflug analyzer. *J Refract Surg.* (2017) 33:266–73. doi: 10.3928/1081597X-20161221-03
29. Joda AA, Shervin MMS, Kook D, Elsheikh A. Development and validation of a correction equation for Corvis tonometry. *Comput Methods Biomech Biomed Engin.* (2016) 19:943–53. doi: 10.1080/10255842.2015.1077515
30. Bennett AG, Rabbetts RB. *Clinical Visual Optics.* London: Butterworth-Heinemann (1989).
31. Delori F, Greenberg JP, Woods RL, Fischer J, Duncker T, Sparrow J, et al. Quantitative measurements of autofluorescence with the scanning laser ophthalmoscope. *Invest Ophthalmol Vis Sci.* (2011) 52:9379–90. doi: 10.1167/iovs.11-8319
32. Sayah DN, Mazzaferri J, Ghesquière P, Duval R, Rezende F, Costantino S, et al. Non-invasive *in vivo* measurement of ocular rigidity: clinical validation, repeatability and method improvement. *Exp Eye Res.* (2020) 190:107831. doi: 10.1016/j.exer.2019.107831
33. Dastiridou AI, Ginis H, Tsilimbaris M, Karyotakis N, Detorakis E, Siganos C, et al. Ocular rigidity, ocular pulse amplitude, and pulsatile ocular blood flow: the effect of axial length. *Invest Ophthalmol Vis Sci.* (2013) 54:2087–92. doi: 10.1167/iovs.12-11576

34. Elham R, Jafarzadehpur E, Hashemi H, Amanzadeh K, Shokrollahzadeh F, Yekta A, et al. Keratoconus diagnosis using Corvis ST measured biomechanical parameters. *J Curr Ophthalmol.* (2017) 29:175–81. doi: 10.1016/j.joco.2017.05.002
35. Nguyen BA, Roberts CJ, Reilly MA. Biomechanical impact of the sclera on corneal deformation response to an air-puff: a finite-element study. *Front Bioeng Biotechnol.* (2019) 6:210. doi: 10.3389/fbioe.2018.00210
36. Nguyen BA, Reilly MA, Roberts CJ. Biomechanical contribution of the sclera to dynamic corneal response in air-puff induced deformation in human donor eyes. *Exp Eye Res.* (2020) 191:107904. doi: 10.1016/j.exer.2019.107904
37. Ulmer M, Li J, Yaspan BL, Ozel AB, Richards JE, Moroi SE, et al. Genome-wide analysis of central corneal thickness in primary open-angle glaucoma cases in the NEIGHBOR and GLAUGEN consortia. *Investig Ophthalmol Vis Sci.* (2012) 53:4468–74. doi: 10.1167/iovs.12-9784
38. Ozel AB, Moroi SE, Reed DM, Nika M, Schmidt CM, Akbari S, et al. Genome-wide association study and meta-analysis of intraocular pressure. *Hum Genet.* (2014) 133:41–57. doi: 10.1007/s00439-013-1349-5
39. Fazio MA, Grytz R, Morris JS, Bruno L, Gardiner SK, Girkin CA, et al. Age-related changes in human peripapillary scleral strain. *Biomech Model Mechanobiol.* (2014) 13:551–63. doi: 10.1007/s10237-013-0517-9
40. Coudrillier B, Pijanka J, Jefferys J, Sorensen T, Quigley HA, Boote C, Nguyen TD. Collagen structure and mechanical properties of the human sclera: analysis for the effects of age. *J Biomech Eng.* (2015) 137:041006. doi: 10.1115/1.4029430
41. Girard MJA, Suh J-KF, Bottlang M, Burgoyne CF, Downs JC. Biomechanical changes in the sclera of monkey eyes exposed to chronic IOP elevations. *Invest Ophthalmol Vis Sci.* (2011) 52:5656–69. doi: 10.1167/iovs.10-6927
42. Coudrillier B, Pijanka JK, Jefferys JL, Goel A, Quigley HA, Boote C, et al. Glaucoma-related changes in the mechanical properties and collagen micro-architecture of the human sclera. *PLoS One.* (2015) 10:e0131396. doi: 10.1371/journal.pone.0131396
43. Quigley HA, Flower RW, Addicks EM, McLeod DS. The mechanism of optic nerve damage in experimental acute intraocular pressure elevation. *Invest Ophthalmol Vis Sci.* (1980) 19:505–17.
44. Ma Y, Kwok S, Sun J, Pan X, Pavlatos E, Clayson K, et al. IOP-induced regional displacements in the optic nerve head and correlation with peripapillary sclera thickness. *Exp Eye Res.* (2020) 200:108202. doi: 10.1016/j.exer.2020.108202
45. Sayah DN, Mazzaferri J, Descovich D, Costantino S, Lesk MR. The association between ocular rigidity and neuroretinal damage in glaucoma. *Invest Ophthalmol Vis Sci.* (2020) 61:11. doi: 10.1167/iovs.61.13.11
46. Scott JA, Roberts CJ, Mahmoud AM, Jain S. Evaluating the relationship of intraocular pressure and anterior chamber volume with use of prostaglandins. *J Glaucoma.* (2020) 30:421–7. doi: 10.1097/IJG.0000000000001736
47. Sherwood JM, Boazak EM, Feola AJ, Parker K, Ethier CR, Overby DR. Measurement of ocular compliance using iPerfusion. *Front Bioeng Biotechnol.* (2019) 7:276. doi: 10.3389/fbioe.2019.00276
48. Anderson DR, Drance SM, Schulzer M. Factors that predict the benefit of lowering intraocular pressure in normal tension glaucoma. *Am J Ophthalmol.* (2003) 136:820–9. doi: 10.1016/S0002-9394(03)00478-1
49. Heijl A, Leske MC, Bengtsson B, Hyman L, Bengtsson B, Hussein M. Reduction of intraocular pressure and glaucoma progression: results from the Early Manifest Glaucoma Trial. *Arch Ophthalmol.* (2002) 120:1268–79. doi: 10.1001/archopht.120.10.1268
50. Meda R, Wang Q, Paoloni D, Harasymowycz P, Brunette I. The impact of chronic use of prostaglandin analogues on the biomechanical properties of the cornea in patients with primary open-angle glaucoma. *Br J Ophthalmol.* (2017) 101:120–5. doi: 10.1136/bjophthalmol-2016-308432
51. Weinreb RN, Toris CB, B'Ann TG, Lindsey JD, Kaufman PL. Effects of prostaglandins on the aqueous humor outflow pathways. *Surv Ophthalmol.* (2002) 47:S53–64. doi: 10.1016/S0039-6257(02)00306-5

Conflict of Interest: SM holds a patent that is not related to this work and receives royalties from Wolters Kluwer Health that is not related to this work. CR is a consultant to OCULUS Optikgerate GmbH and Zeimer Ophthalmic Systems AG.

The remaining author declares that the research was conducted in the absence of any commercial or financial relationships that could be construed as a potential conflict of interest.

frontiers in Medicine

BRIEF RESEARCH REPORT
published: 03 August 2021
doi: 10.3389/fmed.2021.681169

Oral Scutellarin Treatment Ameliorates Retinal Thinning and Visual Deficits in Experimental Glaucoma

Jingyuan Zhu[1,2], Anoop Sainulabdeen[2,3], Krystal Akers[2], Vishnu Adi[2], Jeffrey R. Sims[2], Eva Yarsky[2], Yi Yan[2], Yu Yu[4], Hiroshi Ishikawa[2,5], Christopher K. Leung[6,7,8], Gadi Wollstein[2,5], Joel S. Schuman[2,5,9,10], Wenbin Wei[1†] and Kevin C. Chan[2,5,9,10,11*†]*

[1] Beijing Tongren Eye Center, Beijing Key Laboratory of Intraocular Tumor Diagnosis and Treatment, Beijing Ophthalmology & Visual Sciences Key Lab, Medical Artificial Intelligence Research and Verification Key Laboratory of the Ministry of Industry and Information Technology, Beijing Tongren Hospital, Capital Medical University, Beijing, China, [2] Department of Ophthalmology, NYU Grossman School of Medicine, NYU Langone Health, New York University, New York, NY, United States, [3] Department of Surgery and Radiology, College of Veterinary and Animal Sciences, Kerala Veterinary and Animal Sciences University, Thrissur, India, [4] Pleryon Therapeutics Limited, Shenzhen, China, [5] Department of Biomedical Engineering, Tandon School of Engineering, New York University, New York, NY, United States, [6] Hong Kong Eye Hospital, University Eye Center, Hong Kong, China, [7] Department of Ophthalmology and Visual Sciences, The Chinese University of Hong Kong, Hong Kong, China, [8] Department of Ophthalmology, The University of Hong Kong, Hong Kong, China, [9] Center for Neural Science, College of Arts and Science, New York University, New York, NY, United States, [10] Neuroscience Institute, NYU Grossman School of Medicine, NYU Langone Health, New York University, New York, NY, United States, [11] Department of Radiology, NYU Grossman School of Medicine, NYU Langone Health, New York University, New York, NY, United States

Purpose: Intraocular pressure (IOP) is currently the only modifiable risk factor for glaucoma, yet glaucoma can continue to progress despite controlled IOP. Thus, development of glaucoma neurotherapeutics remains an unmet need. Scutellarin is a flavonoid that can exert neuroprotective effects in the eye and brain. Here, we investigated the neurobehavioral effects of scutellarin treatment in a chronic IOP elevation model.

Methods: Ten adult C57BL/6J mice were unilaterally injected with an optically clear hydrogel into the anterior chamber to obstruct aqueous outflow and induce chronic IOP elevation. Eight other mice received unilateral intracameral injection of phosphate-buffered saline only. Another eight mice with hydrogel-induced unilateral chronic IOP elevation also received daily oral gavage of 300 mg/kg scutellarin. Tonometry, optical coherence tomography, and optokinetics were performed longitudinally for 4 weeks to monitor the IOP, retinal nerve fiber layer thickness, total retinal thickness, visual acuity, and contrast sensitivity of both eyes in all three groups.

Results: Intracameral hydrogel injection resulted in unilateral chronic IOP elevation with no significant inter-eye IOP difference between scutellarin treatment and untreated groups. Upon scutellarin treatment, the hydrogel-injected eyes showed less retinal thinning and reduced visual behavioral deficits when compared to the untreated, hydrogel-injected eyes. No significant difference in retinal thickness or optokinetic measures was found in the contralateral, non-treated eyes over time or between all groups.

OPEN ACCESS

Edited by:
Michele Lanza,
University of Campania Luigi Vanvitelli, Italy

Reviewed by:
Alessio Martucci,
University of Rome Tor Vergata, Italy
Gema Martinez Navarrete,
Universidad Miguel Hernández, Spain
Benjamin Thomson,
Northwestern University, United States
Eduardo Fernandez,
Miguel Hernández University of Elche, Spain
Jeff Gidday,
Louisiana State University, United States

****Correspondence:***
Kevin C. Chan
chuenwing.chan@fulbrightmail.org
Wenbin Wei
tr_weiwenbin@163.com

† These authors share senior authorship

Specialty section:
This article was submitted to Ophthalmology, a section of the journal Frontiers in Medicine

Received: *16 March 2021*
Accepted: *07 July 2021*
Published: *03 August 2021*

Citation:
Zhu J, Sainulabdeen A, Akers K, Adi V, Sims JR, Yarsky E, Yan Y, Yu Y, Ishikawa H, Leung CK, Wollstein G, Schuman JS, Wei W and Chan KC (2021) Oral Scutellarin Treatment Ameliorates Retinal Thinning and Visual Deficits in Experimental Glaucoma. Front. Med. 8:681169. doi: 10.3389/fmed.2021.681169

Conclusion: Using the non-invasive measuring platform, oral scutellarin treatment appeared to preserve retinal structure and visual function upon chronic IOP elevation in mice. Scutellarin may be a novel neurotherapeutic agent for glaucoma treatment.

Keywords: glaucoma, intraocular pressure, scutellarin, retina, optokinetics

INTRODUCTION

Glaucoma is a chronic neurodegenerative disease involving progressive loss of retinal ganglion cells (RGC) and injuries to their dendrites and axons (1). It is the leading cause of irreversible blindness in the world (2). While intraocular pressure (IOP) is currently the only clinically modifiable risk factor, glaucoma can continue to progress even after IOP is controlled (3). Thus, development of effective neurotherapeutics is of paramount importance to further slowdown the progression of the disease beyond IOP control in order to reduce its prevalence.

Several *in vitro* and *in vivo* experiments have attempted to demonstrate the potentials of neuroprotective medications for glaucoma. These include the use of alpha 2 adrenergic agonists (e.g., brimonidine) (4), prostaglandin-related compounds (e.g., tafluprost) (5), N-methyl-D-aspartate receptor antagonists (e.g., memantine) (6), calcium channel blockers (e.g., nilvadipine) (7), choline precursor (e.g., citicoline) (8), brain-derived neurotrophic factors (9), and plant extracts [e.g., ginkgo biloba (10), xanthophylls, and flavonoids (11)]. However, their effectiveness on glaucoma patients has been controversial (12), and the side effects of some of these medications remain a concern (13). Among the plant extracts that have been identified as potential candidates for protective effects, *Erigeron breviscapus* is a multifunctional traditional Chinese herb that has been used to treat various diseases in the brain and body of both humans and experimental animal models (14). Scutellarin, a flavone glucuronide (5,6,4′-trihydroxyflavone-7-O-glucuronide), is one of the major constituents of *Erigeron brevisca*pus (15). It has been reported to exert protective effects on the brain (16) via translocation of the apoptosis-inducing factor pathway (17), and increase in cell survival, proliferation, and contraction (18). In ophthalmic studies, scutellarin promoted the survival of cultured rat retinal neurons at high concentrations (19). Scutellarin was also found to preserve, at least in part, the visual field of post-surgical open-angle glaucoma patients with controlled IOP (20). For acute IOP elevation and retinal hypoxia models, scutellarin inhibited the inflammatory reactions by mediating the nucleotide-binding oligomerization domain-like receptor protein 3 (NLRP3) inflammasome-signaling pathway *in vivo* and *in vitro* (21). It also promoted RGC survival while down-regulating abnormal retinal microglia activation (21). Despite such initial evidence, well-controlled experiments on the neuroprotective effects of scutellarin on chronic glaucoma remain lacking.

To date, pre-clinical testing of glaucoma neurotherapeutics has been limited by existing experimental models that allow chronic elevation of IOP while preserving optical media clarity for non-invasive and longitudinal evaluation of the structure and function of the visual system. Recently, we have developed a novel experimental glaucoma rodent model that satisfies the above requirements via intracameral injection of an optically clear, cross-linked hydrogel (22, 23). In the current study, we used this experimental model in combination with non-invasive imaging and behavioral assessments to investigate if scutellarin is neuroprotective against chronic experimental glaucoma. We hypothesized that oral scutellarin treatment ameliorates the effects of retinal thinning and visual functional deficits induced by chronic IOP elevation.

METHODS

Animal Preparation

All experimental procedures were approved by the Institutional Animal Care and Use Committee at New York University Grossman School of Medicine, and investigators followed guidelines from the Association for Research in Vision and Ophthalmology's statement for Use of Animals in Ophthalmic and Vision Research. Thirty C57BL/6J mice (Jackson Laboratory, Bar Harbor, Maine) aged 15–18 weeks old were housed under a 12-h light/dark cycle with standard chow and water available *ad libitum*, and were assigned to three groups of 10 each via a random number table. Mice in Group 1 received unilateral intracameral injection of hydrogel only (Hydrogel group). Mice in Group 2 received unilateral intracameral injection of phosphate-buffered saline (PBS) only (PBS group). Mice in Group 3 were unilaterally injected with the hydrogel into the anterior chamber along with daily oral gavage of scutellarin at 300 mg/kg/day for 3 consecutive weeks, beginning at 1 week prior to hydrogel injection until 2 weeks post-injection (Hydrogel+Scutellarin group) (**Table 1**). The contralateral eyes were untreated and served as an internal control. A non-invasive *in vivo* measurement system was developed for longitudinal assessments of IOP via tonometry, retinal thickness via optical coherence tomography, and visual function via optokinetic behavioral testing immediately before, and at 3 days (IOP only), and 1, 2, 3, and 4 weeks after intracameral hydrogel or PBS injection (**Table 1**). For Group 3, the same *in vivo* measurements were performed at an additional time point at 1 week before intracameral hydrogel injection (i.e., before daily oral scutellarin treatment began). Throughout the experiments, the researchers did not know which eye had been injected until group data analyses were to be performed.

TABLE 1 | Overall experimental timetable.

Experimental procedures/ Time after intracameral injection	−1 week	0 week	3 day	1 week	2 week	3 week	4 week
Tonometry	Group 3 only	All	All	All	All	All	All
Optical coherence tomography	Group 3 only	All	-	All	All	All	All
Optokinetics	Group 3 only	All	-	All	All	All	All
Intracameral hydrogel or PBS injection	-	All	-	-	-	-	-
Daily scutellarin treatment	Group 3 only	Group 3 only	Group 3 only	Group 3 only	Group 3 only	-	-

-Group 1: Hydrogel-only group.
-Group 2: Phosphate-buffered saline (PBS) group.
-Group 3: Hydrogel+Scutellarin group.
-Sample size (N) for tonometry/optical coherence tomography/optokinetics – visual acuity (VA): Group 1 = 10; Group 2 = 8; Group 3 = 8.
-N for optokinetics – contrast threshold (CT): Group 1 = 9; Group 2 = 8; Group 3 = 4.

Intracameral Hydrogel or PBS Injection

All mice were anesthetized with an intraperitoneal injection of a 5:1 ketamine/xylazine cocktail at 0.01 mL/g body weight (Henry Schein, NY). The side for unilateral intracameral injection in each animal was selected randomly by a coin toss. Proparacaine and tropicamide were then topically applied to the randomly chosen eye to induce analgesia and pupil dilation followed by intracameral injection with 2 μL of a 1:1 mixture of vinyl sulfonated hyaluronic acid and thiolated hyaluronic acid (Groups 1 and 3) or PBS (Group 2) via a glass micropipette (BLAUBRAND®, BR708709-1000EA). The functionalized hyaluronic acid mixture was heat-sensitive and became gelatinous in the anterior chamber since body temperature triggered chemical crosslinking of the polymers. This solidified hydrogel obstructed the aqueous outflow, thereby causing a sustained increase in IOP with long-term preservation of a transparent optical media for at least 4 weeks. Antibiotic ointment was applied topically immediately after injection, and ophthalmic hydrogel was applied to the surface of the eye without intracameral injection. A successful intracameral injection was judged by the absence of iris penetration, lens abrasion, and other traumatic damage. One mouse in Group 1 presented hyphema during intracameral injection as a result of unintentional needle injury to the iris, and was replaced by a spare mouse of the same age in the same cohort. Two mice in Group 2 and two mice in Group 3 did not survive through the entire study period due to other concerns including needs of euthanasia from fighting wounds. These four animals were not replaced and none of their incomplete data was included in the statistical analyses.

Intraocular Pressure Measurements Using Tonometry

The IOPs of both eyes were measured under inhaled isoflurane anesthesia using a rebound tonometer (TonoLab, Icare, Finland) within 5 min after the animal was knocked down. The IOP of both eyes was measured alternately for each mouse and repeated 10 times for each eye. Each of the 10 IOP values was derived by default settings of the TonoLab tonometer using six single IOP readings, whereby the highest and lowest IOP readings were excluded, and the remaining four readings were averaged. All IOP measurements were taken in the afternoon between 1 and 3 p.m. The IOP difference between eyes (ΔIOP) was calculated as the IOP of the injected eye minus that of the contralateral non-injected eye for each mouse (24), and was used for between-group comparisons at each time point to account for any physiological fluctuations on both eyes.

Retinal Thickness Evaluation Using Optical Coherence Tomography

The optic nerve head regions of both eyes of all mice were scanned linearly using spectral-domain optical coherence tomography (Bioptigen, Leica Microsystems, Germany). The retinas were segmented using a custom-written software (25, 26) to determine the retinal nerve fiber layer (RNFL) thickness and total retinal thickness (TRT) along a sampling ring band of 0.234–0.324 mm radius centered on the optic nerve head (**Figure 2A**). RNFL thickness was defined as the average distance between the ILM and the ganglion cell layer within the ring band (**Figure 2B**). TRT was defined as the average distance between the internal limiting membrane (ILM) and the Bruch's membrane (BM) within the ring band (**Figure 2B**).

Visual Function Assessment Using Optokinetic Behavioral Testing

Visual function was assessed using an OptoMotry optokinetic virtual-reality device (CerebralMechanics, Lethbridge, Alberta, Canada) in each awake, freely moving mouse to quantify the visual acuity (VA) and contrast sensitivity for both eyes over time. Each mouse was first habituated in the optokinetic testing device for 5 min. It has been shown that when one eye is closed, only motion in the temporal-to-nasal direction for the contralateral eye evokes the tracking response (27). Thus, the visual capabilities of each eye can be measured under binocular conditions simply by changing the direction of rotation of the visual presentation. Using the OptoMotry system, clockwise and anti-clockwise rotations were alternately presented to examine the left and right eyes, respectively in the same mouse during the same experimental session. The VA testing involved an increasing spatial frequency of sine wave grating starting from 0.042 cycles/degree (c/d) at a constant drift speed of 0.12°/s at

100% contrast. VA was identified as the highest spatial frequency that the mice could track. Contrast sensitivity testing involved a decreasing image contrast from 100% with a constant spatial frequency of 0.103 c/d. Contrast threshold (CT), which is the inverse of contrast sensitivity was determined from this testing, with a higher CT implicative of worse visual function. Both VA and CT measurements used a simple staircase method and ended when the optokinetic response could no longer be elicited.

Statistical Analysis

Comparisons of IOP, ΔIOP, TRT, RNFL, VA and CT were conducted between experimental groups over time using two-way ANOVA and *post-hoc* Tukey's multiple comparisons correction tests. Prior to intracameral hydrogel injection in Group 3, comparisons of each parameter before and after oral scutellarin administrations were conducted using paired *t*-tests. Correlation analyses between cumulative ΔIOP and other parameters at the end time point, and linear regressions between time and TRT, RNFL, VA and CT were also conducted. All statistical analyses were conducted with GraphPad Prism version 9 (GraphPad Software Inc., La Jolla, CA, USA). Data were presented as mean ± standard error of mean (SEM). $P < 0.05$ was considered to be statistically significant.

RESULTS

Chronic IOP Elevation Was Induced After Intracameral Hydrogel Injection With No Effects From Scutellarin

The hydrogel-injected eyes in Groups 1 (**Figure 1A**) and 3 (**Figure 1C**) had significantly higher IOP levels than the contralateral, non-treated eyes irrespective of scutellarin treatment (ANOVA, $p < 0.05$), while both eyes of the PBS group (Group 2, **Figure 1B**) had comparable IOP levels (ANOVA, $p > 0.05$). When comparing IOP of individual eyes, both the injected eyes and the contralateral non-treated eyes exhibited significant IOP differences between the three groups (ANOVA, $p < 0.05$). When comparing ΔIOP over time (**Figure 1D**), significant group differences were observed between the PBS group (Group 2) and the two hydrogel groups (Groups 1 and 3) after intracameral injection. No apparent ΔIOP difference was found between hydrogel-only group (Group 1) and hydrogel+scutellarin group (Group 3) at any experimental time point. No significant IOP difference was observed before and after oral scutellarin treatment prior to intracameral hydrogel injection in Group 3 (**Supplementary Figure 1**).

Oral Scutellarin Treatment Reduced Retinal Thinning Under Hydrogel-Induced Chronic IOP Elevation

Figures 2A,B illustrate the regions of interest for measuring retinal thicknesses in both the *en face* image (**Figure 2A**) and the corresponding cross-sectional b-scan images in different line scans (**Figure 2B**). **Figure 2C** shows the cross-sectional retinal images from both injected and contralateral, non-treated eyes of a representative mouse in each of the 3 groups. The injected eye of the hydrogel-only group (Group 1) showed apparent inner retinal thinning over time, whereas less apparent retinal thinning was observed in the injected eye of the hydrogel+scutellarin group (Group 3). Quantitatively, relative to the PBS-injected eye in Group 2, RNFL thickness (**Figure 3A**) and TRT (**Figure 3C**) significantly decreased in the hydrogel-injected eye of Group 1 only without scutellarin treatment at each post-injection time point, whereas no statistically significant RNFL thickness or TRT change was observed in the hydrogel-injected eye of Group 3 after scutellarin treatment ($p > 0.05$). RNFL thickness and TRT of the injected eye in Group 3 were also significantly higher than those in Group 1 after hydrogel injection. In the hydrogel-only group, the cumulative ΔIOP was linearly correlated to RNFL thickness ($R^2 = 0.607$, $p = 0.008$) and TRT ($R^2 = 0.401$, $p = 0.049$) at 4 week post-injection. No apparent difference in RNFL thickness or TRT was found between the three groups in the injected eye at 0 week before intracameral injection (**Figures 3A,C**), or in the PBS-injected eye and non-treated eye over time (**Figures 3B,D**).

Oral Scutellarin Treatment Ameliorated Visual Acuity Decrease and Contrast Threshold Increase Under Hydrogel-Induced Chronic IOP Elevation

The longitudinal profiles of VA and CT for each group are shown in **Figures 3E–H**, respectively. Relative to the PBS-injected eye in Group 2, VA of the hydrogel-injected eye in Group 1 progressively declined upon intracameral hydrogel injection, whereas upon oral scutellarin treatment in Group 3, VA of the hydrogel-injected eye apparently decreased more slowly than that of Group 1 without scutellarin treatment (**Figure 3E**; **Supplementary Figure 2**). VA of the injected eye in Group 3 was also significantly higher than that of Group 1 at 4 weeks after intracameral hydrogel injection (**Figure 3E**). CT of the hydrogel-injected eye in Group 1 was significantly higher than that of PBS-injected eye in Group 2 at each post-injection time point (**Figure 3G**). In contrast, CT of the hydrogel-injected eye in Group 3 was significantly lower than that in Group 1 at 4 weeks after intracameral injection (**Figure 3G**). Cumulative ΔIOP was not correlated to visual acuity or contrast threshold in any groups ($p > 0.05$). No apparent VA or CT change was observed in the PBS-injected eye in Group 2 throughout the experimental period (**Figures 3E,G**). No significant change in VA or CT was found in the non-treated eye between all three groups over time (**Figures 3F,H**).

DISCUSSION

In the current study, we applied oral scutellarin treatment to our recently developed experimental glaucoma model, and demonstrated the preservation of retinal structure and visual function by scutellarin via non-invasive assessments over time. This crosslinking hydrogel model produces chronic IOP elevation while preserves optical media clarity in the long term (22). The transparency of the bioinert hydrogel allows not only *in vivo* optical imaging of the retina but also longitudinal evaluation of awake optokinetic responses, both of which are important for

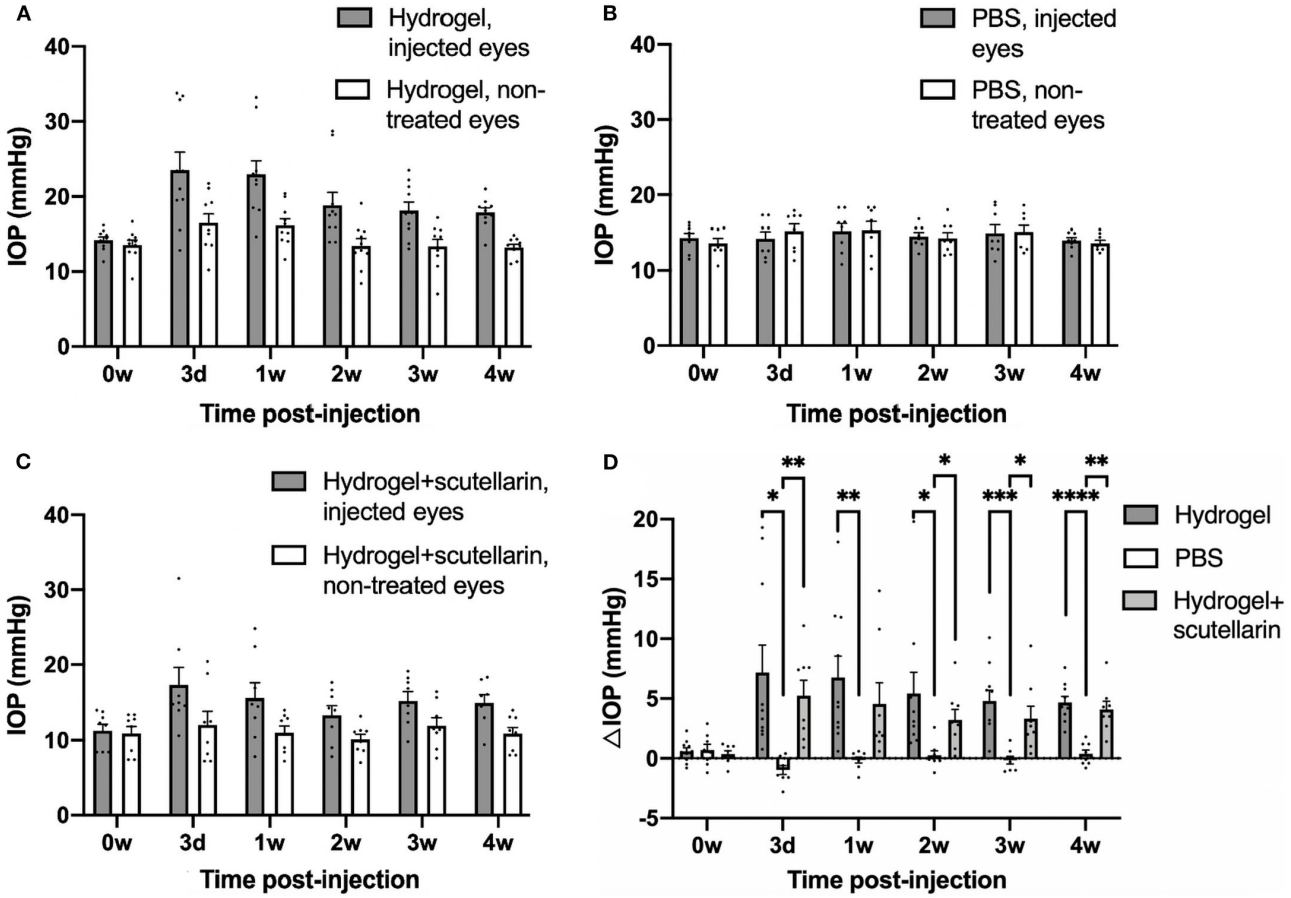

FIGURE 1 | Intraocular pressure (IOP) profiles after unilateral intracameral injections in adult C57BL/6J mice. IOP values of both injected (gray bar) and contralateral, non-treated eyes (white bar) are shown in the hydrogel-only group (Group 1) **(A)**, phosphate-buffered saline (PBS) group (Group 2) **(B)** and hydrogel+scutellarin group (Group 3) **(C)**. Hydrogel-injected eyes in both Groups 1 and 3 **(A,C)** developed sustained elevation of IOP relative to the non-treated eyes (ANOVA, $p < 0.05$), while the PBS-injected eye in Group 2 did not differ in IOP levels from the non-treated eye (ANOVA, $p > 0.05$). **(D)** The inter-eye IOP difference (ΔIOP, injected minus non-injected eye) was significantly higher in both the hydrogel-only group (dark gray bar) and the hydrogel+scutellarin group (light gray bar) when compared to the PBS group (white bar), but was not significantly different between hydrogel-only and hydrogel+scutellarin groups. 0w: 0 week, pre-injection; 3d: 3 days post-injection; 1w to 4w: 1 week to 4 weeks post-injection. Data were represented as mean ± SEM. *Post-hoc* Tukey's multiple comparisons correction tests between groups in **(D)**: $^{*}p < 0.05$, $^{**}p < 0.01$, $^{***}p < 0.001$, $^{****}p < 0.0001$.

understanding glaucomatous neurodegeneration and treatment effects. Here, given that scutellarin did not significantly affect IOP changes after intracameral hydrogel injection, our results may help expedite the development of neuroprotective therapies for glaucoma and other neurodegenerative diseases beyond IOP control.

Scutellarin, a multifunctional flavonoid, has been shown to exert protective effects on diabetes (28, 29), inflammation (30), tumors (31), and multiple organ diseases in the kidney, lung, and liver (32, 33). Within the central nervous system, scutellarin treatment displayed antioxidant and metal-chelating neuroprotective properties against Alzheimer's disease (34). Scutellarin has also been shown to alleviate hypoxia-induced cognitive impairment by promoting the proliferation and differentiation of neural stem cells in a mouse model (35). Chronic IOP elevation can induce ischemia and hypoxia of the optic nerve and its surrounding retinal tissue (36–38) causing retinal cell loss or neurodegeneration, which may lead to inner retinal thinning (39, 40). On the other hand, scutellarin can improve the axoplasmic flow and blood supply of the optic nerve (41), as well as the growth promotion and apoptosis inhibition of RGCs (42).

Scutellarin is also suggested to protect against a cascade of inflammatory events caused by glaucoma. In experimental glaucoma, models of chronic IOP elevation by intracameral microbead injection (43), acute IOP elevation by anterior chamber perfusion (21), and optic nerve crush (44) indicated the involvements of NLRP3 inflammasome activation during retina and optic nerve head damage, whereas pharmacological inhibition of NLRP3 (43) and inhibitor of Fas receptor (45) have been suggested as potential neuroprotective therapeutics in glaucoma. Given a recent experimental glaucoma study demonstrating increased expression of tumor necrosis factor-α, interleukin-1β (IL-1β) and IL-17A protein in the mouse

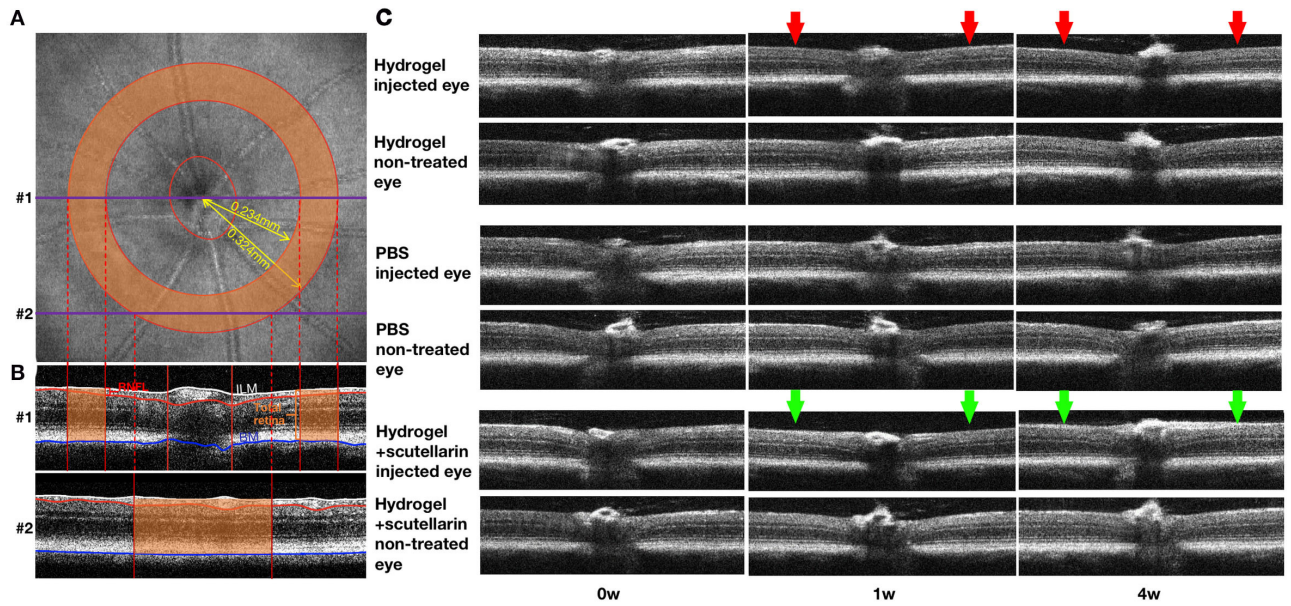

FIGURE 2 | Optical coherence tomography of the mouse retina over time. **(A)** *en face* image showing the optic nerve head (ONH) and a sampling band (orange) of 0.234 to 0.324 mm radius centered on the ONH for measuring retinal nerve fiber layer (RNFL) thickness and total retinal thickness (TRT). **(B)** Two representative cross-sectional retinal B-scan images corresponding to the linear scans #1 (through the optic nerve) and #2 (around the optic nerve) in **(A)**. The RNFL (red bracket), inner limiting membrane (ILM; white line), and Bruch's membrane (BM; blue line) were outlined using a custom-written automated segmentation algorithm. RNFL thickness was defined as the distance between white and red lines, and TRT was defined as the distance between white and blue lines. Only the thicknesses within the orange sampling band were measured and averaged for each eye for further analyses. **(C)** Cross-sectional retinal images from both injected and contralateral, non-treated eyes of a representative mouse in each of the 3 groups at 0 week (0w; pre-injection), 1 week (1w) and 4 weeks (4w) after unilateral intracameral injection. Note the clear images indicating the transparency of the ocular media comprising the hydrogel. Note also the apparent inner retinal thinning in the injected eye of the hydrogel-only group (Group 1; red arrows), and less apparent retinal thinning in the hydrogel+scutellarin group (Group 3; green arrows). No obvious retinal change was observed in the injected eye of the PBS group and in the non-treated eyes of all three groups.

retina after hydrogel-induced chronic IOP elevation (46), whereas scutellarin may inhibit the inflammatory processes of retinal neurodegeneration through the NLRP3 inflammasome signaling pathway, including NLRP3, apoptosis-associated speck-like protein containing a caspase recruitment domain, cleaved caspase-1, IL-1β, and IL-18 (21), it is possible that the mechanism of the reduced retinal thinning in our scutellarin-treated, hydrogel-injected eyes involved intervention of neuroinflammation via the NLRP3 inflammasome pathways. Scutellarin was also found to inhibit abnormally activated microglia and provide protection against neurodegeneration in the eye and the brain (21, 47, 48). Future research is warranted to examine if scutellarin may reduce inflammatory events in experimental chronic glaucoma (49, 50) and its associated damages to the retina and the optic nerve.

In terms of functional recovery, scutellarin has been shown to improve neurological functions in Alzheimer's disease mouse models (51) and in rats with cerebral ischemia (52, 53). Using multifocal electroretinogram, *Erigeron breviscapus* extract was also found to improve the impaired visual function of persistently elevated IOP in rats induced by episcleral vein cauterization (54). Our optokinetics results of ameliorated VA or CT aggravation in the scutellarin-treated, hydrogel-injected eyes further supported the role of oral scutellarin treatment in improving visual behavioral responses upon experimental glaucoma. While the exact mechanisms underlying the visual improvements remain to be elucidated, potential candidates may include mediation of the potassium (55) and calcium ions (56, 57). For example, flavonoid extracts of *Erigeron breviscapus* can suppress outward potassium currents in rat RGCs (55), which may help prevent RGC injury and vision loss caused by glaucoma. In addition, scutellarin may modulate intracellular calcium ion concentrations and voltage-gated calcium channels in the smooth muscle cells of vasculature (56), whereas systemic calcium ion antagonism can constantly improve visual field function in glaucoma patients (57). Further experimentations are necessary to determine the physiological basis of the observed visual recovery along with its linkage to the integrity of the neuroretina and visual pathway in more depth.

Scutellarin administration was found to exert protective effects in a dose-dependent manner (29, 58). We chose our current dosage of 300 mg/kg/day for 3 weeks with reference to similar flavonoid studies (59–61) in an attempt to maximize the delivery of scutellarin to the eye and the neural tissues. We have also attempted a low-dose pilot study ($n = 5$) using 50 mg/kg/day scutellarin treatment before formal experiments following a prior study (21), and did not observe obvious differences in visual behavioral responses from no scutellarin treatment (ANOVA $p > 0.05$, not shown). Therefore, the higher 300 mg/kg/day dose was chosen in the current formal experiments. Scutellarin was found to be minimally toxic or non-toxic in rodents up

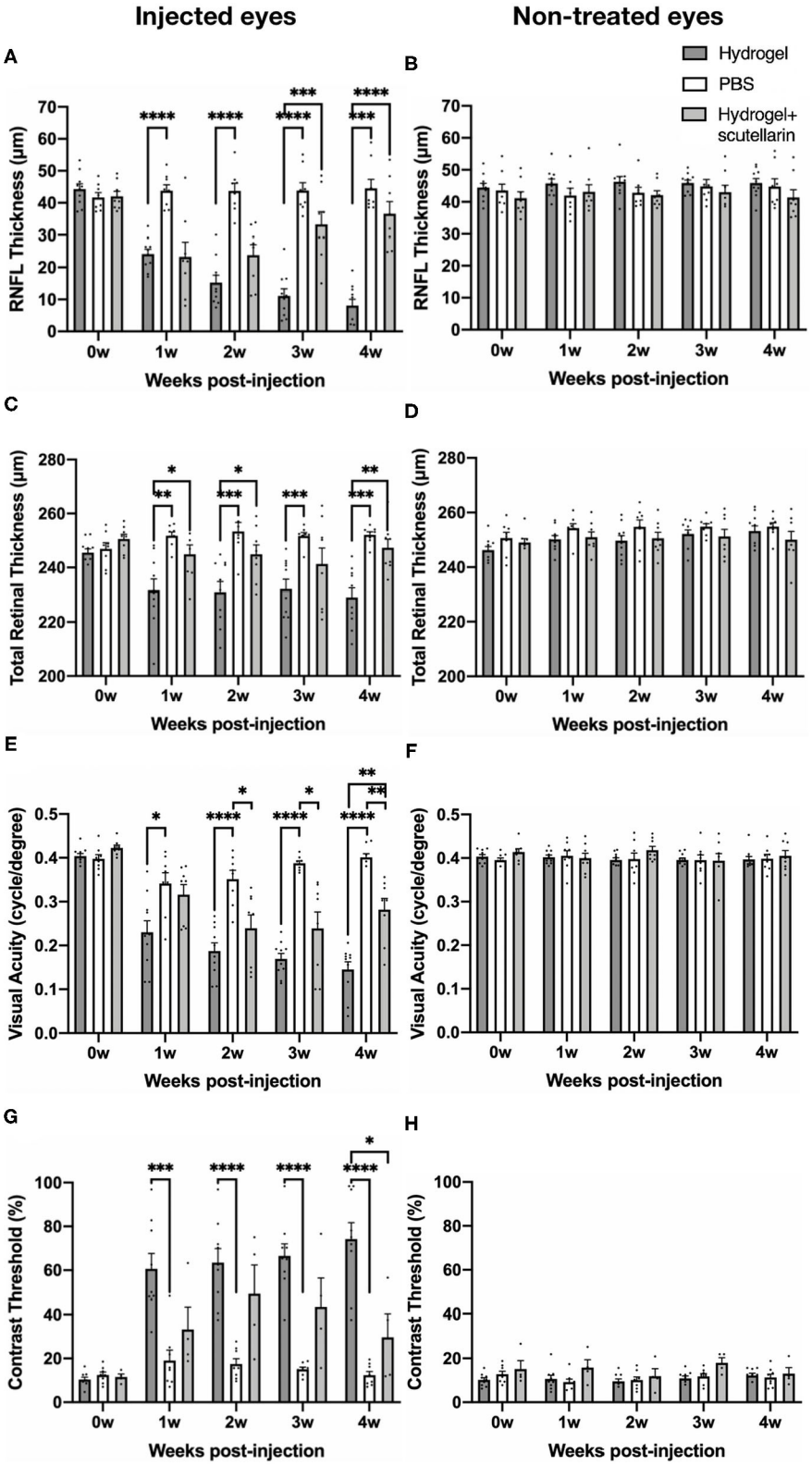

FIGURE 3 | Quantitative analyses of retinal nerve fiber layer (RNFL) thickness, total retinal thickness (TRT), visual acuity, and contrast threshold in the injected (left column) and contralateral, non-treated eyes (right column) among the hydrogel-only group (Group 1, dark gray bar), phosphate-buffered saline (PBS) group (Group 2, *(Continued)*

FIGURE 3 | white bar) and hydrogel+scutellarin group (Group 3, light gray bar). The scutellarin-treated, hydrogel-injected eyes in Group 3 showed less RNFL **(A)** and TRT **(C)** thinning, and reduced visual behavioral deficits **(E,G)** when compared to the untreated, hydrogel-injected eyes in Group 1. Such differences became more apparent toward the later stages of the experimental period. No significant change in RNFL thickness **(B)**, TRT **(D)**, visual acuity **(F)**, or contrast threshold **(H)** was observed in the non-treated eyes of all three groups or in the injected eye of the PBS group **(A,C,E,H)** ($p > 0.05$). 0w: 0 week, pre-injection; 1w to 4w: 1 week to 4 weeks post-injection. Data are represented as mean ± SEM. *Post-hoc* Tukey's multiple comparisons correction tests between groups: $^{*}p < 0.05$, $^{**}p < 0.01$, $^{***}p < 0.001$, $^{****}p < 0.0001$.

to 500 mg/kg/day (62), suggesting that our current dosage had a sufficient margin of safety for therapeutic use. Besides, we did not observe significant differences in body weight between the 3 groups in the current experiments (ANOVA $p > 0.05$, not shown). Scutellarin was suggested to protect visual function in glaucoma patients with controlled IOP at a lower oral dosage than the current study (20), whereas no side effect of scutellarin treatment on the eye has been illustrated in theory or reported in practice (63). At a high scutellarin dosage of more than 10 g/kg, systemic adverse effects including hypoactivity, loss of appetite, and asthenia were observed in mice which disappeared within 48 h (62), while another human study found rare occurrence of adverse drug reactions such as rash, chills and fever upon systemic scutellarin administration (63). Future studies are foreseen that expand upon the current findings to determine the dose-dependent effects of oral scutellarin treatment on vision preservation as well as potential adverse events in the eye.

There are several limitations for the experiments in the current study, one being the potential physiological fluctuations from anesthesia on IOP measurements. We expected that such effect was small, since we measured IOP soon after knocking the animals down from isoflurane induction, while all IOP measurements were taken in the same period between 1 pm and 3 pm to minimize diurnal variation. However, since not only the injected eyes but also the contralateral non-treated eyes exhibited significant IOP differences between the three groups, cautions should be noted when interpreting the IOP levels of individual eyes. Comparing the inter-eye IOP difference allowed us to evaluate the extent of IOP elevation induced by intracameral hydrogel injection more specifically and accurately, accounting for any physiological fluctuations on both eyes. Future studies may consider awake IOP measurements after training to further improve reliability and consistency (64).

With respect to the effects of oral scutellarin treatment on IOP, we compared IOP levels in Group 3 during the week of oral scutellarin treatment prior to hydrogel injection, and did not observe any significant differences before and after scutellarin treatment (**Supplementary Figure 1**). In addition, no significant difference in other parameters (i.e., RNFL thickness, TRT, VA and CT) was observed before and after oral scutellarin administration in Group 3 prior to hydrogel injection (**Supplementary Figure 1**). These findings suggest that 1 week of oral scutellarin treatment did not substantially affect the retinal structure or visual function in healthy adult mice. However, cautions should still be noted about the possibility that the slightly lower baseline IOP observed in the scutellarin-treated animals than the control groups may account for some of the protective effects observed in the experimental group. In addition, more evidence is needed to determine the possibility of secondary reduction of IOP elevation by oral scutellarin treatment after hydrogel injection.

Since scutellarin has been shown to exhibit unique pharmacokinetic behaviors in humans and animals that cannot be explained by the classical compartment model (65), how oral scutellarin administrations and the corresponding neurotherapeutic findings can be translated into the pharmacological activities and concentrations of scutellarin in the target brain tissues such as the visual system compartments remains unclear (63). To the best of our knowledge, the most relevant rodent brain drug distribution studies showed that 22% of orally and 29% of tail vein administered radiolabeled breviscapine (an extract mixture of *Erigeron breviscapus* with ≥90% scutellarin) reached the rat brain tissues when it was administered at a dose of 0.4 mg/kg (66). Despite the limited studies, rodents are considered as a preferred animal model for translating scutellarin studies to humans, as the model better mimics the pharmacokinetic behaviors and bioavailability of scutellarin in humans relative to other species (63). In addition, upon oral scutellarin administration, substantial amounts of scutellarein (i.e., the aglycone form of scutellarin) are present in the blood of both humans and rodents (65). In future studies, plasma measurements of scutellarin and scutellarein, as well as local examination of the NLRP3 inflammasome signaling pathway may help examine more specifically the therapeutic effects, pharmacokinetics, and pharmacological activity of the drug. Since scutellarin has been reported with a relatively low bioavailability upon oral administration (65), solutions can also be exploited to enhance oral delivery efficacy of scutellarin to glaucoma models or patients, such as the use of vitamin B12 derivatives-modified nanoparticles (67).

Given that the course of the disease deterioration in glaucoma is chronic and endures for years, further studies with higher frequencies of experimental measurements, longer periods of experimental follow-ups and large sample sizes can help to determine the safety and effectiveness of long-term scutellarin oral treatment, while histological and immunohistochemical studies would help further investigate the mechanisms underlying the *in vivo* findings observed in the current study. Future studies may also include electroretinography to provide additional functional endpoints to the visual behavioral optokinetic assessments. Future experimental designs can also consider post-IOP elevation treatment only or combined IOP lowering and scutellarin treatment for stronger clinical relevance. Overall, this preliminary but potentially important study demonstrated the use of a non-invasive measuring

platform to examine retinal thinning and visual behavioral deficits after hydrogel-induced chronic IOP elevation, as well as the positive role that scutellarin played on retinal structure and visual function under chronic experimental glaucoma. Scutellarin may be a possible candidate as a novel neurotherapeutic agent for glaucoma treatment beyond IOP control.

DATA AVAILABILITY STATEMENT

The original contributions presented in the study are included in the article/**Supplementary Material**, further inquiries can be directed to the corresponding author/s.

ETHICS STATEMENT

The animal study was reviewed and approved by NYU Grossman School of Medicine's Institutional Animal Care and Use Committee (IACUC).

AUTHOR CONTRIBUTIONS

JZ, CL, GW, JSS, WW, and KC: study conception and design. JZ, AS, KA, VA, JRS, EY, and YYu: data collection. JZ, KA, EY, YYa, HI, and KC: data analysis and interpretation. JZ, JRS, EY, YYa, HI, GW, JSS, and KC: manuscript writing. All authors have read and approved the final manuscript.

FUNDING

This work was supported in part by the National Institutes of Health R01-EY028125 (Bethesda, Maryland); BrightFocus Foundation G20190103 (Clarksburg, Maryland); State Scholarship Fund, China Scholarship Council No. 201908110347 for visiting Ph.D. student in the USA (China); Research to Prevent Blindness/Stavros Niarchos Foundation International Research Collaborators Award (New York, New York); and an Unrestricted Grant from Research to Prevent Blindness to NYU Langone Health Department of Ophthalmology.

ACKNOWLEDGMENTS

The authors would like to thank Nicole Colwell, M.D. for her technical support.

SUPPLEMENTARY MATERIAL

The Supplementary Material for this article can be found online at: https://www.frontiersin.org/articles/10.3389/fmed.2021.681169/full#supplementary-material

REFERENCES

1. Almasieh M, Wilson AM, Morquette B, Vargas J LC, Di Polo A. The molecular basis of retinal ganglion cell death in glaucoma. *Prog Retin Eye Res.* (2012) 31:152–81. doi: 10.1016/j.preteyeres.2011.11.002
2. Tham YC, Li X, Wong TY, Quigley HA, Aung T, Cheng CY. Global prevalence of glaucoma and projections of glaucoma burden through 2040: a systematic review and meta-analysis. *Ophthalmology.* (2014) 121:2081–90. doi: 10.1016/j.ophtha.2014.05.013
3. Susanna R Jr., De Moraes CG, Cioffi GA, Ritch R. Why do people (still) go blind from glaucoma? *Transl Vis Sci Technol.* (2015) 4:1. doi: 10.1167/tvst.4.2.1
4. Wheeler LA, Woldemussie E. Alpha-2 adrenergic receptor agonists are neuroprotective in experimental models of glaucoma. *Eur J Ophthalmol.* (2001) 11:30–35. doi: 10.1177/112067210101102S03
5. Schultz C. Tafluprost for the reduction of interocular pressure in open angle glaucoma and ocular hypertension. *Ophthalmol Eye Dis.* (2011) 3:13–9. doi: 10.4137/OED.S4253
6. Cheung W, Guo L, Cordeiro MF. Neuroprotection in glaucoma: drug-based approaches. *Optom Vis Sci.* (2008) 85:406–16. doi: 10.1097/OPX.0b013e31817841e5
7. Araie M, Mayama C. Use of calcium channel blockers for glaucoma. *Prog Retin Eye Res.* (2011) 30:54–71. doi: 10.1016/j.preteyeres.2010.09.002
8. Faiq MA, Wollstein G, Schuman JS, Chan KC. Cholinergic nervous system and glaucoma: from basic science to clinical applications. *Prog Retin Eye Res.* (2019) 72:100767. doi: 10.1016/j.preteyeres.2019.06.003
9. Johnson JE, Barde YA, Schwab M, Thoenen H. Brain-derived neurotrophic factor supports the survival of cultured rat retinal ganglion cells. *J Neurosci.* (1986) 6:3031–8. doi: 10.1523/JNEUROSCI.06-10-03031.1986
10. Cybulska-Heinrich AK, Mozaffarieh M, Flammer J. Ginkgo biloba: an adjuvant therapy for progressive normal and high tension glaucoma. *Mol Vis.* (2012) 18:390–402.
11. Sena DF, Lindsley K. Neuroprotection for treatment of glaucoma in adults. *Cochrane Database Syst Rev.* (2017) 1:CD006539. doi: 10.1002/14651858.CD006539.pub4
12. Shih GC, Calkins DJ. Secondary neuroprotective effects of hypotensive drugs and potential mechanisms of action. *Expert Rev Ophthalmol.* (2012) 7:161–75. doi: 10.1586/eop.12.13
13. Mei N, Guo X, Ren Z, Kobayashi D, Wada K, Guo L. Review of ginkgo biloba-induced toxicity, from experimental studies to human case reports. *J Environ Sci Health C Environ Carcinog Ecotoxicol Rev.* (2019) 35:1–28. doi: 10.1080/10590501.2016.1278298
14. Zhu JT, Choi RC, Li J, Xie HQ, Bi CW, Cheung AW, et al. Estrogenic and neuroprotective properties of scutellarin from erigeron breviscapus: a drug against postmenopausal symptoms and Alzheimer's disease. *Planta Med.* (2009) 75:1489–93. doi: 10.1055/s-0029-1185776
15. Liu Q, Shi Y, Wang Y, Lu J, Cong W, Luo G, et al. Metabolism profile of scutellarin in urine following oral administration to rats by ultra performance liquid chromatography coupled to time-of-flight mass spectrometry. *Talanta.* (2009) 80:84–91. doi: 10.1016/j.talanta.2009.06.031
16. Lin LL, Liu AJ, Liu JG, Yu XH, Qin LP, Su DF. Protective effects of scutellarin and breviscapine on brain and heart ischemia in rats. *J Cardiovasc Pharmacol.* (2007) 50:327–32. doi: 10.1097/FJC.0b013e3180cbd0e7
17. Zhang HF, Hu XM, Wang LX, Xu SQ, Zeng FD. Protective effects of scutellarin against cerebral ischemia in rats: evidence for inhibition of the apoptosis-inducing factor pathway. *Planta Med.* (2009) 75:121–6. doi: 10.1055/s-0028-1088368
18. Wang J, Zhang L, Liu B, Wang Q, Chen Y, Wang Z, et al. Systematic investigation of the *Erigeron breviscapus* mechanism for treating cerebrovascular disease. *J Ethnopharmacol.* (2018) 224:429–40. doi: 10.1016/j.jep.2018.05.022
19. Zhang Y, Sheng YM, Meng XL, Long Y. [Effect of caffeic acid, seopoletin and scutellarin on rat retinal neurons *in vitro*]. *Zhongguo Zhong Yao Za Zhi.* (2005) 30:907−9. doi: 10.3321/j.issn:1001-5302.2005.12.008. (in Chinese).
20. Zhong Y, Xiang M, Ye W, Cheng Y, Jiang Y. Visual field protective effect of erigeron breviscapus (vant.) hand. Mazz. Extract on glaucoma with controlled intraocular pressure: a randomized, double-blind, clinical trial. *Drugs R D.* (2010) 10:75–82. doi: 10.2165/11539090-000000000-00000

21. Zhu J, Chen L, Qi Y, Feng J, Zhu L, Bai Y, et al. Protective effects of *Erigeron breviscapus* hand.- Mazz. (EBHM) extract in retinal neurodegeneration models. *Mol Vis.* (2018) 24:315–25.
22. Chan KC, Yu Y, Ng SH, Mak HK, Yip YWY, van der Merwe Y, et al. Intracameral injection of a chemically cross-linked hydrogel to study chronic neurodegeneration in glaucoma. *Acta Biomater.* (2019) 94:219–31. doi: 10.1016/j.actbio.2019.06.005
23. van der Merwe Y, Murphy MC, Sims JR, Faiq MA, Yang XL, Ho LC, et al. Citicoline modulates glaucomatous neurodegeneration through intraocular pressure-independent control. *Neurotherapeutics.* (2021). doi: 10.1007/s13311-021-01033-6. [Epub ahead of print].
24. Roubeix C, Godefroy D, Mias C, Sapienza A, Riancho L, Degardin J, et al. Intraocular pressure reduction and neuroprotection conferred by bone marrow-derived mesenchymal stem cells in an animal model of glaucoma. *Stem Cell Res Ther.* (2015) 6:177. doi: 10.1186/s13287-015-0168-0
25. Gabriele ML, Ishikawa H, Schuman JS, Ling Y, Bilonick RA, Kim JS, et al. Optic nerve crush mice followed longitudinally with spectral domain optical coherence tomography. *Invest Ophthalmol Vis Sci.* (2011) 52:2250–4. doi: 10.1167/iovs.10-6311
26. Ho LC, Wang B, Conner IP, van der Merwe Y, Bilonick RA, Kim SG, et al. *In vivo* evaluation of white matter integrity and anterograde transport in visual system after excitotoxic retinal injury with multimodal MRI and OCT. *Invest Ophthalmol Vis Sci.* (2015) 56:3788–800. doi: 10.1167/iovs.14-15552
27. Douglas RM, Alam NM, Silver BD, McGill TJ, Tschetter WW, Prusky GT. Independent visual threshold measurements in the two eyes of freely moving rats and mice using a virtual-reality optokinetic system. *Vis Neurosci.* (2005) 22:677–84. doi: 10.1017/S0952523805225166
28. Mei X, Zhang T, Ouyang H, Lu B, Wang Z, Ji L. Scutellarin alleviates blood-retina-barrier oxidative stress injury initiated by activated microglia cells during the development of diabetic retinopathy. *Biochem Pharmacol.* (2019) 159:82–95. doi: 10.1016/j.bcp.2018.11.011
29. Mei XY, Zhou LY, Zhang TY, Lu B, Ji LL. Scutellaria barbata attenuates diabetic retinopathy by preventing retinal inflammation and the decreased expression of tight junction protein. *Int J Ophthalmol.* (2017) 10:870–7. doi: 10.18240/ijo.2017.06.07
30. Zhang L, Sun S, Li W, Zhang W, Wang X, Yang SY. Effect of scutellarin inhibits collagen-induced arthritis through TLR4/NF-κB-mediated inflammation. *Mol Med Rep.* (2017) 16:5555–60. doi: 10.3892/mmr.2017.7292
31. Sun C, Li C, Li X, Zhu Y, Su Z, Wang X, et al. Scutellarin induces apoptosis and autophagy in NSCLC cells through ERK1/2 and AKT signaling pathways *in vitro* and *in vivo*. *J Cancer.* (2018) 9:3247–56. doi: 10.7150/jca.25921
32. Tan ZH, Yu LH, Wei HL, Liu GT. Scutellarin protects against lipopolysaccharide-induced acute lung injury via inhibition of NF-kappaB activation in mice. *J Asian Nat Prod Res.* (2010) 12:175–84. doi: 10.1080/10286020903347906
33. Tan ZH, Yu LH, Wei HL, Liu GT. The protective action of scutellarin against immunological liver injury induced by concanavalin A and its effect on pro-inflammatory cytokines in mice. *J Pharm Pharmacol.* (2007) 59:115–21. doi: 10.1211/jpp.59.1.0015
34. Simunkova M, Alwasel SH, Alhazza IM, Jomova K, Kollar V, Rusko M, et al. Management of oxidative stress and other pathologies in Alzheimer's disease. *Arch Toxicol.* (2019) 93:2491–513. doi: 10.1007/s00204-019-02538-y
35. Wang WW, Han JH, Wang L, Bao TH. Scutellarin may alleviate cognitive deficits in a mouse model of hypoxia by promoting proliferation and neuronal differentiation of neural stem cells. *Iran J Basic Med Sci.* (2017) 20:272–9. doi: 10.22038/IJBMS.2017.8355
36. Liu HH, Zhang L, Shi M, Chen L, Flanagan JG. Comparison of laser and circumlimbal suture induced elevation of intraocular pressure in albino CD-1 mice. *PLoS ONE.* (2017) 12:e0189094. doi: 10.1371/journal.pone.0189094
37. Wei X, Yu Z, Cho KS, Chen H, Malik MT, Chen X, et al. Neuroglobin is an endogenous neuroprotectant for retinal ganglion cells against glaucomatous damage. *Am J Pathol.* (2011) 179:2788–97. doi: 10.1016/j.ajpath.2011.08.015
38. Jassim AH, Fan Y, Pappenhagen N, Nsiah NY, Inman DM. Oxidative stress and hypoxia modify mitochondrial homeostasis during glaucoma. *Antioxid Redox Signal.* (2021). doi: 10.1089/ars.2020.8180. [Epub ahead of print].
39. Chao WH, Lai MY, Pan HT, Shiu HW, Chen MM, Chao HM. Dendrobium nobile lindley and its bibenzyl component moscatilin are able to protect retinal cells from ischemia/hypoxia by dowregulating placental growth factor and upregulating norrie disease protein. *BMC Complement Altern Med.* (2018) 18:193. doi: 10.1186/s12906-018-2256-z
40. Yang Q, Cho KS, Chen H, Yu D, Wang WH, Luo G, et al. Microbead-induced ocular hypertensive mouse model for screening and testing of aqueous production suppressants for glaucoma. *Invest Ophthalmol Vis Sci.* (2012) 53:3733–41. doi: 10.1167/iovs.12-9814
41. Zhu Y, Jiang Y, Liu Z, Luo X, Wu Z. [The affect of *Erigeron breviscapus* (Vant.) hand-Mazz on axoplasmic transport of optic nerve in rats with experimentally elevated intraocular pressure]. *Zhonghua Yan Ke Za Zhi.* (2000) 36:289–91. doi: 10.3760/j:issn:0412-4081.2000.04.014. (in Chinese).
42. Jia L, Liu Z, Luo X. [The effect of qing guang kang on the metabolism of retinal ganglionic cells in rats after artificial acute high intraocular pressure]. *Zhonghua Yan Ke Za Zhi.* (1995) 31:129–32.
43. Krishnan A, Dua M, Mitchell CH, Lu W, Gregory-Ksander MS. Pharmacologic inhibition of the nLRP3 inflammasome - a novel neuroprotective therapy for glaucoma. In: *ARVO 2019: Association for Research in Vision and Ophthalmology Annual Meeting 2019.* Vancouver, BC (2019). p. 2256
44. Puyang Z, Feng L, Chen H, Liang P, Troy JB, Liu X. Retinal ganglion cell loss is delayed following optic nerve crush in NLRP3 knockout mice. *Sci Rep.* (2016) 6:20998. doi: 10.1038/srep20998
45. Krishnan A, Kocab AJ, Zacks DN, Marshak-Rothstein A, Gregory-Ksander M. A small peptide antagonist of the Fas receptor inhibits neuroinflammation and prevents axon degeneration and retinal ganglion cell death in an inducible mouse model of glaucoma. *J Neuroinflammation.* (2019) 16:184. doi: 10.1186/s12974-019-1576-3
46. Chen J, Sun J, Yu H, Huang P, Zhong Y. Evaluation of the effectiveness of a chronic ocular hypertension mouse model induced by intracameral injection of cross-linking hydrogel. *Front Med.* (2021) 8:643402. doi: 10.3389/fmed.2021.643402
47. Wang SX, Guo H, Hu LM, Liu YN, Wang YF, Kang LY, et al. Caffeic acid ester fraction from erigeron breviscapus inhibits microglial activation and provides neuroprotection. *Chin J Integr Med.* (2012) 18:437–44. doi: 10.1007/s11655-012-1114-y
48. Block ML, Hong JS. Microglia and inflammation-mediated neurodegeneration: multiple triggers with a common mechanism. *Prog Neurobiol.* (2005) 76:77–98. doi: 10.1016/j.pneurobio.2005.06.004
49. Bosco A, Steele MR, Vetter ML. Early microglia activation in a mouse model of chronic glaucoma. *J Comp Neurol.* (2011) 519:599–620. doi: 10.1002/cne.22516
50. Bosco A, Crish SD, Steele MR, Romero CO, Inman DM, Horner PJ, et al. Early reduction of microglia activation by irradiation in a model of chronic glaucoma. *PLoS ONE.* (2012) 7:e43602. doi: 10.1371/journal.pone.0043602
51. Zeng YQ, Cui YB, Gu JH, Liang C, Zhou XF. Scutellarin mitigates Aβ-induced neurotoxicity and improves behavior impairments in AD mice. *Molecules.* (2018) 23:869. doi: 10.3390/molecules23040869
52. Fang M, Yuan Y, Lu J, Li HE, Zhao M, Ling EA, et al. Scutellarin promotes microglia-mediated astrogliosis coupled with improved behavioral function in cerebral ischemia. *Neurochem Int.* (2016) 97:154–71. doi: 10.1016/j.neuint.2016.04.007
53. Liu G, Tang G, Liang W, Wang Z, Xu W, Fan G, et al. PK-PD correlation of *Erigeron breviscapus* injection in the treatment of cerebral ischemia-reperfusion injury model rats. *J Mol Neurosci.* (2021) 71:302–24. doi: 10.1007/s12031-020-01651-3
54. Lu XJ, Zhang FW, Cheng L, Liu AQ, Duan JG. Effect on multifocal electroretinogram in persistently elevated intraocular pressure by *Erigeron breviscapus* extract. *Int J Ophthalmol.* (2011) 4:349–52. doi: 10.3980/j.issn.2222-3959.2011.04.04
55. Yin S, Wang ZF, Duan JG, Ji L, Lu XJ. Extraction (DSX) from *Erigeron breviscapus* modulates outward potassium currents in rat retinal ganglion cells. *Int J Ophthalmol.* (2015) 8:1101–6. doi: 10.3980/j.issn.2222-3959.2015.06.04
56. Zhu BH, Ma L, Pan XD, Huang YL, Liu J. Scutellarin induced ca(2+) release and blocked KCl-induced ca(2+) influx in smooth muscle cells isolated from rat thoracic artery. *J Asian Nat Prod Res.* (2008) 10:583–9. doi: 10.1080/10286020801966633

57. Kitazawa Y, Shirai H, Go FJ. The effect of ca2(+) -antagonist on visual field in low-tension glaucoma. *Graefes Arch Clin Exp Ophthalmol.* (1989) 227:408–12. doi: 10.1007/BF02172889
58. Xiong LL, Du RL, Xue LL, Jiang Y, Huang J, Chen L, et al. Anti-colorectal cancer effects of scutellarin revealed by genomic and proteomic analysis. *Chin Med.* (2020) 15:28. doi: 10.1186/s13020-020-00307-z
59. Hu S, Chen Y, Wang ZF, Mao-Ying QL, Mi WL, Jiang JW, et al. The analgesic and antineuroinflammatory effect of baicalein in cancer-Induced bone pain. *Evid Based Complement Alternat Med.* (2015) 2015:973524. doi: 10.1155/2015/973524
60. Zhao Z, Zhao J. [Effect of baicalin on rat cardiac function during acute respiratory distress syndrome]. *J Environ Occup Med.* (2011) 28:517–20. (in Chinese).
61. Lee G, Kim H, Lee H, Shin M, Hong M, Bae H. Effects of *Scutellaria barbata* on cisplatin induced nephrotoxicity in mice. *Mol Cell Toxicol.* (2010) 6:255–59. doi: 10.1007/s13273-010-0035-0
62. Li X, Wang L, Li Y, Bai L, Xue M. Acute and subacute toxicological evaluation of scutellarin in rodents. *Regul Toxicol Pharmacol.* (2011) 60:106–11. doi: 10.1016/j.yrtph.2011.02.013
63. Wang L, Ma Q. Clinical benefits and pharmacology of scutellarin: a comprehensive review. *Pharmacol Ther.* (2018) 190:105–27. doi: 10.1016/j.pharmthera.2018.05.006
64. Ding C, Wang P, Tian N. Effect of general anesthetics on IOP in elevated IOP mouse model. *Exp Eye Res.* (2011) 92:512–20. doi: 10.1016/j.exer.2011.03.016
65. Huang JM, Weng WY, Huang XB, Ji YH, Chen E. Pharmacokinetics of scutellarin and its aglycone conjugated metabolites in rats. *Eur J Drug Metab Pharmacokinet.* (2005) 30:165–70. doi: 10.1007/BF03190615
66. Shi SL, Xu LY, Wu JJ, Li CY, Ge WH, Dai WY. [Comparison of the distribution of breviscapine in the brain by different administration routes]. *Yao Xue Xue Bao.* (2009) 44:515–8. doi: 10.3321/j.issn:0513-4870.2009.05.014. (in Chinese).
67. Wang J, Tan J, Luo J, Huang P, Zhou W, Chen L, et al. Enhancement of scutellarin oral delivery efficacy by vitamin b12-modified amphiphilic chitosan derivatives to treat type iI diabetes induced-retinopathy. *J Nanobiotechnol.* (2017) 15:18. doi: 10.1186/s12951-017-0251-z

Conflict of Interest: YYu and CL have patents filed related to this study (Induction of chronic elevation of intraocular pressure with intracameral cross-linking hydrogel US 20150250815). YYu was employed by the company Pleryon Therapeutics Limited.

The remaining authors declare that the research was conducted in the absence of any commercial or financial relationships that could be construed as a potential conflict of interest.

Publisher's Note: All claims expressed in this article are solely those of the authors and do not necessarily represent those of their affiliated organizations, or those of the publisher, the editors and the reviewers. Any product that may be evaluated in this article, or claim that may be made by its manufacturer, is not guaranteed or endorsed by the publisher.

frontiers in Medicine

ORIGINAL RESEARCH
published: 03 September 2021
doi: 10.3389/fmed.2021.712332

Microcatheter-Assisted Trabeculotomy Combined With Deep Sclerectomy and Trabeculectomy in Young to Middle-Aged Adults With Advanced Primary Open-Angle Glaucoma: 1-Year Result

*Hengli Zhang, Xiaowei Yan, Fan Li, Lihua Ma, Yulei Geng, Kexin Jiao and Guangxian Tang**

Department of Ophthalmology, Shijiazhuang People's Hospital, Shijiazhuang, China

OPEN ACCESS

Edited by:
Michele Lanza, University of Campania Luigi Vanvitelli, Italy

Reviewed by:
Ronald Fellman, Glaucoma Associates of Texas, United States
Sylvain Roy, École Polytechnique Fédérale de Lausanne, Switzerland
Sameh Mosaed, University of California, Irvine, United States
Ian Murdoch, University College London, United Kingdom

***Correspondence:**
Guangxian Tang
gxtykyy@126.com

Specialty section:
This article was submitted to Ophthalmology, a section of the journal Frontiers in Medicine

Received: *20 May 2021*
Accepted: *02 August 2021*
Published: *03 September 2021*

Citation:
Zhang H, Yan X, Li F, Ma L, Geng Y, Jiao K and Tang G (2021) Microcatheter-Assisted Trabeculotomy Combined With Deep Sclerectomy and Trabeculectomy in Young to Middle-Aged Adults With Advanced Primary Open-Angle Glaucoma: 1-Year Result. Front. Med. 8:712332. doi: 10.3389/fmed.2021.712332

Objective: We aimed to evaluate the safety and clinical efficacy of *ab externo* microcatheter-assisted trabeculotomy combined with deep sclerectomy and trabeculectomy (MATT-DS-Trab) in the surgical management of advanced primary open-angle glaucoma (POAG).

Methods: According to the inclusion criteria, we retrospectively collected and analyzed 37 POAG cases in advanced stage who received MATT-DS-Trab. The intraocular pressure (IOP), best corrected visual acuity (BCVA), use of anti-glaucoma drugs, shape of the filtering bleb, size of the scleral lake, complications, and the surgical success rate were recorded.

Results: The mean IOP was 37.50 ± 8.11 mmHg before the operation, while it depleted to 10.08 ± 2.01 and 11.43 ± 2.07 mmHg at 1 week and 12 months after the operation, respectively (both $P < 0.001$ compared to preoperative IOP). From none to two kinds of anti-glaucoma drugs were used 12 months after surgery on the patients, which were significantly reduced compared with that preoperatively ($P < 0.001$). An L-type filtering bleb was the main form at all time points after the operation. At 12 months following surgery, an F-type filtering bleb accounted for 5.41% and no E-type filtering bleb was recorded. The length and height of the scleral lake shrunk with time, but there was no statistical significance ($P > 0.05$). Also, there was no correlation between the size of the scleral pool and the IOP ($P > 0.05$). At 12 months after the operation, the complete success rates were 94.59, 83.78, and 72.97% according to standards A (≤18 mmHg), B (≤15 mmHg), and C (≤12 mmHg), respectively. Intraoperative complications were mainly anterior chamber hemorrhage, and no complications related to the filtration bleb were observed after the operation.

Conclusion: Based on multichannel mechanisms, MATT-DS-Trab is able to effectively reduce IOP in advanced POAG patients, with few serious complications and a high success rate.

Keywords: primary open angle glaucoma, microcatheter, trabeculotomy, deep sclerectomy, trabeculectomy

INTRODUCTION

Primary open-angle glaucoma (POAG) often causes blindness. Trabeculectomy is a classic operation used to treat glaucoma and is considered one of the primary surgical treatments for POAG. However, the success rates were 86.5, 69.3, and 53.1% at 1, 3, and 5 years after surgery, respectively, after which the failure rate increased by an additional 10% each year (1–3). The primary cause of failure was scarring of the filtering area. *Ab externo* microcatheter-assisted trabeculotomy (MATT) is performed by inserting an iTrack laser microcapsule into the Schlemm's canal (SC) through an incision in the outer wall of 360°. We then incised the inner wall of the SC and the trabecular meshwork (TM). This may promote drainage of aqueous humor and reduce intraocular pressure (IOP) when combined with accurate surgical positioning. The success rate of congenital glaucoma surgery (IOP $<$ 21 mmHg) by MATT could be as high as 83–91% after 6–12 months (4–7), and the 2-year complete success rate may be as high as 67% (IOP $<$ 18 mmHg) (8). Studies have shown that trabeculotomy for POAG in adults is not as effective as in the case of congenital glaucoma in lowering the IOP (9, 10). But the investigation by Grover et al. presented that circumferential *ab interno* trabeculotomy in adults with POAG is effective; the mean IOP ranged from 15.5 to 16.2 mmHg with 1.7 glaucoma drugs 12 months after surgery (10). Grant believed that most of the outflow resistance of the aqueous humor lies in the SC–TM complex. Trabeculotomy can reduce aqueous humor resistance by 75% (11). However, some studies have investigated that trabeculotomy can only eliminate 40–50% of outflow resistance when the IOP perfusion is low (12, 13). Trabeculotomy is more suited to treat patients with POAG in the early and moderate stages who have not adapted to glaucoma filtering surgery and whose IOP values do not need to be reduced to $<$15 mmHg (14).

However, most patients with POAG in China are already in the late stage when diagnosed, and the IOP remains high even after the maximum dose of drug treatment has been administered. Some patients are likely to develop scarring after trabeculectomy, and their IOP must be reduced to protect the remaining visual function (15). For such patients, it is important to discover a safe and effective way to reduce the IOP. In the present study, we describe a series of Chinese patients with advanced POAG who underwent microcatheter-assisted trabeculotomy combined with deep sclerectomy and trabeculectomy (MATT-DS-Trab). The operation aims to reduce the IOP stably to values within the target range based on multichannel aqueous humor drainage mechanisms and to eventually improve long-term efficacy and reduce postoperative complications.

MATERIALS AND METHODS

Retrospective Case Series

We retrospectively collected and analyzed data from 37 patients with advanced POAG who received MATT-DS-Trab between September 2018 and April 2019 at Shijiazhuang People's Hospital. The study included 26 men and 11 women. Their ages ranged between 19 and 57 years (37.46 $\pm$ 12.08). The preoperative IOP was 37.50 $\pm$ 8.11 mmHg despite the patients receiving the maximum dose of IOP-controlling drugs. All operations were performed by the same surgeon in the same manner. All patients were followed up for longer than 12 months after surgery. This study was approved by the ethics committee of Shijiazhuang People's Hospital. All patients were informed and signed a surgery consent form.

Diagnosis and Inclusion and Exclusion Criteria

Diagnostic and Inclusion Criteria

Gonioscopy was performed for patients with open-angle glaucoma and a clear structure, while fundus stereography was for patients with glaucoma optic neuropathy (16), cup/disc (C/D) $>$ 0.8. Patients' signs and symptoms coincided with the diagnostic criteria of advanced POAG according to the Hodapp–Anderson–Parris staging method and the Advanced Glaucoma Intervention Study (AGIS) system rating (17). The inclusion criteria were as follows: (1) patients older than 18 years (based on PubMed's MeSH definition for young middle-aged adults) (18) who did not have a history of previous eye surgery; (2) the patient's IOP was still uncontrolled in the target range ($\geq$21 mmHg) despite taking the maximum tolerable number of anti-glaucoma medications (three or more) or a fluctuation of more than 8 mmHg during a 24-h IOP measurement and the progression of visual field loss over time; and (3) patients who could not tolerate or had serious adverse effects when using anti-glaucoma drugs.

Exclusion Criteria

We excluded the following: (1) patients whose fundus could not be observed due to refractive ocular diseases; (2) patients who had undergone eye surgeries such as cataract surgery, corneal surgery, etc.; (3) patients with secondary glaucoma, e.g., neovascular glaucoma; (4) patients with peripheral anterior synechiae (PAS); (5) monocular patients; (6) patients with severe systemic or mental conditions; and (7) pregnant women.

Surgical Procedure

All surgeries were conducted under topical anesthesia with proparacaine hydrochloride eye drops and subconjunctival anesthesia in the surgical area with 0.2 ml of a 2% lidocaine solution. A fornix-based conjunctival flap was created and a 5 $\times$ 5-mm superficial scleral flap one-third as thick as the sclera, extending $\sim$1 mm into the clear cornea, was excised. A piece of sponge soaked in 0.4 mg/ml mitomycin (MMC) was applied under the conjunctiva and scleral flap for 3–4 min, followed by thorough washing. An $\sim$4 $\times$ 4-mm-deep sclera was then created, leaving a margin of 0.5 mm on each side, along with a thinner layer of deep sclera covering the choroid. The color of the pigmentation in the choroid tissue was visible in the sclera bed. Paracentesis was then performed at a depth of 0.5 mm inside the transparent corneal limbus at the temporal side, and an appropriate amount of the aqueous humor was released to allow the IOP to return to a value within the normal range. Subsequently, the SC in front of the scleral spur was examined and opened, and the end of the SC was dilated by viscoelastic

using a specially designed needle. The illuminated microcatheter (iTrack 250A, iScience Interventional, Menlo Park, CA, USA) was inserted into the SC and threaded circumferentially around it. In four cases, the microcatheter encountered some resistance. When this occurred, the microcatheter was pulled out and threaded again in the opposite direction. An appropriate amount of viscoelastic material was again injected into the anterior chamber through the puncture opening. Then, both exposed ends of the microcatheter were grasped and pulled in opposite directions, thereby conducting the trabeculotomy. The remainder of the trabeculectomy procedure has been described previously (19). The deep scleral flap and a 1.5 × 3-mm portion of the trabeculum were excised, and a peripheral iridectomy was then performed. The two posterior corners of the superficial scleral flap were fixed using a 10–0 nylon suture under moderate tension, and two releasable sutures were made tightly on the vertical incisions of both sides of the superficial scleral flap to temporarily fix the scleral flap firmly in place. Gentle anterior chamber irrigation was performed *via* paracentesis in cases of significant hyphema. The anterior chamber was subsequently rebuilt and the filtering function was evaluated. The conjunctiva was closed using a 10–0 nylon suture. Finally, the IOP was elevated to a normal level. All surgeries were performed by a single experienced glaucoma surgeon (GX Tang).

Observational Indicators

The following parameters were examined and analyzed before surgery and at 1, 7, and 14 days and at 1, 3, 6, and 12 months after surgery. The BCVA was measured using the Snellen chart and the results described using the logarithmic minimum angle of resolution (logMAR). IOP was measured using a calibrated Goldman applanation tonometer. Slit lamp microscopy, gonioscopy (a single-mirror Gonio diagnostic lens), ultrasound biomicroscopy (UBM) (300, Meda Co., Ltd., Tianjin, China), stereoscopic optic disc photography (Kowa Nonmyd WX 3D, Tokyo, Japan), the number of anti-glaucoma medications, surgical success rate, and the occurrence of complications were observed. We also assessed the head of the optic nerve and the visual field (VF) using optical coherence tomography (Heidelberg, Germany) and a Humphrey-750i Field Analyzer (Carl Zeiss Meditec, Oberkochen, Germany). All examinations were performed by experienced ophthalmologists and technicians.

Postoperative Management

The subjects were prescribed tobramycin dexamethasone drops four times a day and tobramycin dexamethasone ointment once a day after the procedure. The medication frequency gradually subsided following relief from ocular inflammatory reaction during the follow-up period. A 2% pilocarpine solution was given four times a day for 3 months to prevent PAS (20). Postoperative gonioscopy was performed at each hospital visit.

We obtained the images using UBM and examined the area at a depth of 5 mm with a probe frequency of 50 MHz and observed the scope displayed on the monitor (8 × 5.5 mm). Additional observations with UBM were conducted if the IOP was >18 mmHg. All patients underwent a scan of the surgical area and an evaluation according to the UBM procedure and calculation method described in a previous study (21). Quantitative observation included measurements of the scleral lake size, maximum anteroposterior length (MAPL) of the longitudinal scan, and maximum height (MH). The filtration blebs were classified as L-type (low-reflective), H-type (high-reflective), E-type (encapsulated), and F-type (flattened) in accordance with the methods used in a previous study and the parameters assessed with UBM (22). Morphological changes in the filtration bleb and intrascleral lake were measured 1, 3, 6, and 12 months postoperatively using UBM.

Surgical Success Rate

Complete success was defined as IOP values ranging between 5 and 18 mmHg with a reduction of at least 30% from the baseline IOP (23). Postsurgical IOP ≤18 mmHg was defined as criterion A, ≤15 mmHg as criterion B, and ≤12 mmHg as criterion C. These criteria had to be fulfilled without the use of anti-glaucoma drugs. Qualified success referred to an IOP that fulfilled the above-mentioned criteria after the topical application of anti-glaucoma medications. Failure was defined as two consecutive determinations of IOP that exceeded the aforementioned IOP values after topical application of three or more anti-glaucoma drugs.

Statistical Analysis

SPSS 19.0 software (IBM, Chicago, IL, USA) was used for all data analyses. The Shapiro–Wilk test was used to test normality, and parametric or non-parametric tests were applied accordingly. Descriptive data for numeric variables were presented as the mean ± SD, as medians and interquartile range for continuous variables, or as *n* (%) for categorical variables. Preoperative and postoperative IOP values were compared using a paired *t*-test. The Wilcoxon paired signed-rank test was used to compare BCVA and the number of drugs used before and after surgery. The Kruskal–Wallis *H* test was conducted to compare changes in the number of drugs at different time points after surgery. Filtration bleb morphologies were assessed using Fisher's exact test. MAPL and MH at different time points after surgery were compared using parametric one-way analysis of variance (ANOVA). Pearson's correlation coefficient or Spearman's correlation coefficient was used to evaluate the correlation between IOP and scleral lake parameters. Kaplan–Meier curve analysis was performed to determine the cumulative probability of complete surgical success. Statistical significance was set at $P < 0.05$.

RESULTS

Characteristics of Patients

The mean follow-up time was 17.20 ± 3.4 months (13–25 months). **Table 1** shows the preoperative information for all patients.

Best Corrected Visual Acuity

The Shapiro–Wilk test showed that the BCVA (LogMAR) was statistically significant both before and after surgery (all *P*

TABLE 1 | Baseline parameters for the subjects.

Parameter	Results
Subjects (*n*, %)	37 (100.00)
Eyes (*n*, %)	37 (100.00)
Gender	
Male (*n*, %)	26 (70.27)
Female (*n*, %)	11 (29.73)
Age (years)	
<30 years	12 (32.43)
30–40 years (included 30 and 40 years)	10 (27.03)
40–50 years (included 50 years)	9 (24.32)
>50 years	6 (16.22)
C/D	
0.9	17 (45.95)
1.0	20 (54.05)
MD (dB)	
Mean ± SD	−20.62 ± 7.63
Minimum, maximum	−30.72, −13.08
AL (mm)	
Mean ± SD	23.43 ± 0.99
Minimum, maximum	22.66, 24.06
Refractive error (D)	
Mean ± SD	−0.23 ± 1.27
Minimum, maximum	−2.25, +2
Number of medications	
3	9 (24.32)
4	25 (67.57)
5	3 (8.11)

C/D, cup/disc; MD, mean deviation; SD, standard deviation; AL, axial length; D, diopter.

TABLE 2 | Changes in the BCVA (LogMAR) before and after surgery.

Time point	Median	Q1	Q3	*Z*	*P*[a]
Preoperative	0.11	0.00	0.19	–	–
12 months postoperative	0.12	0.00	0.22	−0.834	0.404

BCVA, best corrected visual acuity; LogMAR, logarithmic minimum angle of resolution; Q1, lower quartile; Q3, upper quartile.
[a]*Wilcoxon paired signed-rank test was used before and after surgery.*

< 0.001) and did not conform to normal distribution. The Wilcoxon paired signed-rank test did not reveal a significant difference in the BCVA (LogMAR) before and 12 months after the procedure ($Z = -0.834$, $P = 0.404$) (**Table 2**).

Intraocular Pressure

The mean IOP before surgery was 37.50 ± 8.11 mmHg. The mean IOP and the corresponding pressure decrease at 1 and 2 weeks and at 1, 3, 6, and 12 months after surgery are shown in **Table 3**. Compared with the preoperative IOP, the postoperative IOP at 1 and 2 weeks and at 1, 3, 6, and 12 months diminished by 69.91, 69.67, 68.59, 67.93, 68.06, and 68.14%, respectively. There were significant differences in the IOP at all time points before and after surgery (all $P < 0.001$).

Medications

Patients required three to five kinds of anti-glaucoma medication before the operation and none or only one medication at 3 and 6 months after surgery; the number of anti-glaucoma medications was significantly less than that used preoperatively ($P < 0.001$). There was also a marked reduction in the number of medications used at 12 months postoperatively (from none to two types) compared to the number used preoperatively ($P < 0.001$) (**Table 4**).

Changes in the Morphology of the Filtering Bleb and Sclera Pool Before and After Operation

Morphology of the Filtering Bleb and the Appearance of Anterior Chamber Angle

At 1, 3, 6, and 12 months after the operation, the L-type filtering bleb accounted for 97.30, 97.30, 97.30, and 94.59% and the F-type accounted for 0.00, 2.70, 2.70, and 5.41% of the blebs, respectively. One month after the operation, the proportion of H-type filtering blebs was 2.70%. No E-type filtering blebs were observed during the entire follow-up period. There was no statistical difference between the groups ($F = 4.98$, $P = 0.55$) (**Table 5** and **Figure 1**). The appearance of the anterior chamber angle after surgery is presented in **Figure 2**.

Sclera Pool

Hypoechoic images were taken under the scleral flap at different time points after surgery. The length and the height of the scleral pool are shown in **Table 6**. The length and height of the scleral cistern tended to shrink after a longer observation time had elapsed, but the difference was not significant (MAPL: $F = 1.13$, $P = 0.34$; MH: $F = 1.24$, $P = 0.30$) (**Table 6** and **Figure 3**). No significant correlation was observed between IOP and the scleral pool length or height during the entirety of the follow-up period (**Table 7**).

Intraoperative, Postoperative Complications, and Follow-Up

During the operation, 33 eyes were simultaneously threaded circumferentially with the illuminated microcatheter tip. Resistance was encountered in four eyes during the threading process. After withdrawing from the original route, we successfully completed the procedure in the reverse direction. The rate of success was 100%. Intraoperative complications, such as hyphema in the anterior chamber, occurred in all patients, but blood was absorbed within 2 weeks following the operation. During the operation, one eye experienced Descemet's layer detachment with a range of 2 × 3 mm at six points below the cornea. Sterile gas was administered in the anterior chamber after the operation and the patient recovered well.

One eye developed a shallow anterior chamber and a relatively low IOP (9 mmHg) 1 week postoperatively, but the eye was left untreated and recovered after 1 month. Two weeks after surgery, one eye had a flat choroidal detachment, and the IOP was

TABLE 3 | Changes in IOP before and after surgery.

Time point	*n*	IOP (mmHg)		IOP decrease from baseline		*t*	*P*[a]
		Mean ± SD	95% CI	Mean ± SD	95% CI		
Preoperative	37	37.50 ± 8.11	33.78–39.19			–	–
Postoperative							
1 week	37	10.08 ± 2.01	9.60–10.94	26.22 ± 8.12	23.51–28.92	19.644	<0.001
2 weeks	37	10.58 ± 1.76	9.99–11.20	26.13 ± 8.50	23.25–29.00	18.449	<0.001
1 month	37	11.44 ± 1.71	10.42–11.58	25.72 ± 8.38	22.89–28.56	18.412	<0.001
3 months	37	11.57 ± 2.20	10.50–11.99	25.48 ± 8.49	22.60–28.35	18.006	<0.001
6 months	37	11.39 ± 2.10	10.79–12.24	25.52 ± 8.62	22.61–28.44	17.390	<0.001
12 months	37	11.43 ± 2.07	10.82–12.27	25.55 ± 8.36	22.98–28.65	18.011	<0.001

IOP, intraocular pressure; CI, confidence interval.
[a]*Paired t-test was conducted before and after surgery.*

TABLE 4 | Number of medications before surgery and at 3, 6, and 12 months after surgery.

Time point	No. of medication, median (range)	*Z*	*P*[a]
Preoperative	4 (3–5)		
Postoperative			
3 months	0 (0–1)	−5.50	<0.001
6 months	0 (0–1)	−5.50	<0.001
12 months	0 (0–2)	−5.476	<0.001

[a]*Wilcoxon paired signed-rank test between baseline and post-baseline values.*

TABLE 5 | Changes in the filtering bleb morphology after surgery.

Time point	Filtering bleb morphology				*F*	*P*[a]
	L (*n*)	H (*n*)	E (*n*)	F (*n*)		
1 month	36	1	0	0		
3 months	36	0	0	1		
6 months	36	0	0	1		
12 months	35	0	0	2		
					4.98	0.55

L, low-reflective type; H, high-reflective type; E, encapsulated type; F, flattened type.
[a]*Fisher's exact test was used.*

maintained at 7 mmHg. Hypotony maculopathy did not occur, and no special treatment was given except for regular follow-up in the clinic.

In addition, the IOP increased to 42 mmHg in one eye. The ciliary body band was observed with gonioscopy, and UBM images showed hyperechoic reflection under the filtering bleb and scleral flap 3 weeks postoperatively. Interestingly, after the scleral flap suture was released by laser under a slit lamp, the filtering bleb diffused and swelled and the IOP dropped to 9 mmHg. At the last follow-up, the IOP of the patient was 11 mmHg. In addition, four eyes experienced PAS, among which three had synechia under 90° (IOP = 11–13 mmHg) and one underwent 180° adhesion (the IOP fluctuated between 13 and 15 mmHg); no special treatment was administered. The IOP was 21 mmHg in one eye and abated to 14 mmHg at 3 months postoperatively after one anti-glaucoma drug was administered. During the follow-up period, the IOP of another eye peaked at 22 mmHg during a 24-h IOP measurement, with a fluctuation of 11.3 mmHg. The IOP decreased to 13.7 mmHg after treatment with two topical medications. At the last follow-up, no complications (e.g., a thin-walled filtering bleb or filtering bleb leakage) were observed.

Surgical Success Rates

The complete success rates at 3, 6, and 12 months after surgery were 97.29, 97.29, and 94.59%, respectively, according to criterion A; 97.29, 89.19, and 83.78%, respectively, according to criterion B; and 81.08, 75.68, and 72.97%, respectively, according to criterion C. The conditional success rates at 3, 6, and 12 months were 100% for standards A and B and 94.59% for standard C. The Kaplan–Meier survival curve for the complete success rates of standard A–C operations is shown in **Figure 4**.

DISCUSSION

The IOP increase in POAG patients is thought to be caused by the elevated outflow resistance of the aqueous humor at the TM adjacent and distal to the SC. Trabeculotomy can reduce the resistance in the SC and promote drainage of the aqueous humor by opening the TM and SC complex (TM, adjacent SC tissue, and inner SC wall). Thus, it can reduce the IOP in patients with POAG. In the past 10 years, circumferential trabeculotomy has been performed in adult patients with open-angle glaucoma (14). However, only a few reports have been conducted on the effectiveness of a 360° external trabeculotomy in treating adults with POAG or secondary open-angle glaucoma thus far (24). Chin et al. used a modified 360° external suture trabeculotomy to manage adult open-angle glaucoma (25). They discovered that the success rate of this surgery in POAG patients was 84% (IOP < 18 mmHg) 1 year postoperatively. The IOP decreased from 27.8 ± 12.2 to 13.1 ± 3.2 mmHg after the operation, and the average number of medications used also decreased from 2.8 to

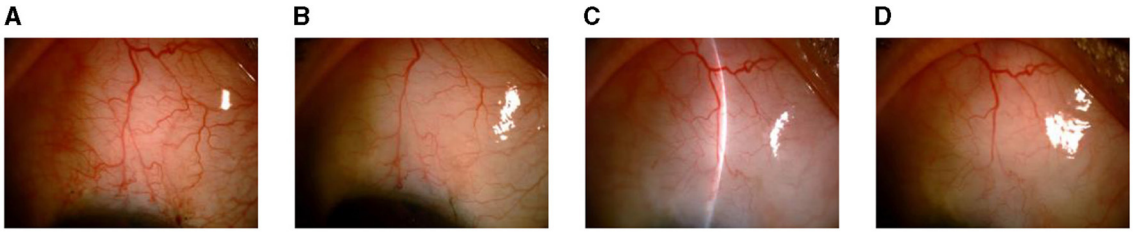

FIGURE 1 | Changes in the filtering blebs in the slit lamp images at different time points after surgery. **(A)** At 1 month after surgery. **(B)** At 3 months after surgery. **(C)** At 6 months after surgery. **(D)** At 12 months after surgery.

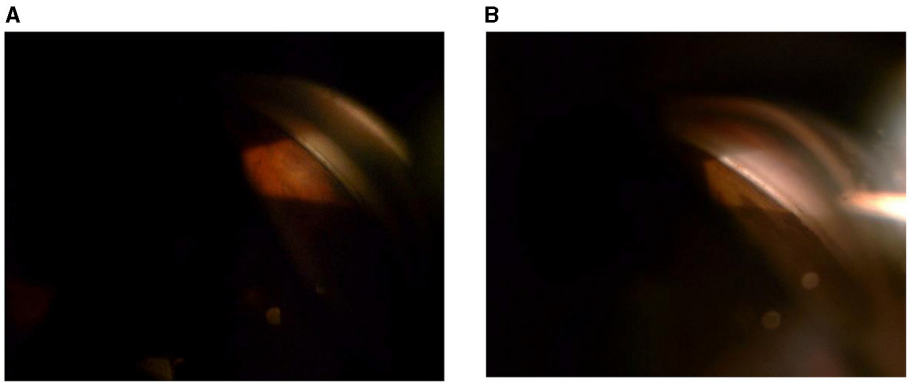

FIGURE 2 | (A,B) Appearance of the anterior chamber angle after microcatheter-assisted trabeculotomy combined with deep sclerectomy and trabeculectomy (MATT-DS-Trab) at 1 month **(A)** and at 12 months **(B)** after surgery.

TABLE 6 | Changes in the scleral lake after surgery.

Time point	MAPL (μm)		MH (μm)	
	Mean ± SD	95% CI	Mean ± SD	95% CI
1 month	3,450.30 ± 495.77	3,285.00–3,615.60	711.81 ± 106.33	676.36–747.26
3 months	3,360.62 ± 482.87	3,199.63–3,521.62	688.95 ± 102.89	654.64–723.25
6 months	3,336.43 ± 479.37	3,176.60–3,496.26	676.22 ± 100.99	642.55–709.89
12 months	3,246.03 ± 466.46	3,090.50–3,401.55	669.03 ± 99.90	635.72–702.34
F	1.13	–	1.24	–
P[a]	0.34	–	0.30	–

MAPL, maximum anteroposterior length; MH, maximum height; CI, confidence interval.
[a]*ANOVA (parametric).*

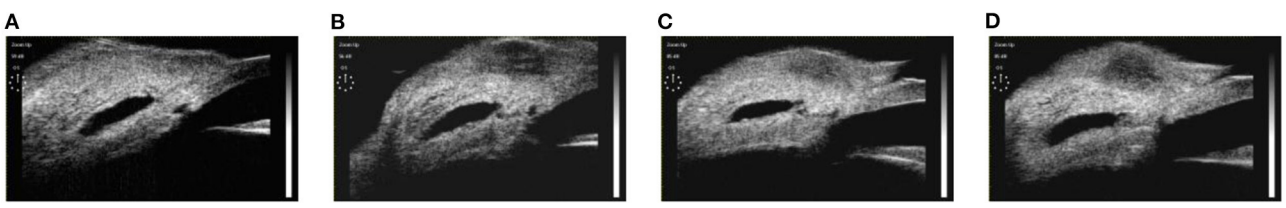

FIGURE 3 | Changes in the scleral reservoirs in ultrasound biomicroscopy (UBM) images at different time points after surgery. **(A)** At 1 month after surgery. **(B)** At 3 months after surgery. **(C)** At 6 months after surgery. **(D)** At 12 months after surgery.

TABLE 7 | Correlations between MAPL, MH, and IOP after surgery.

	Correlation with IOP (mmHg)							
	1 month		3 months		6 months		12 months	
	r	*P*[a]	*r*	*P*[a]	*r*	*P*[a]	*r*	*P*[a]
MAPL (μm)	−0.173	0.306	−0.154	0.364	−0.269	0.107	−0.203	0.228
MH (μm)	−0.223	0.184	−0.193	0.253	−0.147	0.387	−0.184	0.276

MAPL, maximum anteroposterior length; MH, maximum height; IOP, intraocular pressure.
[a]*Spearman's rank correlation coefficient.*

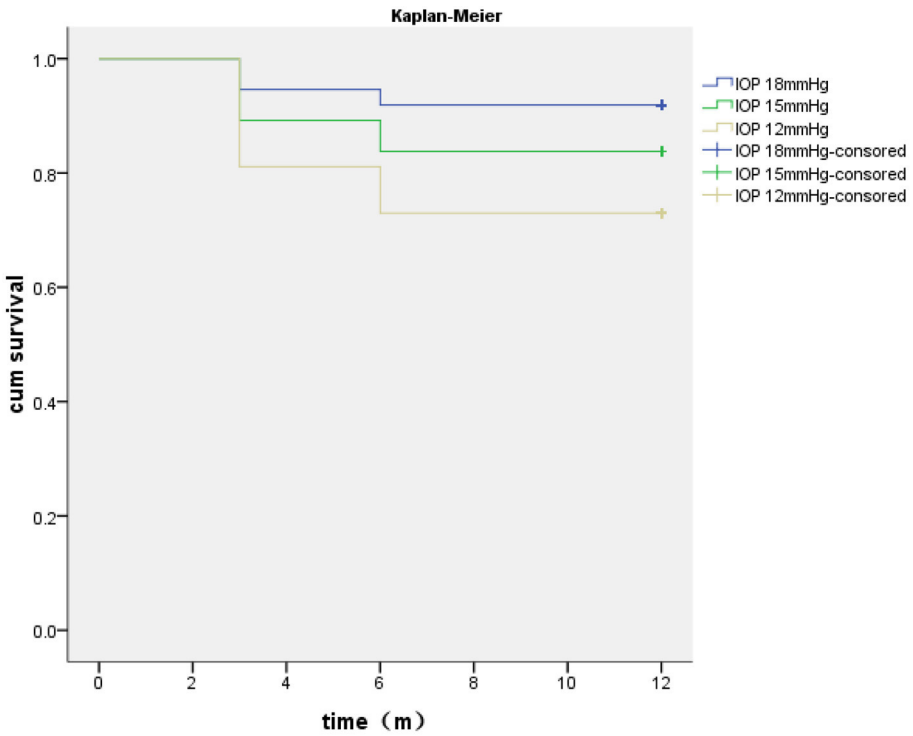

FIGURE 4 | Kaplan–Meier analysis of the surgical complete success rates based on the different intraocular pressure (IOP) criteria.

0.5 postoperatively (25). Shi et al. performed a 1-year follow-up of 22 eyes of patients who were diagnosed with congenital glaucoma and underwent MATT (7). They discovered that the conditional success rate was 86.4% (IOP $\leq$ 21 mmHg). The mean IOP decreased from 33.1 $\pm$ 6.1 to 14.8 $\pm$ 2.5 mmHg after surgery, and the number of drugs the patients used to treat their condition also lessened from three kinds (range = 1–5) to none (range = 0–1) after the surgery (7).

Previous studies have shown that damage to the collector canals in adults with POAG is related to the severity of the disease and the time of onset (26–28). Race, atrophy of the collecting duct in adult patients with POAG, the disease severity, treatment duration, superior scleral venous flow wave, and ocular surface conditions may also influence the effect of SC surgery on the reduction of IOP (29). All the patients who participated in the present study had advanced POAG. The target IOP according to the AGIS was <18 mmHg. However, in a clinical study, the researchers found that the 6-year visual field mean deviation (MD) of patients was lowered by 2.5 dB when the IOP was kept below 15 mmHg; when the IOP was kept below 12.3 mmHg, the visual field remained stable. Palmberg et al. revealed that, when the IOP of patients with advanced glaucoma was controlled at 15 mmHg, the condition worsened over time in 30% of patients (30). The European Glaucoma Society recommends that the target IOP for patients with advanced-stage glaucoma should be <12 mmHg and <10 mmHg for those in terminal stages. Many studies have also shown that maintaining the IOP between 10 and 12 mmHg would be of help to control the progression of glaucoma pathology (31–34).

In view of the characteristics of patients with POAG in China (15), the filtering areas of young patients after glaucoma filtering surgery are more likely to develop scarring and require

a lower target IOP (35). We performed MATT-DS-Trab on our patients, and several key points need to be emphasized regarding this procedure. Firstly, the IOP should be kept as stable as possible during the operation to avoid excessive anterior chamber bleeding. Secondly, the scleral flap should be sufficiently large (5 mm × 5 mm). The scleral pool should not only be large (4 × 4 mm) but also deep enough (the color of the choroid under the scleral bed should be visible). This is in accordance with the methodology of a study performed by Zhang et al. (15) to ensure smooth drainage and filtration of the aqueous humor. When the aqueous humor is stored in a large and deep scleral pool, it is easier to maintain IOP stability for longer periods. Thirdly, trabeculectomy should be performed as soon as possible after catheterization and trabeculotomy in order to maintain anterior chamber stability and reduce the incidence of hyphema and postoperative PAS. The scleral flap was then sutured tightly using two adjustable sutures. It is very important to remove the adjustable sutures within 4 weeks after the operation according to the IOP and the morphology of the filtration blebs. It also makes sense to use MMC during the operation and apply both topical anti-inflammatory drugs and pilocarpine during the perioperative period.

Our results showed that the mean IOP decreased to 11.43 ± 2.07 mmHg at 12 months postoperatively. We inferred that the significant decrease in IOP due to our operation might be caused by the joint promotion of aqueous humor drainage by internal and external channels, including the removal of resistance at the proximal end of the SC, leakage of the deep scleral pool, and suprachoroidal cavity. The broken end of the SC is directly exposed to the internal drainage channel of the anterior chamber, and the external drainage channel of conjunctival filtration promotes the outflow of the aqueous humor, thus reducing IOP. In addition, surgical operation proficiency and perioperative management also influence the success rate and IOP reduction.

UBM is an important method used to evaluate the correlation between aqueous humor outflow and IOP after trabeculectomy and non-penetrating deep sclerectomy (NPDS). In our study, the UBM images clearly showed all the paths under the filtering bleb and scleral flap, suggesting that aqueous filtration occurred and that the trabeculectomy and deep sclerectomy were successful. During the follow-up period, we revealed that the L-type filtering bleb was the main form at all time points, and we did not observe E-type filtering blebs. At 12 months after the operation, the F-type filtering bleb only accounted for 5.41% of blebs. Previous studies have shown that the shape of the filtering blebs is related to IOP control. Ninety-six percent of patients with ideal IOP control after undergoing deep sclerectomy developed L-shaped filtering blebs, which is consistent with the results of our study (22). We disclosed that the length and height of the scleral pool declined over time, but the difference was not statistically significant ($P > 0.05$). Zhang et al. confirmed that IOP in the stable scleral pool group was higher than that in the unstable group 12 and 24 months after CO_2 laser-assisted deep sclerectomy surgery (CLASS) and that the difference was statistically significant (15). In other words, the stability of the scleral cistern after surgery is related to the preoperative IOP. The exact mechanism is still unclear, possibly because a high IOP before the operation causes rapid circulation of liquid after the operation, which causes a "flushing effect" and, thus, results in a more stable scleral pool. In addition, there was no significant correlation between the scleral pool size by UBM and the IOP after surgery. Similar results were determined in the studies by Zhang et al. and Jankowska-Szmul (15, 36). This indicates that the drop in IOP may not depend on the size and shape of the scleral cistern; on the contrary, the presence of the scleral cistern is very important for IOP reduction.

All of the patients enrolled in our study experienced hyphema during the operation, which is consistent with the results of previous studies (25). However, there was only a small amount of bleeding (all <3 mm), which was absorbed within 2 weeks without special treatment. In addition, Chin et al. reported that 47% of patients experienced transient high IOP after circumferential trabeculotomy (25). Some patients with an IOP >30 mmHg must receive additional medication. However, in our study, transient or persistent high IOP was not observed >2 weeks postoperatively, which may be due to the adjustable sutures in all patients during the operation, allowing doctors to regulate the IOP in a timely fashion. This could avoid damage to the optic nerve due to a high IOP or fluctuations in the IOP.

During follow-up, we measured the IOP of one patient climbing to 42 mmHg at 21 days after the operation. The ciliary body band could be observed by gonioscopy, and UBM revealed hyperechoic reflection under a filtering bleb and the scleral flap. After the suture of the scleral flap was released by laser under slit lamp, the filtering bleb was diffused and lifted and the IOP was lowered to 9 mmHg. At the last follow-up, the patient's IOP was recorded as 11 mmHg. In general, whether glaucoma surgery based on SC could work effectively depends primarily on the patency and function of the TM outflow pathway, as well as the collecting tube and its downstream passage near the incision site. This patient had advanced POAG and a C/D of 1.0, and the patient had also been taking medication for a long time before undergoing surgery. Therefore, we speculate that the function of the collecting duct and its downstream pathway may be seriously damaged. It is worth noting that, at the last follow-up, the UBM images showed that more than 90% of the filtering blebs were hypoechoic, and the results of split lamp photography revealed that the filtering blebs were diffuse and protruding. During the entire follow-up period, no thin-walled bleb-related complications were observed.

Our study has several limitations. We did not set up a control group to compare the effects of IOP reduction and the postoperative complications of other types of anti-glaucoma surgeries. The follow-up duration was also limited. Prospective, controlled, randomized multicenter studies with a larger sample size, enrollment of multiple races, and a longer follow-up period are needed to confirm the long-term efficacy and IOP reduction effect of this procedure.

CONCLUSIONS

Microcatheter-assisted trabeculotomy combined with deep sclerectomy and trabeculectomy is based on multichannel

mechanisms and has a good effect on reducing IOP 1 year after the surgery. It is safe and effective in the management of advanced POAG patients with a high success rate, but few serious complications.

DATA AVAILABILITY STATEMENT

The original contributions presented in the study are included in the article/supplementary material, further inquiries can be directed to the corresponding author/s.

ETHICS STATEMENT

The studies involving human participants were reviewed and approved by The ethics committee of Shijiazhuang People's Hospital. The patients/participants provided their written informed consent to participate in this study. Written informed consent was obtained from the individual(s) for the publication of any potentially identifiable images or data included in this article.

AUTHOR CONTRIBUTIONS

All authors listed have made a substantial, direct and intellectual contribution to the work, and approved it for publication.

FUNDING

This study was supported by a grant (no. G2015062) from the Hebei Province Medical Applicable Technology Tracking Project.

ACKNOWLEDGMENTS

The authors thank Dr. Mei Han of Beijing University of Chinese Medicine and PhD Xuejing Zhang of Shijiazhuang People's Hospital for their comments on the manuscript. We also would like to thank Editage (www.editage.cn) for English language editing.

REFERENCES

1. Gedde SJ, Schiffman JC, Feuer WJ, Herndon LW, Brandt JD, Budenz DL. Treatment outcomes in the tube versus trabeculectomy (TVT) study after five years of follow-up. *Am J Ophthalmol.* (2012) 153:789–803. e2. doi: 10.1016/j.ajo.2011.10.026
2. Gedde SJ, Schiffman JC, Feuer WJ, Herndon LW, Brandt JD, Budenz DL. Treatment outcomes in the tube versus trabeculectomy study after one year of follow-up. *Am J Ophthalmol.* (2007) 143:9–22. doi: 10.1016/j.ajo.2006.07.020
3. Gedde SJ, Schiffman JC, Feuer WJ, Herndon LW, Brandt JD, Budenz DL. Three-year follow-up of the tube versus trabeculectomy study. *Am J Ophthalmol.* (2009) 148:670–84. doi: 10.1016/j.ajo.2009.06.018
4. Girkin CA, Marchase N, Cogen MS. Circumferential trabeculotomy with an illuminated microcatheter in congenital glaucomas. *J Glaucoma.* (2012) 21:160–3. doi: 10.1097/IJG.0b013e31822af350
5. Girkin CA, Rhodes L, McGwin G, Marchase N, Cogen MS. Goniotomy versus circumferential trabeculotomy with an illuminated microcatheter in congenital glaucoma. *J AAPOS.* (2012) 16:424–7. doi: 10.1016/j.jaapos.2012.05.013
6. Lim ME, Neely DE, Wang J, Haider KM, Smith HA, Plager DA. Comparison of 360-degree versus traditional trabeculotomy in pediatric glaucoma. *J AAPOS.* (2015) 19:145–9. doi: 10.1016/j.jaapos.2015.01.008
7. Shi Y, Wang H, Yin J, Li M, Zhang X, Xin C, Chen X, Wang N. Microcatheter-assisted trabeculotomy versus rigid probe trabeculotomy in childhood glaucoma. *Br J Ophthalmol.* (2016) 100:1257–62. doi: 10.1136/bjophthalmol-2015-307880
8. Y. El Sayed and G. Gawdat. Two-year results of microcatheter-assisted trabeculotomy in paediatric glaucoma: a randomized controlled study. *Acta Ophthalmol.* (2017) 95:e713–9. doi: 10.1111/aos.13414
9. Luntz MH, Livingston DG. Trabeculotomy ab externo and trabeculectomy in congenital and adult-onset glaucoma. *Am J Ophthalmol.* (1977) 83:174–9. doi: 10.1016/0002-9394(77)90612-2
10. Grover DS, Godfrey DG, Smith O, Feuer WJ, Montes de Oca I, Fellman RL. Gonioscopy-assisted transluminal trabeculotomy, ab interno trabeculotomy: technique report and preliminary results. *Ophthalmology.* (2014) 121:855–61. doi: 10.1016/j.ophtha.2013.11.001
11. Grant WM. Further studies on facility of flow through the trabecular meshwork. *AMA Arch Ophthalmol.* (1958) 60(4 Part 1):523–33. doi: 10.1001/archopht.1958.00940080541001
12. Ellingsen BA, Grant WM. The relationship of pressure and aqueous outflow in enucleated human eyes. *Invest Ophthalmol.* (1971) 10:430–7
13. Johnstone MA, Grant WG. Pressure-dependent changes in structures of the aqueous outflow system of human and monkey eyes. *Am J Ophthalmol.* (1973) 75:365–83. doi: 10.1016/0002-9394(73)91145-8
14. Godfrey DG, Fellman RL, Neelakantan A. Canal surgery in adult glaucomas. *Curr Opin Ophthalmol.* (2009) 20:116–21. doi: 10.1097/ICU.0b013e32831eef65
15. Zhang Y, Cheng G. Modified CO2 laser-assisted sclerectomy surgery in chinese patients with primary open-angle glaucoma and pseudoexfoliative glaucoma: a 2-year follow-up study. *J Glaucoma.* (2020) 29:367–73. doi: 10.1097/IJG.0000000000001460
16. Prum BE Jr, Rosenberg LF, Gedde SJ, Mansberger SL, Stein JD, Moroi SE, et al. Primary open-angle glaucoma preferred practice pattern((R)) guidelines. *Ophthalmology.* (2016) 123: P41–P111. doi: 10.1016/j.ophtha.2015.10.053
17. Kim NR, Lee ES, Seong GJ, Kim JH, An HG, Kim CY. Structure-function relationship and diagnostic value of macular ganglion cell complex measurement using Fourier-domain OCT in glaucoma. *Invest Ophthalmol Vis Sci.* (2010) 51:4646–51. doi: 10.1167/iovs.09-5053
18. Salimi A, Nithianandan H, Al Farsi H, Harasymowycz P, Saheb H. Gonioscopy-assisted transluminal trabeculotomy in younger to middle-aged adults: one-year outcomes. *Ophthalmol Glaucoma.* (2021) 4:162–72. doi: 10.1016/j.ogla.2020.08.014
19. Zhang H, Tang G, Liu J. Effects of phacoemulsification combined with goniosynechialysis on primary angle-closure glaucoma. *J Glaucoma.* (2016) 25:e499–503. doi: 10.1097/IJG.0000000000000297
20. Shi Y, Wang H, Oatts J, Cao K, Xin C, Liang X, et al. Ab interno vs ab externo microcatheter-assisted trabeculotomy for primary congenital glaucoma with clear cornea. *Clin Exp Ophthalmol.* (2020) 48:1201–9. doi: 10.1111/ceo.13868
21. Yan X, Zhang H, Li F, Ma L, Geng Y, Tang G. Surgical site characteristics after CLASS followed by ultrasound biomicroscopy and clinical grading scale: a 2-year follow-up. *Eye.* (2020) 35:2283–93. doi: 10.1038/s41433-020-01235-w
22. Yamamoto T, Sakuma T, Kitazawa Y. An ultrasound biomicroscopic study of filtering blebs after mitomycin C trabeculectomy. *Ophthalmology.* (1995) 102:1770–6. doi: 10.1016/s0161-6420(95)30795-6
23. Warjri GB, Sidhu T, Kishan A, Behera AK, Shakrawal J, Selvan H, et al. Achieving low target intraocular pressures in severe glaucoma. *Eur J Ophthalmol.* (2020) 8:1–6. doi: 10.1177/1120672120979903

24. Elhusseiny AM, El Sayed YM, El Sheikh RH, Gawdat GI, Elhilali HM. Circumferential Schlemm's canal surgery in adult and pediatric glaucoma. *Curr Eye Res.* (2019) 44:1281–90. doi: 10.1080/02713683.2019.1659975
25. Chin S, Nitta T, Shinmei Y, Aoyagi M, Nitta A, Ohno S, et al. Reduction of intraocular pressure using a modified 360-degree suture trabeculotomy technique in primary and secondary open-angle glaucoma: a pilot study. *J Glaucoma.* (2012) 21:401–7. doi: 10.1097/IJG.0b013e318218240c
26. Fellman RL, Grover DS. Episcleral venous fluid wave: intraoperative evidence for patency of the conventional outflow system. *J Glaucoma.* (2014) 23:347–50. doi: 10.1097/IJG.0b013e31827a06d8
27. Aktas Z, Ozmen MC, Atalay HT, Ucgul AY. Evaluation of episcleral venous fluid wave during gonioscopy assisted transluminal trabeculotomy in patients with advanced glaucoma. *Eye.* (2019) 33:668–73. doi: 10.1038/s41433-018-0254-5
28. Brian AF, Steven RS, James CT. *Minimally Invasive Glaucoma Surgery*. New York, NY: Thieme Medical Publishers (2017).
29. Aktas Z, Ucgul AY, Bektas C, Sahin Karamert S. Surgical outcomes of prolene gonioscopy-assisted transluminal trabeculotomy in patients with moderate to advanced open-angle glaucoma. *J Glaucoma.* (2019) 28:884–8. doi: 10.1097/IJG.0000000000001331
30. Palmberg P. Evidence-based target pressures: how to choose and achieve them. *Int Ophthalmol Clin.* (2004) 44:1–14. doi: 10.1097/00004397-200404420-00003
31. Burr J, Azuara-Blanco A, Avenell A, Tuulonen A. Medical versus surgical interventions for open angle glaucoma. *Cochrane Database Syst Rev.* (2012) 12:CD004399. doi: 10.1002/14651858.CD004399.pub3
32. Sihota R, Rao A, Srinivasan G, Gupta V, Sharma A, Dada T, Kalaiwani M. Long-term scanning laser ophthalmoscopy and perimetry in different severities of primary open and chronic angle closure glaucoma eyes. *Indian J Ophthalmol.* (2017) 65:963–8. doi: 10.4103/0301-4738.216734
33. Gazzard G, Foster PJ, Devereux JG, Oen F, Chew P, Khaw PT, Seah S. Intraocular pressure and visual field loss in primary angle closure and primary open angle glaucomas. *Br J Ophthalmol.* (2003) 87:720–5. doi: 10.1136/bjo.87.6.720
34. Sharmini AT, Yin NY, Lee SS, Jackson AL, Stewart WC. Mean target intraocular pressure and progression rates in chronic angle-closure glaucoma. *J Ocul Pharmacol Ther.* (2009) 25:71–5. doi: 10.1089/jop.2008.0061
35. Wang Y, Sun XH, Meng FR, Wang JJ. [The failure causes of non-penetrating trabecular surgery and reoperation]. *Zhonghua Yan Ke Za Zhi.* (2003) 39:87–90.
36. Jankowska-Szmul J, Wylegala E. The CLASS surgical site characteristics in a clinical grading scale and anterior segment optical coherence tomography: a one-year follow-up. *J Healthc Eng.* (2018) 2018:5909827. doi: 10.1155/2018/5909827

Conflict of Interest: The authors declare that the research was conducted in the absence of any commercial or financial relationships that could be construed as a potential conflict of interest.

Publisher's Note: All claims expressed in this article are solely those of the authors and do not necessarily represent those of their affiliated organizations, or those of the publisher, the editors and the reviewers. Any product that may be evaluated in this article, or claim that may be made by its manufacturer, is not guaranteed or endorsed by the publisher.

frontiers in Medicine

REVIEW
published: 13 September 2021
doi: 10.3389/fmed.2021.733080

Glaucoma Clinical Research: Trends in Treatment Strategies and Drug Development

Line Storgaard[1], *Thuy Linh Tran*[2], *Josefine Clement Freiberg*[1], *Alexander S. Hauser*[1] *and Miriam Kolko*[1,2]*

[1] Department of Drug Design and Pharmacology, University of Copenhagen, Copenhagen, Denmark, [2] Department of Ophthalmology, Copenhagen University Hospital, Rigshospitalet-Glostrup, Copenhagen, Denmark

OPEN ACCESS

Edited by:
Michele Lanza,
University of Campania Luigi Vanvitelli, Italy

Reviewed by:
Riccardo Sacco,
Politecnico di Milano, Italy
Annagrazia Adornetto,
University of Calabria, Italy
Jamss Tsai,
Icahn School of Medicine at Mount Sinai, United States
Daniela Montorio,
Federico II University Hospital, Italy

***Correspondence:**
Miriam Kolko
miriamk@sund.ku.dk

Specialty section:
This article was submitted to Ophthalmology, a section of the journal Frontiers in Medicine

Received: 29 June 2021
Accepted: 11 August 2021
Published: 13 September 2021

Citation:
Storgaard L, Tran TL, Freiberg JC, Hauser AS and Kolko M (2021) Glaucoma Clinical Research: Trends in Treatment Strategies and Drug Development. Front. Med. 8:733080. doi: 10.3389/fmed.2021.733080

Purpose: To investigate the trends and progresses in glaucoma research by searching two major clinical trial registries; clinicaltrials.gov, and australianclinicaltrials.gov.

Methods: All clinical trials with glaucoma covered by Clinicaltrials.gov, and Australianclinicaltrials.gov starting the study before 1 January 2021 were included. Trials evaluating glaucoma treatment were separated from non-treatment trials and divided into three major categories: "laser treatment," "surgical treatment," and "medical treatment." In the category of "medical treatment," new compounds and their individual targets were identified and subcategorized according to treatment strategy; intraocular pressure (IOP)-lowering, neuroprotective or vascular. The phase transition success rates were calculated.

Results: One-thousand five hundred and thirty-seven trials were identified. Sixty-three percent ($n = 971$) evaluated glaucoma treatment, of which medical treatment accounted for the largest proportion (53%). The majority of medical trials evaluated IOP-lowering compounds, while trials with neuroprotective or vascular compounds accounted for only 5 and 3%, respectively. Eighty-eight new compounds were identified. Phase I, II, and III transition success rates were 63, 26, and 47%, respectively.

Conclusion: The number of clinical trials in glaucoma research has increased significantly over the last 30 years. Among the most recently evaluated compounds, all three main treatment strategies were represented, but clinical trials in neuroprotection and vascular modalities are still sparse. In addition to traditional medicines, dietary supplements and growth factors are assessed for a potential anti-glaucomatous effect. Phase II and III success rates were below previously reported success rates for all diseases and ophthalmology in general. A stricter phenotyping of patients can improve the success rates in glaucoma and ophthalmological research and gain a better understanding of responders and non-responders.

Keywords: glaucoma, clinical trials, trends, treatment, drug development

INTRODUCTION

Glaucoma is one of the leading causes of global irreversible blindness, and the prevalence is increasing (1, 2). Glaucoma is characterized by a progressive degeneration of the optic nerve with corresponding visual field loss and ultimately blindness if left untreated. The pathophysiology of glaucoma is multifactorial and there are several clinical phenotypes (3). In short, glaucoma can be divided into primary glaucoma, secondary glaucoma and the rarer forms of juvenile and congenital glaucoma. Within primary glaucoma, there are two clinical phenotypes, open-angle glaucoma (POAG) and angle-closure glaucoma. In all glaucoma subtypes, elevated intraocular pressure (IOP) is recognized as a major risk factor for the development and progression of glaucoma and lowering IOP is currently the only documented method of treating glaucoma.

Numerous trials are being conducted around the world to examine glaucoma with the aim of improving glaucoma diagnosis, management, and treatment of the disease. Among these, clinical trials evaluating either medical, surgical, or behavioral intervention are of great interest. Clinical trials advance through four phases to test a particular treatment, find an appropriate dose of a given drug, and evaluate side effects of the treatment. When U. S. Food and Drug Administration (FDA) or a similar ruling authority decide whether a drug should be approved, Phase I, II, and III trials are usually conducted in advance. Phase IV trials are post-marketing or surveillance studies performed to monitor adverse reactions, safety, long-term risks, benefits and efficacy in large and diverse populations over several years (4).

The first interventional glaucoma trial dates back to 1978, according to the database ClinicalTrails.gov, whereas the first article listed in PubMed based on a clinical trial was published in 1961 (5). Various aspects of glaucoma are evaluated in clinical trials, including diagnostic tests, procedures, devices, drugs, and behavioral factors. This paper presents data on all clinical trials of glaucoma covered by the two major trials registers clinicaltrials.gov and australianclinicaltrials.gov.au. ClinicalTrials.gov is a database provided by the U.S. national Library of Medicine at the National Institutes of Health. It provides information on both privately and publicly funded clinical studies and provides access to summary information and trial results on a wide range of diseases and conditions (6). australianclinicaltrials.gov.au is a joint initiative between the National Health and Medical Research Council and the Department of Industry, Innovation and Science in Australia (7). The Australian registry was included to ensure that clinical trials conducted at Melbourne Centre for Eye Research Australia would be covered by this review. We were aware that important trials evaluating the role of vitamin B3 supplementation in treating glaucoma did not appear in the registry clinicaltrials.gov.

All new compounds evaluated for the treatment of glaucoma and their individual targets are presented with the aim of showing the trends in drug development over the last decades. The objective of this paper is to provide an overview of the different types of glaucoma treatments and to investigate whether the strategies and targets in glaucoma drug development have changed over time. Furthermore, this paper examines how the different compounds perform in progressing through the different phases of clinical trials. Additional, personalized medicine and mathematical modeling are discussed as potential strategies to improve the possibility of successful glaucoma therapy in the future.

Treatment of Glaucoma

Glaucoma treatment falls into three basic categories: laser treatment, incisional surgery, and medication (8, 9).

Laser treatment can be used in several ways to treat glaucoma: targeting the trabecular meshwork and thereby reducing IOP; performing peripheral laser iridotomy to prevent pupillary block; ablating the ciliary processes to reduce production of aqueous humor; and facilitating surgical procedures, such as trabeculectomy (10, 11).

Argon laser trabeculoplasty (ALT) was introduced as a treatment modality by Wise and Witter in 1979 (12), and ∼20 years later in 1998, selective laser trabeculoplasty (SLT) was introduced by Latina et al. SLT is currently the most frequently used and accepted laser therapy in the treatment of POAG (13). Most clinical trials regarding glaucoma laser treatment registered in clinicaltrials.gov evaluate traditional laser modalities, whereas more recently micropulse laser trabeculoplasty and micropulse transscleral cyclophotocoagulation have been evaluated in clinical trials (14, 15).

Surgery is typically performed when non-invasive efforts (maximal tolerated medical therapy and/or laser trabeculoplasty) have not reached target IOP levels. Trabeculectomy is currently the most frequently performed glaucoma filtration procedure. Recently, less invasive glaucoma procedures, such as minimally invasive glaucoma surgery (MIGS), have gained popularity with new devices entering the market on a regular basis (13, 16). Recent trials have focused on examining the outcomes of conventional glaucoma surgery, including trabeculectomy and glaucoma drainage devices. In addition, the use of minimally invasive devices for glaucoma surgery devices has been investigated.

Medical treatment (e.g., topical eye drops) is considered a reasonable first choice of therapy in published guidelines for the treatment of POAG (17, 18). Clinicians usually prescribe a single drug selected from one of four drug classes—prostaglandin analogs (PGAs), beta-blockers, carbonic anhydrase inhibitors, and alpha-2 adrenergic agonists. Furthermore, miotic drugs can be an alternative, but are now almost never used as a first-line treatment due to side effects (19).

History of Glaucoma Pharmacology

The history of glaucoma pharmacology began almost 150 years ago. Cholinergic drugs, also known as parasympathomimetics or miotics, were the first class of drugs used to treat glaucoma. Eserine (physostigmine) was the first glaucoma drug, a cholinergic agonist from 1876. Pilocarpine, the second miotic, was launched just a year later and showed fewer adverse events and was thus better tolerated by patients (20). Osmotic agents were added to the list of available agents in the early 1900s (21).

The second class of IOP-lowering drugs, the adrenergic agonist, debuted with epinephrine in 1901. Epinephrine first became commercially available for glaucoma in the 1950s, followed shortly after by clonidine (20). Systemic carbonic anhydrase inhibitors were introduced in 1954 (22), but patients experienced a number of side effects. Topical formulations of the systemic carbonic anhydrase inhibitors were attempted to be prepared, but the formulations at that time had little or no effect on IOP (20).

In the early 1960s, propranolol was discovered and became the first commercially successful beta-blocker (23). The IOP-lowering effects of beta-adrenergic antagonists were discovered in 1967. However, the drug was not available as a topical agent due to corneal anesthetic properties and a negative effect on tear production (20). A decade later, timolol became available in 1978 (24). For a while, topical beta-blockers became the most prescribed anti-glaucomatous treatment until prostaglandin analogs were introduced on the market. The alpha-adrenergic agonist apraclonidine, a derivative of clonidine that is highly selective for the alpha2 receptor, was introduced around 1987. In 1996, brimonidine reached the market and largely replaced apraclonidine as the preferred adrenergic agonist for glaucoma.

In 1995, after many years of research, dorzolamide, a topical carbonic anhydrase inhibitor, finally reached the market following FDA approval. Today, dorzolamide is still widely used in the clinic (25). In the mid-1990s, prostaglandin analogs revolutionized the medical treatment of glaucoma (26, 27). Latanoprost was the first prostaglandin analog to receive FDA approval in 1996. Hereafter, bimatoprost, travoprost, tafluprost and the partial agonist unoprotone were subsequently approved (27). In 2017, a nitric oxide-donating prostaglandin analog, latanoprostene bunod (27) was approved by FDA.

Preservatives used in topical glaucoma medications may have toxic effects on the ocular surface, especially in patients receiving a multiple drop regimen (28, 29). In particular, the adverse effects of by far the most common preservative benzalkonium chloride (BAK) are well-described (30, 31). In recent decades, several glaucoma eye drops have been reformulated into preservative-free versions, and some have changed preservatives. A challenge of preservative-free formulations is the absence of an antimicrobial effect and thus an increased risk of contamination (28). Single-dose units are therefore frequently used as alternative but are more expensive and can be difficult to handle. Newer multi-dose formulations have been developed which dispense droplets either by a non-return valve or a filtration systems to ensure sterility after opening (28).

A new class of glaucoma drugs and the first major innovation in glaucoma therapy after 2000s were signaled by the approval of the first Rho kinase inhibitors, ripasudil in Japan in 2014 followed by netarsudil in the U.S in 2017 (32) and by European Medicine Agency (EMA) in 2019. The combination therapy netarsudil/latanoprost was approved by the FDA in 2019 and by the EMA in January 2021. Currently, the combination of ripasudil with the alpha2 agonist brimonidine (started Phase III in Japan February 2020) and the combination of ripasudil (or netarsudil) with sepetaprost (32) are in the pipeline.

Neuroprotection in Glaucoma

Current available therapies for glaucoma have the primary aim of reducing IOP without directly addressing the associated optic neuropathy and retinal ganglion cell loss (33, 34).

Although lowering IOP is the primary treatment target in glaucoma management, there is a growing interest in neuroprotective strategies, as reducing IOP is often not sufficient to slow disease progression.

Neuroprotection in glaucoma refers to non-IOP-related interventions that prevent or delay glaucomatous neurodegeneration independent of IOP. Neuroprotection for glaucoma has been demonstrated in several animal models (35). So far, however, no relevant effect has been demonstrated in clinical trials in humans. Memantine, an N-methyl-d-aspartate antagonist, has been shown to be effective in neurodegenerative disorders but has no effect in glaucoma. A comprehensive phase 3 randomized multicenter clinical trial lasting more than 5 years at significant costs did not reveal benefits for memantine treatment by preventing the progression of visual field loss in glaucoma patients (36). Brimonidine, an α2-adrenoreceptor agonist widely distributed in the retina and anterior segment of the eye, may slow visual field deterioration, but a randomized controlled trial comparing 0.2% brimonidine with 0.5% timolol did not provide convincing evidence (37).

Ocular Blood Flow in Glaucoma

It has been suggested that changes in ocular blood flow may alter the retinal functions affecting the prognosis for glaucoma. Several studies have shown a reduction of ocular blood supply in patients with both preperimetric as well as advanced glaucoma, suggesting an association between reduction in blood flow and glaucomatous damage (38–40). Abnormalities in retinal blood flow may play a role in the etiology of glaucoma, but the underlying pathophysiological mechanisms are still uncertain. Furthermore, only a limited proportion of patients with vascular deficiency develop glaucoma, and therefore vascular dysregulation is thought to be only one of many risk factors for developing glaucoma (41).

Dietary Supplements

A number of trials are investigating the potential beneficial anti-glaucomatous effects of dietary supplements. Dietary supplements include vitamins, minerals, herbs, amino acids, and enzymes. Dietary supplements are not intended for the treatment, diagnosis, prevention or cure of diseases (42). Unlike pharmaceutical products, which must be proven safe and effective by regulatory authorities before marketing, manufacturers, and distributors of dietary supplements are solely responsible for ensuring that their products are safe before entering the market.

METHODS

An in-dept query on Clinicaltrials.gov and Australianclinicaltrials.gov.au was performed using the keyword "glaucoma" and all registered trials were included. We did not

distinguish between investigational and observational trials. Data were extracted January 2021. All trials were sorted by start date of the study and grouped into time intervals: before 2000, 2000–2004, 2005–2009, 2010–2014, 2015–2019, and 2020. Based on the details of the study record, we separated studies regarding treatment of glaucoma from non-treatment studies. We included studies evaluating medical treatment aimed at other diseases than glaucoma, but with a possible secondary effect on IOP. These studies were not included in the figures, but the numbers are shown in the tables.

The non-treatment group included studies that assessed quality of life, adherence, diagnostic methods, and epidemiology.

The treatment group was further sub-divided into laser treatment, surgical treatment, or medical treatment. For all trials evaluating medical treatment, we identified the specific compound being evaluated. We distinguished between compounds already approved for the treatment of glaucoma and new compounds, including repurposed drug candidates. New compounds were subcategorized according to treatment strategy; IOP-lowering, neuroprotective, or agents that act on microvascular blood flow. Trials characterized as vascular research included studies that analyzed the following parameters: retinal or choroidal blood flow, optic disc blood flow, or retrobulbar vascular resistance.

We recorded recruitment status and phase for each trial. Target information for all new compounds was collected from the online resources Drugbank, Open Targets and from the literature (43, 44). A new compound was defined successful if it went from one phase to the next. Trials registered with the following recruitment status were defined as ongoing: "Not yet recruiting," "recruiting," "enrolling by invitation," "active, not recruiting," and "unknown." New compounds were defined as treatment with the indication of glaucoma approved after 2015. Ongoing trials and trials completed within 2 years were considered potentially successful and categorized as such. However, compounds evaluated in ongoing trials with a start date of the study more than 4 years ago were marked as unsuccessful in the success calculation due to an expected duration of maximum 4 years of a clinical trial (45). Success rates were calculated per phase. By calculating the number of compounds that advance to the next phase vs. the total number of compounds per phase, we assessed the success rate at each of the three development phases. The phase transition success rates per phase were compared with previously reported success rates for clinical drug development (46).

RESULTS

A total of 1,537 trials were identified. One-thousand five hundred and twenty-three trials were identified in the ClinicalTrials database, and in addition, 14 trials were identified in the Australian Clinical Database. The majority of all trials evaluated glaucoma treatment (n = 971, 63%, **Figure 1A**). Within the treatment group, trials of medical treatment dominated, covering a total of 55% (**Figure 1B**; **Table 1**). Medical trials accounted for the majority of the trials for a long time. From 2015 to 2019, the proportion of trials evaluating surgery increased, and by 2020, the balance shifted, and trials investigating surgical treatment dominated by 63% of the total numbers of trials. Clinical trials with laser treatment accounted for a small proportion of all trials. The percentage of laser trials has been slightly increasing over time and ranges from 4% in 2000–2004 to 12% in 2015–2019.

Most studies evaluated the IOP-lowering effect as primary efficacy outcome (**Table 2**). Overall, 92% of the trials registered in the two databases evaluated IOP, ranging from 69% (before 2000) to 95% (2010–2014). An increasing number of trials evaluating neuroprotective strategies have been registered, reaching 13% in 2015–2019, but overall, this subgroup of studies accounts for only a small proportion of the total number of trials (5%) over time. Evaluation of vascular targets or compounds represented 11% of the studies in 2020–2021 with an overall representation of 3% over time.

We identified 88 new compounds including supplements and a few compounds that investigated a secondary IOP-lowering effect of non-glaucoma treatment (**Figures 2**, **3**). The compounds were sorted by category, phase, drug name and target. Most drug candidates are named, while others are listed with codes used by individual pharmaceutical companies. 11 compounds are labeled "unknown" as the mode of action is unknown.

Due to differences in the regulation of dietary supplements and drugs, we present dietary supplements separately in **Figure 3**. **Figure 3** also includes trials evaluating growth factors and stem cell therapy. A total of 20 compounds were categorized as supplement, stimulants, or transplants (**Figure 3**).

Figure 4 shows recently approved glaucoma treatments (approved within 5 years, $n = 4$) along with pipeline compounds defined as candidates seen in clinical trials with study start date of the study within the last 4 years ($n = 16$).

The success rates for the transition of the drug development phase were 63% in phase I, 26% in phase II and 47% in phase III (**Table 3**; **Figure 5**). The number of compounds that succeed decreases during each phase.

DISCUSSION

Pipeline Drugs and Tendencies in Glaucoma Clinical Trials

The number of clinical trials evaluating both non-treatment and treatment of glaucoma has increased significantly over the last 30 years. There is a tendency for relatively fewer clinical trials of medical treatment compared to surgical and laser treatment. However, medical treatment is still an essential part of glaucoma treatment, and several trials are assessing traditional and new approaches to medical treatment. We found 105 different drug targets, but these targets compromise only a small proportion of the possible drug targets of glaucoma, as there are more than 2,700 possible targets associated with glaucoma (48). We identified 88 new compounds, 22 of which are of particular interest, as they are either recently approved for glaucoma treatment or possible future candidates (**Figure 4**). The compounds listed in **Figure 4** are discussed below.

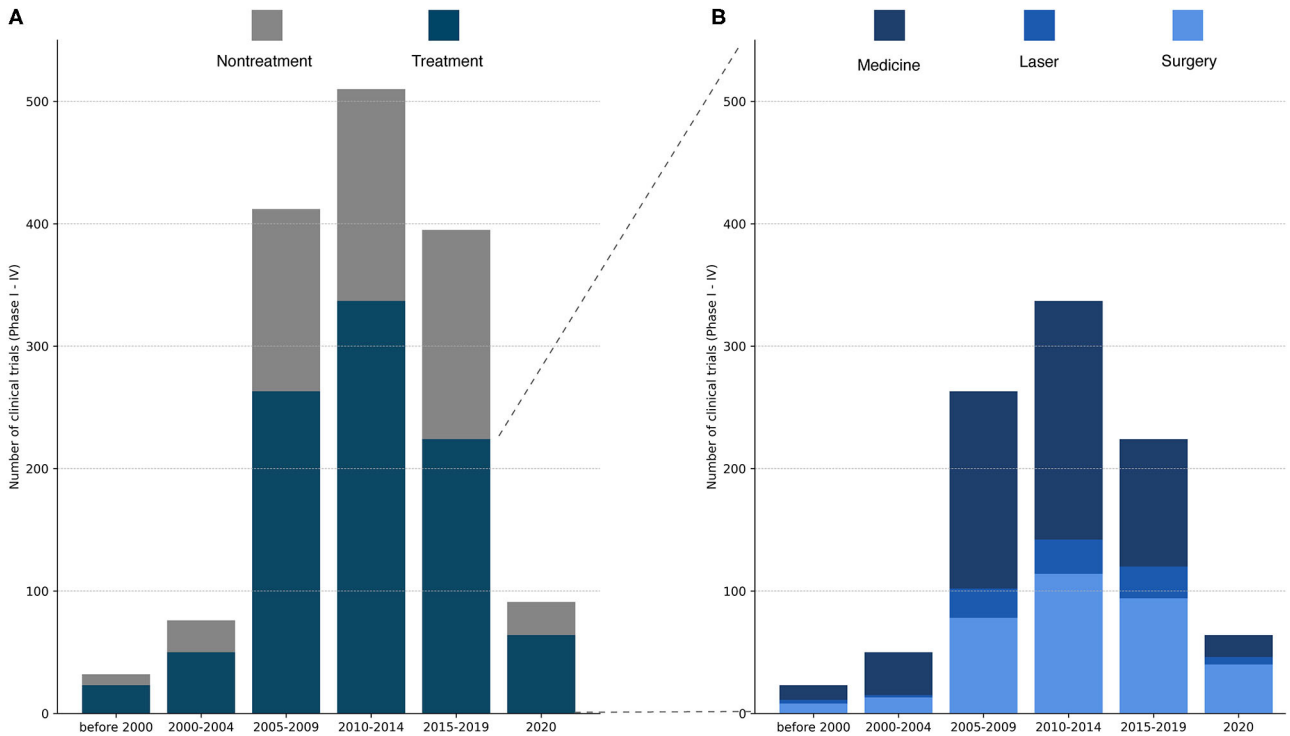

FIGURE 1 | (A) Total number of registered glaucoma clinical trials (Phase I–IV) over time. Each study was categorized as treatment or non-treatment. The number of clinical trials increased dramatically from 2000–2004 to 2005–2009, peaking in 2010–2014 and declining in 2025–2019. Of important note, the last column contains only trials from 2020, while the other columns cover a period of at least 4 years. **(B)** Total number of registered clinical trials in the treatment group divided into medical treatment, laser treatment or surgical treatment. Medical treatments constitute the majority of the assessed glaucoma treatments except from 2020, where surgery was the most frequently evaluated treatment in glaucoma trials.

TABLE 1 | Total number of registered glaucoma clinical trials listed for surgery, laser and medical treatment with total number of trials (*n*, %).

Year	Surgery	Laser	Medicine
Before 2000	8 (33%)	3 (13%)	13 (54%)
2000–2004	13 (25%)	2 (4%)	36 (71%)
2005–2009	78 (30%)	24 (9%)	161 (61%)
2010–2014	114 (34%)	27 (8%)	197 (58%)
2015–2019	94 (42%)	26 (12%)	104 (46%)
2020	40 (63%)	6 (9%)	18 (28%)
Total	347 (36%)	88 (9%)	529 (55%)

In total 347 (36%) trials examined surgery, 88 (9%) examined laser treatment, and 529 (55%) examined medical treatments. In 2020, surgery was the most frequently examined treatment of glaucoma trials, while prior medical treatment accounted for the majority of trials. Laser treatment consistently covered 4–13% of glaucoma trials.

TABLE 2 | Trials evaluating glaucoma medical treatment categorized by treatment strategy: IOP lowering, vascular or neuroprotective.

Year	IOP lowering	Vascular	Neuroprotective
Before 2000	9 (69%)	2 (15%)	2 (15%)
2000–2004	33 (92%)	2 (6%)	1 (3%)
2005–2009	152 (94%)	4 (2%)	5 (3%)
2010–2014	187 (95%)	4 (2%)	6 (3%)
2015–2019	89 (86%)	1 (1%)	14 (13%)
2020	15 (79%)	2 (11%)	1 (5%)
Total	485 (92%)	15 (3%)	29 (5%)

IOP-lowering agents cover the vast majority of clinical trials in glaucoma. A total of 485 (92%) evaluated IOP-lowering treatments, 15 (3%) evaluated drugs acting on microvascular blood flow, and 29 (5%) trials examined neuroprotective treatments.

Prostaglandin Analogs and NO-Donating Prostaglandin Analogs

Prostaglandin analogs (PGAs) reduce IOP by targeting prostaglandin F receptor (PTGFR) and prostaglandin E receptor (PTGER 1-4) to increase the outflow of aqueous humor primarily through the uveoscleral pathway, but significant effects have also been reported on trabecular outflow facility (27, 49, 50). Several PGAs have been evaluated in clinical trials over the past decades to find new PGAs with improved tolerability and therapeutic benefits. Omidenepag Isopropyl (DE-117) is a selective PTGER2 agonist currently under development for the treatment of glaucoma and ocular hypertension (OHT) (51–53). Based on results from phase III trials, it received approval in Japan in September 2019 for this indication (53, 54). In February 2021, Santen and Ube Industries announced that the

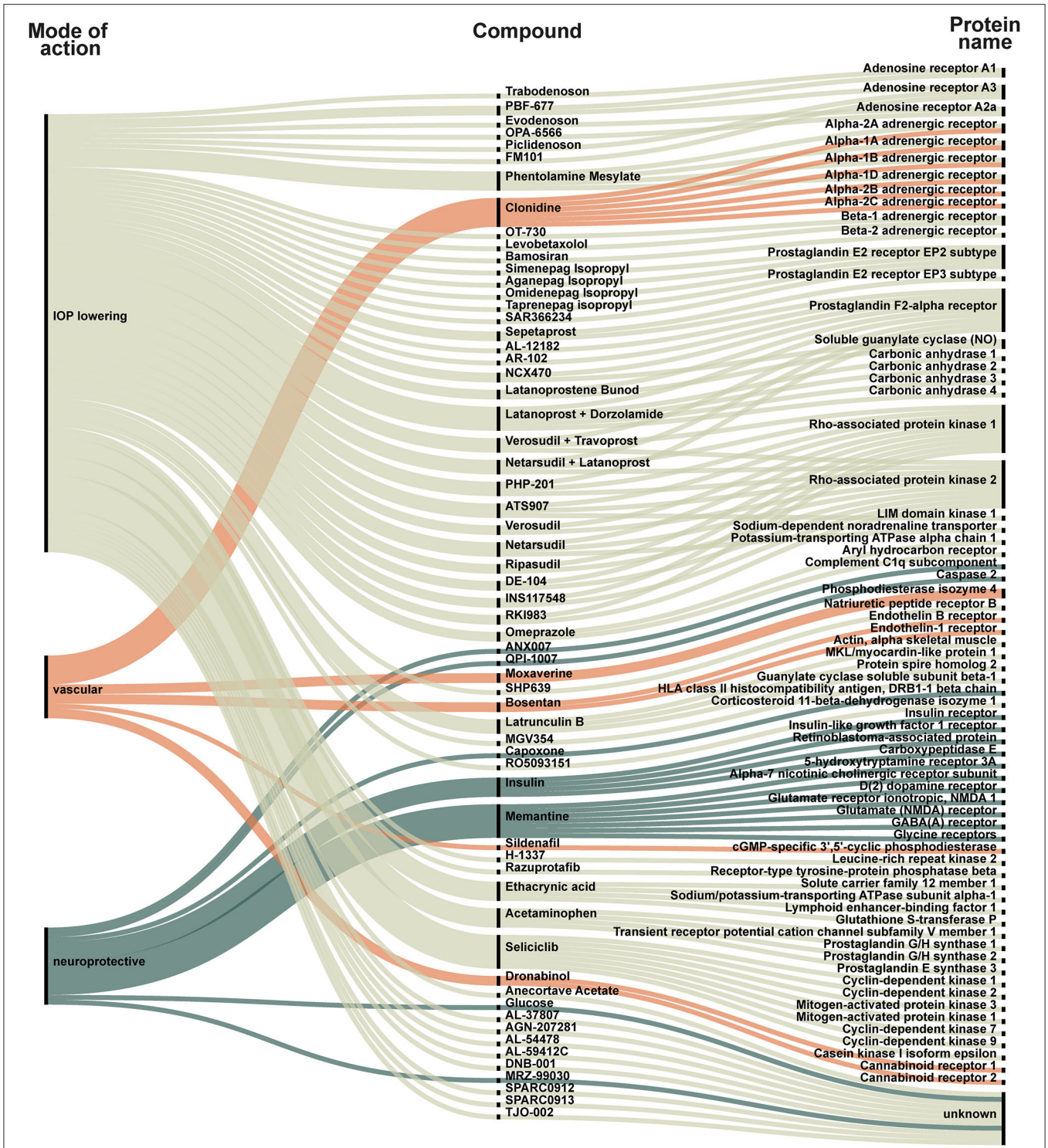

FIGURE 2 | New compounds represented in all included trials. Each compound is categorized as IOP-lowering (light green), vascular (orange) or neuroprotective (dark green). The compound is linked to its target. The targets are listed to the right and visualize how some compounds act on several targets. For example: (1) Trabodenoson is an IOP-lowering compound that targets adenosine receptor A1; (2) Clonidine is a vascular compound targeting six different alpha-adrenergic receptors (1A, 1B, 1D, 2A, 2B, and 2C); (3) Insulin is a neuroprotective compound that acts on insulin receptor, insulin-like growth factor 1 receptor, retinoblastoma-associated protein, and carboxypeptidase E.

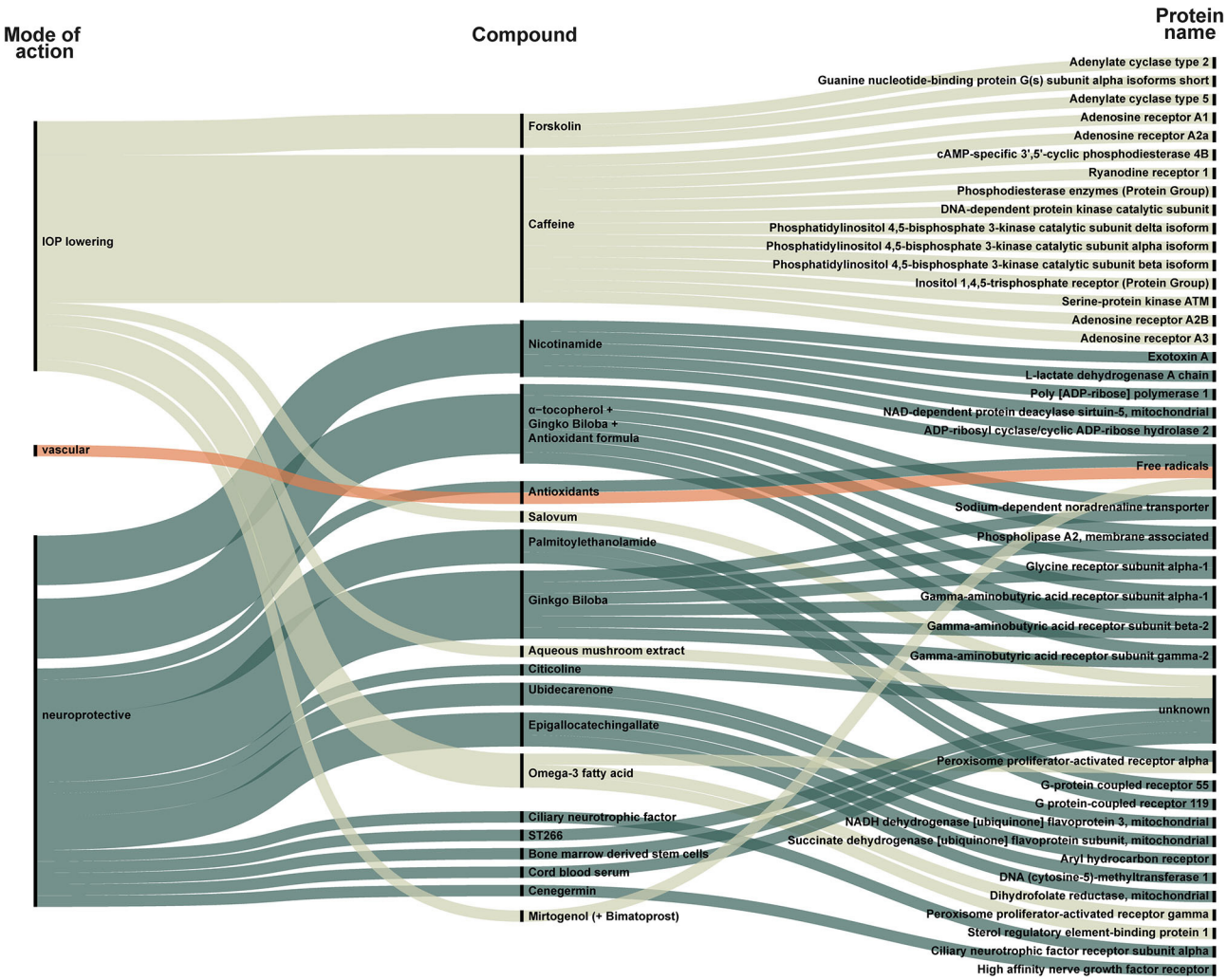

FIGURE 3 | New compounds classified as supplements, stimulants, or transplant identified in all included trials. Each compound is categorized as IOP-lowering (light green), vascular (orange), or neuroprotective (dark green). The compound is linked to its target. The targets are listed to the right and visualize how some compounds act on several targets. For example, forskolin is an IOP-lowering compound that targets adenylate cyclase type 2, G(s) subunit alpha-isoforms short, and adenylate cyclase type 5. Only one group of vascular compounds, namely antioxidants, that act on free radicals, is represented.

FDA had accepted the New Drug Application for Omidenepag Isopropyl (55).

Sepetaprost is a prodrug that is hydrolyzed by esterase to its active metabolite. It was developed as a dual agonist of PTGFR and PTGER3, in contrast to the classical PGAs, which function primarily through PTGFR (56, 57). With this new dual-mechanism approach, IOP reduction may be improved. A phase IIb dose-finding study was completed in 2018 [NCT03216902]. Enrolment has just begun for a multicenter phase II trial to evaluate efficacy and safety of Sepetaprost [NCT04742283].

Nitric oxide (NO), which donates PGAs, has been evaluated in clinical trials since the late 2000s. A Phase IIb dose-finding study was completed in 2018 [NCT03216902]. The release of NO results in further IOP-lowering effect through increased trabecular meshwork outflow by cAMP-mediated relaxation of trabecular meshwork cells (58, 59). Non-IOP related physiological functions of NO may also be important in terms of glaucoma pathophysiology and treatment. Since NO is an important regulator of vascular tone, it has been suggested that NO helps maintain adequate blood supply to the optic nerve (59, 60). A possible neuroprotective effect of NO has been evaluated in preclinical studies, but needs to be investigated further (59). The first NO-donating PGA was approved by FDA in 2017, a NO-donating latanoprost derivative Vyzulta. Another compound, NCX 470, is composed of the prostamide Bimatoprost with an NO-donating moiety. NCX 470 recently advanced to phase III clinical development [NCT04445519].

Adenosine Receptor Agonists

There are four subtypes of adenosine receptors, described as A_1, A_{2A}, and A_{2B} and A_3 receptor. Adenosine receptors are widely distributed throughout the body including the eye. Adenosine

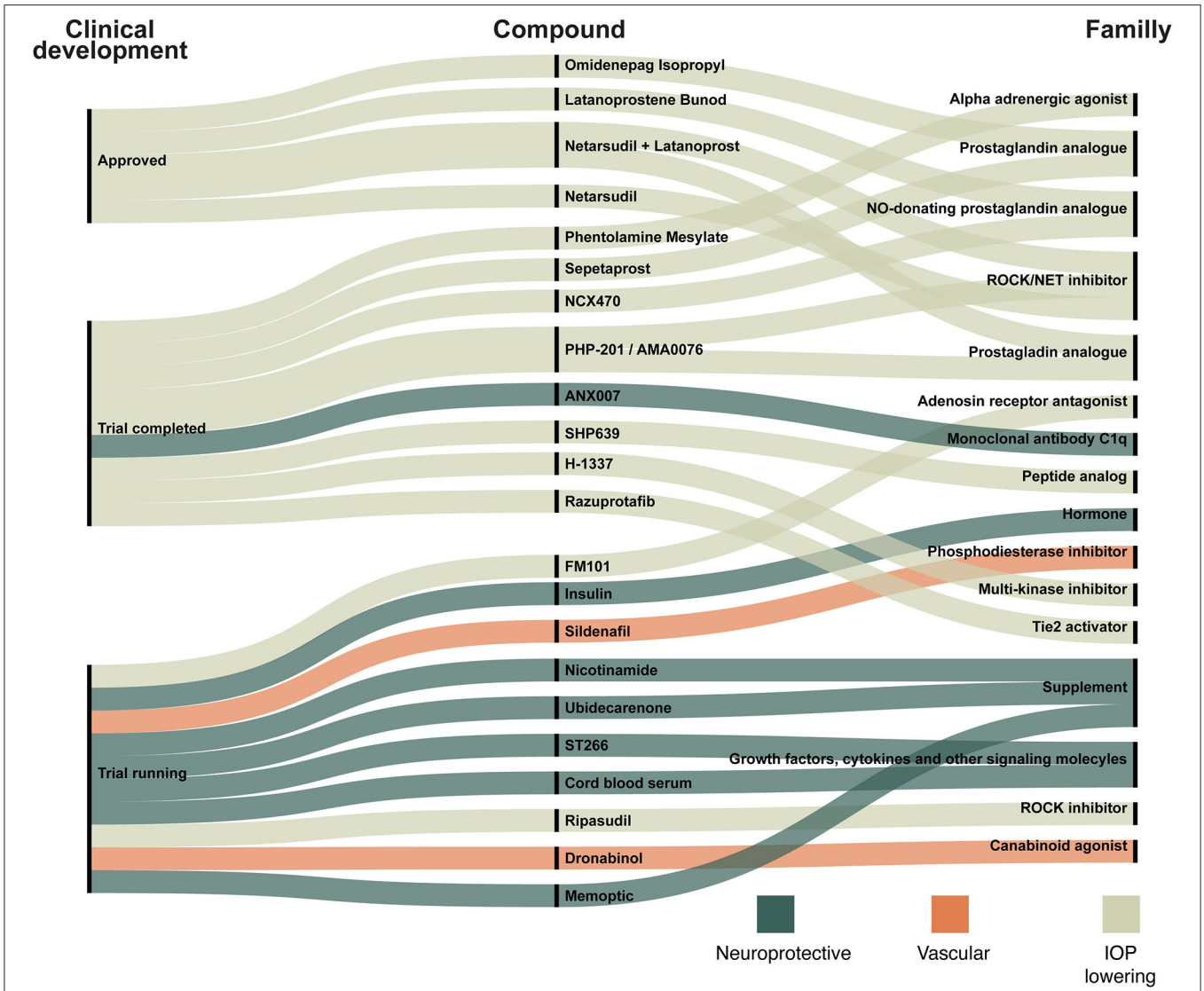

FIGURE 4 | New compounds in ongoing trials, trials completed within 2 years and compounds resulting in recently approved glaucoma treatment drugs. The compounds are linked to the target family listed on the right site. The three colors indicate whether a compound is categorized as neuroprotective (dark green), vascular (orange), or IOP-lowering (light green). For example: (1) Omidenepag Isopropyl, a prostaglandin analog, has been approved and works by lowering IOP; (2) ANX007 is a neuroprotective monoclonal antibody c1q and trials with this compound have been completed; (3) Sildenafil is a phosphodiesterase inhibitor that acts on the microvascular blood flow and trials are still ongoing.

receptors are numerous in ocular tissue, such as the ciliary body, the trabecular meshwork, the sclera, and the retina (61). We identified nine clinical trials that evaluated compounds acting on an adenosine receptor, but to date none of the compounds have succeeded in progressing to FDA approval (62–64). A single phase I/IIA trials is currently underway [NCT04585100]. FM101 is an oral tablet formulation of an A_3 receptor modulator that has been shown to be safe in preclinical studies (65).

Small Molecule Inhibitor of VE-PTP

A phase II clinical trial evaluating Razuprotafib/AKB-9778 was completed in November 2020 [NCT04405245]. AKB-9778 binds to and inhibits vascular endothelial protein tyrosine phosphatase (VE-PTP), an important negative regulator of Tie2. In mice, VE-PTP was expressed by Schlemm's canal endothelium. Topical ocular administration of AKB-9778 increased Tie2 activation, enhanced SC filtration area, and increased outflow facility, resulting in reduced IOP. The effects appear to be mediated by both eNOS activation and Rho kinase pathway inhibition (66).

Multikinase Inhibitor

H-1337 is a multikinase inhibitor proposed to stimulate the drainage of aqueous humor from the main outflow tract *via* the trabecular meshwork and the Schlemms canal. The mechanism of action of H-1337 has been explained in two pathways, LRRK2 (leucine-rich repeat kinase 2) inhibition as the main

TABLE 3 | Success rates for new compounds in glaucoma clinical trials 2000–2020.

Phase	Success per phase	Compounds per phase, total (*n*)	Success rate (%)
Phase I	24	38	63
Phase II	12	46	26
Phase III	9	19	47

Success per phase represents the number of compounds that reach next phase. Compounds per phase represents total number of agents in each phase. Success rate represents the percentage of compounds that succeed to the next phase. 24/38 (63%) compounds succeeded from phase I, 12/46 (26%) compounds succeeded from phase II, and 9/19 (47%) compounds succeeded from phase III.

pathway and ROCK inhibition as the secondary pathway. LRRK2 is a type of serine/threonine kinase that acts to control the polymerization of intracellular microtubules. When LRRK2 is inhibited, the microtubules that make up the cytoskeleton of trabecular meshwork cells in the eye depolymerize and change the structure. The results of phase I/IIa trial completed in September 2018 [NCT03452033] showed that IOP was reduced vs. placebo and H-1337 was well tolerated (67, 68).

C-type Natriurectic Peptide Analog

TAK-639/SHP-639 is a topical, 9-amino acid, synthetic, C-type natriuretic peptide analog in phase I development for the treatment of patients with OHT and POAG. The mechanism for lowering IOP is relaxation of the trabecular meshwork *via* activation of the type B natriuretic peptide receptor (NPR-B). TAK-630 has shown potential as an ocular hypotensive agent in preclinical studies (69, 70). Data from the phase I clinical trial report marginal reduction in IOP from baseline values, but only at the highest dose group and at the most frequent dosing regimen (71).

α-antagonist

Phentolamine has been studied in preclinical studies with promising IOP-lowering effect (72). In 2019, phentolamine was evaluated in a clinical phase II trial for multiple ocular indications. Data were recently published (73) and it was found that phentolamine did not significantly reduce IOP in patients with glaucoma or OHT. There was a tendency for a greater decrease in patients with lower IOP at baseline (73). The authors suggest combination therapy with topical prostaglandins as a possible way for further development of phentolamine in POAG (73).

ROCK Inhibitors

Among the few new compounds introduced since latanoprost in 1996 are the rho-associated protein kinase (ROCK) inhibitors. Ripasudil 0.4% ophthalmic solution was approved in Japan in September 2014 (74), and netarsudil 0.02% in 2017 by FDA US (75). We found 36 clinical trials investigating the effect of ROCK inhibitors, either as monotherapy ($n = 5$) or combination therapy with prostaglandin analogs ($n = 31$). As ROCK inhibitors were first approved in Japan, the numbers of clinical trials are likely to be higher than 36, as we did not conduct a search in clinicaltrials.jp.

ROCK is a serine/threonine protein kinase and is divided into ROCK1 and ROCK2. ROCK1and ROCK2 are activated by a GTP-binding protein named Rho A. When ROCK1 or ROCK2 are phosphorylated and activated by Rho A, they act on several intracellular molecules such as myosin light chain, LIM-kinase, calponin and ERM. This range of functions contributes to the different features of ROCK inhibitors, as they act directly on the trabecular meshwork and Schlemm's canal by modulating cell adhesion, cell motility, proliferation, and cell differentiation (76). The mentioned actions lead to a reduction in IOP. In addition, several studies suggest that ROCK inhibitors act on multiple other parameters, and both neuroprotection and beneficial effects on retinal blood flow may increase its anti-glaucomatous effects (76). Overall, ROCK inhibitors are well tolerated, with conjunctival hyperemia as the most common adverse effect of treatment. As ROCK inhibitors act on different targets compared to traditional IOP-lowering agents, combining ROCK-inhibitors with other IOP-lowering drugs may be an additive, which may be a future strategy when monotherapy is not sufficient to achieve disease control.

Vascular Compounds

Interest in finding treatment strategies other than lowering IOPs has increased in recent decades. As our data suggest, research into vascular compounds is still limited with 15 trials conducted over time. In 2019, a phase III trial investigating phosphodiesterase (PDE) inhibitors effect on blood circulation in the retina and the choroid was initiated [NCT04052269]. PDE is an enzyme subgrouped into 12 isoenzymes. The isoenzymes are differently distributed in various tissues in the body. For example, PDE5 is found in platelets and vascular smooth muscle cells in the corpus cavernosum. PDE5 inhibitors are used primarily to treat of erectile dysfunction and work by increasing blood circulation in the corpus cavernosum. PDE5 is also present in the choroidal and retinal vessels (77). In the above-mentioned study, the drug was dispensed as an oral pill and not as a topical administration. The aim of the study was to investigate whether it is possible to detect changes in blood flow in the retina and choroid assessed by OCT scans.

In 2020, a phase II trial was launched to investigate retinal blood flow [NCT04596826]. The trial focuses on dronabinol, a synthetic Tetrahydrocannabinol (THC) agent. THC binds to two cannabinoid G protein coupled receptors: CB_1 and CB_2. CB_1 receptors are distributed in neurons and a variety of peripheral organs and tissues, such as endocrine glands, leucocytes, spleen, heart, reproductive system, urinary tract, and gastrointestinal tracts. CB_2 is distributed in the immune system. Thus, binding to CB_1 affects the psyche and circulation, while CB_2 does not (78). The study mentioned above investigated whether THC affects the retinal hemodynamic after oral administration evaluated by OCT, retinal vessel diameter, retinal oxygen saturation, and retinal blood velocity among others.

Data from the two trials examining PDE5 and THC have not yet been published. The small number of trials evaluating compounds acting on microvascular blood may be an indicator

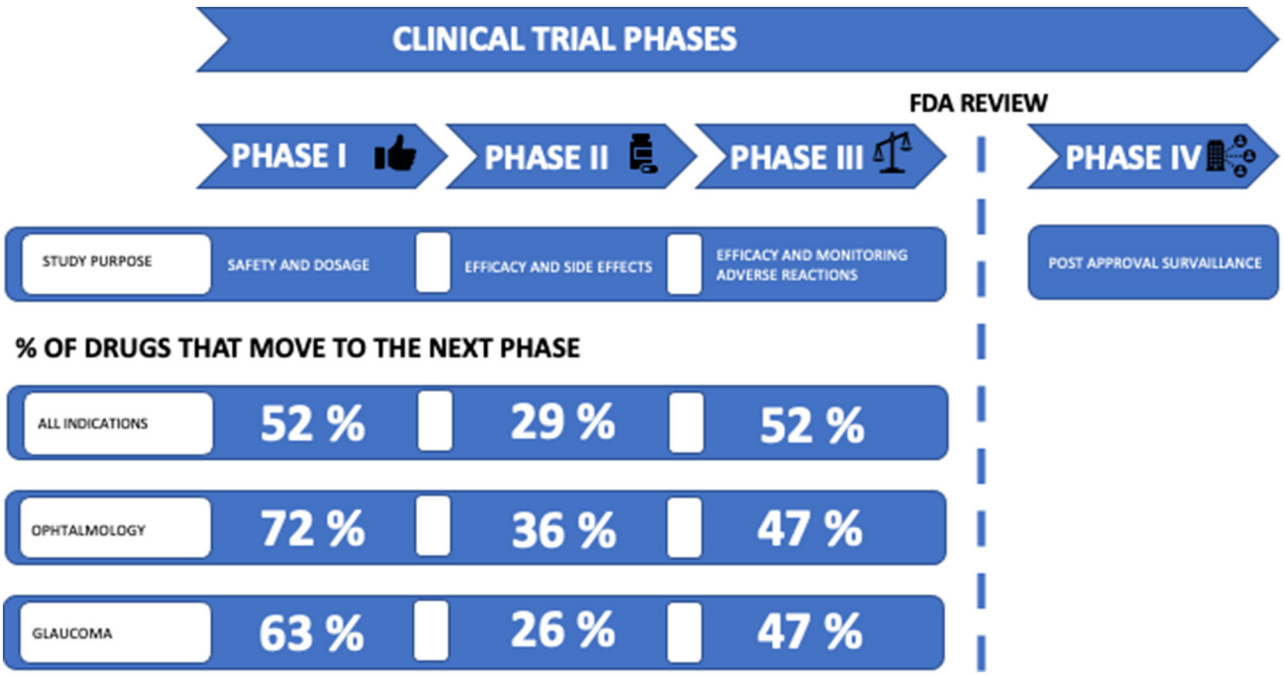

FIGURE 5 | Clinical development success rates. Clinical trial phases are linked to study purpose; phase I studies investigate safety and dosage, phase II studies investigate efficacy and side effects, phase III studies investigate efficacy and monitoring of adverse events, and phase IV studies investigate post-approval surveillance. Before entering phase IV, an FDA review is required. The percentage of drugs that proceed to next phase is listed. Success rates from **Table 3** are listed as "Glaucoma" and compared with success rates for ophthalmology and for all indications in the period 2011–2021 in general. Source: BIO (Biotechnology, Innovation, Organization) (47).

of insufficient methods to evaluate the effect of a particular compound on ocular blood flow. Suitable endpoints are needed for clinical trials to determine if modification of ocular blood flow is an effective therapeutic target for glaucoma.

Neuroprotective Compounds

Neuroprotection in glaucoma can be addressed from several starting points. Among many deprivation of neurotrophic factors, excitotoxicity and oxidative stress are some examples (79). The compounds that have been investigated in clinical trials for neuroprotection in glaucoma can be categorized accordingly.

Neurotrophic factors (NFs) are soluble polypeptides with several functions in the nervous system. They are important for the survival, maintenance, and regeneration of neuronal cells (80). Depletion of various neurotrophic factors has been associated with specific disease pathology.

Brain-derived neurotrophic factor (BDNF), which is known to regulate neuronal survival and function in the central nervous system, plays an important role in the treatment of neurodegenerative diseases and has been associated with Parkinson's, Alzheimer's, and Huntington's diseases (80).

ST266 is a novel biologic drug candidate made by a method of culturing amnion epithelial cells harvested from the placenta after birth (81). It contains biologically active proteins and other factors that promote wound healing and preservation of retinal ganglion cells (RGC). A phase I trial is currently running [NCT03901781] (81). Similarly, a study investigating eye drops prepared from umbilical cord blood serum containing growth factors is registered in clinicaltrial.gov, but recruitment status is unknown and last updated in 2018 [NCT03609125].

Citicoline (cytidine 5-diphos-phocholine) is an FDA-approved supplement. Citicoline is an endogenous molecule that participates in the synthesis of membrane proteins. It has been shown to be beneficial in ischemic stroke, traumatic brain injury, Parkinson's disease, Alzheimer's disease, and cerebrovascular diseases (19). In animal models, citicoline has an anti-apoptotic effect on RGC by decreasing glutamate excitotoxicity and oxidative stress (19, 79, 82). Clinical trials do not show consistent results. Parisi et al. (83) showed improvement on retinal function and neural conduction along the visual pathways. Marino et al. (84) found improvement in contrast sensitivity and quality of life, but there were no significant effects on the visual field. A new trial is recruiting patients to evaluate the effect of Memoptic; citicoline in combination with ginkgo biloba, magnesium, vitamin B5 and zinc on visual field performance [NCT04499157].

Nicotinamide, also known as niacinamide, is a water-soluble form of vitamin B3 and is an FDA-approved dietary supplement. Nicotinamide is the precursor of nicotinamide adenine dinucleotide (NAD), which is a coenzyme in several cellular processes, including energy metabolism and DNA repair. Aging causes a decrease in NAD levels leading to metabolic and mitochondrial dysfunction, leaving RGC more prone to cell death. Animal models show that nicotinamide prevents RGC death during IOP elevation. Improvement of

mitochondrial function also protects RGCs (85, 86). A clinical trial is currently underway to show whether nicotinamide is beneficial in humans for visual field-testing performance [NCT03797469]. Early results from NCT03797469 have shown a promising neuroprotective potential of nicotinamide. Thus, Hui et al. (87) have shown improved inner retinal function measured by photopic negative response after 3 months treatment with nicotinamide.

Oxidative stress is also a likely contributing factor in the pathogenesis of glaucoma. Studies have shown that antioxidants such as Coenzyme Q10, alpha-lipoic acid, superoxide dismutase, ginkgo biloba leaf extract, and bilberry leaf extract decrease RGC loss in rat models of glaucoma (88).

Another contributing factor to glaucomatous loss of RGC is low-grade inflammation, also called neuroinflammation (89–91). ANX007 is an investigational monoclonal antibody antigen binding fragment (Fab) for the treatment of patients with complement-mediated neurodegenerative ophthalmic diseases. ANX007 completed phase I and has progressed into phase II trial, however, for geographic atrophy and not for glaucoma [NCT04656561] (92).

Insulin resistance has been associated with neurodegeneration in diseases characterized by dendritic pathology, notably Alzheimer's and Parkinson's disease. Insulin may promote the regeneration of dendrites following traumatic injury (93). A phase I trial using topical insulin for glaucoma patients is recruiting patients [NCT04118920].

Neuroprotection in glaucoma is certainly an important approach to treating glaucoma. However, as Liu and Pang (41) describe, there are the following challenges in the discovery and development of neuroprotective drugs: uncertain mechanisms of pathogenesis, uncertain therapeutic targets, preclinical models yet to be validated, and limitations in clinical detection of disease progression.

A general challenge in ophthalmological research is the choice of primary endpoint. As mentioned earlier, IOP is the only evidence-based treatable risk factor for slowing the worsening of glaucoma. Thus, the primary endpoint of most trials is related to IOP, making it difficult to evaluate potential neuroprotective properties of the drug, as progression of visual field defects or OCT scans are rarely evaluated alongside to IOP control. Using electrophysiology, hereunder photopic negative response (87), as a primary endpoint along with biomarkers to stratify treatment effectiveness can help improve positive outcomes of ongoing and future glaucoma trials.

The ultimate goal of drug development is to introduce a promising new compound with a proven therapeutic effect on the market. It is a milestone when a compound moves from preclinical to clinical phase. However, <10% of the drugs entering clinical trials will be approved by regulatory authorities (94). Consistent with previous studies of success rates for the transition to the next phase of drug development, we found the success rate for phase II to be lower than any other phase (46, 95, 96). In this study, we found that the success rate in phase II was 26% (**Table 3**; **Figure 5**). Thomas et al. (47) recently reported a phase II success rate for all indications of 29%. We found that the transition success rates for phase I and phase III were 63 and 47%, respectively. Although glaucoma compounds are more successful in progressing from phase I than reported by Thomas et al. (52%), we found the success rate from phase III to approval to be lower than reported by Thomas et. al. (47) (58%). Thomas et al. (47) report phase transition success rates for major disease areas. In ophthalmology, the phase I, II, and III transition success rates were 72, 36, and 47%, respectively. Thus, the phase transition success rates in clinical glaucoma research appear to be below the general level in ophthalmology.

Gower et al. (97) suggest that personalized medicine could be a way to improve the success rate in ophthalmic research. When randomizing people to clinical trials, biomarkers and underlying disease pathophysiology should be considered. This can potentially improve the sensitivity of analysis by investigating whether a particular subgroup responds better to a current treatment.

Gower et al. argues that the lack of discovering new drugs may be due to the special properties of the eye, such as the immediate dilution of the eye drops caused by the tear film, which results in reduced effect of the drug. To succeed with the new strategies in glaucoma research, it is very important to continue to improve knowledge and understanding of the pathogenesis of glaucoma in order to optimize disease modeling and thereby improve the understanding of potential new targets and compounds with promising opportunities (97). In a review by Gross et al., the authors suggest that biophysical models could provide an effective tool in glaucoma risk assessment and may improve the understanding of the inconsistency in treatment response among patients. The biophysical models and mathematical modeling are still at an early stage, and it is challenging to incorporate, e.g., the circadian curve of IOP into the models (98). Also, genetic prediction models could potentially identify individuals most at risk for disease development and progression (99). As previously mentioned, more than 2,700 potential targets for glaucoma exists, but only a fraction are represented in clinical trials. Drug compounds targeting glaucoma risk genes may be potential therapeutic candidates. New technologies using genetic information could also assist in predicting if a patient likely would benefit from a certain treatment. With future innovative drug development where the above-mentioned aspects of personalized medicine and mathematical modeling are considered, we might see an increasing phase transition success rate in glaucoma clinical trials.

CONCLUSION

The number of clinical trials in glaucoma research has increased significantly over the last 30 years. A total of 1,537 trials were identified, with the majority evaluating glaucoma treatment ($n =$ 971, 63%). Medical treatments covered 55% of these trials over time with IOP evaluation as the most common primary endpoint. In 2020, clinical trials evaluating surgical treatment dominated with 63%. Eighty-eight new compounds were identified with 22 compounds that are currently in clinical development or recently approved for glaucoma treatment. New PGAs and NO donating

PGAs are in late-stage development. Dietary supplements currently being evaluated for neuroprotective effects are nicotinamide, citicoline in combination and Coenzyme Q10. Overall, research into neuroprotection and vascular modalities is still sparse with non-uniform results. However, the early results of the nicotinamide trial give rise to some hope for an IOP-independent treatment for glaucoma. The phase transition success rates were below the level of success rates in ophthalmology, potentially caused by the particular anatomy and physiology of the eye, thus reducing the effectiveness of a drug. A future strategy to improve the success rates in glaucoma and ophthalmological research can be achieved from personalized medicine. This paper contributes to the literature by highlighting the difficulties of finding other treatment strategies than lowering IOP and by showing, that only a fraction of the new drugs reaches the market despite comprehensive research. It underlines the need for further research in the complex pathophysiology of glaucoma and for future innovative drug development.

AUTHOR CONTRIBUTIONS

The manuscript has been conceptualized by MK. LS and TT have performed data collection and analysis with advices from MK and AH. AH has designed the figures with input from all authors. LS, TT, and JF have written the manuscript with supervision from MK. All authors have provided feedback and helped shape the data analysis and final manuscript.

REFERENCES

1. Kolko M, Horwitz A, Thygesen J, Jeppesen J, Torp-Pedersen C. The prevalence and incidence of glaucoma in Denmark in a fifteen year period: a Nationwide Study. *PLoS One.* (2015) 10:e0132048. doi: 10.1371/journal.pone.0132048
2. Tham YC, Li X, Wong TY, Quigley HA, Aung T, Cheng CY. Global prevalence of glaucoma and projections of glaucoma burden through 2040: a systematic review and meta-analysis. *Ophthalmology.* (2014) 121:2081–90. doi: 10.1016/j.ophtha.2014.05.013
3. Agarwal R, Gupta SK, Agarwal P, Saxena R, Agrawal SS. Current concepts in the pathophysiology of glaucoma. *Indian J Ophthalmol.* (2009) 57:257–66. doi: 10.4103/0301-4738.53049
4. Minneci PC, Deans KJ. Clinical trials. *Semin Pediatr Surg.* (2018) 27:332–7. doi: 10.1053/j.sempedsurg.2018.10.003
5. Luntz MH. GLAUCOMA TREATED WITH DARANIDE A CLINICAL TRIAL. *Br J Ophthalmol.* (1961) 45:125–9.
6. ClinicalTrials.gov. *U. S. National Library and Medicine.* Available online at: https://clinicaltrials.gov/ct2/home (accessed June 8, 2021).
7. Australian Government NHaMRC, Department of Industry, Innovation and Science. *Australian Clinical Trials.* (2021). Available online at: https://www.australianclinicaltrials.gov.au/copyright-information (accessed August 2, 2021).
8. Gupta N, Aung T, Congdon N, Dada T, Lerner F, Olawoye S, et al. *ICO Guidelines for Glaucoma Eye Care.* (2016). Available online at: http://www.icoph.org/downloads/ICOGlaucomaGuidelines.pdf (accessed June 8, 2021).
9. John MECfCD, Communications S. *AHRQ Comparative Effectiveness Reviews Comparisons of Medical, Laser, and Incisional Surgical Treatments for Open-Angle Glaucoma in Adults. Comparative Effectiveness Review Summary Guides for Clinicians*. Rockville, MD: Agency for Healthcare Research and Quality (US) (2007).
10. Ekici F, Waisbourd M, Katz LJ. Current and Future of Laser Therapy in the Management of Glaucoma. *Open Ophthalmol J.* (2016) 10:56–67. doi: 10.2174/1874364101610010056
11. Kumar H, Mansoori T, Warjri GB, Somarajan BI, Bandil S, Gupta V. Lasers in glaucoma. *Indian J Ophthalmol.* (2018) 66:1539–53. doi: 10.4103/ijo.IJO_555_18
12. Wise JB, Witter SL. Argon laser therapy for open-angle glaucoma. A pilot study. *Arch Ophthalmol.* (1979) 97:319–22.
13. Conlon R, Saheb H, Ahmed, II. Glaucoma treatment trends: a review. *Can J Ophthalmol.* (2017) 52:114–24. doi: 10.1016/j.jcjo.2016.07.013
14. Preda MA, Karancsi OL, Munteanu M, Stanca HT. Clinical outcomes of micropulse transscleral cyclophotocoagulation in refractory glaucoma-18 months follow-up. *Lasers Med Sci.* (2020) 35:1487–91. doi: 10.1007/s10103-019-02934-x
15. Sun CQ, Chen TA, Deiner MS, Ou Y. Clinical outcomes of micropulse laser trabeculoplasty compared to selective laser trabeculoplasty at one year in open-angle glaucoma. *Clin Ophthalmol.* (2021) 15:243–51. doi: 10.2147/OPTH.S285136
16. Bar-David L, Blumenthal EZ. Evolution of glaucoma surgery in the last 25 years. *Rambam Maimonides Med J.* (2018) 9:e0024. doi: 10.5041/RMMJ.10345
17. Gedde SJ, Lind JT, Wright MM, Chen PP, Muir KW, Vinod K, et al. Primary open-angle glaucoma suspect preferred practice pattern®. *Ophthalmology.* (2021) 128:P151–P92.
18. National Collaborating Centre for Acute C. *National Institute for Health and Clinical Excellence: Guidance. Glaucoma: Diagnosis and Management of Chronic Open Angle Glaucoma and Ocular Hypertension*. London: National Collaborating Centre for Acute Care (UK) Copyright © 2009, National Collaborating Centre for Acute Care (2009).
19. Faiq MA, Wollstein G, Schuman JS, Chan KC. Cholinergic nervous system and glaucoma: From basic science to clinical applications. *Prog Retin Eye Res.* (2019) 72:100767. doi: 10.1016/j.preteyeres.2019.06.003
20. Realini T. A history of glaucoma pharmacology. *Optom Vis Sci.* (2011) 88:36–8. doi: 10.1097/OPX.0b013e3182058ead
21. Keith CG. INTRAVENOUS UREA IN GLAUCOMA. *Br J Ophthal.* (1961) 45:307–11.
22. Becker B. Decrease in intraocular pressure in man by a carbonic anhydrase inhibitor, diamox; a preliminary report. *Am J Ophthalmol.* (1954) 37:13–5. doi: 10.1016/0002-9394(54)92027-9
23. Srinivasan AV. Propranolol: a 50-year historical perspective. *Ann Indian Acad Neurol.* (2019) 22:21–6. doi: 10.4103/aian.AIAN_201_18
24. Sambhara D, Aref AA. Glaucoma management: relative value and place in therapy of available drug treatments. *Ther Adv Chronic Dis.* (2014) 5:30–43. doi: 10.1177/2040622313511286
25. Pfeiffer N. Dorzolamide: development and clinical application of a topical carbonic anhydrase inhibitor. *Surv Ophthalmol.* (1997) 42:137–51. doi: 10.1016/S0039-6257(97)00053-2
26. Costagliola C, dell'Omo R, Romano MR, Rinaldi M, Zeppa L, Parmeggiani F. Pharmacotherapy of intraocular pressure - part II. Carbonic anhydrase inhibitors, prostaglandin analogues and prostamides. *Expert Opin Pharmacother.* (2009) 10:2859–70. doi: 10.1517/14656560903300129
27. Impagnatiello F, Bastia E, Almirante N, Brambilla S, Duquesroix B, Kothe AC, et al. Prostaglandin analogues and nitric oxide contribution in the treatment of ocular hypertension and glaucoma. *Br J Pharmacol.* (2019) 176:1079–89. doi: 10.1111/bph.14328
28. Bagnis A, Papadia M, Scotto R, Traverso CE. Antiglaucoma drugs: the role of preservative-free formulations. *Saudi J Ophthalmol.* (2011) 25:389–94. doi: 10.1016/j.sjopt.2011.08.004
29. Thygesen J. Glaucoma therapy: preservative-free for all? *Clin Ophthalmol.* (2018) 12:707–17. doi: 10.2147/OPTH.S150816
30. Steven DW, Alaghband P, Lim KS. Preservatives in glaucoma medication. *Br J Ophthalmol.* (2018) 102:1497–503. doi: 10.1136/bjophthalmol-2017-311544
31. Baudouin C, Labbe A, Liang H, Pauly A, Brignole-Baudouin F. Preservatives in eyedrops: the good, the bad and the ugly. *Prog Retin Eye Res.* (2010) 29:312–34. doi: 10.1016/j.preteyeres.2010.03.001

32. Berrino E, Supuran CT. Rho-kinase inhibitors in the management of glaucoma. *Expert Opin Ther Pat.* (2019) 29:817–27. doi: 10.1080/13543776.2019.1670812
33. Cvenkel B, Kolko M. Current medical therapy and future trends in the management of glaucoma treatment. *J Ophthalmol.* (2020) 2020:6138132. doi: 10.1155/2020/6138132
34. Kolko M. Present and new treatment strategies in the management of glaucoma. *Open Ophthalmol J.* (2015) 9:89–100. doi: 10.2174/1874364101509010089
35. Khatib TZ, Martin KR. Neuroprotection in Glaucoma: towards clinical trials and precision medicine. *Curr Eye Res.* (2020) 45:327–38. doi: 10.1080/02713683.2019.1663385
36. Weinreb RN, Liebmann JM, Cioffi GA, Goldberg I, Brandt JD, Johnson CA, et al. Oral memantine for the treatment of glaucoma: design and results of 2 randomized, placebo-controlled, phase 3 studies. *Ophthalmology.* (2018) 125:1874–85. doi: 10.1016/j.ophtha.2018.06.017
37. Sena DF, Lindsley K. Neuroprotection for treatment of glaucoma in adults. *Cochrane Database Syst Rev.* (2017) 1:CD006539. doi: 10.1002/14651858.CD006539.pub4
38. Kim JM, Sae Kim M, Ju Jang H, Ho Park K, Caprioli J. The association between retinal vessel diameter and retinal nerve fiber layer thickness in asymmetric normal tension glaucoma patients. *Invest Ophthalmol Vis Sci.* (2012) 53:5609–14. doi: 10.1167/iovs.12-9783
39. Hwang JC, Konduru R, Zhang X, Tan O, Francis BA, Varma R, et al. Relationship among visual field, blood flow, and neural structure measurements in glaucoma. *Invest Ophthalmol Vis Sci.* (2012) 53:3020–6. doi: 10.1167/iovs.11-8552
40. Jia Y, Morrison JC, Tokayer J, Tan O, Lombardi L, Baumann B, et al. Quantitative OCT angiography of optic nerve head blood flow. *Biomed Opt Express.* (2012) 3:3127–37. doi: 10.1364/BOE.3.003127
41. Liu Y, Pang IH. Challenges in the development of glaucoma neuroprotection therapy. *Cell Tissue Res.* (2013) 353:253–60. doi: 10.1007/s00441-013-1584-z
42. Chen ST. Regulation of research: is it a drug trial or a supplement trial? *Fitoterapia.* (2011) 82:14–6. doi: 10.1016/j.fitote.2010.11.011
43. Drugbank. *Drugbank.* (2021). Available online at: https://go.drugbank.com/ (accessed June 8, 2021).
44. *Open Targets Platform: Open Targets Platform.* (2021). Available online at: https://platform.opentargets.org/ (accessed June 8, 2021).
45. *Step 3: Clinical Research: US Food and Drug Administation*. Available online at: https://www.fda.gov/patients/drug-development-process/step-3-clinical-research (accessed June 9, 2021).
46. Thomas D, Burns J, Audette J, Carroll A, Dow-Hygelund C, Hay M. *Clinical Development Success Rates 2006-2015*. Available online at: https://www.bio.org/sites/default/files/legacy/bioorg/docs/Clinical%20Development%20Success%20Rates%202006-2015%20-%20BIO,%20Biomedtracker,%20Amplion%202016.pdf (accessed June 2, 2021).
47. Thomas D, Chancellor D, Micklus A, LaFever S, Hay M. *Clinical Development Success Rates and Contributing Factors 2011–2020.* (2021). Available online at: https://pharmaintelligence.informa.com/$\sim$/media/informa-shop-window/pharma/2021/files/reports/2021-clinical-development-success-rates-2011-2020-v17.pdf (accessed April 22, 2021).
48. *Glaucoma: Open Targets Platform.* Available online at: https://platform.opentargets.org/disease/EFO_0000516/associations (accessed June 8, 2021).
49. Winkler NS, Fautsch MP. Effects of prostaglandin analogues on aqueous humor outflow pathways. *J Ocul Pharmacol Ther.* (2014) 30:102–9. doi: 10.1089/jop.2013.0179
50. Toris CB, Gabelt BT, Kaufman PL. Update on the mechanism of action of topical prostaglandins for intraocular pressure reduction. *Surv Ophthalmol.* (2008) 53(Suppl. 1):S107–S20. doi: 10.1016/j.survophthal.2008.08.010
51. Kirihara T, Taniguchi T, Yamamura K, Iwamura R, Yoneda K, Odani-Kawabata N, et al. Pharmacologic characterization of omidenepag isopropyl, a novel selective EP2 receptor agonist, as an ocular hypotensive agent. *Invest Ophthalmol Vis Sci.* (2018) 59:145–53. doi: 10.1167/iovs.17-22745
52. Iwamura R, Tanaka M, Okanari E, Kirihara T, Odani-Kawabata N, Shams N, et al. Identification of a selective, non-prostanoid EP2 receptor agonist for the treatment of glaucoma: omidenepag and its prodrug omidenepag isopropyl. *J Med Chem.* (2018) 61:6869–91. doi: 10.1021/acs.jmedchem.8b00808
53. Ferro Desideri L, Cutolo CA, Barra F, Ferrero S, Traverso CE. Omidenepag isopropyl for the treatment of glaucoma and ocular hypertension. *Drugs Today (Barc).* (2019) 55:377–84. doi: 10.1358/dot.2019.55.6.2984806
54. Duggan S. Omidenepag isopropyl ophthalmic solution 0.002%: first global approval. *Drugs.* (2018) 78:1925–9. doi: 10.1007/s40265-018-1016-1
55. Santen Ube Announces U.S. FDA Acceptance of New Drug Application for STN10117 (DE-117) (JAN: Omidenepag Isopropyl) as a Treatment for Patients with Glaucoma and Ocular Hypertension: Santen and Ube (2021). Available online at: https://www.santen.com/en/news/20210202.pdf (accessed June 2, 2021).
56. Berlin MS, Rowe-Rendleman C, Ahmed I, Ross DT, Fujii A, Ouchi T, et al. EP3/FP dual receptor agonist ONO-9054 administered morning or evening to patients with open-angle glaucoma or ocular hypertension: results of a randomised crossover study. *Br J Ophthalmol.* (2016) 100:843–7. doi: 10.1136/bjophthalmol-2015-307000
57. Harris A, Ward CL, Rowe-Rendleman CL, Ouchi T, Wood A, Fujii A, et al. Ocular hypotensive effect of ONO-9054, an EP3/FP receptor agonist: results of a randomized, placebo-controlled, dose escalation study. *J Glaucoma.* (2016) 25:e826–e33. doi: 10.1097/IJG.0000000000000449
58. Addis VM, Miller-Ellis E. Latanoprostene bunod ophthalmic solution 0.024% in the treatment of open-angle glaucoma: design, development, and place in therapy. *Clin Ophthalmol.* (2018) 12:2649–57. doi: 10.2147/OPTH.S156038
59. Garhöfer G, Schmetterer L. Nitric oxide: a drug target for glaucoma revisited. *Drug Discov Today.* (2019) 24:1614–20. doi: 10.1016/j.drudis.2019.05.033
60. Mao YJ, Wu JB, Yang ZQ, Zhang YH, Huang ZJ. Nitric oxide donating anti-glaucoma drugs: advances and prospects. *Chin J Nat Med.* (2020) 18:275–83. doi: 10.1016/S1875-5364(20)30035-2
61. Santiago AR, Madeira MH, Boia R, Aires ID, Rodrigues-Neves AC, Santos PF, et al. Keep an eye on adenosine: its role in retinal inflammation. *Pharmacol Ther.* (2020) 210:107513. doi: 10.1016/j.pharmthera.2020.107513
62. Qiu TG. Trabodenoson on trabecular meshwork rejuvenation: a comprehensive review of clinical data. *Expert Opin Investig Drugs.* (2021) 30:227–36. doi: 10.1080/13543784.2021.1873276
63. Jacobson KA, Tosh DK, Jain S, Gao ZG. Historical and current adenosine receptor agonists in preclinical and clinical development. *Front Cell Neurosci.* (2019) 13:124. doi: 10.3389/fncel.2019.00124
64. Spinozzi E, Baldassarri C, Acquaticci L, Del Bello F, Grifantini M, Cappellacci L, et al. Adenosine receptors as promising targets for the management of ocular diseases. *Med Chem Res*. (2021) 30:1–18. doi: 10.1007/s00044-021-02704-x
65. Park CW, Han CT, Sakaguchi Y, Lee J, Youn HY. Safety evaluation of FM101, an A3 adenosine receptor modulator, in rat, for developing as therapeutics of glaucoma and hepatitis. *Excli J.* (2020) 19:187–200. doi: 10.17179/excli2019-2058
66. Li G, Nottebaum AF, Brigell M, Navarro ID, Ipe U, Mishra S, et al. A small molecule inhibitor of VE-PTP activates tie2 in Schlemm's canal increasing outflow facility and reducing intraocular pressure. *Invest Ophthalmol Vis Sci.* (2020) 61:12. doi: 10.1167/iovs.61.14.12
67. Jayanetti V, Sandhu S, Lusthaus JA. The latest drugs in development that reduce intraocular pressure in ocular hypertension and glaucoma. *J Exp Pharmacol.* (2020) 12:539–48. doi: 10.2147/JEP.S281187
68. Company Report D. *Western Therapeutics Institute, Inc.* (2020). Available online at: https://pdf.irpocket.com/C4576/yCGV/Fnnr/DXyw.pdf (accessed June 15, 2021).
69. Savinainen A, Prusakiewicz JJ, Oswald J, Spencer E, Lou Z, Cohen ML, et al. Pharmacokinetics and intraocular pressure-lowering activity of TAK-639, a novel C-type natriuretic peptide analog, in rabbit, dog, and monkey. *Exp Eye Res.* (2019) 189:107836. doi: 10.1016/j.exer.2019.107836
70. Millar JC, Savinainen A, Josiah S, Pang IH. Effects of TAK-639, a novel topical C-type natriuretic peptide analog, on intraocular pressure and aqueous humor dynamics in mice. *Exp Eye Res.* (2019) 188:107763. doi: 10.1016/j.exer.2019.107763
71. Martin P, Cohen A, Uddin S, Epelbaum L, Josiah S. Randomized, Double-Masked, Placebo-controlled dose escalation study of TAK-639 topical ophthalmic solution in subjects with ocular hypertension or primary open-angle glaucoma. *Clin Ophthalmol.* (2020) 14:885–96. doi: 10.2147/OPTH.S242932

72. Kiel JW, Reitsamer HA. Paradoxical effect of phentolamine on aqueous flow in the rabbit. *J Ocul Pharmacol Ther.* (2007) 23:21–6. doi: 10.1089/jop.2006.0102
73. Pepose JS, Hartman PJ, DuBiner HB, Abrams MA, Smyth-Medina RJ, Moroi SE, et al. Phentolamine mesylate ophthalmic solution provides lasting pupil modulation and improves near visual acuity in presbyopic glaucoma patients in a randomized phase 2b clinical trial. *Clin Ophthalmol.* (2021) 15:79–91. doi: 10.2147/OPTH.S278169
74. Garnock-Jones KP. Ripasudil: first global approval. *Drugs.* (2014) 74:2211–5. doi: 10.1007/s40265-014-0333-2
75. (FDA) FaDA. *Novel Drug Approvals for 2017 Food and Drug Administration (FDA).* Food and Drug Administration (FDA). Available online at: https://www.fda.gov/drugs/new-drugs-fda-cders-new-molecular-entities-and-new-therapeutic-biological-products/novel-drug-approvals-2017 (accessed March 04, 2020).
76. Honjo M, Tanihara H. Impact of the clinical use of ROCK inhibitor on the pathogenesis and treatment of glaucoma. *Jpn J Ophthalmol.* (2018) 62:109–26. doi: 10.1007/s10384-018-0566-9
77. Kerr NM, Danesh-Meyer HV. Phosphodiesterase inhibitors and the eye. *Clin Exp Ophthalmol.* (2009) 37:514–23. doi: 10.1111/j.1442-9071.2009.02070.x
78. Grotenhermen F. Pharmacokinetics and pharmacodynamics of cannabinoids. *Clin Pharmacokinet.* (2003) 42:327–60. doi: 10.2165/00003088-200342040-00003
79. Parisi V, Oddone F, Ziccardi L, Roberti G, Coppola G, Manni G. Citicoline and retinal ganglion cells: effects on morphology and function. *Curr Neuropharmacol.* (2018) 16:919–32. doi: 10.2174/1570159X15666170703111729
80. Zuccato C, Cattaneo E. Brain-derived neurotrophic factor in neurodegenerative diseases. *Nat Rev Neurol.* (2009) 5:311–22. doi: 10.1038/nrneurol.2009.54
81. Noveome Biotherapeutics Inc. *ST266—A Next-Generation Anti-Inflammatory and Neuroprotective Platform Biologic.* Biopharmadealmakers.nature.com (2019).
82. Gandolfi S, Marchini G, Caporossi A, Scuderi G, Tomasso L, Brunoro A. Cytidine 5'-Diphosphocholine (Citicoline): evidence for a neuroprotective role in glaucoma. *Nutrients.* (2020) 12:793. doi: 10.3390/nu12030793
83. Parisi V, Centofanti M, Ziccardi L, Tanga L, Michelessi M, Roberti G, et al. Treatment with citicoline eye drops enhances retinal function and neural conduction along the visual pathways in open angle glaucoma. *Graefes Arch Clin Exp Ophthalmol.* (2015) 253:1327–40. doi: 10.1007/s00417-015-3044-9
84. Marino PF, Rossi GCM, Campagna G, Capobianco D, Costagliola C, On Behalf Of Qualicos Study G. Effects of citicoline, homotaurine, and vitamin e on contrast sensitivity and visual-related quality of life in patients with primary open-angle glaucoma: a preliminary study. *Molecules.* (2020) 25:5614. doi: 10.3390/molecules25235614
85. Tribble JR, Otmani A, Sun S, Ellis SA, Cimaglia G, Vohra R, et al. Nicotinamide provides neuroprotection in glaucoma by protecting against mitochondrial and metabolic dysfunction. *Redox Biol.* (2021) 43:101988. doi: 10.1016/j.redox.2021.101988
86. Williams PA, Harder JM, Cardozo BH, Foxworth NE, John SWM. Nicotinamide treatment robustly protects from inherited mouse glaucoma. *Commun Integr Biol.* (2018) 11:e1356956. doi: 10.1080/19420889.2017.1356956
87. Hui F, Tang J, Williams PA, McGuinness MB, Hadoux X, Casson RJ, et al. Improvement in inner retinal function in glaucoma with nicotinamide (vitamin B3) supplementation: a crossover randomized clinical trial. *Clin Exp Ophthalmol.* (2020) 48:903–14. doi: 10.1111/ceo.13818
88. Song W, Huang P, Zhang C. Neuroprotective therapies for glaucoma. *Drug Des Devel Ther.* (2015) 9:1469–79. doi: 10.2147/DDDT.S80594
89. Williams PA, Marsh-Armstrong N, Howell GR. Neuroinflammation in glaucoma: a new opportunity. *Exp Eye Res.* (2017) 157:20–7. doi: 10.1016/j.exer.2017.02.014
90. Vohra R, Tsai JC, Kolko M. The role of inflammation in the pathogenesis of glaucoma. *Surv Ophthalmol.* (2013) 58:311–20. doi: 10.1016/j.survophthal.2012.08.010
91. Baudouin C, Kolko M, Melik-Parsadaniantz S, Messmer EM. Inflammation in glaucoma: from the back to the front of the eye, and beyond. *Prog Retin Eye Res.* (2020) 83:100916. doi: 10.1016/j.preteyeres.2020.100916
92. *ANX007: ANNEXON Bioscience*. Available online at: https://annexonbio.com/pipeline/anx007 (accessed June 15, 2021).
93. Agostinone J, Alarcon-Martinez L, Gamlin C, Yu WQ, Wong ROL, Di Polo A. Insulin signalling promotes dendrite and synapse regeneration and restores circuit function after axonal injury. *Brain.* (2018) 141:1963–80. doi: 10.1093/brain/awy142
94. Akhondzadeh S. The importance of clinical trials in drug development. *Avicenna J Med Biotechnol.* (2016) 8:151.
95. Takebe T, Imai R, Ono S. The current status of drug discovery and development as originated in United States Academia: the influence of industrial and academic collaboration on drug discovery and development. *Clin Transl Sci.* (2018) 11:597–606. doi: 10.1111/cts.12577
96. Wong CH, Siah KW, Lo AW. Estimation of clinical trial success rates and related parameters. *Biostatistics.* (2019) 20:273–86. doi: 10.1093/biostatistics/kxx069
97. Gower NJD, Barry RJ, Edmunds MR, Titcomb LC, Denniston AK. Drug discovery in ophthalmology: past success, present challenges, and future opportunities. *BMC Ophthalmol.* (2016) 16:11. doi: 10.1186/s12886-016-0188-2
98. Gross JC, Harris A, Siesky BA, Sacco R, Shah A, Guidoboni G. Mathematical modeling for novel treatment approaches to open-angle glaucoma. *Expert Rev Ophthalmol.* (2017) 12:443–55. doi: 10.1080/17469899.2017.1383896
99. Khawaja AP, Cooke Bailey JN, Wareham NJ, Scott RA, Simcoe M, Igo RP, et al. Genome-wide analyses identify 68 new loci associated with intraocular pressure and improve risk prediction for primary open-angle glaucoma. *Nat Genet.* (2018) 50:778–82. doi: 10.1038/s41588-018-0126-8

Conflict of Interest: The authors declare that the research was conducted in the absence of any commercial or financial relationships that could be construed as a potential conflict of interest.

frontiers in Medicine

ORIGINAL RESEARCH
published: 09 December 2021
doi: 10.3389/fmed.2021.730327

Change of Retinal Vessel Density After Lowering Intraocular Pressure in Ocular Hypertension

Xuhao Chen[1,2], *Ying Hong*[1,2], *Haohao Di*[3], *Qianru Wu*[1,2], *Di Zhang*[1,2] *and Chun Zhang*[1,2]*

[1] Department of Ophthalmology, Peking University Third Hospital, Beijing, China, [2] Beijing Key Laboratory of Restoration of Damaged Ocular Nerve, Peking University Third Hospital, Beijing, China, [3] Department of Ophthalmology, Zhengzhou Second Hospital, Zhengzhou, China

Purpose: To investigate the relationship between retinal microvasculature changes and intraocular pressure (IOP) for ocular hypertension (OHT) patients and further assess the factors associated with retinal microcirculation changes.

Methods: This was a single-center prospective study designed for OHT patients, which consisted of two visits. After collecting baseline data of those who met the eligibility criteria, these patients were treated with latanoprost 0.005% ophthalmic solution for 4 weeks. Peripapillary vessel density (VD) of radial peripapillary capillaries (RPC) layer, macular VD in both superficial and deep layers, and foveal avascular zone (FAZ) area were measured by optical coherence tomography angiography (OCTA) before and after the treatment. We compared the changes in IOP and VD among the two visits by paired-sample *t*-test. Bonferroni correction was applied. Factors associated with VD changes were analyzed by linear regression analysis.

Results: Thirty-four eyes of thirty-four patients were included. The mean IOP decreased by 6.5 ± 2.2 mmHg ($p < 0.001$). The peripapillary RPC VD increased significantly from 51.8 ± 2.5 to 53.0 ± 3.1% (Adjusted-$p = 0.012$). We found no significant difference in detailed sectors of the peripapillary region after correction. In the macular area, both the superficial and deep layers in foveal (superficial: 0.2 ± 1.9%, $p = 0.523$; deep: 0.0 ± 2.3%, $p = 0.969$) and parafoveal (superficial: 0.3 ± 3.0%, $p = 0.565$; deep: 0.5 ± 3.1%, $p = 0.423$) VD remained unchanged. The decrease of the mean FAZ area was insignificant ($p = 0.295$). The percentage of IOP reduction (β = 0.330, $p = 0.031$) and the baseline RNFL thickness (β = 0.450, $p = 0.004$) significantly correlated with the percentage of peripapillary RPC VD improvement in the multivariate linear regression analysis.

Conclusion: The peripapillary VD in OHT patients increased after the reduction of IOP. The mild change of IOP did not alter the microcirculation in the macula. In addition, the percentage of IOP change and the baseline RNFL thickness were independent factors for the peripapillary RPC VD improvement.

Keywords: ocular hypertension, optical coherence tomography angiography, vessel density, intraocular pressure, latanoprost

OPEN ACCESS

Edited by:
Michele Lanza,
University of Campania Luigi Vanvitelli, Italy

Reviewed by:
Katarzyna Krysik,
Wojewódzki Szpital Specjalistyczny nr 5 Sosnowiec, Poland
Xiangmei Kong,
Fudan University, China
Jianqin Lei,
The First Affiliated Hospital of Xi'an Jiaotong University, China

***Correspondence:**
Chun Zhang
zhangc1@yahoo.com

Specialty section:
This article was submitted to Ophthalmology, a section of the journal Frontiers in Medicine

Received: *24 June 2021*
Accepted: *19 November 2021*
Published: *09 December 2021*

Citation:
Chen X, Hong Y, Di H, Wu Q, Zhang D and Zhang C (2021) Change of Retinal Vessel Density After Lowering Intraocular Pressure in Ocular Hypertension. Front. Med. 8:730327. doi: 10.3389/fmed.2021.730327

INTRODUCTION

Intraocular pressure (IOP) and retinal circulation were influenced by autoregulation in normal tissue (1, 2). A mild change of IOP within a short time exerts little influence on the peripapillary (3) or macular (3, 4) microcirculation. With the broader range of IOP changes, however, such homeostasis will be affected. Previous studies have revealed that an IOP spike is associated with reduced retinal perfusion in healthy controls (5, 6) and patients with narrow anterior chamber angles (4, 7). However, based on the models' nature, the long-term effect of IOP change on retinal circulation remained unsolved. Recent studies mainly discussed such interplay on glaucoma patients, with an emphasis on the impact of surgeries (8–13) and medication applications (14–18). Given the damaging retinal circulation with glaucoma progression (19), the correlation between the extent of microcirculation improvement and IOP reduction was inconsistent among studies. In comparison, ocular hypertension (OHT) patients present no signs of glaucomatous defects but suffer the risk of developing and progressing into primary open-angle glaucoma (POAG) with long-term IOP elevation (20–22). Previous studies revealed that the IOP reduction for OHT showed little impact on the ophthalmic artery (23). However, based on the nature of OHT, the retinal microcirculation may be influenced by topical hypotensive treatment (18). The peripapillary and macular microcirculation and their associations with IOP change for OHT were not thoroughly evaluated, which may affect the robustness to its therapeutic value. Further, the factors associated with microcirculation changes still need to be explored.

Optical coherence tomography angiography (OCTA) is an updated imaging technique based on the mechanism of optical coherence tomography (OCT) (24). It has been widely used as a non-invasive tool to assess glaucoma patients' retinal microcirculation (24, 25). The motion contrast generated by red blood cells provides a means to visualize the retinal microvasculature in both the macula and peripapillary region (25). With OCTA, the capillaries were automatically divided into different layers of both regions. To our knowledge, limiting studies had explored the retinal vascular response to IOP change by OCTA on OHT. Hereby, we used OCTA to assess the relationship between retinal microcirculation changes and IOP for OHT patients and further evaluated the factors associated with such vascular changes.

METHODS

This single-center prospective study was approved by the Institutional Review Board of Peking University Third Hospital (M2017242) and adhered to the tenets of the Declaration of Helsinki. Written informed consent was obtained from each participant before the enrollment.

Participants

Patients with OHT were prospectively enrolled in the glaucoma clinics of Peking University Third Hospital between July 2018 and June 2021. The criteria for ocular hypertension had been mentioned in the previous guideline (26). Inclusion criteria for all subjects were: (1) age between 10 and 70 years old, (2) open anterior chamber angles on gonioscopy, (3) IOP >21 mmHg, (4) best-corrected visual acuity (BCVA) $\geq$20/40 and refractive error within $+3.00$D and -8.00D, (5) without signs of RNFL retinal nerve fiber layer (RNFL) defect on fundus examination, (6) without signs of glaucomatous visual fields defects, and (7) treatment-naïve OHT. The study excluded those with (1) an IOP decrease of $<10\%$ of baseline after the treatment, (2) a history of systemic diseases including ischemic heart disease and diabetes, (3) a history of retinal or neurological disease, ocular trauma, or surgeries, and (4) poor OCT scans with scan quality (SQ)<6, the presence of motion artifacts or segmentation errors. One eye of each subject was enrolled in the study.

The study was comprised of two visits for each patient. All participants underwent standard ophthalmic examinations, including a best-corrected visual acuity measurement, slit-lamp examination, gonioscopy, Goldmann applanation tonometry, fundus examination, central corneal thickness (CCT), visual fields, and OCTA during the first visit. After collecting baseline data, the patients were treated topically with latanoprost 0.005% ophthalmic solution (XALATAN, Pfizer Manufacturing Belgium NV, Puurs, Belgium) once for four weeks in the ocular hypertension eye. The IOP and OCTA were re-evaluated after the four-week treatment at the same time of a day as one's first visit.

OCTA Image Acquisition and Processing

The OCTA scans were acquired via the Avanti spectral-domain system (RTVue-XR Avanti, software version 2017.1.0.155; Optovue, Inc.; Fremont, CA, USA). The perfused retinal vasculature was identified according to a split-spectrum amplitude-decorrelation angiography algorithm by capturing the motion of particles. Trained and experienced technicians were in charge of acquiring the scans. The Angio Disc 4.5 $\times$ 4.5 mm and Angio Retina 3.0 $\times$ 3.0 mm scans were obtained for both eyes within the same visit of the participants. Under these scan patterns, B-scans were equally spaced along the horizontal and vertical dimensions. Each scan was repeated at least twice. The built-in Angiovue software was centered on the optic disc and fovea automatically after the imaging process. Vascular information was featured quantitatively as vessel density (%), which calculated the proportion of perfused blood vessels within the measured area. The peripapillary region was defined as a 1 mm-wide annulus extending from a 2 mm ring centered on the disc, based on the disc margin. A modified Garway-Heath sector grid was overlaid on the Angio Disc en face images, dividing the peripapillary region into eight sections (**Figure 1A**) (27). The VD was measured on the radial peripapillary capillaries (RPC) plexus ranged from the inner limiting membrane (ILM) to the lower boundary of RNFL. Similarly, the parafovea region was defined as a 1 mm-wide annulus extending from a 1 mm circle centered on the fovea. The fovea center was automatically identified by searching for the thinnest part of the retinal slab ranging from ILM to the inner plexiform layer (IPL). The central foveal and parafoveal subfields were divided in accordance with the early treatment of diabetic retinopathy study (ETDRS) retinal grid definition (**Figure 1B**). And the VD of both superficial and deep

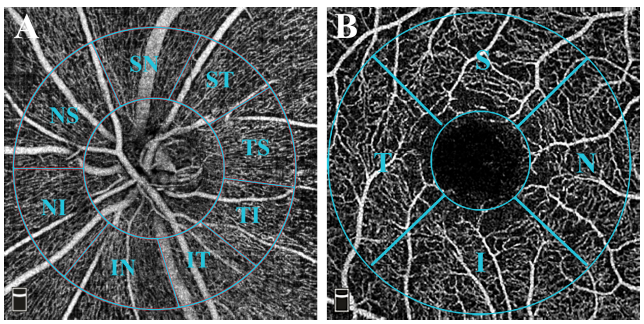

FIGURE 1 | OCTA measurement of vessel density. **(A)** Angio Disc 4.5 × 4.5 mm scan (left eye). The inner-circle represented the inside disc sector. The peripapillary region is defined by a 2-mm and a 4-mm ring centered on the disc. The image presented the peripapillary sectors according to a modified Garway-Heath method. The eight sectors included Nasal Superior (NS), Nasal Inferior (NI), Inferior Nasal (IN), Inferior Temporal (IT), Temporal Inferior (TI), Temporal Superior (TS), Superior Temporal (ST), and Superior Nasal (SN) regions. **(B)** Angio Retina 3 × 3 mm scan (right eye). The 1-mm circle in the center referred to the fovea. The parafovea region was defined as a 1 mm-wide annulus extending from a 1 mm circle centered on the fovea. The central foveal and parafoveal subfields were divided in accordance with the early treatment of diabetic retinopathy study (ETDRS) retinal grid definition, which included Nasal (N), Superior (S), Temporal (T), and Inferior (I) regions.

capillary plexus was measured on each subfield. Specifically, the superficial layer ranged from ILM to 10 μm above the IPL, while the deep layer ranged from 10 μm above IPL to 10 μm below the outer plexiform layer (OPL). A built-in Projection Artifact removal (PAR) algorithm was automatically applied to minimize the artifacts from the overlying vasculature. The foveal avascular zone (FAZ) area was automatically detected and measured. Any misalignment of OCTA scans was corrected manually. In order to repeat the scan location of the first visit, a follow-up mode was applied to both the retina and disc images. The VD will be excluded from the final analysis if one of the subfields lacks>30% of pixels as calculated by the built-in software due to scan de-centration. SQ indicated the image quality based on the signal strength index, eye motion, and focus. All scans were individually reviewed by two investigators (XC, HD) for evaluation of scan quality. The repeatability of the OCTA VD and FAZ measurement was assessed by the same investigators on different days in a random subset of ten eyes from our cohort.

Statistical Analysis

The sample size was preliminarily estimated by PASS (Version 11.0; NCSS Statistical Software, Kaysville, UT, USA). To detect a paired difference between the two visits, a sample size of 30 can achieve more than 80% power with a significance level of 0.05. Data analysis was performed using SPSS Statistics Software (Version 24.0; IBM Corp., Armonk, NY, USA). Figures were drawn by GraphPad Prism (Version 7.0; GraphPad Software, Inc., San Diego, CA, USA). The repeatability of the OCTA measurements was assessed using the intraclass correlation coefficient (ICC) by employing a two-way random-effects model. The Shapiro-Wilk test and Q-Q plots were used to assess the normality of each variable. Data were presented as means ± standard deviation (SD). Data before and after the treatment were compared and analyzed with a paired-sample *t*-test or Wilcoxon signed-rank test based on the normality. ΔVD and ΔIOP were defined as the percentage of change between the two visits. Regression analysis was performed to investigate the factors associated with the decrease of peripapillary VD. A univariate model was first introduced to explore potential factors. Variables with $p < 0.10$ in the univariate model were then introduced to a multivariate model by the stepwise method. $P < 0.05$ was considered statistically significant. *P*-values were adjusted by Bonferroni correction considering the multiple comparisons of vessel density in scans before and after the treatment.

TABLE 1 | Demographics of the participants ($N = 34$).

Characteristic	Mean ± SD; No. (%)
Age (years)	32.7 ± 13.0
Gender	
Male	19 (56)
Female	15 (44)
Eye	
OD	23 (68)
OS	11 (32)
SBP	120.8 ± 12.1
DBP	74.5 ± 12.0
BCVA (logMAR)	0.01 ± 0.04
SE	−3.46 ± 2.66
CCT (μm)	556.2 ± 32.0
C/D area ratio (%)	0.25 ± 0.13
C/D vertical ratio (%)	0.50 ± 0.18
C/D horizontal ratio (%)	0.45 ± 0.16
Rim area (mm^2)	1.6 ± 0.36
Disc area (mm^2)	2.17 ± 0.48
Cup volume (mm^3)	0.12 ± 0.10
IOP (mmHg)	
Pre-treatment	24.7 ± 2.6
Post-treatment	18.2 ± 2.6
Angio disc SQ	
Pre-treatment	8.4 ± 0.7
Post-treatment	8.4 ± 0.8
Angio retina SQ	
Pre-treatment	7.7 ± 1.0
Post-treatment	8.0 ± 0.9

BCVA, best-corrected visual acuity; CCT, central corneal thickness; C/D, cup/disc; DBP, diastolic blood pressure; DS, diopter of spherical power; IOP, intraocular pressure; SBP, systolic blood pressure; SE, spherical equivalent; SQ, scan quality.

RESULTS

Demographics

Following the eligibility criteria, a total of 34 eyes of 34 patients were included in the final analysis. **Table 1** shows the demographic, clinical, and optic nerve head (ONH) structure of all the subjects. The mean age was 32.7 ± 13.0 years, ranging from 12 to 68 years. The mean RNFL thickness

TABLE 2 | Peripapillary vessel density improved after IOP decrease ($N = 34$).

Sectors	Pre-treatment (%, Mean ± SD)	Post-treatment (%, Mean ± SD)	*t*	*p*	Adjusted *p*
Inside disc	50.6 ± 5.9	51.0 ± 6.2	−0.676	0.504	1.00
Peripapillary	51.8 ± 2.5	53.0 ± 3.1	−3.664	**0.001**	**0.01**
NS	46.5 ± 4.7	47.3 ± 5.5	−2.029	0.051	0.51
NI	45.5 ± 4.5	46.8 ± 4.8	−2.968	**0.006**	0.06
IN	50.2 ± 4.2	52.0 ± 5.0	−2.691	**0.011**	0.11
IT	57.8 ± 4.8	59.1 ± 4.2	−2.615	**0.013**	0.13
TI	54.7 ± 3.4	55.5 ± 3.4	−1.718	0.095	0.95
TS	56.3 ± 3.3	57.8 ± 3.5	−2.785	**0.009**	0.09
ST	56.7 ± 3.6	58.1 ± 3.5	−2.545	**0.016**	0.16
SN	50.6 ± 4.8	52.0 ± 4.9	−2.408	**0.022**	0.22

The peripapillary region was divided into eight sectors including Nasal Superior (NS), Nasal Inferior (NI), Inferior Nasal (IN), Inferior Temporal (IT), Temporal Inferior (TI), Temporal Superior (TS), Superior Temporal (ST), and Superior Nasal (SN). P < 0.05 were marked in bold. P-values were adjusted by Bonferroni correction.

TABLE 3 | Vessel density changes in macula scan after IOP decrease ($N = 31$).

Sectors	Superficial layer				Deep layer			
	Pre-treatment (%, Mean ± SD)	Post-treatment (%, Mean ± SD)	*t*	*p*	Pre-treatment (%, Mean ± SD)	Post-treatment (%, Mean ± SD)	*t*	*p*
Fovea	16.2 ± 6.4	16.4 ± 5.8	−0.646	0.523	30.4 ± 6.8	30.4 ± 6.1	−0.039	0.969
Parafovea	50.0 ± 2.9	50.3 ± 2.9	−0.583	0.565	52.9 ± 3.1	53.5 ± 3.1	−0.813	0.423
Temporal	48.7 ± 3.0	48.8 ± 2.9	−0.338	0.738	53.2 ± 2.8	53.2 ± 3.0	−0.017	0.987
Superior	51.0 ± 3.5	51.7 ± 2.8	−1.086	0.286	52.6 ± 3.9	53.0 ± 3.7	−0.556	0.582
Nasal	49.5 ± 2.8	49.4 ± 3.5	0.143	0.887	53.6 ± 3.6	54.2 ± 3.6	−0.984	0.333
Inferior	50.9 ± 3.9	51.3 ± 3.8	−0.710	0.484	52.1 ± 3.4	52.9 ± 3.4	−1.079	0.289

P < 0.05 were considered statistically significant.

was 114.1 ± 12.2 μm at baseline, while the mean parafoveal retinal thickness was 328.3 ± 14.7 μm. The mean IOP before treatment was 24.7 ± 2.6 mmHg (range: 22–32 mmHg). Latanoprost decreased the IOP by 6.5 ± 2.4 mmHg ($t = 15.612$, $p < 0.001$) after four weeks. The difference between the OCTA SQ of the two visits was insignificant in both scans (Angio Disc: $Z = -0.423$, $p = 0.672$; Angio Retina: $Z = -0.664$, $p = 0.507$). The ICCs for VD and FAZ measurement ranged from 0.967 to 1.000 (all $p < 0.001$, **Supplementary Table 1**).

Peripapillary VD

We compared RPC VD's data to evaluate the peripapillary microcirculation changes after IOP decrease for four weeks. The VD in the peripapillary region, indicating RPC's conditions, significantly increased from 51.8 ± 2.5% to 53.0 ± 3.1% ($t = -3.664$, $p = 0.001$) (**Table 2**). However, the VD inside the disc, which displayed the microcirculation of ONH, was not increased (0.4 ± 3.7%, $t = -0.697$, $p = 0.504$). In the comparison of a detailed segmentation, six of the eight sectors showed a significant increase. However, after the Bonferroni correction, only the overall peripapillary RPC VD increase remained statistically significant (adjusted-$p = 0.01$).

Macular VD

Both the superficial and the deep layers were investigated in the macula. In the fovea region, the vessel density remained stable after the treatment in both layers (superficial layer: 0.2 ± 1.9%, $t = -0.646$, $p = 0.523$; deep layer: 0.0 ± 2.3%, $t = 0.039$, $p = 0.969$). In a detailed analysis of FAZ, its mean area decreased from 0.331 ± 0.104 mm^2 to 0.328 ± 0.102 mm^2, but such a trend was insignificant ($t = 1.066$, $p = 0.295$). Similarly, the changes in parafoveal region were insignificant after the IOP decreased (superficial layer: 0.3 ± 3.0%, $t = -0.583$, $p = 0.565$; deep layer: 0.5 ± 3.1%, $t = 0.813$, $p = 0.423$). The detailed segmentation of the parafoveal region revealed no significant VD increase in all the quadrants (**Table 3**). To analyze the potential differences in response to IOP, we further compare the VD change between the superficial and deep layers. No significant difference was found in both foveal ($t = 0.620$, $p = 0.540$) and parafoveal ($t = -0.313$, $p = 0.756$) regions.

Factors Associated With RPC VD Increment

As we found a significant increase in peripapillary RPC VD, we further explored its association with different parameters using linear regression analysis. Age, blood pressure, spherical equivalent, CCT, IOP, RNFL thickness, SQ difference between

TABLE 4 | Factors associated with increase of peripapillary VD after treatment in linear regression analysis.

Factors	Univariate model			Multivariate model		
	β	95% CI	*p*	β	95% CI	*p*
Age	−0.525	(−0.252, −0.066)	**0.001**			
SBP	−0.052	(−0.181, 0.143)	0.810			
DBP	−0.139	(−0.213, 0.111)	0.519			
CCT	0.153	(−0.025, 0.062)	0.389			
SE	−0.157	(−0.759, 0.294)	0.375			
SQ difference	−1.015	(−2.639, 0.609)	0.212			
Baseline IOP	0.251	(−0.147, 0.902)	0.152			
Percentage of Δ IOP	0.447	(0.057, 0.347)	**0.008**	0.330	(0.015, 0.283)	**0.031**
Baseline VD	−0.108	(−0.722, 0.387)	0.543			
Baseline RNFL thickness	0.536	(0.075, 0.270)	**0.001**	0.450	(0.049, 0.240)	**0.004**
C/D area ratio	0.052	(−9.268, 12.426)	0.769			
C/D vertical ratio	0.008	(−7.602, 7.952)	0.964			
C/D horizontal ratio	0.007	(−8.545, 8.867)	0.970			
Rim area	0.120	(−2.636, 5.284)	0.501			
Disc area	0.105	(−2.093, 3.835)	0.554			
Cup volume	0.092	(−10.739, 18.101)	0.607			

CCT, central corneal thickness; C/D, cup/disc; CI, confidence interval; DBP, diastolic blood pressure; IOP, intraocular pressure; RNFL, retinal nerve fiber layer; SBP, systolic blood pressure; SE, spherical equivalent; SQ, scan quality; VD, vessel density. P < 0.05 were marked in bold.

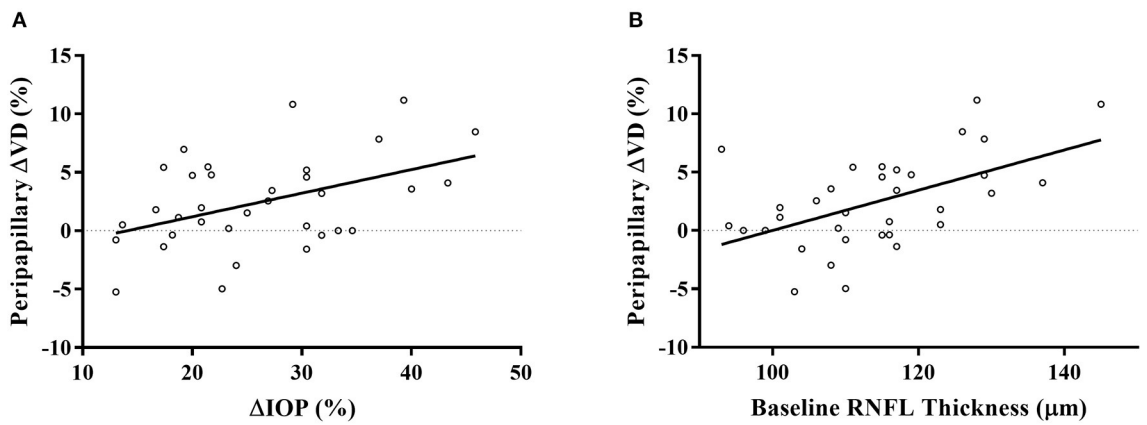

FIGURE 2 | Scatterplots displayed the significant association of IOP reduction percentage **(A)** and baseline RNFL thickness **(B)** with the percentage of peripapillary VD increase after treatment. ΔVD represented the percentage of VD change after a 4-week latanoprost application. ΔIOP represented the percentage of IOP reduction of each subject.

the visits, VD, and ONH measurements were included in the analysis. In the univariate model, age, percentage of IOP change, and the baseline RNFL thickness were significantly associated with the percentage of increase in peripapillary VD. Specifically, none of the other ONH parameters or their changes after IOP reduction was significantly correlated with peripapillary ΔVD. The further multivariate analysis displayed that both the percentage of IOP change ($\beta = 0.330$, $p = 0.031$) and baseline RNFL thickness ($\beta = 0.450$, $p = 0.004$) were significantly associated with the percentage of peripapillary VD improvement in the two models (**Table 4**; **Figure 2**).

DISCUSSION

The response of retinal microcirculation to IOP stimuli holds great promise to reveal the mechanism of the development and progression of glaucoma (28). Nonetheless, such relation was seldom reported on OHT patients (18, 23), who tend to progress into POAG with sustained high IOP (20, 21). The present study investigated the relationship of retinal VD and IOP change by latanoprost application using OCTA in OHT patients. To summarize, in OHT patients, (1) The peripapillary RPC VD increased significantly after lowering IOP. (2) The mild change of IOP did not alter the microcirculation in the macula. (3)

Regression analysis indicated that the percentage of IOP change and the baseline RNFL thickness were both independent factors for the peripapillary RPC VD improvement.

The improvement of peripapillary RPC VD by long-term IOP reduction was shown on OHT patients. The OCTA data after the hypotensive treatment had proved a significant trend of increment in RPC VD (**Table 2**). Similar hypotensive treatment had shown little impact on ophthalmic artery blood supply (23). The conclusion was drawn based on the phase-contrast magnetic resonance imaging (PC-MRI) technique after the 1-week treatment of latanoprost (23). However, the applied technique's resolution was insufficient to assess the capillaries (29), which were autoregulated based on the local feedback and tissue demands (28). In comparison, OCTA displayed the structural signal of vessels and capillaries instead of functional signals like velocity (24, 25). It has shown good effectiveness in measuring VD of both children and adult OHT patients (18, 30). Currently, limiting studies have investigated the influence of medical anti-glaucomatous therapy on retinal microcirculation by OCTA. In a group of treatment-naïve subjects, latanoprost decreased the mean IOP by 26.1% but did not improve the peripapillary VD (18). However, due to the varying severity and subtypes of the including glaucoma patients, such a conclusion may be flawed. In our prospective study, we only enrolled OHT patients above the age of 10 years, with better compliance in IOP measurement (31). The peripapillary VD increased significantly with a mean IOP decrease of 26.3%. After Bonferroni adjustment, such difference became insignificant in all the sectors, but the increase of overall peripapillary VD was significant. Our study indicated the susceptibility to the IOP decrease was consistent among all the sectors. To further investigate the peripapillary microcirculation on glaucoma patients, previous studies had focused on surgical-induced IOP decrease (8–13). Within a 12-month follow-up period, filtering surgeries did not improve the peripapillary VD under an IOP reduction of 24.6–51.1% (8, 9, 11, 13). Specifically, Shin et al. observed improved peripapillary microcirculation in 61.3% of participants within three months, but the mean VD did not increase significantly for all the included patients (10). Such neutral response of ocular perfusion to anti-glaucomatous treatment may originate from the retinal vascular defects caused by glaucoma progression (28). Typically, those in need of glaucoma surgery may suffer advanced microcirculatory defects. In OHT patients, the regulatory function of peripapillary retinal vasculature was possibly preserved, which possibly explained our differences from previous studies. Our findings indicated that the RPC VD increased significantly after reducing IOP in OHT patients, revealing the potential of peripapillary vascular improvement after treatment.

The mild change of IOP did not alter the microcirculation in the macula. In our study, the IOP decreased by 6.5 $\pm$ 2.4 mmHg, much lower than the surgical-induced IOP decrease in the previous studies (8–11, 32). In OHT patients, unlike the peripapillary region, the macular VD measured in different layers and FAZ area remained stable (**Table 3**). Similar results were observed in glaucoma patients (8, 11, 13, 18). Within about one month, both the surgical (8, 11, 13) and medical (18) therapy failed to improve VD in the macula. Previous studies have revealed a more prominent vascular damage in the peripapillary areas (33). Compared with this region, macular VD had shown a lower diagnostic value for glaucoma (33–36). Therefore, the macular VD may be less susceptible to external factors. Despite this, with a more extended follow-up period after surgery, some claimed that the foveal VD had revealed an increasing trend (13), accompanied by a decreasing FAZ area (13, 32). It was postulated that such a pattern of VD change might be induced by surgical inflammation (13). However, such delayed trends were not observed in the peripapillary region, which was unparallel to its susceptibility. The exact role of surgical-induced IOP change on the retina still needs to be explored. As we had applied a topical medication to the participants, the induction of inflammation will be milder than surgery. During our one-month follow-up, the VD change of different layers in the foveal and parafoveal region revealed no significant difference, which further proved the insusceptibility of macular microcirculation toward IOP in OHT patients. Therefore, the mild change of IOP did not alter the vasculature condition in the macula.

The reduction of IOP and the baseline RNFL thickness were independent factors associated with peripapillary RPC VD improvement, as shown in the multivariate linear regression model (**Figure 2**; **Table 4**). Although the image quality (37) and myopic status (38) correlated with retinal VD, we did not find their correlation with VD improvement. Previous cross-sectional studies have demonstrated an insignificant prediction value of IOP on the measurements of peripapillary parameters (39, 40). To further explore the role of IOP change in the retinal microcirculation by OCTA, previous studies had provoked an IOP spike by laser peripheral iridotomy (LPI) (4, 7) or darkroom prone provocative test (3). Wang et al. had observed a significant correlation with RPC VD change and IOP spike after LPI, with a mean IOP increase of 6.3 mmHg (7). However, possibly due to the short duration of IOP increase, such correlation was insignificant in other studies, even with a more significant IOP reduction (3, 4). The existence of vascular autoregulation, which adjusts the retinal capillaries, may confound the response to acute pressure elevation (28). In our study, with a mild IOP change similar to Wang et al. (7), we observed a significant correlation after a long-term duration, indicating a prolonged influence of IOP. Similarly, the change of peripapillary VD was found to correlate with IOP change in glaucoma patients after three weeks (18), which adds robustness to our findings. Studies have shown abnormal ocular vascular autoregulation in glaucoma patients, indicating the reduction of vascular resistance to perfusion pressure changes (2). Given that the RPC is damaged with glaucoma progression (19), those in need of surgery may have impaired regulation patterns of retinal microcirculation compared to healthy controls or early-stage patients. It was reported that prostaglandin analog could improve retinal microcirculation (15, 17, 41), but the exact role of its interaction on IOP and microcirculation was not thoroughly studied. The pharmacological effect can't be completely ruled out unless further studies compare different doses or categories of IOP-lowering medication. Nevertheless, our results on OHT patients indicated the relationship between IOP and retinal blood supply on normal tissues. As for another

factor, RNFL thickness remained stable after IOP reduction, but the baseline RNFL thickness correlated with peripapillary RPC VD improvement (**Table 4**). It was claimed that VD change introduced by IOP reduction after trabeculectomy in POAG was not associated with RNFL thickness (9). In normal structures, perfusion will be regulated based on the metabolic condition (2). However, as POAG patients have suffered RNFL and RPC defects (42), the relationship between RNFL thickness and RPC may be affected. Together, our study indicated that thicker RNFL might possess more significant potential to adjust the circulation conditions due to its metabolic requirement. The additional perfusion promoted by anti-glaucomatous treatments will increase the metabolic supply for peripapillary RNFL. Consequently, extra nourishment to the RNFL will be provided by IOP reduction, adding therapeutic value to the OHT patients. As topical hypotensive treatment had revealed its effectiveness in preventing or delaying POAG onset in OHT patients (20), the accompanying improvement of peripapillary microcirculation might serve as a protection mechanism. Together, both the IOP reduction and thicker baseline RNFL were independent factors for peripapillary RPC VD improvement.

Recent studies have focused on the application of OCT and OCTA on the early detection of development and progression in glaucoma suspects and patients. Specifically, the longitudinal structural and vascular metrics changes have been frequently studied (43, 44). In the early diagnosis of glaucoma, both ONH, RNFL, and macular parameters have shown a high level of value (44). For an experimental IOP spike, OCT detected an immediate change of vascular metrics (4, 7) and retinal structures (45, 46). While in varied surgical treatment for glaucoma patients, the OCT technique provides an objective index for follow-up (8–13, 47–50). Therefore, the current application of the OCT technique can provide information about the retinal response to stimulation or treatment for glaucoma patients. Similarly, our study shed light on the longitudinal influence of IOP lowering on the OHT, which indicated the potential of early treatment for these patients. Further studies comparing different medications or other IOP lowering techniques may be helpful in the early treatment of glaucoma.

There are still several limitations that need attention and further addressed in our study. First, we only included a relatively small sample of OHT patients whose retinal microcirculation may differ from glaucoma patients. The effect of latanoprost on the peripapillary microcirculation of glaucoma patients in different stages required further analysis. Second, the follow-up time of our study was limited to four weeks. The relationship between retinal microcirculation and IOP reduction induced by medications with a longer duration still needs to be explored, especially for treatment-naïve patients. Third, as measured by OCTA, vessel density did not display the exact velocity of retinal perfusion. Possible changes of velocity in both large vessels and microcirculation in the peripapillary region should be assessed in future studies.

In conclusion, the peripapillary VD in OHT patients increased after the reduction of IOP. The mild change of IOP did not alter the microcirculation in the macula. In addition, the percentage of IOP change and the baseline RNFL thickness were independent factors for the peripapillary RPC VD improvement.

DATA AVAILABILITY STATEMENT

The raw data supporting the conclusions of this article will be made available by the authors, without undue reservation.

ETHICS STATEMENT

The studies involving human participants were reviewed and approved by Peking University Third Hospital. Written informed consent to participate in this study was provided by the participants' legal guardian/next of kin.

AUTHOR CONTRIBUTIONS

XC, YH, and CZ: conception and design. XC, YH, HD, QW, and DZ: data collection. XC, YH, and HD: analysis and interpretation of data. XC: drafting the manuscript. YH, HD, QW, DZ, and CZ: critical revesion of the manuscript. All authors contributed to the article and approved the submitted version.

FUNDING

This study was supported by National Natural Science Foundation of China (No. 81970798) and Capital's Funds for Health Improvement and Research (No. CFH-2020-2-40911).

SUPPLEMENTARY MATERIAL

The Supplementary Material for this article can be found online at: https://www.frontiersin.org/articles/10.3389/fmed.2021.730327/full#supplementary-material

REFERENCES

1. Prada D, Harris A, Guidoboni G, Siesky B, Huang AM, Arciero J. Autoregulation and neurovascular coupling in the optic nerve head. *Surv Ophthalmol.* (2016) 61:164–86. doi: 10.1016/j.survophthal.2015.10.004
2. Schmidl D, Garhofer G, Schmetterer L. The complex interaction between ocular perfusion pressure and ocular blood flow - relevance for glaucoma. *Exp Eye Res.* (2011) 93:141–55. doi: 10.1016/j.exer.2010.09.002
3. Zhang Q, Jonas JB, Wang Q, Chan SY, Xu L, Wei WB, et al. Optical coherence tomography angiography vessel density changes after acute intraocular pressure elevation. *Sci Rep.* (2018) 8:6024. doi: 10.1038/s41598-018-24520-x
4. Ma ZW, Qiu WH, Zhou DN, Yang WH, Pan XF, Chen H. Changes in vessel density of the patients with narrow antenior chamber after an acute intraocular pressure elevation observed by OCT angiography. *BMC Ophthalmol.* (2019) 19:132. doi: 10.1186/s12886-019-1146-6
5. Kiyota N, Shiga Y, Ichinohasama K, Yasuda M, Aizawa N, Omodaka K, et al. The impact of intraocular pressure elevation on optic nerve head

and choroidal blood flow. *Invest Ophthalmol Vis Sci.* (2018) 59:3488–96. doi: 10.1167/iovs.18-23872
6. Iwase T, Akahori T, Yamamoto K, Ra E, Terasaki H. Evaluation of optic nerve head blood flow in response to increase of intraocular pressure. *Sci Rep.* (2018) 8:17235. doi: 10.1038/s41598-018-35683-y
7. Wang X, Chen J, Kong X, Sun X. Immediate changes in peripapillary retinal vasculature after intraocular pressure elevation -an optical coherence tomography angiography study. *Curr Eye Res.* (2020) 45:749–56. doi: 10.1080/02713683.2019.1695843
8. Lommatzsch C, Rothaus K, Koch JM, Heinz C, Grisanti S. Retinal perfusion 6 months after trabeculectomy as measured by optical coherence tomography angiography. *Int Ophthalmol.* (2019) 39:2583–94. doi: 10.1007/s10792-019-01107-7
9. Kim JA, Kim TW, Lee EJ, Girard M, Mari JM. Microvascular changes in peripapillary and optic nerve head tissues after trabeculectomy in primary open-angle glaucoma. *Invest Ophthalmol Vis Sci.* (2018) 59:4614–21. doi: 10.1167/iovs.18-25038
10. Shin JW, Sung KR, Uhm KB, Jo J, Moon Y, Song MK, et al. Peripapillary microvascular improvement and lamina cribrosa depth reduction after trabeculectomy in primary open-angle glaucoma. *Invest Ophthalmol Vis Sci.* (2017) 58:5993–9. doi: 10.1167/iovs.17-22787
11. Zeboulon P, Leveque PM, Brasnu E, Aragno V, Hamard P, Baudouin C, et al. Effect of surgical intraocular pressure lowering on peripapillary and macular vessel density in glaucoma patients: an optical coherence tomography angiography study. *J Glaucoma.* (2017) 26:466–72. doi: 10.1097/IJG.0000000000000652
12. Alnawaiseh M, Muller V, Lahme L, Merte RL, Eter N. Changes in flow density measured using optical coherence tomography angiography after istent insertion in combination with phacoemulsification in patients with open-angle glaucoma. *J Ophthalmol.* (2018) 2018:2890357. doi: 10.1155/2018/2890357
13. Ch'ng TW, Gillmann K, Hoskens K, Rao HL, Mermoud A, Mansouri K. Effect of surgical intraocular pressure lowering on retinal structures - nerve fibre layer, foveal avascular zone, peripapillary and macular vessel density: 1 year results. *Eye.* (2020) 34:562–71. doi: 10.1038/s41433-019-0560-6
14. Kurysheva NI. Assessment of the optic nerve head, peripapillary, and macular microcirculation in the newly diagnosed patients with primary open-angle glaucoma treated with topical tafluprost and tafluprost/timolol fixed combination. *Taiwan J Ophthalmol.* (2019) 9:93–9. doi: 10.4103/tjo.tjo_108_17
15. Iida Y, Akagi T, Nakanishi H, Ohashi IH, Morooka S, Suda K, et al. Retinal blood flow velocity change in parafoveal capillary after topical tafluprost treatment in eyes with primary open-angle glaucoma. *Sci Rep.* (2017) 7:5019. doi: 10.1038/s41598-017-05258-4
16. Harris A, Garzozi HJ, McCranor L, Rechtman E, Yung CW, Siesky B. The effect of latanoprost on ocular blood flow. *Int Ophthalmol.* (2009) 29:19–26. doi: 10.1007/s10792-008-9190-x
17. Gherghel D, Hosking SL, Cunliffe IA, Armstrong RA. First-line therapy with latanoprost 0.005% results in improved ocular circulation in newly diagnosed primary open-angle glaucoma patients: a prospective, 6-month, open-label study. *Eye.* (2008) 22:363–9. doi: 10.1038/sj.eye.6702639
18. Liu C, Umapathi RM, Atalay E, Schmetterer L, Husain R, Boey PY, et al. The effect of medical lowering of intraocular pressure on peripapillary and macular blood flow as measured by optical coherence tomography angiography in treatment-naïve eyes. *J Glaucoma.* (2021) 30:465–72. doi: 10.1097/IJG.0000000000001828
19. Geyman LS, Garg RA, Suwan Y, Trivedi V, Krawitz BD, Mo S, et al. Peripapillary perfused capillary density in primary open-angle glaucoma across disease stage: an optical coherence tomography angiography study. *Br J Ophthalmol.* (2017) 101:1261–8. doi: 10.1136/bjophthalmol-2016-309642
20. Kass MA, Heuer DK, Higginbotham EJ, Johnson CA, Keltner JL, Miller JP, et al. The Ocular Hypertension Treatment Study: a randomized trial determines that topical ocular hypotensive medication delays or prevents the onset of primary open-angle glaucoma. *Arch Ophthalmol.* (2002) 120:701–13; discussion 829–30. doi: 10.1001/archopht.120.6.701
21. Gordon MO, Beiser JA, Brandt JD, Heuer DK, Higginbotham EJ, Johnson CA, et al. The Ocular Hypertension Treatment Study: baseline factors that predict the onset of primary open-angle glaucoma. *Arch Ophthalmol.* (2002) 120:714–20; discussion 829–30. doi: 10.1001/archopht.120.6.714
22. Selvan H, Gupta S, Wiggs JL, Gupta V. Juvenile-onset open-angle glaucoma - a clinical and genetic update. *Surv Ophthalmol.* (2021). doi: 10.1016/j.survophthal.2021.09.001. [Epub ahead of print].
23. Jóhannesson G, Qvarlander S, Wåhlin A, Ambarki K, Hallberg P, Eklund A, et al. Intraocular pressure decrease does not affect blood flow rate of ophthalmic artery in ocular hypertension. *Invest Ophthalmol Vis Sci.* (2020) 61:17. doi: 10.1167/iovs.61.12.17
24. Bojikian KD, Chen PP, Wen JC. Optical coherence tomography angiography in glaucoma. *Curr Opin Ophthalmol.* (2019) 30:110–6. doi: 10.1097/ICU.0000000000000554
25. Kashani AH, Chen CL, Gahm JK, Zheng F, Richter GM, Rosenfeld PJ, et al. Optical coherence tomography angiography: a comprehensive review of current methods and clinical applications. *Prog Retin Eye Res.* (2017) 60:66–100. doi: 10.1016/j.preteyeres.2017.07.002
26. European-Glaucoma-Society. European Glaucoma Society Terminology and Guidelines for Glaucoma, 4th Edition - Chapter 2: classification and terminology supported by the EGS foundation: Part 1: foreword; introduction; glossary; chapter 2 classification and terminology. *Br J Ophthalmol.* (2017) 101:73–127. doi: 10.1136/bjophthalmol-2016-EGSguideline.002
27. Garway-Heath DF, Poinoosawmy D, Fitzke FW, Hitchings RA. Mapping the visual field to the optic disc in normal tension glaucoma eyes. *Ophthalmology.* (2000) 107:1809–15. doi: 10.1016/S0161-6420(00)00284-0
28. Venkataraman ST, Flanagan JG, Hudson C. Vascular reactivity of optic nerve head and retinal blood vessels in glaucoma–a review. *Microcirculation.* (2010) 17:568–81. doi: 10.1111/j.1549-8719.2010.00045.x
29. Ambarki K, Hallberg P, Jóhannesson G, Lindén C, Zarrinkoob L, Wåhlin A, et al. Blood flow of ophthalmic artery in healthy individuals determined by phase-contrast magnetic resonance imaging. *Invest Ophthalmol Vis Sci.* (2013) 54:2738–45. doi: 10.1167/iovs.13-11737
30. Chen X, Wang X, Hu X, Sun X. The evaluation of juvenile ocular hypertension by optical coherence tomography angiography. *BMC Ophthalmol.* (2020) 20:423. doi: 10.1186/s12886-020-01641-4
31. Feng CS, Jin KW, Yi K, Choi DG. Comparison of intraocular pressure measurements obtained by rebound, noncontact, and goldmann applanation tonometry in children. *Am J Ophthalmol.* (2015) 160:937–43.e1. doi: 10.1016/j.ajo.2015.07.029
32. Shoji T, Kanno J, Weinreb RN, Yoshikawa Y, Mine I, Ishii H, et al. OCT angiography measured changes in the foveal avascular zone area after glaucoma surgery. *Br J Ophthalmol.* (2020). doi: 10.1136/bjophthalmol-2020-317038. [Epub ahead of print].
33. Triolo G, Rabiolo A, Shemonski ND, Fard A, Di Matteo F, Sacconi R, et al. Optical coherence tomography angiography macular and peripapillary vessel perfusion density in healthy subjects, glaucoma suspects, and glaucoma patients. *Invest Ophthalmol Vis Sci.* (2017) 58:5713–22. doi: 10.1167/iovs.17-22865
34. Yip V, Wong HT, Yong V, Lim BA, Hee OK, Cheng J, et al. Optical coherence tomography angiography of optic disc and macula vessel density in glaucoma and healthy eyes. *J Glaucoma.* (2019) 28:80–7. doi: 10.1097/IJG.0000000000001125
35. Yarmohammadi A, Zangwill LM, Manalastas PIC, Fuller NJ, Diniz-Filho A, Saunders LJ, et al. Peripapillary and macular vessel density in patients with primary open-angle glaucoma and unilateral visual field loss. *Ophthalmology.* (2018) 125:578–87. doi: 10.1016/j.ophtha.2017.10.029
36. Richter GM, Chang R, Situ B, Chu Z, Burkemper B, Reznik A, et al. Diagnostic performance of macular versus peripapillary vessel parameters by optical coherence tomography angiography for glaucoma. *Transl Vis Sci Technol.* (2018) 7:21. doi: 10.1167/tvst.7.6.21
37. Dastiridou A, Kassos I, Samouilidou M, Koutali D, Mataftsi A, Androudi S, et al. Age and signal strength-related changes in vessel density in the choroid and the retina: an OCT angiography study of the macula and optic disc. *Acta Ophthalmol.* (2021). doi: 10.1111/aos.15028. [Epub ahead of print].
38. Liu M, Wang P, Hu X, Zhu C, Yuan Y, Ke B. Myopia-related stepwise and quadrant retinal microvascular alteration and its correlation with axial length. *Eye.* (2021) 35:2196–205. doi: 10.1038/s41433-020-01225-y
39. Yun YI, Kim YW, Lim HB, Lee DH, Kim JH, Oh BL, et al. Peripapillary vessel parameters and mean ocular perfusion pressure in young healthy

eyes: OCT angiography study. *Br J Ophthalmol.* (2021) 105:862–8. doi: 10.1136/bjophthalmol-2020-316222
40. Juliano J, Burkemper B, Lee J, Nelson A, LeTran V, Chu Z, et al. Longer axial length potentiates relationship of intraocular pressure and peripapillary vessel density in glaucoma patients. *Invest Ophthalmol Vis Sci.* (2021) 62:37. doi: 10.1167/iovs.62.9.37
41. Weindler H, Spitzer MS, Schultheiß M, Kromer R. OCT angiography analysis of retinal vessel density in primary open-angle glaucoma with and without Tafluprost therapy. *BMC Ophthalmol.* (2020) 20:444. doi: 10.1186/s12886-020-01707-3
42. Mansoori T, Sivaswamy J, Gamalapati JS, Balakrishna N. Radial peripapillary capillary density measurement using optical coherence tomography angiography in early glaucoma. *J Glaucoma.* (2017) 26:438–43. doi: 10.1097/IJG.0000000000000649
43. Miguel A, Silva A, Barbosa-Breda J, Azevedo L, Abdulrahman A, Hereth E, et al. OCT-angiography detects longitudinal microvascular changes in glaucoma: a systematic review. *Br J Ophthalmol.* (2021). doi: 10.1136/bjophthalmol-2020-318166. [Epub ahead of print].
44. Vazquez LE, Bye A, Aref AA. Recent developments in the use of optical coherence tomography for glaucoma. *Curr Opin Ophthalmol.* (2021) 32:98–104. doi: 10.1097/ICU.0000000000000733
45. Wang YX, Zhang Q, Yang H, Chen JD, Wang N, Jonas JB. Lamina cribrosa pore movement during acute intraocular pressure rise. *Br J Ophthalmol.* (2019) 104:800–6. doi: 10.1136/bjophthalmol-2019-314016
46. Wang YX, Jiang R, Wang NL, Xu L, Jonas JB. Acute peripapillary retinal pigment epithelium changes associated with acute intraocular pressure elevation. *Ophthalmology.* (2015) 122:2022–8. doi: 10.1016/j.ophtha.2015.06.005
47. Gietzelt C, von Goscinski C, Lemke J, Schaub F, Hermann MM, Dietlein TS, et al. Dynamics of structural reversal in Bruch's membrane opening-based morphometrics after glaucoma drainage device surgery. *Graefes Arch Clin Exp Ophthalmol.* (2020) 258:1227–36. doi: 10.1007/s00417-020-04621-y
48. Kiessling D, Christ H, Gietzelt C, Schaub F, Dietlein TS, Cursiefen C, et al. Impact of ab-interno trabeculectomy on Bruch's membrane opening-based morphometry of the optic nerve head for glaucoma progression analysis. *Graefes Arch Clin Exp Ophthalmol.* (2019) 257:339–47. doi: 10.1007/s00417-018-4187-2
49. Gietzelt C, Lemke J, Schaub F, Hermann MM, Dietlein TS, Cursiefen C, et al. Structural reversal of disc cupping after trabeculectomy alters bruch membrane opening-based parameters to assess neuroretinal rim. *Am J Ophthalmol.* (2018) 194:143–52. doi: 10.1016/j.ajo.2018.07.016
50. Lyssek-Boroń A, Wylegała A, Polanowska K, Krysik K, Dobrowolski D. Longitudinal changes in retinal nerve fiber layer thickness evaluated using avanti Rtvue-XR optical coherence tomography after 23G vitrectomy for epiretinal membrane in patients with open-angle glaucoma. *J Healthc Eng.* (2017) 2017:4673714. doi: 10.1155/2017/4673714

Conflict of Interest: The authors declare that the research was conducted in the absence of any commercial or financial relationships that could be construed as a potential conflict of interest.

Publisher's Note: All claims expressed in this article are solely those of the authors and do not necessarily represent those of their affiliated organizations, or those of the publisher, the editors and the reviewers. Any product that may be evaluated in this article, or claim that may be made by its manufacturer, is not guaranteed or endorsed by the publisher.

frontiers in Medicine

ORIGINAL RESEARCH
published: 17 January 2022
doi: 10.3389/fmed.2021.736792

The Relationship Between Plasma Tetrahydrocannabinol Levels and Intraocular Pressure in Healthy Adult Subjects

Sameh Mosaed[1,2], *Andrew K. Smith*[1,2]*, *John H. K. Liu*[3], *Donald S. Minckler*[2], *Robert L. Fitzgerald*[4], *David Grelotti*[5], *Emily Sones*[5], *Robert N. Weinreb*[3] and *Thomas D. Marcotte*[5]

[1] Gavin Herbert Eye Institute, University of California, Irvine, Irvine, CA, United States, [2] Irvine School of Medicine, University of California, Irvine, Irvine, CA, United States, [3] Viterbi Family Department of Ophthalmology, University of California, San Diego, San Diego, CA, United States, [4] Department of Pathology, University of California, San Diego, San Diego, CA, United States, [5] Department of Psychiatry, University of California, San Diego, San Diego, CA, United States

OPEN ACCESS

Edited by:
Michele Lanza,
University of Campania Luigi Vanvitelli, Italy

Reviewed by:
Parul Ichhpujani,
Government Medical College and Hospital, India
Luciano Quaranta,
University of Pavia, Italy

***Correspondence:**
Andrew K. Smith
andrewks@hs.uci.edu

Specialty section:
This article was submitted to Ophthalmology, a section of the journal Frontiers in Medicine

Received: 05 July 2021
Accepted: 24 December 2021
Published: 17 January 2022

Citation:
Mosaed S, Smith AK, Liu JHK, Minckler DS, Fitzgerald RL, Grelotti D, Sones E, Weinreb RN and Marcotte TD (2022) The Relationship Between Plasma Tetrahydrocannabinol Levels and Intraocular Pressure in Healthy Adult Subjects. Front. Med. 8:736792. doi: 10.3389/fmed.2021.736792

Background: Δ9-tetrahydrocannabinol (THC) has been shown to decreased intraocular pressure (IOP). This project aims to define the relationship between plasma THC levels and IOP in healthy adult subjects.

Methods: Eleven healthy subjects received a single dose of inhaled cannabis that was self-administered in negative pressure rooms. Measurements of IOP and plasma THC levels were taken at baseline and every 30 min for 1 h and afterwards every hour for 4 h. IOP reduction and percent change in IOP over time were calculated. Linear regression models were used to measure the relationship between IOP and plasma THC levels. Two line linear regression models with F-tests were used to detect change points in the regression. Then, Pearson correlations were computed based on the change point.

Results: Twenty-two eyes met inclusion criteria. The average peak percentage decrease in IOP was 16% at 60 min. Percent IOP reduction as well as total IOP reduction demonstrated a negative correlation with THC plasma levels showing r-values of −0.81 and −0.70, respectively. *F*-tests revealed a change point in the regression for plasma levels >20 ng/ml. For levels >20 ng/ml, the correlation coefficients changed significantly with *r*-values of 0.21 and 0.29 ($p < 0.01$).

Conclusion: Plasma THC levels are significantly correlated with IOP reduction up to plasma levels of 20 ng/ml. Plasma levels >20 ng/ml were not correlated with further decrease in IOP. More research is needed to determine the efficacy of THC in reducing IOP for eyes with ocular hypertension and glaucoma.

Keywords: tetrahydrocannabinol (THC), glaucoma, cannabis, intraocular pressure (IOP), treatment

INTRODUCTION

Although not yet adopted in clinical practice, prior studies have demonstrated the intraocular pressure (IOP)-lowering effects of cannabis (1–4). Inhaled marijuana has been shown to decrease IOP by 25% in some studies while intravenous THC lowered IOP by 37% (3, 4). Topically applied THC in animal models and sublingual THC in humans have likewise demonstrated significant IOP-lowering effects (1, 2). Despite the IOP-lowering effects of cannabis, clinical adoption of THC for the treatment of elevated IOP has been limited.

There are several reasons for this, namely that topically administered pharmaceutical formulations of THC have historically poor corneal penetration, and hence limited IOP-lowering effects, and systemic administration is associated with psychotropic and potential cardiovascular side effects, thereby limiting use in clinical practice (5–9). Improving corneal penetration is an area of active research and some have shown promise through various methods (10–14).

When inhaled, THC is detected in the serum within seconds after the first puff, achieving peak plasma levels within 3–10 min (15). The bioavailability of THC varies greatly, with ranges reported between 2 and 56% (16). This variability is attributed to the differences in smoking practices and is influenced by the depth of inhalation, number of puffs, time between puffs as well as hold time of each user. After stopping inhalation, plasma levels fall rapidly. For example, when subjects smoked a cigarette containing 3.55% THC, peak concentrations ranged from 76 to 267 ng/ml but were <5 ng/ml within 2 h for all subjects (17). The average plasma clearance has been reported to be 11.8 ± 3 L/h for women and 14.9 ± 3.7 L/h for men with plasma half-life ranging from 18.7 h to 4.1 days (18, 19). The speed at which THC leaves the serum is attributed to its wide distribution into tissues including brain, heart, lungs, and adipose tissue as well as its metabolism by the liver (20). Metabolism by P450 enzymes in the liver turn the compound into a number of different metabolites including most prominently THC-COOH (17). These metabolites are then excreted in the feces and urine.

Recently, the first double-blinded randomized controlled trial demonstrated that inhaled THC reduced IOP by 16% in healthy adult subjects (21). This study reports on the correlation between THC plasma levels and IOP reduction of those patients. This is the first study to assess the correlation between THC plasma levels and IOP in adult healthy subjects.

MATERIALS AND METHODS

Regulatory Process

This study was approved by the University of California, San Diego (UCSD) Human Research Protections, and adhered to the Declaration of Helsinki. The parent study was conducted under IND 131268, and approved by the Research Advisory Panel of California. This study was conducted at the University of California, Center for Medicinal Cannabis Research (CMCR). Two rooms were specifically outfitted with a negative pressure system to enable cannabis to be vented to the atmosphere without contaminating the workspace of others. Cannabis was harvested at the University of Mississippi under the supervision of the National Institute on Drug Abuse (NIDA).

Participant Selection

Informed consent was obtained from all participants. Participants were a consecutive subset of individuals enrolled in a larger study examining the impact of acute cannabis inhalation on driving performance. Subjects were recruited from the community. Eligible participants (healthy adults between 21 and 55 years of age) were scheduled for a baseline session and one, 8-h experimental session at the CMCR.

Patients were included who were older than 21 years, a licensed driver and driven a minimum of 1,000 miles in the past year, a regular cannabis smoker (>/=4 times in the past month), willing to not disclose details of the simulator and iPad-based assessments, and willing to complete the IOP tonometer evaluations. Exclusion criteria for this study included a known history of glaucoma or other eye disorder other than refractive error, the inability to refrain from contact lens use on the day of visits, history of traumatic brain injury, an unwillingness to abstain from cannabis for: 2 days prior to screening visit (so driving simulation will not be impaired) and 2 days prior to experimental visit (2–3 half-lives of THC), a positive pregnancy test, a positive result on toxicity screening for cocaine, amphetamines, opiates, and phencyclidine (PCP). However, a positive result for a prescribed or recommended drug (cannabis) was not exclusionary. Individuals with current substance use disorders as assessed using the Drug Abuse Screening Test (DAST) and Alcohol Use Disorders Identification Test (AUDIT) were excluded. Subjects were also excluded for being unwilling to be transported by cab or have a responsible adult drive them home after experimental session or inability to complete study procedures (i.e., poor veins, unwillingness to be transported home by taxi, or friend).

Study Design

Three-hundred participants were recruited with the intention to study up to 220 participants who met inclusion/exclusion criteria and ultimately provide complete data. Eleven participants were screened and enrolled in the IOP component. At the beginning of the screening/baseline visit and the experimental visit, subjects underwent a urine drug screen and breathalyzer for alcohol and drugs. In addition, an oral fluid sample was run for the presence of delta-9 THC using a testing device (Draeger 5000) which identifies THC levels at above vs. below 5 ng. A positive reading on the Draeger was considered indicative of use within the past day. Any participants with a positive reading were excluded (none occurred within the subsample for this study).

Participants were divided into two groups and each received either a 5.9 or 13.4 w/w % cannabis cigarette at their visits. Group assignment were assigned using a permuted blocks randomization with stratification by prior cannabis exposure [frequent user (>4x per week) vs. occasional user (<4x per week)]. They were asked to smoke 700 mg cigarettes with either 5.9, or 13.4% (at the beginning of the day, and to measure IOP, complete driving simulations, iPad-based performance assessments, and bodily fluid draws [e.g., blood, oral fluid

(OF) saliva, breath] before the cannabis smoking and over the subsequent 6 h after cannabis smoking. Participants were instructed to "*smoke the joint/cigarette the way you do at home to get high*" (i.e., there was no requirement that they finish the entire cigarette). Though not mandatory to incinerate the cigarette to the proximal tip, a minimum of 4 puffs was required for a participant to remain in the study. They were allowed 10 min to smoke. The allocation schedule was kept in the pharmacy and concealed from other study personnel. Patients and assessors were blinded to group assignments.

Monitoring of Vital Signs

Vital signs were monitored throughout the experiment at hourly intervals to monitor the subject's health status as well as to quantify marijuana's general effects. At any sign of an adverse reaction (e.g., a change in blood pressure or pulse rate or development of psychological distress), an investigator was called. Subjects remained in the laboratory under direct observation for 7 h after the marijuana smoking inhalations were completed. At that time, a final vital sign and self-report status check was made and upon satisfactory readings, the subject was released and driven back to his/her domicile by taxicab or prearranged transportation. The return transport procedure was observed directly by staff to ensure compliance.

Cardiovascular Monitoring

Blood pressure and pulse were assessed pre-smoking, and at approximately every 30 min for 2 h post-smoking session, then up to every hour for the additional 3 h.

IOP and THC Plasma Monitoring

THC plasma levels were taken prior to smoking, and then at ∼12 min after, 40, 80, 120 min, and every hour for the additional 3 h after smoking. The average of three IOP readings at each of these time points were taken for each eye. IOP readings were obtained by trained research assistants. Measurements of IOP were taken using the non-contact Ocular Response Analyzer (Reichert Technologies, Depew, NY). This device is FDA approved and was used in our protocol in accordance to the FDA label. Of note, if the participant had high IOP (21 mmHg or higher) prior to smoking, we recommended follow-up with an ophthalmologist.

Data Analysis Overview

In this analysis, data from the low-dose and high-dose group were combined as there were no statistically significant differences in the plasma levels between the two groups. This is because the participants were permitted to self-administer the quantity of puffs until they felt a psychotropic effect. Total IOP reduction in mmHg was calculated along with the percent reduction for each participant. The peak THC plasma level was determined for each participant. Linear regression models were then used to assess the relationship between IOP and THC plasma levels. Two-line linear regression models with *F*-tests were used to detect change points in the regression models. Pearson correlations were then calculated for values under and over the change point.

RESULTS

Twenty-two eyes of 11 subjects were included in the analysis. There are no missing values or outliers in the data. The IOP was normally distributed. The average peak THC plasma level was 45 ng/ml and occurred at 12 min. THC plasma levels spiked reaching peak levels at 12 min and then rapidly declined, achieving levels of <10 ng/ml by 55 min (**Figure 1**). THC levels continued to gradually decline for the remaining time periods. Average IOP before inhalation was 17.5 mmHg. After inhalation, IOP percent reduction ranged from 7 to 16% with the greatest IOP percent reduction of 16% seen at 60 min (**Figure 2**). This percent reduction of IOP gradually decreased for the remaining time periods.

IOP and plasma THC levels showed a strong negative correlation (**Figures 3**, **4**). Two line linear regression models revealed a change point at 20 ng/ml. Percent IOP reduction and THC plasma levels demonstrated a correlation coefficient of −0.81 for THC plasma levels up to 20 ng/ml and 0.21 for levels over 20 ng/ml (F-statistic = 16.93, $p < 0.01$). Total IOP reduction and plasma THC showed similar results with correlation coefficients of −0.70 for THC plasma levels up to 20 ng/ml and 0.29 for values over 20 ng/ml (F-statistic = 7.92, $p < 0.01$).

DISCUSSION

The results of this study indicate that in healthy adult subjects, inhaled THC significantly lowers IOP, and that this effect correlates with plasma THC levels. IOP reduction occurred soon after inhalation and was reduced by as much as 16%. Both percent IOP reduction and absolute IOP reduction in mmHg demonstrated a strong negative correlation with plasma THC levels. The IOP was lowered significantly for 4 h after inhalation. Furthermore, increasing plasma levels up to a concentration of 20 ng/ml was strongly correlated with increasing reduction in IOP. THC plasma levels >20 ng/ml were not correlated with further reduction in IOP.

Consistent with prior descriptions of THC metabolism, participants demonstrated a rapid spike in plasma THC levels that quickly decreased (15, 20). At 30 min, IOP reduction was already at 15%, but this reduction continued ranging from 11 to 16% for 4 h despite the fall in THC plasma levels (**Figure 2**). Indeed, THC plasma levels are known to decrease quickly as the lipophilic substance leaves the serum and deposits in the tissues of the body where it exerts its various effects (16, 17). As such, IOP reduction continued despite the rapid fall in serum levels.

Correlation between THC plasma levels and its other effects in the body have been described. The lipophilicity of THC results in a rapid withdrawal from the serum into the tissues, causing a situation where THC effects correlate with early THC plasma levels rather than concurrent THC plasma levels (22). For example, psychotropic effects have been correlated with THC plasma levels during the first 4 h after inhalation (23). Furthermore, models for predicting effects on heart rate, alertness, and psychotropic effects have been developed to predict

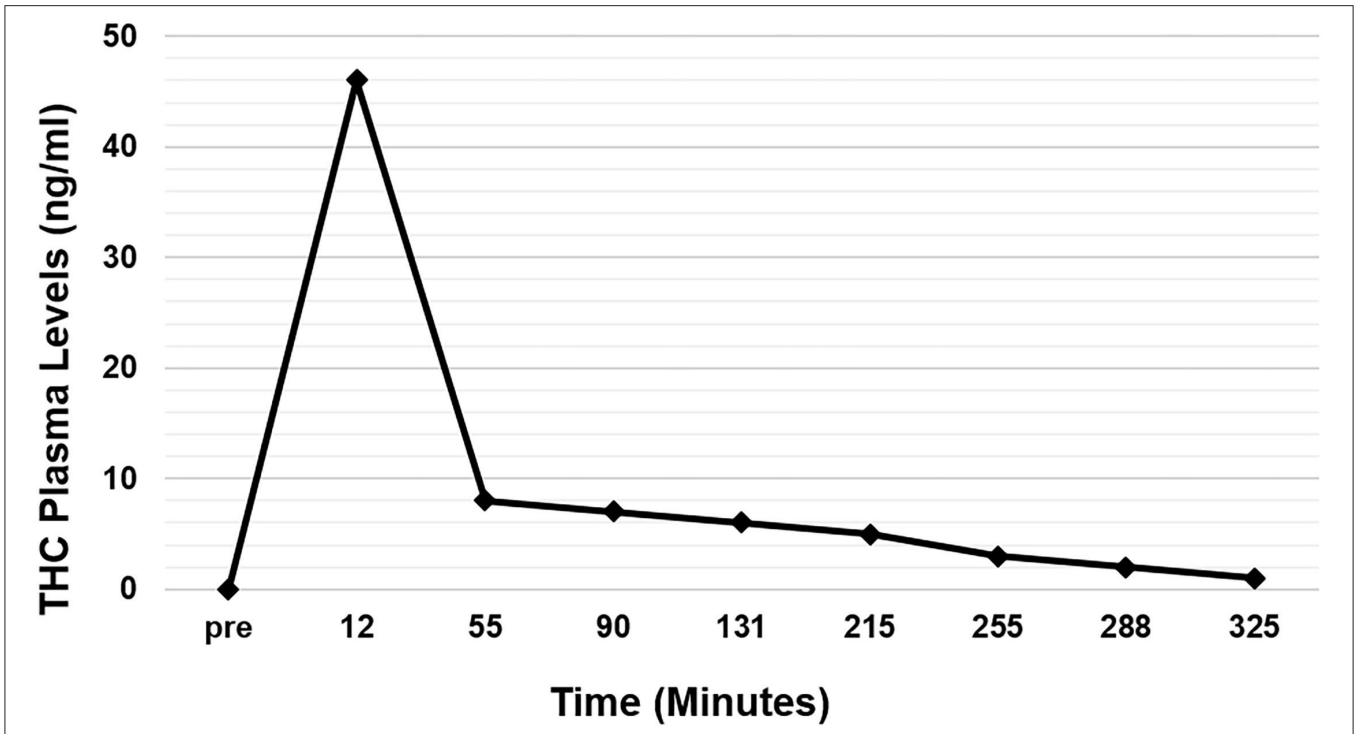

FIGURE 1 | Average THC plasma levels over time.

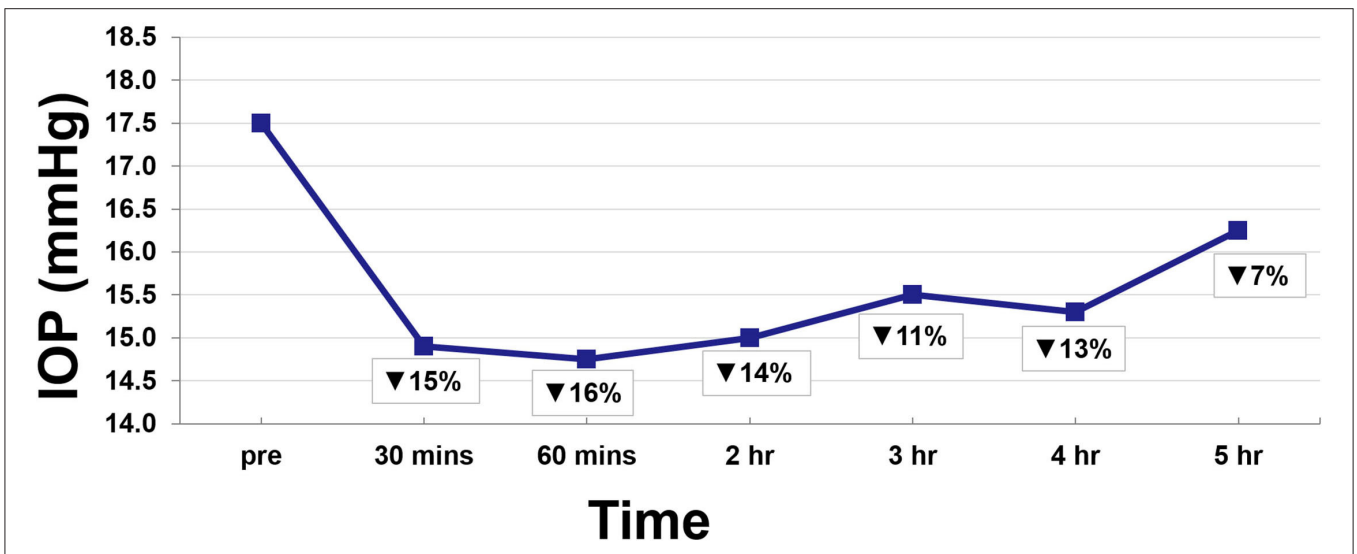

FIGURE 2 | Average IOP reduction over time.

the degree of these effects based on THC plasma levels (22). They suggest plasma levels above which additional effect on the body are less likely or impactful. This study shows similar results for IOP, and represents the first analysis to describe IOP reduction as it correlates with THC plasma levels. It further suggests a plasma level of 20 ng/ml as a target plasma level above which additional IOP-lowering is not strongly correlated.

The specific mechanisms by which cannabis lowers IOP are the subject of active investigation. It is known that there are cannabinoid receptors located throughout the eye, in particular in the ciliary muscle, ciliary epithelium, trabecular meshwork, and Schlemm's canal (24). These receptors, part of the endocannabinoid system, result in a series of varied changes such as ciliary body contraction,

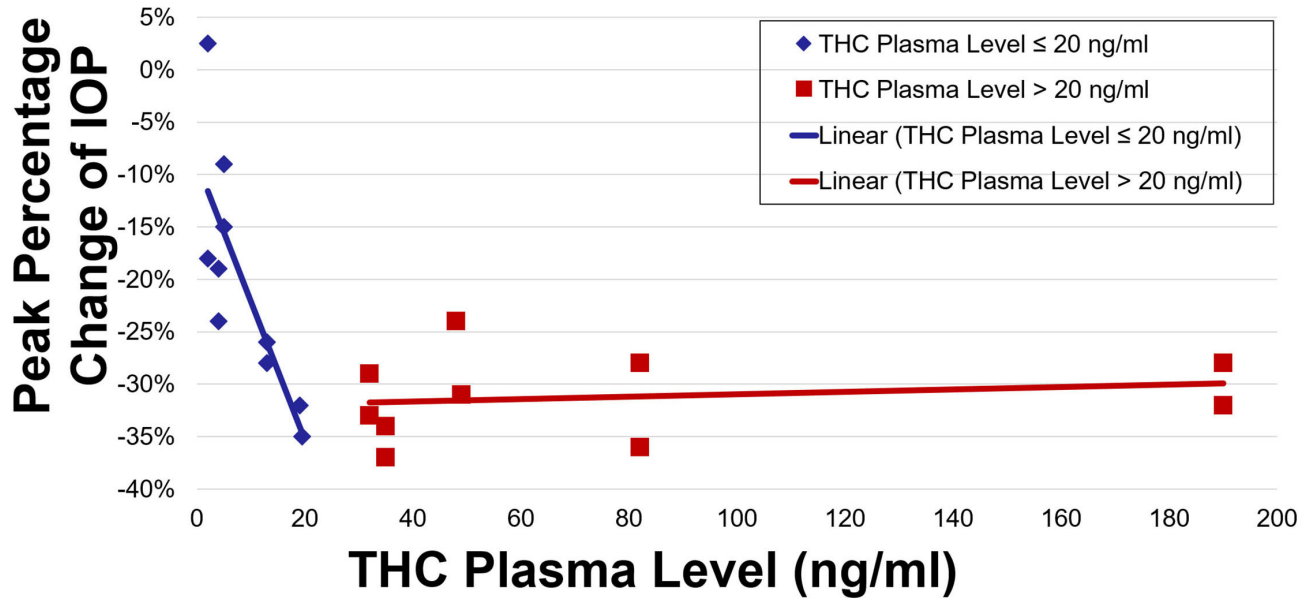

FIGURE 3 | Peak percentage change of IOP by THC plasma level.

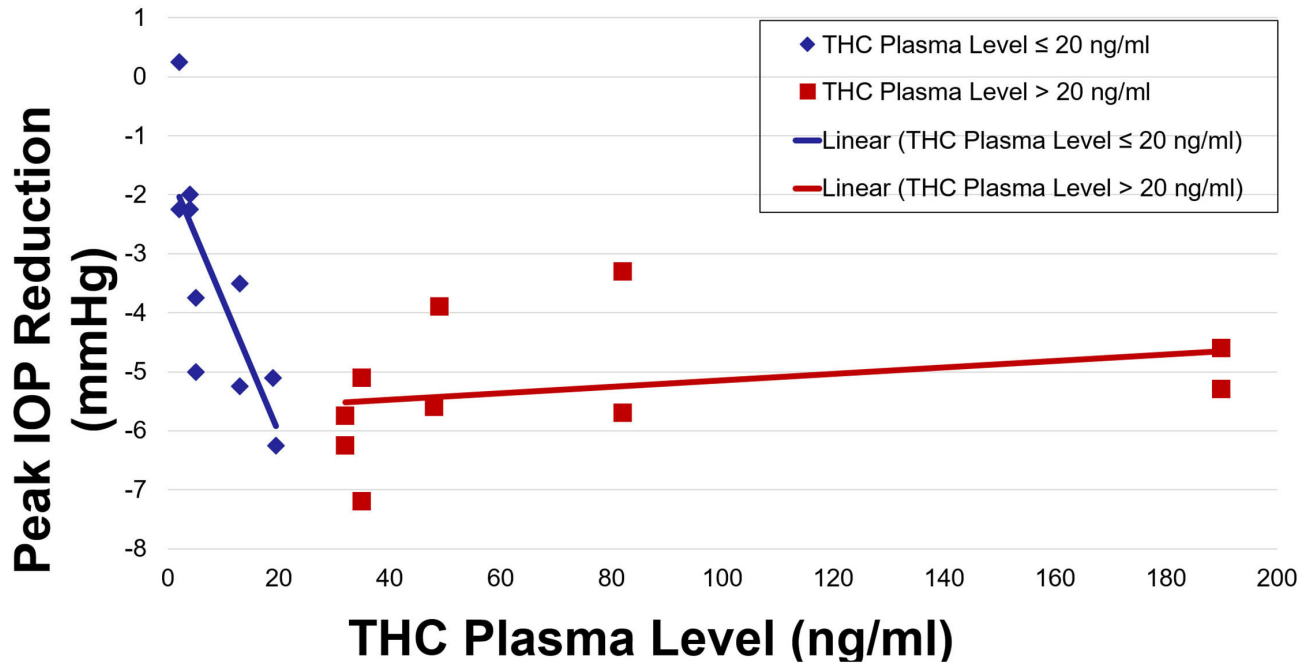

FIGURE 4 | Peak IOP reduction by THC plasma level.

widening of Schlemm's canal, and activation of matrix metalloproteinase, which enhances outflow of the trabecular meshwork (25, 26). Moreover, cannabinoids also upregulate COX-2, potentially increasing the presence of prostaglandin E2 and metalloproteinases, enhancing the outflow of aqueous humor, and reducing IOP (27, 28). It has also been suggested that some cannabinoids lower IOP through adrenergic receptors within the eye as well as through a mechanism involving prostaglandins by action of endocannabinoid metabolites (29–31). Besides any manipulation on ocular blood flow, the potential role of cannabis in neuroprotection has been suggested by many studies, although no clear evidence

of neuroprotection in glaucoma has yet been established (32, 33).

Given the wide range of systemic considerations, the routine use of inhaled or ingested cannabis for glaucoma treatment has not been clinically practical. However, novel compounds with improved corneal penetration are being developed for topical administration, thereby mitigating systemic side-effects (10–14, 34). Non-psychotropic cannabinoids and other CB1 receptor targets are being investigated for potential treatments that avoid systemic effects (35, 36). In addition, formulations are being developed to improve duration of action (37).

This study is not without limitations. First, the method of obtaining the IOP data was through a non-contact tonometry method, thereby facilitating the acquisition of IOP data in contact lens wearers, and decreasing the invasiveness of measurements for this pilot study. Future studies would ideally use more consistently accurate methods of tonometry. In addition, this study only involved healthy normal adults, and does not characterize the IOP-lowering effects of marijuana in subjects with glaucoma, ocular hypertension, or in subjects with concomitant IOP-lowering medications. Future studies can also focus on IOP-lowering response based on patient characteristics such as sex, ethnicity, etc…

In conclusion, the current study demonstrates a strong correlation between IOP and THC plasma levels. This study further suggests that a peak THC plasma level above 20 ng/mL is not correlated with further IOP reduction, and that non-physiologic IOP levels are not seen with increasing plasma levels of THC in healthy subjects. Defining the role of cannabis in glaucoma treatment requires further studies to better characterize these effects in different patient populations.

DATA AVAILABILITY STATEMENT

The raw data supporting the conclusions of this article will be made available by the authors, without undue reservation.

ETHICS STATEMENT

The studies involving human participants were reviewed and approved by University of California, San Diego (UCSD) Human Research Protections. The patients/participants provided their written informed consent to participate in this study.

AUTHOR CONTRIBUTIONS

SM, JL, RF, TM, RW, and DM contributed to the conception and design of the study. AS, DG, and ES organized and analyzed the data as well as performed the statistical analysis. AS wrote the first draft of the manuscript. SM, ES, and DG wrote the methods section of the manuscript. All authors contributed to the revising and editing of the manuscript and approved the submitted version of the manuscript.

FUNDING

This study was conducted using departmental funds from the University of California, Irvine, Gavin Herbert Eye Institute.

REFERENCES

1. Tomida I, Azuara-Blanco A, House H, Flint M, Pertwee RG, Robson PJ. Effect of sublingual application of cannabinoids on intraocular pressure: a pilot study. *J Glaucoma.* (2006) 15:349–53. doi: 10.1097/01.ijg.0000212260.04488.60
2. Miller S, Daily L, Leishman E, Bradshaw H, Straiker A. Δ9-Tetrahydrocannabinol and cannabidiol differentially regulate intraocular pressure. *Invest Ophthalmol Vis Sci.* (2018) 59:5904–11. doi: 10.1167/iovs.18-24838
3. Hepler RS, Frank IR. Marihuana smoking and intraocular pressure. *JAMA.* (1971) 217:1392. doi: 10.1001/jama.1971.03190100074024
4. Cooler P, Gregg JM. Effect of delta-9-tetrahydrocannabinol on intraocular pressure in humans. *South Med J.* (1977) 70:951–4. doi: 10.1097/00007611-197708000-00016
5. Alshaarawy O, Elbaz HA. Cannabis use and blood pressure levels: United States National Health and Nutrition Examination Survey, 2005-2012. *J Hypertens.* (2016) 34:1507–12. doi: 10.1097/HJH.0000000000000990
6. Malinowska B, Toczek M, Pedzińska-Betiuk A, Schlicker *E. Cannabinoids* in arterial, pulmonary and portal hypertension - mechanisms of action and potential therapeutic significance. *Br J Pharmacol.* (2019) 176:1395–411. doi: 10.1111/bph.14168
7. Singh A, Saluja S, Kumar A, Agrawal S, Thind M, Nanda S, et al. Cardiovascular complications of marijuana and related substances: a review. *Cardiol Ther.* (2018) 7:45–59. doi: 10.1007/s40119-017-0102-x
8. Green K, Roth M. Ocular effects of topical administration of delta 9-tetrahydrocannabinol in man. *Arch Ophthalmol.* (1982) 100:265–7. doi: 10.1001/archopht.1982.01030030267006
9. Jay WM, Green K. Multiple-drop study of topically applied 1% delta 9-tetrahydrocannabinol in human eyes. *Arch Ophthalmol.* (1983) 101:591–3. doi: 10.1001/archopht.1983.01040010591012
10. Taskar P, Adelli G, Patil A, Lakhani P, Ashour E, Gul W, et al. Analog derivatization of cannabidiol for improved ocular permeation. *J Ocul Pharmacol Ther.* (2019) 35:301–10. doi: 10.1089/jop.2018.0141
11. Adelli GR, Bhagav P, Taskar P, Hingorani T, Pettaway S, Gul W, et al. Development of a Δ9-tetrahydrocannabinol amino acid-dicarboxylate prodrug with improved ocular bioavailability. *Invest Ophthalmol Vis Sci.* (2017) 58:2167–79. doi: 10.1167/iovs.16-20757
12. Punyamurthula NS, Adelli GR, Gul W, Repka MA, ElSohly MA, Majumdar S. Ocular disposition of Δ8-tetrahydrocannabinol from various topical ophthalmic formulations. *AAPS PharmSciTech.* (2017) 18:1936–45. doi: 10.1208/s12249-016-0672-2
13. Hingorani T, Gul W, Elsohly M, Repka MA, Majumdar S. Effect of ion pairing on in vitro transcorneal permeability of a Δ(9) -tetrahydrocannabinol prodrug: potential in glaucoma therapy. *J Pharm Sci.* (2012) 101:616–26. doi: 10.1002/jps.22791
14. Hingorani T, Adelli GR, Punyamurthula N, Gul W, Elsohly MA, Repka MA, et al. Ocular disposition of the hemiglutarate ester prodrug of Δ?-Tetrahydrocannabinol from various ophthalmic formulations *Pharm Res.* (2013) 30:2146–56. doi: 10.1007/s11095-013-1072-x
15. Owens SM, McBay AJ, Reisner HM, Perez-Reyes M. 125I radioimmunoassay of delta-9-tetrahydrocannabinol in blood and plasma with a solid-phase second-antibody separation method. *Clin Chem.* (1981) 27:619–24. doi: 10.1093/clinchem/27.4.619
16. Huestis MA, Henningfield JE, Cone EJ. Blood cannabinoids. I Absorption of THC and formation of 11-OH-THC and THCCOOH during and after smoking marijuana. *J Anal Toxicol.* (1992) 16:276–82. doi: 10.1093/jat/16.5.276

17. Huestis MA. Human cannabinoid pharmacokinetics. *Chem Biodivers.* (2007) 4:1770–804. doi: 10.1002/cbdv.200790152
18. Cone EJ, Huestis MA. Relating blood concentrations of tetrahydrocannabinol and metabolites to pharmacologic effects and time of marijuana usage. *Ther Drug Monit.* (1993) 15:527–32. doi: 10.1097/00007691-199312000-00013
19. Karschner EL, Schwilke EW, Lowe RH, Darwin WD, Herning RI, Cadet JL, et al. Implications of plasma Delta9-tetrahydrocannabinol, 11-hydroxy-THC, and 11-nor-9-carboxy-THC concentrations in chronic cannabis smokers. *J Anal Toxicol.* (2009) 33:469–77. doi: 10.1093/jat/33.8.469
20. Lemberger L, Silberstein SD, Axelrod J, Kopin IJ. Marihuana: studies on the disposition and metabolism of delta-9-tetrahydrocannabinol in man. *Science.* (1970) 170:1320–2. doi: 10.1126/science.170.3964.1320
21. Mosaed S, Liu J, Minckler D, Fitzgerald D, Grelotti D, Sones E, et al. The effect of inhaled cannabis on intraocular pressure in healthy adult subjects. *Touch Ophthalmology*. (2020) 15:1. doi: 10.17925/OPHT.2021.15.1.33
22. Strougo A, Zuurman L, Roy C, Pinquier JL, van Gerven JM, Cohen AF, et al. Modelling of the concentration–effect relationship of THC on central nervous system parameters and heart rate – insight into its mechanisms of action and a tool for clinical research and development of cannabinoids. *J Psychopharmacol.* (2008) 22:717–26. doi: 10.1177/0269881108089870
23. Chiang CW, Barnett G. Marijuana effect and delta-9-tetrahydrocannabinol plasma level. *Clin Pharmacol Ther.* (1984) 36:234–8. doi: 10.1038/clpt.1984.168
24. Straiker AJ, Maguire G, Mackie K, Lindsey J. Localization of cannabinoid CB1 receptors in the human anterior eye and retina. *Invest Ophthalmol Vis Sci.* (1999) 40:2442–8.
25. Panahi Y, Manayi A, Nikan M, Vazirian M. The arguments for and against cannabinoids application in glaucomatous retinopathy. *Biomed Pharmacother.* (2017) 86:620–7. doi: 10.1016/j.biopha.2016.11.106
26. Rösch S, Ramer R, Brune K, Hinz B. R(+)-methanandamide and other cannabinoids induce the expression of cyclooxygenase-2 and matrix metalloproteinases in human nonpigmented ciliary epithelial cells. *J Pharmacol Exp Ther.* (2006) 316:1219–28. doi: 10.1124/jpet.105.092858
27. Kozak KR, Rowlinson SW, Marnett LJ. Oxygenation of the endocannabinoid, 2-arachidonylglycerol, to glyceryl prostaglandins by cyclooxygenase-2. *J Biol Chem.* (2000) 275:33744–9. doi: 10.1074/jbc.M007088200
28. Rouzer CA, Marnett LJ. Endocannabinoid oxygenation by cyclooxygenases, lipoxygenases, and cytochromes P450: cross-talk between the eicosanoid and endocannabinoid signaling pathways. *Chem Rev.* (2011) 111:5899–921. doi: 10.1021/cr2002799
29. Green K, Kearse EC, McIntyre OL. Interaction between delta-9-tetrahydrocannabinol and indomethacin. *Ophthalmic Res.* (2001) 33:217–20. doi: 10.1159/000055673
30. Green K, Podos SM. Antagonism of arachidonic acid-induced ocular effects by delta1-tetrahydrocannabinol. *Invest Ophthalmol.* (1974) 13:422–9.
31. Hudson BD, Beazley M, Szczesniak AM, Straiker A, Kelly ME. Indirect sympatholytic actions at β-adrenoceptors account for the ocular hypotensive actions of cannabinoid receptor agonists. *J Pharmacol Exp Ther.* (2011) 339:757–67. doi: 10.1124/jpet.111.185769
32. Nucci C, Bari M, Spanò A, Corasaniti M, Bagetta G, Maccarrone M, et al. Potential roles of (endo)cannabinoids in the treatment of glaucoma: from intraocular pressure control to neuroprotection. *Prog Brain Res.* (2008) 173:451–64. doi: 10.1016/S0079-6123(08)01131-X
33. Rapino C, Tortolani D, Scipioni L, Maccarrone M. Neuroprotection by (endo)cannabinoids in glaucoma and retinal neurodegenerative diseases. *Curr Neuropharmacol.* (2018) 16:959–70. doi: 10.2174/1570159X15666170724104305
34. Goyal H, Awad HH, Ghali JK. Role of cannabis in cardiovascular disorders. *J Thorac Dis.* (2017) 9:2079–92. doi: 10.21037/jtd.2017.06.104
35. Miller S, Kulkarni S, Ciesielski A, Nikas SP, Mackie K, Makriyannis A, et al. Controlled-deactivation cb1 receptor ligands as a novel strategy to lower intraocular pressure. *Pharmaceuticals.* (2018) 11:50. doi: 10.3390/ph11020050
36. Szczesniak AM, Maor Y, Robertson H, Hung O. Kelly ME. Nonpsychotropic cannabinoids, abnormal cannabidiol and canabigerol-dimethyl heptyl, act at novel cannabinoid receptors to reduce intraocular pressure. *J Ocul Pharmacol Ther.* (2011) 27:427–35. doi: 10.1089/jop.2011.0041
37. Sweeney C, Dudhipala N, Thakkar R, Mehraj T, Marathe S, Gul W, et al. Effect of surfactant concentration and sterilization process on intraocular pressure-lowering activity of Δ^9-tetrahydrocannabinol-valine-hemisuccinate (NB1111) nanoemulsions. *Drug Deliv Transl Res.* (2020) 11:2096–107. doi: 10.1007/s13346-020-00871-9

Conflict of Interest: The authors declare that the research was conducted in the absence of any commercial or financial relationships that could be construed as a potential conflict of interest.

Publisher's Note: All claims expressed in this article are solely those of the authors and do not necessarily represent those of their affiliated organizations, or those of the publisher, the editors and the reviewers. Any product that may be evaluated in this article, or claim that may be made by its manufacturer, is not guaranteed or endorsed by the publisher.

Advantages of publishing in Frontiers

OPEN ACCESS
Articles are free to read for greatest visibility and readership

FAST PUBLICATION
Around 90 days from submission to decision

HIGH QUALITY PEER-REVIEW
Rigorous, collaborative, and constructive peer-review

TRANSPARENT PEER-REVIEW
Editors and reviewers acknowledged by name on published articles

Frontiers
Avenue du Tribunal-Fédéral 34
1005 Lausanne | Switzerland

Visit us: www.frontiersin.org
Contact us: frontiersin.org/about/contact

REPRODUCIBILITY OF RESEARCH
Support open data and methods to enhance research reproducibility

DIGITAL PUBLISHING
Articles designed for optimal readership across devices

FOLLOW US
@frontiersin

IMPACT METRICS
Advanced article metrics track visibility across digital media

EXTENSIVE PROMOTION
Marketing and promotion of impactful research

LOOP RESEARCH NETWORK
Our network increases your article's readership